

MASS, HEAT AND NUTRIENT FLUXES IN THE ATLANTIC OCEAN  
DETERMINED BY INVERSE METHODS

by

Stephen Rich Rintoul

A.B., Harvard College  
(1982)

SUBMITTED IN PARTIAL FULFILLMENT OF THE  
REQUIREMENTS FOR THE DEGREE OF

DOCTOR OF PHILOSOPHY

at the

MASSACHUSETTS INSTITUTE OF TECHNOLOGY

and the

WOODS HOLE OCEANOGRAPHIC INSTITUTION

March, 1988

©Stephen R. Rintoul 1988

The author hereby grants to MIT and WHOI permission to reproduce  
and distribute copies of this thesis document in whole or in part.

Signature of the author

---

Joint Program in Oceanography,  
Massachusetts Institute of Technology –  
Woods Hole Oceanographic Institution

Certified by

---

Carl Wunsch  
Thesis supervisor

Accepted by

---

Joseph Pedlosky  
Chairman, Joint Committee for Physical Oceanography.  
Massachusetts Institute of Technology –  
Woods Hole Oceanographic Institution.

Mass, Heat and Nutrient Fluxes in the Atlantic Ocean  
Determined by Inverse Methods

by

Stephen Rich Rintoul

Submitted to the Massachusetts Institute of Technology - Woods Hole Oceanographic Institution Joint Program in March, 1988 in partial fulfillment of the requirements for the degree of Doctor of Philosophy.

**Abstract**

Inverse methods are applied to historical hydrographic data to address two aspects of the general circulation of the Atlantic Ocean. The method allows conservation statements for mass and other properties, along with a variety of other constraints, to be combined in a dynamically consistent way to estimate the absolute velocity field and associated property transports.

The method is first used to examine the exchange of mass and heat between the South Atlantic and the neighboring ocean basins. The Antarctic Circumpolar Current (ACC) carries a surplus of intermediate water into the South Atlantic through Drake Passage which is compensated by a surplus of deep and bottom water leaving the basin south of Africa. As a result, the ACC loses  $.25 \pm .18 \times 10^{15} W$  of heat in crossing the Atlantic. At  $32^\circ S$  the meridional flux of heat is  $.25 \pm .19 \times 10^{15} W$  equatorward, consistent in sign but smaller in magnitude than other recent estimates. This heat flux is carried primarily by a meridional overturning cell in which the export of 17 Sv of North Atlantic Deep Water (NADW) is balanced by an equatorward return flow equally split between the surface layers, and the intermediate and bottom water. No "leak" of warm Indian Ocean thermocline water is necessary to account for the equatorward heat flux across  $32^\circ S$ ; in fact, a large transfer of warm water from the Indian Ocean to the Atlantic is found to be inconsistent with the present data set. Together these results demonstrate that the Atlantic as a whole acts to convert intermediate water to deep and bottom water, and thus that the global thermohaline cell associated with the formation and export of NADW is closed primarily by a "cold water path," in which deep water leaving the Atlantic ultimately returns as intermediate water entering the basin through Drake Passage.

The second problem addressed concerns the circulation and property fluxes across  $24^\circ$  and  $36^\circ N$  in the subtropical North Atlantic. Conservation statements are considered for the nutrients as well as mass, and the nutrients are found to contribute significant information independent of temperature and salinity. Silicate is particularly effective in reducing the indeterminacy of circulation estimates based on mass conservation alone.

In turn, the results demonstrate that accurate estimates of the chemical fluxes depend on relatively detailed knowledge of the circulation.

The zonal-integral of the circulation consists of an overturning cell at both latitudes, with a net export of 19 Sv of NADW. This cell results in a poleward heat flux of  $1.3 \pm 2 \times 10^{15} \text{ W}$  and an equatorward oxygen flux of  $2900 \pm 180 \text{ kmol s}^{-1}$  across each latitude. The net flux of silicate is also equatorward:  $138 \pm 38 \text{ kmol s}^{-1}$  and  $152 \pm 56 \text{ kmol s}^{-1}$  across  $36^\circ$  and  $24^\circ\text{N}$ , respectively. However, in contrast to heat and oxygen, the overturning cell is not the only important mechanism responsible for the net silicate transport. A horizontal recirculation consisting of northward flow of silica-rich deep water in the eastern basin balanced by southward flow of low silica water in the western basin results in a significant silicate flux to the north. The net equatorward flux is thus smaller than indicated by the overturning cell alone.

The net flux of nitrate across  $36^\circ\text{N}$  is  $119 \pm 35 \text{ kmol s}^{-1}$  to the north and is indistinguishable from zero at  $24^\circ\text{N}$  ( $-8 \pm 39 \text{ kmol s}^{-1}$ ), leading to a net divergence of nitrate between these two latitudes. Forcing the system to conserve nitrate leads to an unreasonable circulation. The dominant contribution to the nitrate flux at  $36^\circ\text{N}$  results from the correlation of strong northward flow and relatively high nitrate concentrations in the sub-surface waters of the Gulf Stream. The observed nitrate divergence between  $24^\circ$  and  $36^\circ\text{N}$ , and convergence north of  $36^\circ\text{N}$ , can be accounted for by a shallow cell in which the northward flow of inorganic nitrogen (nitrate) in the Gulf Stream is balanced by a southward flux of dissolved organic nitrogen in the recirculation gyre. Oxidation of the dissolved organic matter during its transit of the subtropical gyre supplies the required source of regenerated nitrate to the Gulf Stream and consumes oxygen, consistent with recent observations of oxygen utilization in the Sargasso Sea.

Thesis supervisor: Prof. Carl Wunsch

*Cecil and Ida Green Professor of Physical Oceanography  
Department of Earth, Atmospheric and Planetary Sciences  
Massachusetts Institute of Technology*

## Table of contents

|  |     |
|--|-----|
| <b>Abstract</b> . . . . .  | 2   |
| <b>Overview</b> . . . . .  | 5   |
| <b>Chapter 1: A Review of the Inverse Method</b> . . . . .               | 8   |
| <b>Chapter 2: South Atlantic Interbasin Exchange</b>                     |     |
| 1. Introduction . . . . .  | 20  |
| 2. The model . . . . .   | 31  |
| 2.1 The data . . . . .   | 31  |
| 2.2 Design of a standard model . . . . .                                 | 48  |
| 3. Results of the standard model . . . . .                               | 60  |
| 3.1 The velocity field . . . . .   | 65  |
| 3.2 Mass and heat transport . . . . .                                    | 73  |
| 3.3 Interpretation of the residuals . . . . .                            | 82  |
| 4. Discussion . . . . .  | 91  |
| 4.1 Water mass transports . . . . .                                      | 91  |
| 4.2 The meridional heat flux across 32°S . . . . .                       | 98  |
| 4.3 North Atlantic Deep Water and the thermohaline circulation . . . . . | 106 |
| 5. Summary and conclusions . . . . .                                     | 119 |
| <b>Chapter 3: Mass, Heat and Nutrient Fluxes in the North Atlantic</b>   |     |
| 1. Introduction . . . . .  | 125 |
| 2. The data . . . . .  | 131 |
| 3. The model . . . . .   | 156 |
| 4. Results . . . . .   | 164 |
| 4.1 Model 1: Total mass conserved . . . . .                              | 164 |
| 4.2 Model 2: Mass conserved in isopycnal layers . . . . .                | 166 |
| 4.3 Model 3: Total silicate conserved . . . . .                          | 181 |
| 4.4 Model 4: Mass and silicate conserved in isopycnal layers . . . . .   | 189 |
| 5. Discussion . . . . .  | 199 |
| 5.1 The velocity field . . . . .   | 199 |
| 5.2 Mass transport results . . . . .                                     | 211 |
| 5.3 Heat, oxygen and nutrient fluxes . . . . .                           | 229 |
| 6. Summary and conclusions . . . . .                                     | 264 |
| <b>Concluding Remarks</b> . . . . .                                      | 269 |
| <b>Acknowledgments</b> . . . . .   | 272 |
| <b>Appendix: Sensitivity of property flux estimates</b> . . . . .        | 273 |
| <b>References</b> . . . . .  | 276 |





## Overview

A primary goal of physical oceanographers is to understand the role of the oceans in the global climate system. The ocean circulation influences the heat budget, and hence the climate, of the earth in several ways. The heat capacity of sea water is large relative to that of the atmosphere and consequently the sea stores a substantial amount of heat, moderating seasonal or perhaps longer term variations in solar insolation. In addition, the ocean is thought to play an important role in balancing the global radiation budget. The earth absorbs more solar radiation in the tropics than it emits, in the annual mean, while the reverse is true at the poles. The ocean and atmosphere act to keep the system in balance by transporting heat from the tropics to the poles, moderating the climatic extremes that would otherwise result from the uneven heating of the earth by the sun. Although the relative importance of the atmosphere and the ocean in the net poleward heat flux is still a matter of debate, both appear to be of roughly the same magnitude. The poleward transport of heat by the oceans is thought to be effected primarily by a meridional overturning cell, in which warm water flows poleward in the upper layers of the ocean, is made more dense by cooling and evaporation, and returns equatorward as cooler deep water.

In addition to being the dominant mode responsible for the poleward transport of heat by the ocean, the thermohaline circulation resulting from the formation of deep water is also important to the climate problem as the primary means of exchange between the atmosphere and the deep sea. As newly-formed deep water sinks from the sea surface at high latitude, it carries with it dissolved gases such as oxygen and radiatively-active, or "greenhouse," gases such as carbon dioxide. Understanding the pathways and rates involved in the thermohaline circulation is therefore an important step toward being able to predict the response of the climate system to natural or man-made changes in the earth's atmosphere.

A second path by which carbon enters the ocean is through the biology. When sea water that is rich in nutrients is exposed to sunlight at the sea surface, photosynthetic organisms take up nutrients and carbon dioxide to form the organic and inorganic compounds of which their cells are made. As the primary production is consumed at higher trophic levels in the food chain, a fraction of the organic matter sinks out of the euphotic zone, providing a source of carbon to the deep sea. As it falls, bacteria and chemical dissolution act to decompose the organic matter, releasing nutrients and carbon to the sea water. Indeed, the carbon supplied by the thermohaline circulation and biological processes to the deep sea, where it is found in the form of carbonate and bicarbonate ions, represents easily the largest single reservoir of carbon on the earth.

The work presented in this thesis consists of two essentially independent parts, each of which focuses on a specific aspect of the larger problem sketched above. The first part examines the exchange of mass and heat between the South Atlantic and the neighboring ocean basins. The goal is to learn something about the mechanisms controlling the global thermohaline circulation associated with the formation of deep water at high latitudes. Since the primary sources of dense water to the world ocean are found in the Atlantic (the Norwegian-Greenland Sea and the Weddell Sea), the South Atlantic is a convenient "choke-point" at which to study the global cell resulting from the export of dense water from the basin, and the compensating inflow of less dense water.

The second half of the thesis is concerned with the circulation of the subtropical North Atlantic, and considers the transport of oxygen and the nutrients as well as mass and heat. The objects of this study are two-fold: the first is to use the information contained in the nutrient fields to better determine the velocity field and transports of heat and mass; the second is to determine the nutrient transports themselves, in order to understand what processes are important in maintaining the nutrient cycles in the ocean.

In addition to their common focus on the mechanisms responsible for the transport of chemical and physical properties in the ocean, the two studies are also linked by use of the same mathematical machinery, that of inverse methods. In the geostrophic inverse method introduced by Wunsch (1978), mass conservation statements and other information are combined to estimate the absolute velocity field. Although the solution obtained is non-unique, as is that obtained by more classical methods, the inverse machinery has the advantage of providing useful information concerning what one has been able to determine and how well. The method is also very flexible: one can include diverse types of information as model constraints, and specific hypotheses can be tested for consistency with the data in a straightforward and explicit way.

The thesis consists of three main chapters. First, the inverse method is reviewed in Chapter 1. Chapter 2 presents the results of the study of interbasin exchange in the South Atlantic. The investigation of mass, heat and nutrient fluxes in the subtropical North Atlantic is discussed in Chapter 3.

## Chapter 1

### A Review of the Inverse Method

A brief review of the geostrophic inverse method is given in this chapter. A more thorough discussion of the application of inverse methods to ocean circulation problems can be found in Wunsch (1978), Roemmich (1980), and Wunsch and Grant (1982); in the more general geophysical context, I have found the presentations by Wiggins (1972) and Parker (1970,1977) particularly useful.

Studies of the general circulation of the ocean have traditionally relied on two classical types of analysis: water mass analysis and the dynamic method. In the former technique the distributions of temperature, salinity and other properties are used to infer the direction of the flow. Wüst's (1935) core-layer method is one example, in which a property extremum is used to define the "core" of a water mass, which is interpreted as the primary "spreading path". Isentropic analysis, in which properties are mapped on constant density surfaces, is another example (Montgomery, 1938). By themselves, such methods can indicate flow patterns but not flow volume. Moreover, there is an ambiguity in the interpretation of spreading paths as axes of flow due to our poor understanding of the relative roles of advection and diffusion in the transport of properties in the ocean. Nevertheless the large-scale distribution of properties is thought to accurately portray the mean flow field.

The second classical tool of physical oceanographers is the dynamic method. The mean circulation is assumed to be steady and in hydrostatic and geostrophic balance to lowest order:

$$\frac{\partial p}{\partial z} = -g\rho$$

$$fv = \frac{1}{\rho_o} \frac{\partial p}{\partial x} \qquad fu = -\frac{1}{\rho_o} \frac{\partial p}{\partial y}$$

Combining these equations gives an expression for the vertical derivative of the velocity, the thermal wind relation:

$$f \frac{\partial v}{\partial z} = -\frac{g}{\rho_o} \frac{\partial \rho}{\partial x} \quad f \frac{\partial u}{\partial z} = \frac{g}{\rho_o} \frac{\partial \rho}{\partial y}$$

In the dynamic method, hydrographic data is used to estimate the horizontal gradient of density along the section and hence the vertical shear. Integrating once from some level  $z_o$  gives the horizontal velocity normal to the section to within an integration constant, the velocity at the reference level  $z_o$ . Some assumption about the unknown reference level velocity is required to obtain the absolute velocity field.

Most commonly the velocity has been assumed to vanish at some level, the level-of-no-motion. There is no dynamical argument for the existence of such a level, and water mass features are generally used to justify a particular choice, such as between two layers whose properties indicate they are flowing in opposing directions. Alternatively, attempts have been made to measure the velocity directly using floats or current meters at a given depth to find the integration constant needed to reference the dynamic computations. However, there is a mismatch that is difficult to resolve between time-mean velocity measurements from a single point, or Lagrangian measurements, and the 'instantaneous' but spatially-averaged shear obtained from hydrographic observations.

The geostrophic inverse method used here is in a sense a synthesis of the two classical techniques: dynamic calculations are combined with property conservation statements and other constraints to estimate the absolute velocity. As in the dynamic method, we start by assuming the flow is in hydrostatic and geostrophic balance, and integrate the thermal wind relation to compute the velocity relative to some initial reference level. The absolute velocity is then given by  $\mathbf{v}_{abs} = \mathbf{v}_{rel} + \mathbf{b}$ , where  $\mathbf{v}_{rel}$  is the relative velocity from the thermal wind and  $\mathbf{b}$  is the unknown reference level velocity. (Throughout the text, vector quantities are denoted by boldface type and matrices by boldface capital letters.) In order to determine the reference level velocities we make

a further assumption that mass (and other properties) are approximately conserved in closed volumes of ocean, and use the continuity equation to solve for  $b$ .

In particular, we consider an area of ocean bounded by hydrographic sections and land, divided vertically into  $M$  layers defined by surfaces of constant density. Conservation of mass or some other property with concentration  $C$  in layer  $m$  then takes the form:

$$\sum_{j=1}^N \delta_j \Delta x_j \int_{P_m}^{P_{m+1}} \rho C_j (v_{rel} + b)_j dp + (w^* a C)_m - (w^* a C)_{m+1} \cong 0 \quad (1.1)$$

$N$  = the number of station pairs

$P_m, P_{m+1}$  = depths of isopycnal surfaces bounding layer  $m$

$\delta_j$  = unit normal

$\int(v_j)$  = relative velocity at station pair  $j$

$b_j$  = reference level velocity at station pair  $j$

$\Delta x_j$  = station spacing at pair  $j$

$C_j$  = property value/unit mass at pair  $j$

$(w^* a C)_{m,m+1}$  = cross-isopycnal flux across each interface (discussed below)

A variety of other statements about the flow can also be written as linear constraints and included in the system of equations. For example, the volume transport can be required to agree with estimates based on direct current meter observations, or the net heat or nitrate flux across a section can be fixed at a particular value. Examples of the use of such constraints will be shown in Chapters 2 and 3.

The resulting system of linear equations can be written in matrix form as

$$\mathbf{A} \mathbf{b} = -\mathbf{d}$$

where  $\mathbf{A}$  is a matrix whose elements are the product of the area times the concentration at each station pair in each layer;  $\mathbf{d}$  is a column vector whose elements are the property

imbalances in each layer due to the relative velocity field; and  $\mathbf{b}$  is the vector of unknowns. The problem then is to find the reference level velocities and cross-isopycnal transfers satisfying this set of linear equations.

In the ocean circulation problems considered in this thesis the system of equations is underdetermined (fewer independent equations than unknowns) and therefore an infinite number of solutions exists. The data alone do not select any particular solution as preferable to any other; the selection of a "unique" solution requires imposing some additional criteria. Here the system of equations will be solved using the singular value decomposition (SVD) (Lanczos, 1961). This procedure selects the solution that simultaneously minimizes the misfit in each equation and the deviation from the initial model; in this case, with  $\mathbf{b}=0$  at the reference level initially, the magnitude of  $\mathbf{b}$  is minimized. Of the infinite set of consistent solutions the SVD solution is the simplest or smoothest one in the sense that no structure is introduced that is not required to satisfy the constraints. The SVD has the additional advantage of being able to handle underdetermined, inexact, incompatible or redundant systems of equations (e.g. see Lanczos, 1961).

The SVD of a matrix  $\mathbf{A}$  can be written:

$$\mathbf{A} = \mathbf{U}\mathbf{\Lambda}\mathbf{V}^T$$

where the  $\mathbf{U}$  and  $\mathbf{V}$  matrices are made up of the eigenvectors of the coupled eigenvalue problem:

$$\mathbf{A}\mathbf{A}^T\mathbf{U} = \lambda^2\mathbf{U} \quad \mathbf{A}^T\mathbf{A}\mathbf{V} = \lambda^2\mathbf{V}$$

and  $\mathbf{\Lambda}$  is a diagonal matrix whose diagonal elements are equal to the eigenvalues  $\lambda$ . ( $\mathbf{V}^T$  is the transpose of the matrix  $\mathbf{V}$ .) The  $\mathbf{U}$  and  $\mathbf{V}$  vectors each form a complete orthonormal set, the  $\mathbf{U}$ 's spanning the observation space of dimension  $M$  ( $M$ =the number of equations) and the  $\mathbf{V}$ 's spanning the  $N$ -space ( $N$ =the number of unknowns). Using the SVD the original problem  $\mathbf{A}\mathbf{b} = -\mathbf{d}$  can be solved for the unknowns:



$$\mathbf{b} = \sum_{l=1}^k \frac{\mathbf{u}_l \cdot (-\mathbf{d})}{\lambda_l} \mathbf{v}_l \quad (1.2)$$

where  $k$  = the number of non-zero eigenvalues. In an underdetermined problem ( $M < N$ ) there can be at most  $M$  non-zero eigenvalues. In practice the  $M$  equations may not all be independent, and the number of non-zero eigenvalues is then less than  $M$ . Due to errors in the observations some eigenvalues that should be zero will actually be very small but finite. Including these eigenvalues in the summation in equation (1.2) causes the solution to grow rapidly since the solution elements are inversely proportional to the eigenvalues. Choosing how many eigenvalues to keep in the summation is the problem of determining the rank of  $\mathbf{A}$ . Wiggins (1972) and Lawson and Hanson (1974) discuss several approaches to making this decision. As additional eigenvectors are added to the summation in equation (1.2) the residual norm  $\|\mathbf{Ab} + \mathbf{d}\|$  decreases while the solution norm  $\|\mathbf{b}^t \mathbf{b}\|$  increases. The best choice of the rank is one for which the residuals have been made acceptably small but the solution has not been made too large.

The trade-off between the relative magnitude of the the residuals and the solution can be illustrated by plotting the residual norm vs. the solution norm for each rank  $k$  (as in the Levenberg-Marquardt stabilization method; Lawson and Hanson, 1974). In Fig. 1 such a diagram is shown for one of the models discussed in Chapter 2. Also shown is a plot of the eigenvalues as a function of  $k$ . The optimum rank is near the "knee" of the curve, where the residuals have been reduced to a satisfactory extent and the solution norm has not become unreasonably large. This corresponds to  $k=36$  in this case, just before the first steep drop-off in the magnitude of the eigenvalues. Another way to choose the proper rank is to examine the estimated error variance, as discussed below. Each of the methods usually led to a similar choice for  $k$  for the

models discussed in this paper, and the results in any case tend to be insensitive to small changes in the rank.

At a given rank the  $U$  and  $V$  vectors provide useful information on the nature of the solution. This comes under the topic of resolution. It can be shown (e.g. Roemmich, 1980) that the solution given in equation (1.2) can be rewritten:

$$\mathbf{b}_{est} = \mathbf{V}_k \mathbf{V}_k^T \mathbf{b}_{true}$$

where  $\mathbf{V}_k$  is the matrix made up of the first  $k$   $V$  vectors, and  $\mathbf{b}_{est}$  is our estimate of the true solution  $\mathbf{b}_{true}$ .  $\mathbf{V}_k \mathbf{V}_k^T$  is called the model resolution matrix; our estimate of the model parameters is a weighted average of the true model parameters, with the weights given by the columns of the  $\mathbf{V}_k \mathbf{V}_k^T$  matrix. If the rank of the system is  $N$  then  $\mathbf{V}_k \mathbf{V}_k^T = \mathbf{I}$ , the identity matrix, and each model parameter is uniquely determined; if  $\mathbf{V}_k \mathbf{V}_k^T$  is close to being the identity matrix, in that the largest elements are clustered around the diagonal, the matrix acts as a filter that performs a local smoothing. In this case the resolution is said to be "compact." The applications of the inverse method discussed in Chapters 2 and 3 will be shown to generally have compact resolution. A good illustration of compact vs. non-compact resolution in several simple cases is given by Roemmich (1980). As he shows, station pairs with similar ratios of layer depths, or equivalently, whose corresponding columns in  $\mathbf{A}$  are most nearly linearly dependent, tend to be grouped together in the solution.

The  $\mathbf{U}_k \mathbf{U}_k^T$  matrix also acts as a filter, but in the  $M$ -space; it is the data resolution matrix. Suppose we want to know how well our estimated model parameters  $\mathbf{b}$  predict the original data  $\mathbf{d}$ . Substituting the expression for  $\mathbf{b}$  in equation (1.1) we find:

$$\mathbf{d}_{pred} = \mathbf{A}\mathbf{b} = (\mathbf{U}\mathbf{\Lambda}\mathbf{V}^T)(\mathbf{V}\mathbf{\Lambda}\mathbf{U}^T)\mathbf{d} = \mathbf{U}\mathbf{U}^T\mathbf{d}.$$

Thus the columns of the data resolution matrix show how much weight each observation has in determining the predicted value, or the information content in each equation. A diagonal element of 1 indicates that the corresponding constraint is completely independent of the other constraints. In the models discussed below we will see that

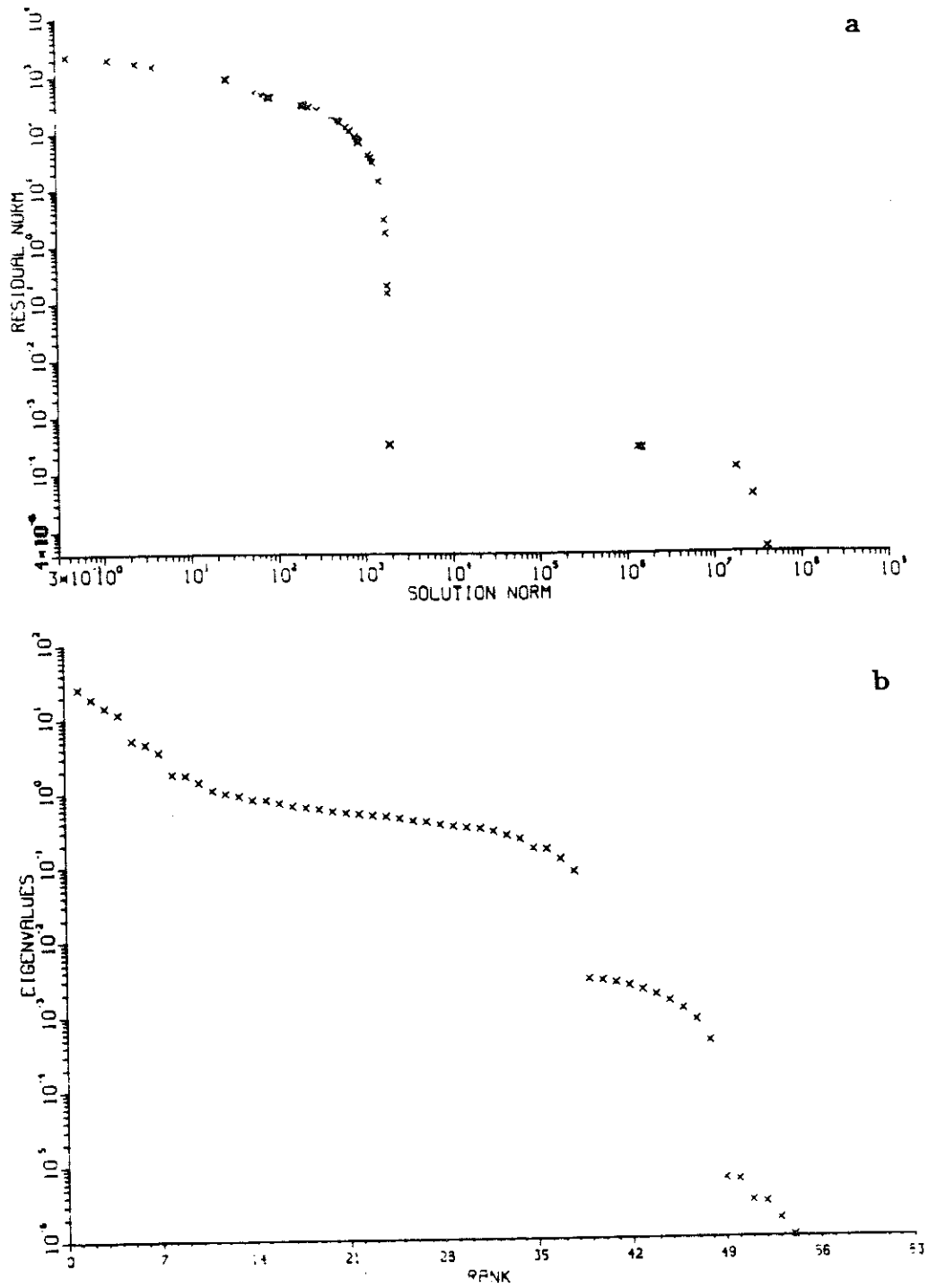


Fig. 1. (a) Example of plot of residual norm vs. solution norm for determining rank of A. Optimum choice of rank is near the "knee" of the curve. (b) Plot of the magnitude of the eigenvalues vs. rank k for the same problem.

examination of the  $U_k U_k^T$  matrix is useful in designing models and evaluating the degree of independent information contributed by different properties.

Before solving the system of equations using the SVD the rows and columns of the coefficient matrix  $A$  are usually weighted (Wunsch, 1978). The solution elements  $b_i$  are proportional to the corresponding elements of  $A$ . Thus large velocities tend to appear at deep, wide station pairs in the unweighted problem. To remove the bias due to unequal station pair areas the columns of  $A$  are divided by their length in the problems discussed in the following chapters; this choice of weighting puts each station pair on an *a priori* equal footing. The original problem now takes the form:

$$AW^{-1/2}W^{1/2}b = -d$$

where  $W$  in this case is a diagonal matrix with elements equal to the column length. Formally  $W$  is the covariance matrix of the solution  $b$ .

The constraint equations (the rows of  $A$ ) are also weighted before applying the SVD to account for the relative confidence one has in each constraint. Including the weighting of the constraints the original system of equations becomes:

$$S^{1/2}AW^{-1/2}W^{1/2}b = -S^{1/2}d$$

where  $S^{-1} = \sigma^2 I$ , and  $\sigma^2 =$  the problem variance. In this case, the constraints were weighted by the estimated uncertainty in each equation, as discussed below. With this choice of row weighting each equation has unit expected error variance. The matrix  $S$  is the covariance matrix of the observations. By assuming a simple diagonal form for  $S$  we have assumed that the noise in each of the equations is not correlated.

To perform the row weighting we need an estimate of the problem variance,  $\sigma^2$ . Error estimates can be made by considering *a priori* the errors due to observational noise, or by examining the residuals, or the goodness of fit. Wiggins (1972) points out that the two estimates should be of similar magnitude. If they are not, then either the estimates of the observational errors are too large relative to the internal consistency of the observations - in which case one is justified in concluding that the observational

errors were overestimated - or the variance of the observations was underestimated and/or the physical model is inadequate to explain the data.

The contribution due to some sources of observational error are easier to estimate than others. Errors in the transport by the relative velocity ( $\mathbf{d}$ ) arise from a variety of sources: navigation errors; measurement errors in temperature, salinity and pressure; and errors in interpolation. Roemmich (1979) estimated the uncertainty in the mass balance due to these sources to be roughly  $\pm 2$  Sv for the IGY sections in the North Atlantic. Thompson and Veronis (1980) and Fiadeiro and Veronis (1982) added random errors of the magnitude of the measurement errors to the observed T, S and P values and found they resulted in a transport uncertainty of similar magnitude. An additional error is incurred in extrapolating the shear to the bottom when adjacent stations reach to different depths. In this paper the isopycnal slope at the deepest common sample depth was kept constant below this depth to extrapolate the shear to the bottom. This is equivalent to assuming that the geostrophic shear decreases with depth roughly proportional to the stratification (Roemmich, 1979). It is difficult to estimate the error in layer transports arising from ignorance of the shear over a sloping bottom; here the uncertainty was assumed to be of the same magnitude as that due to measurement errors ( $\pm 2$  Sv).

The SVD also provides a formal estimate of the uncertainty in the solution  $\mathbf{b}$  due to random errors in the data (Wiggins, 1972; Wunsch, 1978). The relative variance of the  $j$ 'th solution element is given by

$$\frac{\langle b_j^2 \rangle}{\sigma^2} = \sum_{i=1}^k \frac{v_{ji}^2}{\lambda_i^2} \quad (1.3)$$

where  $\langle b_j^2 \rangle$  is the solution variance and  $\sigma^2$  is the problem variance. Note that this illustrates the trade-off between resolution and variance that enters into the determination of the rank  $k$ : as more eigenvalues and eigenvectors are included in the solution,

the resolution increases but so does the variance of the solution as the smaller  $\lambda$ 's are included in the summation. The problem variance can be estimated by *a priori* consideration of errors in the data, as above, or by examining the residuals in the constraint equations:

$$\sigma^2 = \sum_{i=1}^k \frac{(Ab + d)_i^2}{M - k} \quad (1.4)$$

where  $M$  is the total number of constraints and  $k$  is the rank, or the number of independent constraints (Wiggins, 1972).

Observational errors in T, S and P can also lead to errors in determining the depth of the isopycnal surfaces used to define the layers. A more serious problem can arise in defining the isopycnals themselves, due to the nonlinearity of the equation of state of sea water. In fact, the term "isopycnal" is somewhat ambiguous when dealing with density surfaces of changing depth since the compressibility of sea water depends on temperature. For the purposes of the model, we are interested in defining layers whose water mass properties are approximately conservative. Therefore the boundaries of the layers should correspond to surfaces across which the transfer of properties by mixing or other processes is minimized. Montgomery (1938) suggested that potential density surfaces were the appropriate choice, since cross-isopycnal motions would then be most strongly opposed by the bouyancy force. Reid and Lynn (1971) showed that isentropic analysis could be extended to the deep ocean by changing the reference pressure used to calculate potential density as the depth of the surface changed. More recently, McDougall (1984,1986,1987) has considered in detail the subtleties of neutral surfaces in the ocean, defined to be the surface for which at every point the normal gradient to the surface is parallel to the bouyancy force. Neutral surfaces and potential density surfaces coincide at the reference pressure. For the models in this paper I have approximated the neutral surfaces bounding each layer by changing the reference pressure as the density surfaces change depth. By never permitting the difference in

pressure between a given surface and the reference pressure to exceed 500 db, the error introduced is much smaller than that due to measurement error. The effect of the layer definitions on the solution will be addressed in more detail in the discussion of the model results.

The "cross-isopycnal flux" term included in equation (1.1) also bears on the discussion of neutral surfaces vs. potential density surfaces. McDougall (1987) has criticized the use of such a term in the inverse models of Wunsch (1984a,b). Part of the confusion lies in the interpretation of ' $w^*$ ' as a vertical or cross-isopycnal velocity. Although  $w^*$  enters the equation as a velocity-like term, it is properly interpreted as representing the net cross-isopycnal transfer due to a variety of unresolved processes. These processes might include vertical advection, turbulent mixing, cabelling, thermobaricity, etc. In the problem considered in Chapter 2, for example, it is argued that the cross-isopycnal flux reflects the transfer between layers due to air-sea interaction at the layer outcrops. By lumping all such processes into one term, we are recognizing the fact that with the available information we cannot resolve the contribution due to the individual processes.

If the system of equations is incompatible with such a simple parameterization, the residuals will tell us that the model is inadequate. Examination of the residuals is indeed an important step in any inverse problem. The equation residuals should appear to be randomly distributed. The presence of non-random structure in the residuals indicates that some important physics has been left out of the model. We will see in the problems considered below that the structure of the residuals can often be interpreted to identify the physical processes not included.

In the ocean circulation studies described in the following chapters the full inverse method machinery is used. In this way we can not only find a velocity field consistent with the imposed constraints, but also show explicitly what parts of the flow we have been able to determine, and how well. We will also take advantage of the flexibility of

the method by incorporating a variety of *a priori* information in the model constraints. Finally, we will see that the inverse method provides a powerful tool with which to test hypotheses of how the ocean behaves, and to examine the sensitivity of the results to particular model assumptions.



## Chapter 2

### South Atlantic Interbasin Exchange

#### 1. Introduction

The South Atlantic is unique in being the only ocean basin extending to high latitudes in which the meridional flux of heat is equatorward, counter to the global requirement that the ocean-atmosphere system carry heat from the equator to the poles (Model, 1950; Jung, 1955; Bryan, 1962; Bennett, 1978; Hastenrath, 1982). This heat transport is primarily the result of an overturning meridional cell in which warm water flows northward in the upper layers of the ocean, is made more dense by cooling and evaporation in the North Atlantic, and returns southward as cold North Atlantic Deep Water (Jung, 1952,1955; Bryan, 1962). The second major source of cold water to the world ocean, Antarctic Bottom Water formed in the Weddell Sea, is also found in the Atlantic. Since the ocean basins are nearly closed to the north, the South Atlantic acts as a conduit through which the dense water masses formed in the Atlantic are introduced to the other oceans, and through which water must return to close the global thermohaline cell. Determining the general circulation of the South Atlantic is therefore an important step toward a better understanding of the thermohaline circulation and, in turn, the role of the ocean in the global climate system.

The meridional circulation in the South Atlantic was first described by Wüst (1935). Using the zonal sections of the *Meteor* expeditions, he identified various property extrema, or "core-layers," which he interpreted as the primary "spreading path" of each water mass away from its source region. The circulation scheme he derived from these observations consisted of a stack of layers moving alternately to the north and south: northward flow of the surface waters and the relatively fresh Antarctic Intermediate Water (AAIW) at mid-depth; southward flow of saline North Atlantic Deep

Table 1.1 *Estimates of meridional heat transport in the South Atlantic ( $10^{15}$  W). Positive flux is equatorward.*

| Latitude | Heat flux |                         |
|----------|-----------|-------------------------|
| 28°S     | .81,.85   | Fu (1981)               |
| 30°S     | .038      | Hsiung (1985)           |
|          | .69       | Hastenrath (1982)       |
|          | 1.15      | Hastenrath (1980)       |
|          | .41       | Bunker (1976)           |
| 32°S     | .66,.88   | Fu (1981)               |
|          | .16,.18   | Bennett (1978)          |
|          | .4        | Bryan (1962)            |
| 40°S     | .088      | Hsiung (1985)           |
|          | .17,.67   | Georgi and Toole (1982) |

Water (NADW) at deeper levels; and a thin layer of cold fresh Antarctic Bottom Water (AABW) at abyssal depths, also moving to the north.

Wüst was apparently aware that such a scheme implied a heat transport of the “wrong” sign, but he evidently found such a result too strong a violation of his intuition to mention in his discussion of the *Meteor* data (letter from Wüst’s research assistant to H. Stommel, 1980). The first study to comment on the anomalous heat transport implied by the oceanographic observations was that of Model (1950) fifteen years later. Since the early work of Model and Jung (1952,1955), several studies, using a variety of methods, have confirmed that the meridional flux of heat in the South Atlantic is equatorward (Bryan, 1962; Hastenrath, 1980,1982; Bryan, 1982; Fu, 1981; Bunker, 1980; Georgi and Toole, 1982; Hsiung, 1985). However, estimates of the magnitude of the heat flux vary over a wide range, as seen in Table 1.1.

Wüst’s picture of the vertical-meridional circulation has survived intact to the present day. However, his core-layer arguments could not determine the strength of the meridional cell, or the formation rates and transports of individual water masses.

Indeed, many of these questions are still unresolved and provide motivation for the present work.

The circulation in the upper layers of the ocean is particularly uncertain. The zonal sections of the *Meteor* and IGY expeditions have been very useful in developing a picture of the meridional circulation in the South Atlantic, but they are of less help in defining the more zonal flows of the wind-forced circulation in the upper waters. Maps of dynamic height constructed from the historical hydrographic data show evidence of an anticyclonic gyre at mid-latitudes, with a Sverdrup interior flow equatorward, closed on the west by the Brazil Current (e.g. Reid, 1981). But the Brazil Current is anomalously weak and shallow compared to other western boundary currents, and appears to return somewhat less than half of the 30 Sv carried by the Sverdrup interior (Evans and Signorini, 1985; Hellerman and Rosenstein, 1984). The remainder of the equatorward flow in the surface and thermocline layers is thought to cross the equator to balance the export of deep water from the North Atlantic resulting in the "inverted estuary" circulation of the Atlantic basin (Stommel, 1957).

The Brazil Current follows the coast of South America to 40°S, where it meets a branch of the ACC flowing to the north, the Falkland/Malvinas Current (Deacon, 1937). At the confluence the two currents leave the coast and turn to the east to form the poleward boundary of the subtropical gyre (Gordon and Greengrove, 1986). The confluence region itself is complex and highly variable, and may play a role in the formation of intermediate water and ventilation of the South Atlantic thermocline (Gordon, 1981).

The eastern boundary current of the South Atlantic, the Benguela Current, may also play a significant role in the meridional flux of heat. This current is somewhat mysterious, and is difficult to define: while it often appears as a series of meanders and eddies, with no identifiable current core, other investigators have inferred northward transports along the African coast of 16-39 Sv (Wooster and Reid, 1963; Fu, 1981). The

path taken by drifters released off southern Africa also suggests a continuous northward flow parallel to the bottom contours reaching as far as 25°S before leaving the coast and heading to the northwest through a gap in the Walvis Ridge (Harris and Shannon, 1979). Associated with the current is a zone of extensive upwelling extending from the Agulhas Bank to 18°S (Shannon, 1985).

In addition, the eastern basin of the South Atlantic is influenced by the Agulhas Current, the western boundary current of the South Indian Ocean. The Agulhas Current is the most energetic feature in the southern hemisphere, with maximum surface currents of  $>1 \text{ m s}^{-1}$  and a volume transport of up to 130 Sv (Jacobs and Georgi, 1977). The Agulhas Current flows poleward along the east coast of southern Africa until the continent ends at 35°S; here the current abruptly turns back on itself - "retroreflects" - and flows eastward into the Indian Ocean (Bang, 1970). The flow appears to reach to at least 4000 m depth, based on water-mass properties (Jacobs and Georgi, 1977). The relatively warm Indian Ocean water carried poleward by the current experiences an annual heat loss greater than  $150 \text{ W m}^{-2}$  in the retroreflection region (Bunker, 1980).

At intermediate depths in the Atlantic a striking low salinity tongue extends from the Polar Front at 55°S as far north as 15°N, identifying the spreading path of the AAIW (Wüst, 1935). The volume transport and details of the flow path taken by the AAIW in the South Atlantic, however, are not well known. From the property distributions, it appears that the circulation at intermediate depths is influenced both by the western-intensified thermohaline circulation and the anticyclonic wind-driven gyre in the upper layers. Wüst (1935), for example, inferred from the distributions of oxygen and salinity that the flow of AAIW was concentrated along the coast of South America. Other authors (Martineau, 1953; Reid, 1965; and Buscaglia, 1971), however, have concluded that the AAIW moves north along the coast only as far as the Brazil/Malvinas confluence at 40°S, there turning to the east and following the path of the anticyclonic gyre into the South Atlantic. More recently, Evans and

Signorini (1985) have made direct current measurements along the western boundary using the PEGASUS velocity profiler and found northward flow of AAIW along the South American coast at 23°S.

Below the intermediate water lies a thick saline layer of deep water formed in the North Atlantic. The NADW includes water types formed at several sites in the North Atlantic: a dense component (Lower NADW) formed in the Norwegian/Greenland Sea, a fresher and less dense contribution from the Labrador Sea (Middle NADW), and a salinity maximum layer produced by the Mediterranean Sea outflow (Upper NADW) (Wüst, 1935). In each case the dense water is produced by deep convection driven by a strong loss of buoyancy at the sea surface. Once formed, the NADW flows away from the source regions along the western boundary of both the North and South Atlantic basins. The presence of such a deep western boundary current in the Atlantic and other oceans has been taken as evidence supporting the schematic model of the deep circulation introduced by Stommel and Arons (1960).

The deep water formed in the northern North Atlantic is thought to be the primary source of deep water to the world ocean (Warren, 1981). The formation rates, however, are not well known. The convection appears to occur sporadically in time and space and is difficult to observe. The transport of this water mass as it flows away from the source region in the western boundary current, which depends both on the rate at which water upwells in the interior and on the rate of production, is also not very well known. Estimates of the southward transport of NADW in the South Atlantic vary by a factor of 3 (9-26 Sv) (Wright, 1970; Wüst, 1935): with few direct velocity measurements available with which to reference geostrophic calculations, the results are necessarily sensitive to each investigator's choice of reference level.

The second major water mass by which the deep waters of the ocean are renewed is the Antarctic Bottom Water (AABW). The flow of AABW away from its source region in the Antarctic is marked by a tongue of cold, fresh and silica-rich water along the

western boundary of the South Atlantic. There is evidence that dense water is formed at many locations around Antarctica, but the primary source of AABW is thought to be the Weddell Sea (Warren, 1981). However, the details and rates of the production of this water mass are also not well known, and estimates of the volumes involved vary wildly.

Most estimates have been based on a meridional-vertical circulation scheme first presented by Sverdrup (1933) (Fig. 1.1). In this scheme Circumpolar Deep Water (CDW) flows poleward and upward, reaches the sea surface south of the Polar Front and is modified by interaction with the atmosphere, and returns to the north as AAIW and AABW. Gordon and co-workers (Gordon, 1971,1975; Gordon and Taylor, 1975) have used box models based on this circulation to estimate the production of AABW. These models set the strength of the meridional cell by assuming a value for the upwelling rate of CDW or the net air-sea heat flux south of the Polar Front. Since these quantities are poorly known, it is difficult to know how much confidence to have in the resulting transport estimates. In fact, the large formation rates of AABW predicted by the box models (30-40 Sv) are in stark contrast to those suggested by the dynamical models of bottom water formation of Gill (1973), Killworth (1977) and Carmack and Foster (1975).

The transport of AABW into the Atlantic along the western boundary seems to be somewhat better known. Hogg *et al.*(1982) took advantage of the fact that the deep northward flow was forced to pass through the narrow Vema Channel at 30°S. Dynamic computations and direct measurements both suggested that about 4 Sv of AABW left the Argentine Basin to the north. Wright (1969), using a reference level chosen to correspond to a kink in the  $\Theta$ -S curve at 2.0°C, found slightly higher values (5-6 Sv).

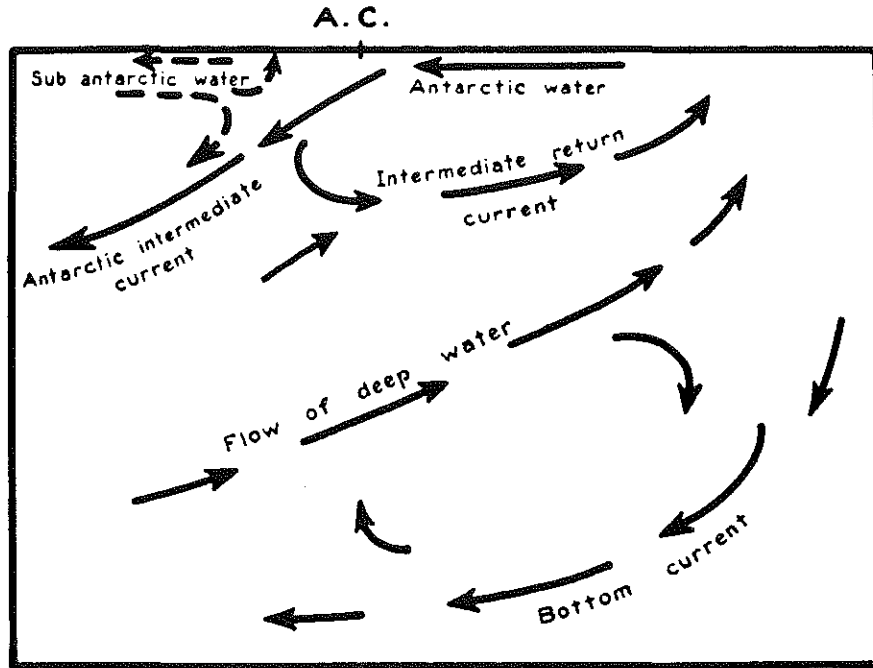


Fig. 23. Schematic representation of the north-south circulations within the Antarctic circumpolar current.

Fig. 1.1 Circulation in the meridional-vertical plane in the Southern Ocean, from Sverdrup (1933). North is on the left.

The discussion above suggests that our present picture of the general circulation of the South Atlantic is incomplete. A basic sketch of the flow patterns can be synthesized from earlier studies based on the dynamic method and the observed property distributions, but determining the formation rates and transports of the major water masses has been more difficult. Estimates of volume transports in the literature generally vary over a wide range, depending on each investigator's choice of reference level, or on values assumed for poorly known quantities such as the net air-sea heat flux. A major goal of this part of the thesis is to determine the transports of the major water masses and boundary currents in the South Atlantic.

A related goal of this work is to quantify the extent to which mass and heat are exchanged between the South Atlantic and the neighboring ocean basins, in order to gain some insight into how the deep water formation processes occurring within the Atlantic are linked to the global thermohaline circulation. The distribution of properties in the deep ocean clearly shows that some exchange takes place. Reid and Lynn (1971), for example, were able to trace the salinity maximum of the NADW into low latitudes of the South Pacific. Since the ocean basins are nearly closed to the north, the strong eastward flow in the Antarctic Circumpolar Current (ACC) is the primary means by which such exchange is achieved.

The ACC is now thought to consist of several narrow jets associated with deep-reaching fronts which separate relatively quiescent regions of distinct water mass characteristics (Nowlin, 1981). The wide range of transport estimates made in Drake Passage using direct current measurements (-15 Sv (Foster, 1972) to 237 Sv (Reid and Nowlin, 1971)) is in part due to this banded structure: short duration, widely-spaced current meters gave wildly different estimates of absolute flow, depending on how often a front meandered across the mooring. The most recent estimate of the mean transport through Drake Passage is  $134 \pm 13$  Sv, based on geostrophic calculations referenced to an array of current meter observations across the Passage (Nowlin and Klinck, 1986).



Some of the variability is due to inadequate sampling but a large part is apparently due to real fluctuations in transport. Whitworth (1980) suggests that there is a seasonal variability, with winter transports  $\approx 20$  Sv greater than summer, but mentions that intraseasonal variation may dominate the signal: week long averages of six current meters across Drake Passage showed a range in transport estimates of over 200 Sv due to the passage of energetic features through the array (Bryden and Pillsbury, 1977). Wearn and Baker (1980) and Whitworth (1983) find a variation of  $\pm 40$  Sv on time scales of days to weeks that appears to be correlated with the zonal wind, although Chelton (1982) pointed out that the apparent coherence in the former case may have resulted from the strong seasonal signals present in both records. Fu and Chelton (1984), using SEASAT altimeter data, observed a zonally coherent increase of 10-30 cm in the cross-stream sea level difference over the three month duration of the experiment.

Although the ACC is easily the dominant means of interbasin exchange in terms of volume transport, it may not be the only important mechanism. The magnitude of the transfer between the Indian and Atlantic Oceans in the Agulhas Retroflexion region is uncertain and a topic of active debate, as discussed in detail in Section 4. The flow in this region varies on a range of temporal and spatial scales: the retroflexion occurs in one of two modes, one at  $13^{\circ}\text{E}$ , or more commonly at  $19^{\circ}\text{E}$  (Harris *et al.*, 1978); the retroflexion itself often pinches off to form large eddies, which may drift to the northwest and enter the South Atlantic (Lutjeharms, 1981); and cyclonic eddies are occasionally formed inshore of the current core (Lutjeharms and Baker, 1980). Recently Gordon (1985) has presented evidence of 13.5 Sv of Indian Ocean water entering the Atlantic southwest of Cape Town; depending on the path of the return flow, this could result in a large flux of heat and other properties between the oceans. Piola and Georgi (1981), on the other hand, see a sharp shift in water mass characteristics south of Africa, suggesting that at least at the depth of the AAIW the exchange is minimal.

The exchange of mass and heat between the Southern Ocean and the rest of the Atlantic north of 32°S was considered by Fu (1981), in his study of the subtropical South Atlantic circulation using inverse methods. His results were for the most part consistent with the general pattern described earlier: a meridional cell carrying 20 Sv of NADW poleward across 32°S balanced by an equatorward flow of equal magnitude in the upper layers, resulting in an equatorward heat flux of .66–.88 PW ('PW' =  $10^{15}$  W); and a horizontal circulation consisting of zonal flow in the interior and strong boundary currents in the east and west. He also demonstrated that forcing a poleward heat transport across 32°S resulted in an unreasonable circulation. One purpose of this work is to test whether imposing constraints on the flow poleward of 32°S alters any of these conclusions.

In another study of interbasin exchange, Georgi and Toole (1982) considered the Southern Ocean as a whole and asked whether the ACC gained or lost heat and freshwater as it traversed each of the ocean basins. They assumed zero velocity at the bottom to reference their geostrophic calculations. In the Atlantic the ACC was found to lose heat and gain freshwater, but the uncertainties were large and neither estimate could be distinguished from zero. Georgi and Toole inferred from their estimate of the heat divergence and estimates of the air-sea heat exchange in the Southern Ocean that the meridional heat flux across 40°S was  $17.5 \times 10^{13}$  W equatorward. They noted, however, that their estimates were possibly sensitive to horizontal variations in the unknown barotropic velocity field. Another motivation for this work was the hope that by using additional conservation statements we could determine the reference level contribution to the absolute velocity adequately to narrow the range of uncertainty in estimates of the net interocean exchange of heat and freshwater.

The most recent discussion of the problem of interbasin exchange and its relation to the global thermohaline circulation is Gordon's (1986) study of the fate of NADW exported from the North Atlantic. He suggested that the global thermohaline cell

associated with NADW formation is closed primarily by a "warm water path:" NADW leaving the Atlantic upwells uniformly into the thermocline of the Pacific and Indian Oceans, flows westward through the Indonesian Passages and across the tropical Indian Ocean, and ultimately reenters the Atlantic via a branch of the Agulhas Current that does not complete the retroflection. Gordon concluded that the "cold water path," in which water leaving the Atlantic returns through Drake Passage in the ACC, could account for no more than 25% of the return flow.

This idea is considered in detail in Section 4. It will be seen that the argument used to demonstrate the dominance of the warm water path is not conclusive, and that the inverse models suggest that a significant fraction of the return flow does reenter the Atlantic through Drake Passage.

The goal of this part of the thesis, then, is to use the inverse method described in Chapter 1 to determine the transports and pattern of the circulation in the South Atlantic, and to quantify the exchange of mass and heat between the South Atlantic and the neighboring ocean basins. In Section 2 the set up of the inverse model is described. Section 3 presents the results of a standard model, which represents my optimal choice of weighting and constraints. These results are compared to other studies in Section 4, and several additional experiments designed to test the compatibility of the data with the heat or mass transport estimates of other investigators are described. The main conclusions are summarized in Section 5.

## 2. The model

The set up of the inverse model is discussed in this section. The location and major hydrographic features of the sections used are described first, followed by a discussion of the specific constraints and weighting applied in the model.

### 2.1 The data

Five hydrographic sections are used to divide the area of the South Atlantic poleward of 32°S into three closed regions, as shown in Fig. 2.1. The potential temperature, salinity and potential density distributions at most of these sections have been discussed previously. The major features revealed in the vertical sections are briefly reviewed here to orient the reader and to define terminology used later in the paper. Readers interested in a more thorough discussion of the details of the property fields are referred to the original papers cited below.

The three meridional sections cross the ACC. The first of these, in Drake Passage, was occupied in February-March, 1975 by the R/V *Melville* as part of the FDRAKE 75 experiment. The hydrographic sections and current meter results from that experiment have been described by Nowlin *et al.* (1977). Temperature, salinity and density along this line are shown in Fig. 2.2. The isopleths slope upward to the south, reflecting the strong eastward shear (relative to a deep level) of the ACC. The slope of the isopleths, however, is not smooth but occurs in a series of vertically-coherent steps or fronts. From north to south these fronts are referred to as the Subantarctic Front (SAF), the Polar Front (PF) and the Continental Water Boundary (Nowlin and Klinck, 1986). Several distinct water masses are indicated by extrema in the property fields. Following Gordon's (1967) terminology, the deep salinity maximum shoaling toward Antarctica indicates the core of the Lower Circumpolar Deep Water (LCDW). At shallower depths a weak temperature maximum south of the Polar Front is defined to be the Upper CDW. In addition to its higher temperature, the UCDW is distinguished from the LCDW by

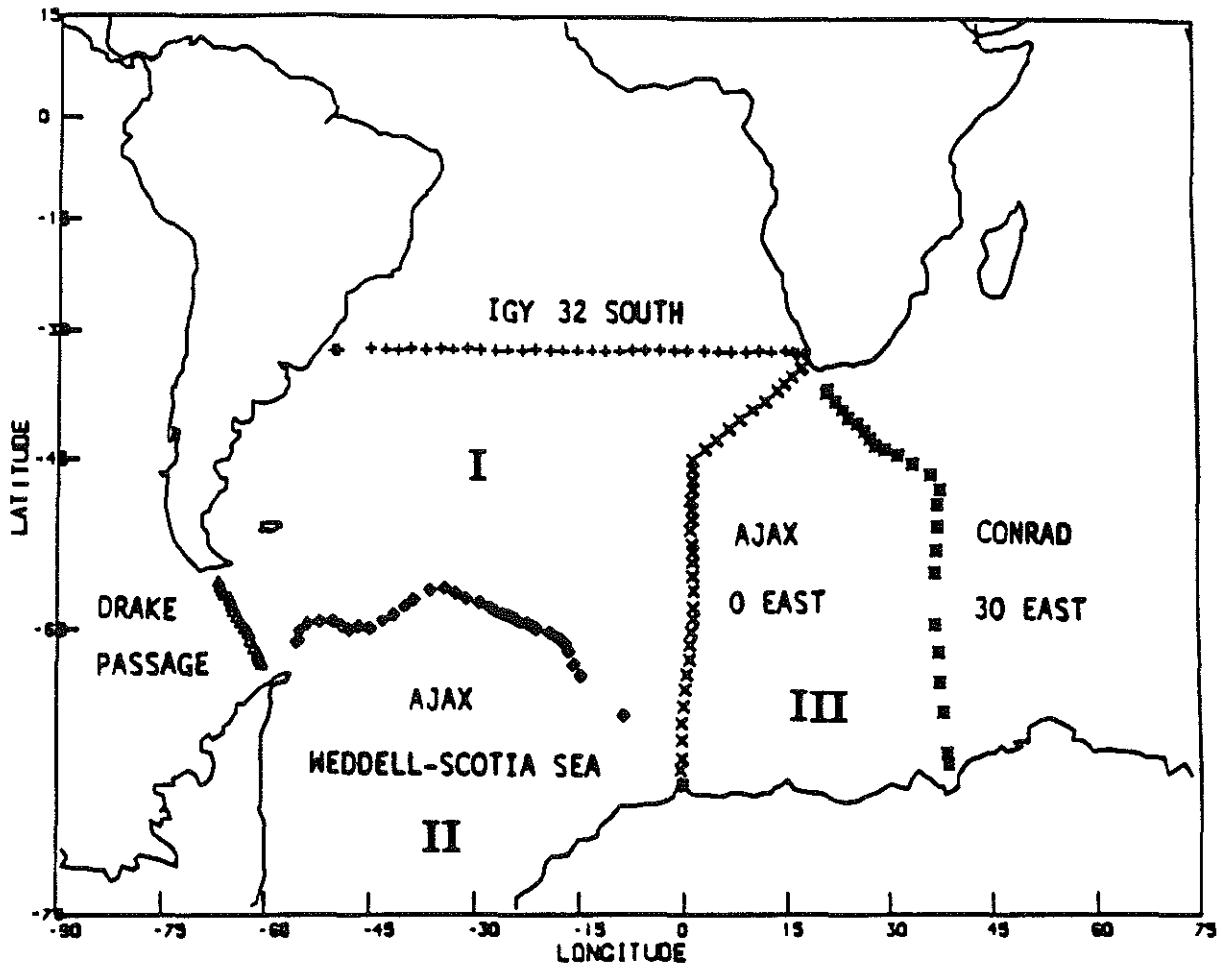


Fig. 2.1 Station locations for the five hydrographic sections used to define three closed volumes in the inverse model.

lower oxygen and higher nutrient concentrations (Sievers and Nowlin, 1984). North of the SAF a low salinity thermostad is found above 1000 m; this is Subantarctic Mode Water formed in the Pacific, one of the complex of water masses which together make up the AAIW (McCartney, 1977).

The second section crossing the ACC is the AJAX line along the Greenwich Meridian taken in January-February, 1984 from the R/V *Knorr*. Whitworth and Nowlin (1987) have recently described the water masses and currents along this section. (The section used here is not identical to that discussed by Whitworth and Nowlin: seven stations from Leg I of the AJAX expedition have been used to fill in gaps between the African coast and the beginning of Leg II at 50°S, 1°E. There is a two month gap between Legs I and II.)

In the vertical sections shown in Figure 2.3 the ACC again appears as several narrow fronts embedded in a general shoaling of the isopleths toward Antarctica. The core of the AAIW is marked by a salinity minimum which descends from the sea surface between the Subantarctic and Polar Fronts to 800 m at 40°S. At deeper levels there is a broad salinity maximum corresponding to the LCDW, as seen in Drake Passage. However, the salinity maximum water is warmer and saltier at this latitude, particularly to the north, the result of "new" NADW being incorporated into the ACC during its passage through the Atlantic (Georgi, 1981). The ACC is mostly confined to the north of the Mid-Ocean Ridge. Further south there is a doming of the isopleths at all depths, corresponding to the cyclonic Weddell Sea gyre. The deep water in the Weddell gyre is relatively isohaline and cold ( $\theta < 0^\circ$  C below 1000 m) and is easily the densest water on the section. At mid-depths there is a temperature and salinity maximum layer due to CDW being carried into the Weddell Sea from the east in the southern limb of the Weddell gyre (Deacon, 1979). Above the CDW layer is a temperature minimum layer which is a remnant of the very cold winter mixed layer.

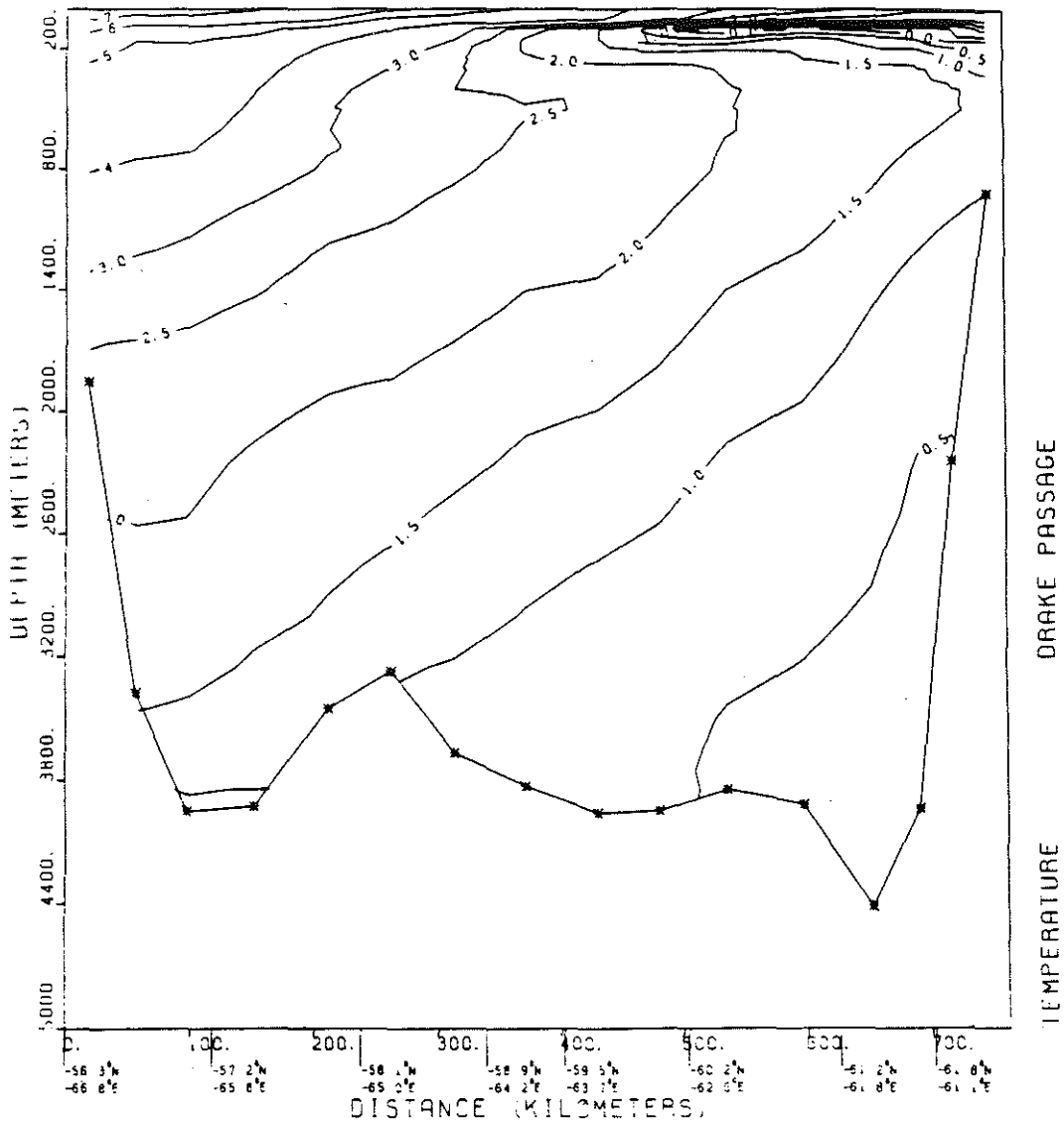


Fig. 2.2a Potential temperature ( $^{\circ}\text{C}$ ) at the Drake Passage section. North is to the left.

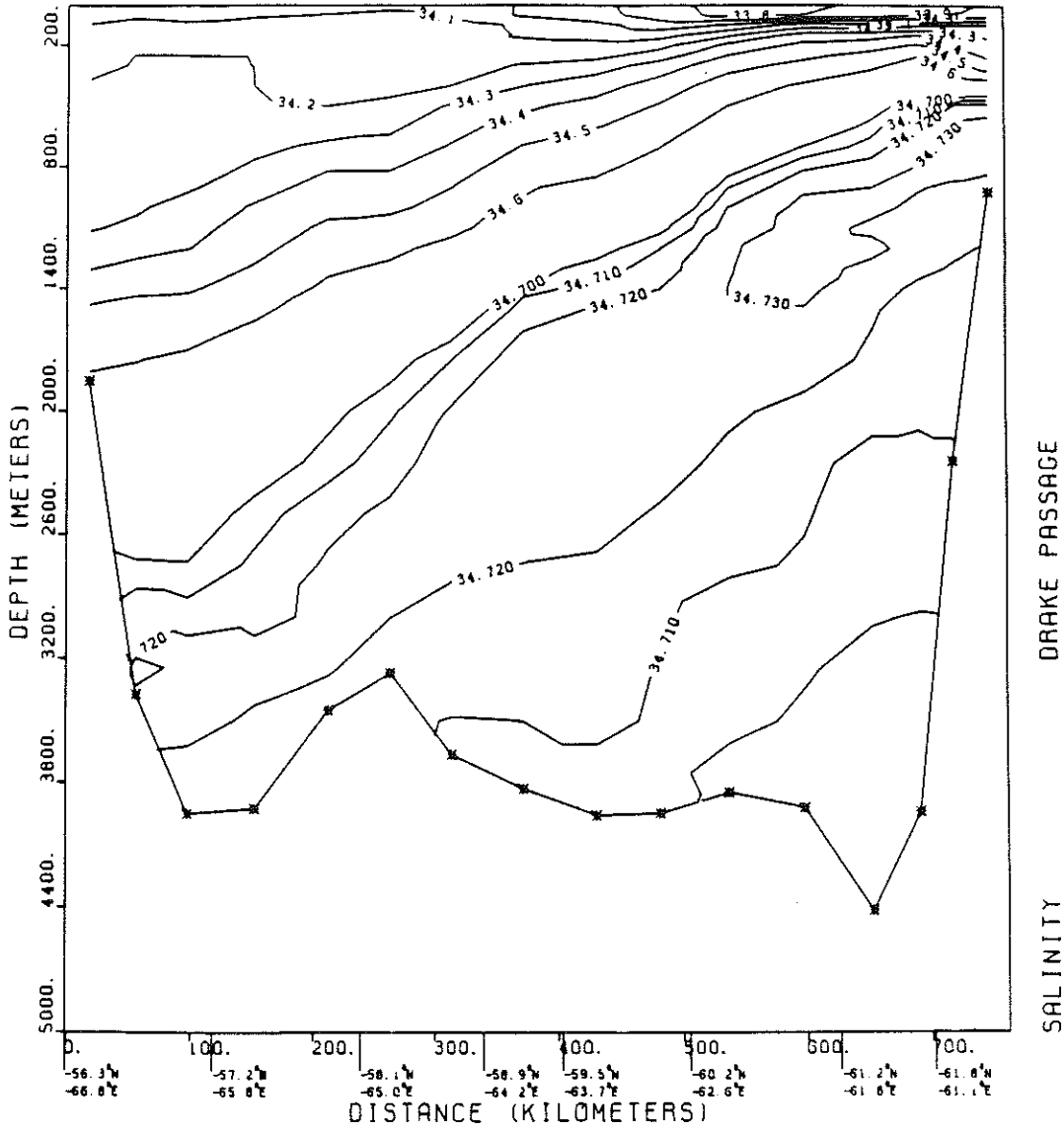


Fig. 2.2b Salinity (psu) at Drake Passage.



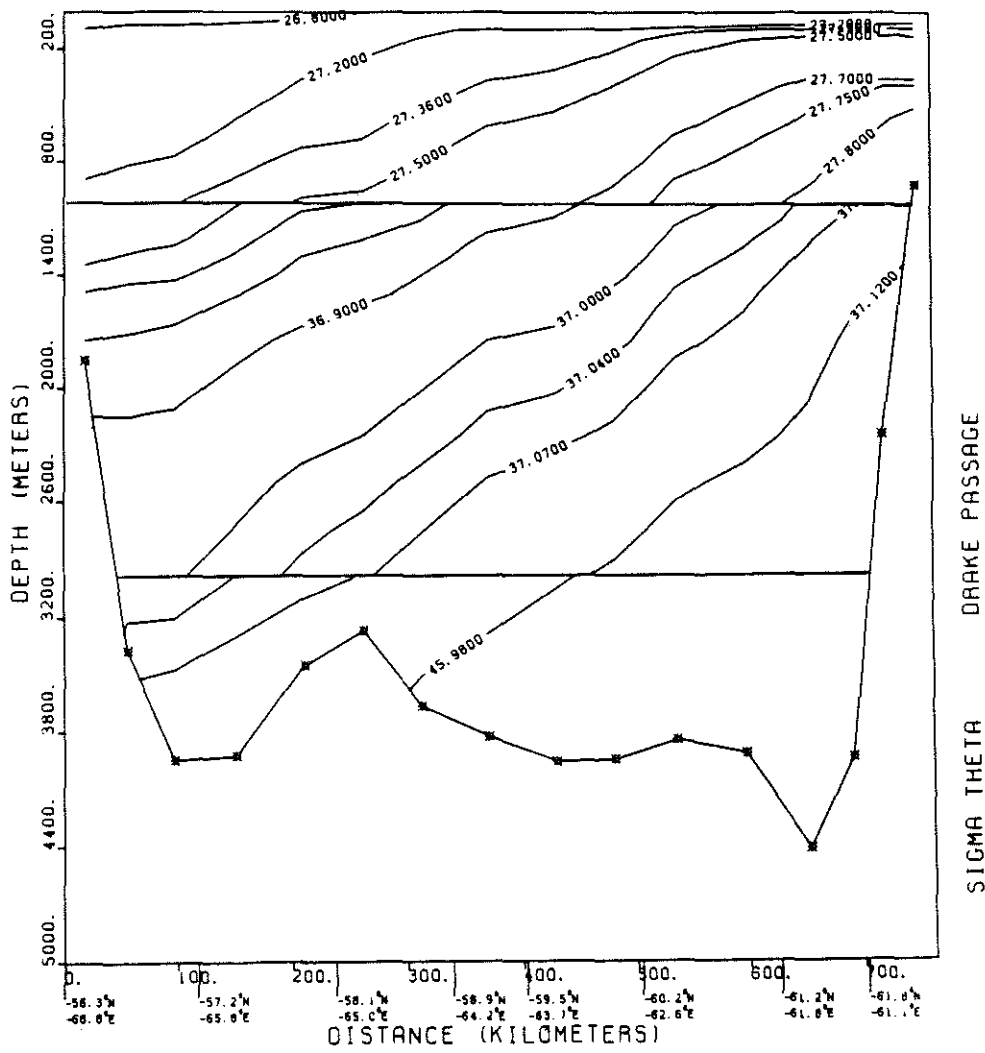


Fig. 2.2c Potential density anomaly at Drake Passage. Values plotted are  $\sigma_0$  between 0 and 1000 db;  $\sigma_2$  between 1000 and 3000 db;  $\sigma_4$  between 3000 db and the bottom.

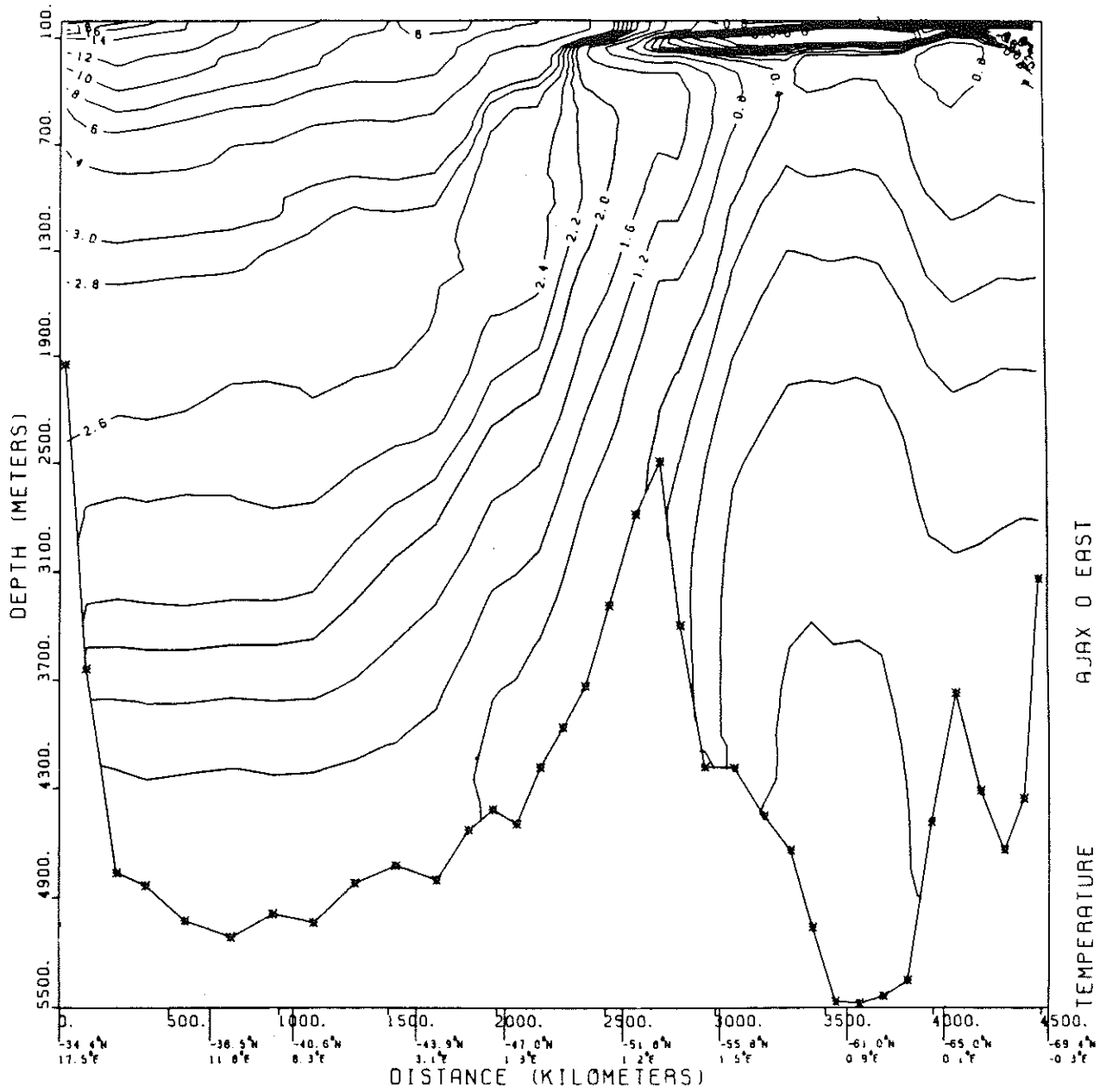


Fig. 2.3a Potential temperature at the AJAX section at 0°E .

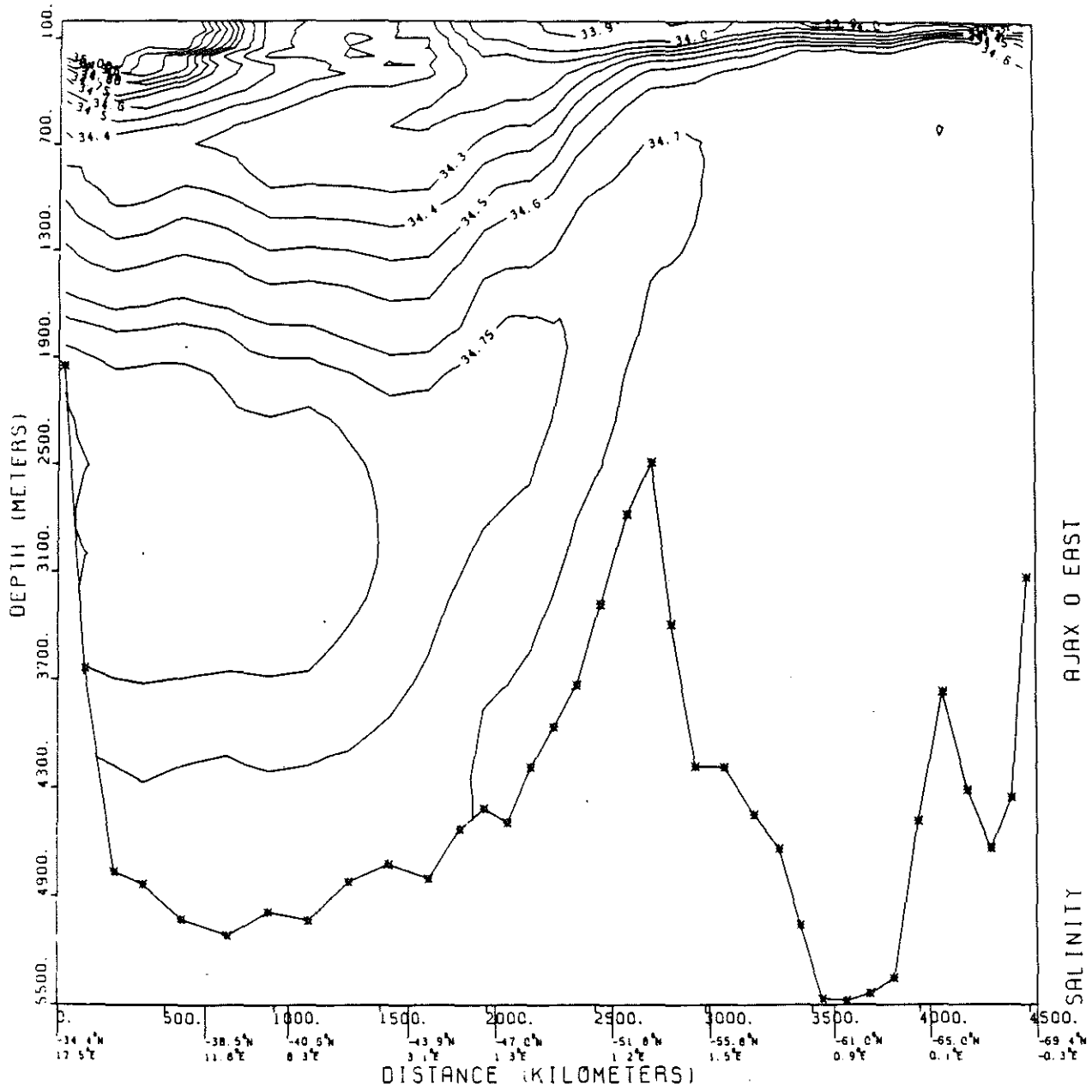


Fig. 2.3b Salinity at 0°E.



The second half of Leg II of the AJAX expedition recrossed the Weddell gyre from 0°E to the South Sandwich Trench near 28°W, and then followed the Weddell-Scotia Confluence (Gordon, 1967) through the Scotia Sea to the southern end of Drake Passage (Fig. 2.4). The Weddell gyre appears to be asymmetrical at this section, with the isopleths gradually shoaling to the north in the interior before returning steeply to greater depths near the northern boundary of the basin at the America-Antarctica Ridge. The temperature and salinity maximum water in the southern limb of the gyre is the signal of CDW entering the Weddell Sea from the east. North and west of the America-Antarctica Ridge the bottom topography plunges abruptly at the South Sandwich Trench. The isopleths slope steeply over this feature, suggesting that there is a narrow recirculating gyre, or jets of opposing flow, associated with the topography. Within the Scotia Sea there is a great deal of structure in each of the fields, due in part to the more complicated ship track. The relatively cold, fresh Weddell Sea waters are separated from the warmer and saltier water of the central Scotia Sea by a frontal system called the Weddell-Scotia Confluence (Gordon *et al.*, 1977). This section crosses the Confluence several times as the cruise track runs from the South Scotia Ridge into the interior of the Scotia Sea and returns.

A third crossing of the ACC is provided by the R/V *Conrad* section at 30°-40°E (Fig. 2.5). This section was occupied in January-February, 1974 and has been discussed by Jacobs and Georgi (1977). The ACC at this section appears much broader than to the west, but the station spacing is wider on this section and sharper features may not be resolved. The most steeply-sloping isopleths are found to the north, where the section crosses the retroflexion loop of the Agulhas Current. Jacobs and Georgi concluded on the basis of salinity, oxygen and nutrient observations that the southwestward flow of the Agulhas Current extended to 4000 m. The salinity section again shows the deep maximum marking the core of the NADW and CDW, with the most extreme values near the northern end of the section where the NADW signal is strongest. The AAIW

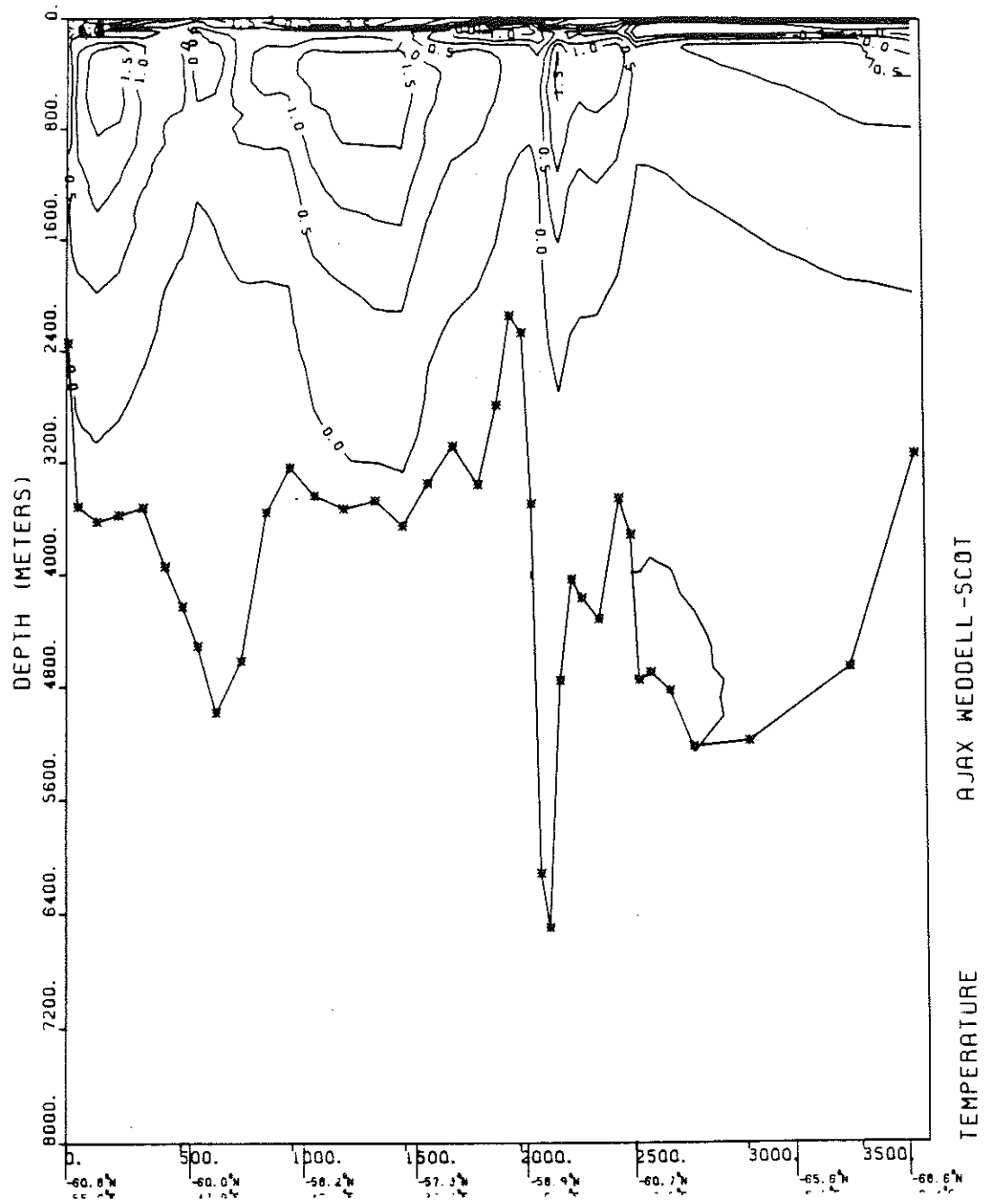


Fig. 2.4a Potential temperature at the AJAX Weddell-Scotia section.

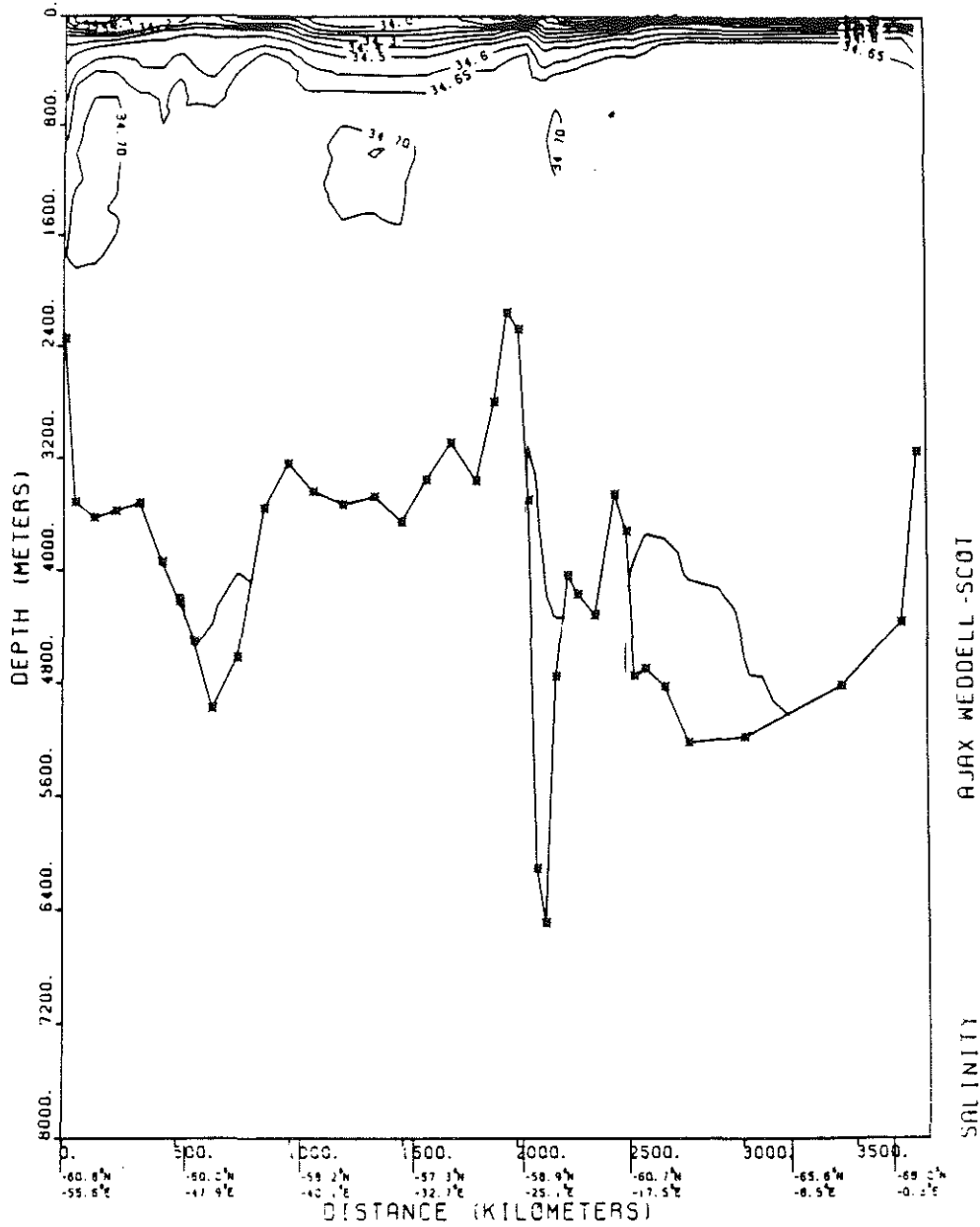


Fig. 2.4b Salinity at the Weddell-Scotia section.

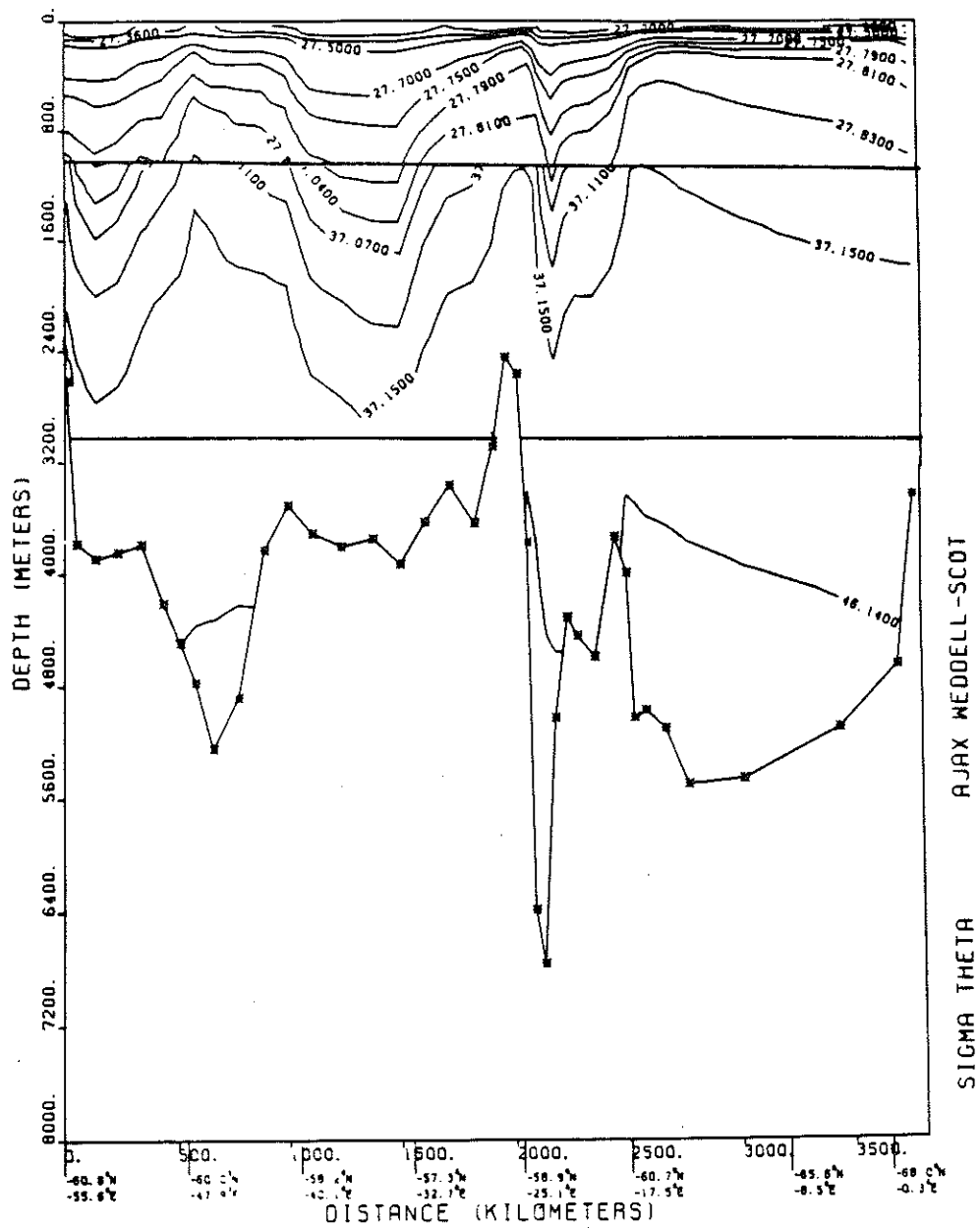


Fig. 2.4c Potential density anomaly at the Weddell-Scotia section, as in Fig. 2.2c.



appears as a salinity minimum between the Subtropical Convergence and the Agulhas Current at 600-1000 m. In contrast to the AJAX section at 0°E, there is little hint of the cyclonic Weddell gyre in the southern part of this section. Closer to Antarctica, the Antarctic Coastal Current (Gill, 1973) appears as a region of steeply plunging isopleths above 1000 m near the coast.

The final section used in this study is a zonal line from the IGY crossing the Atlantic at 32°S. Color plates of temperature and salinity along this section appeared in the IGY atlas (Fuglister, 1960). Fu (1981) used this section and the other IGY lines in the South Atlantic in an inverse model of the circulation between 32° and 8°S. The salinity values used here have been edited slightly from the values listed in the IGY atlas. In the deep water of the eastern basin several very high salinity values ( $>.15\text{‰}$  higher than any other deep water in the basin) were retained but flagged with a small question mark in the atlas. The anomalous values are thought to be due to a leaky replacement bottle used after the deep cast of bottles and thermometers were lost (Fuglister, 1960). I chose to replace the questionable salinities by constructing a  $\Theta$ -S curve for all other deep observations in the Cape Basin and reading off the salinity values corresponding to the observed temperatures.

Several features stand out in the temperature and salinity sections shown in Fig. 2.6. The Brazil Current appears as a narrow region of isopleths sloping downward offshore from the coast of South America, consistent with flow to the south relative to a deeper level. Further offshore, the slope of the isopleths reverses above 2000 m. In the deep water there is a temperature and salinity maximum which is strongest in the west but extends across a large fraction of the western basin. These extrema mark the core of the NADW. Below the NADW layer the cold fresh signal of the AABW is also strongest in the west. The salinity minimum layer associated with the AAIW stretches across the basin between 600 and 1200 m, with the lowest salinity values again found in the west, in the recirculation offshore of the Brazil Current. In the eastern basin

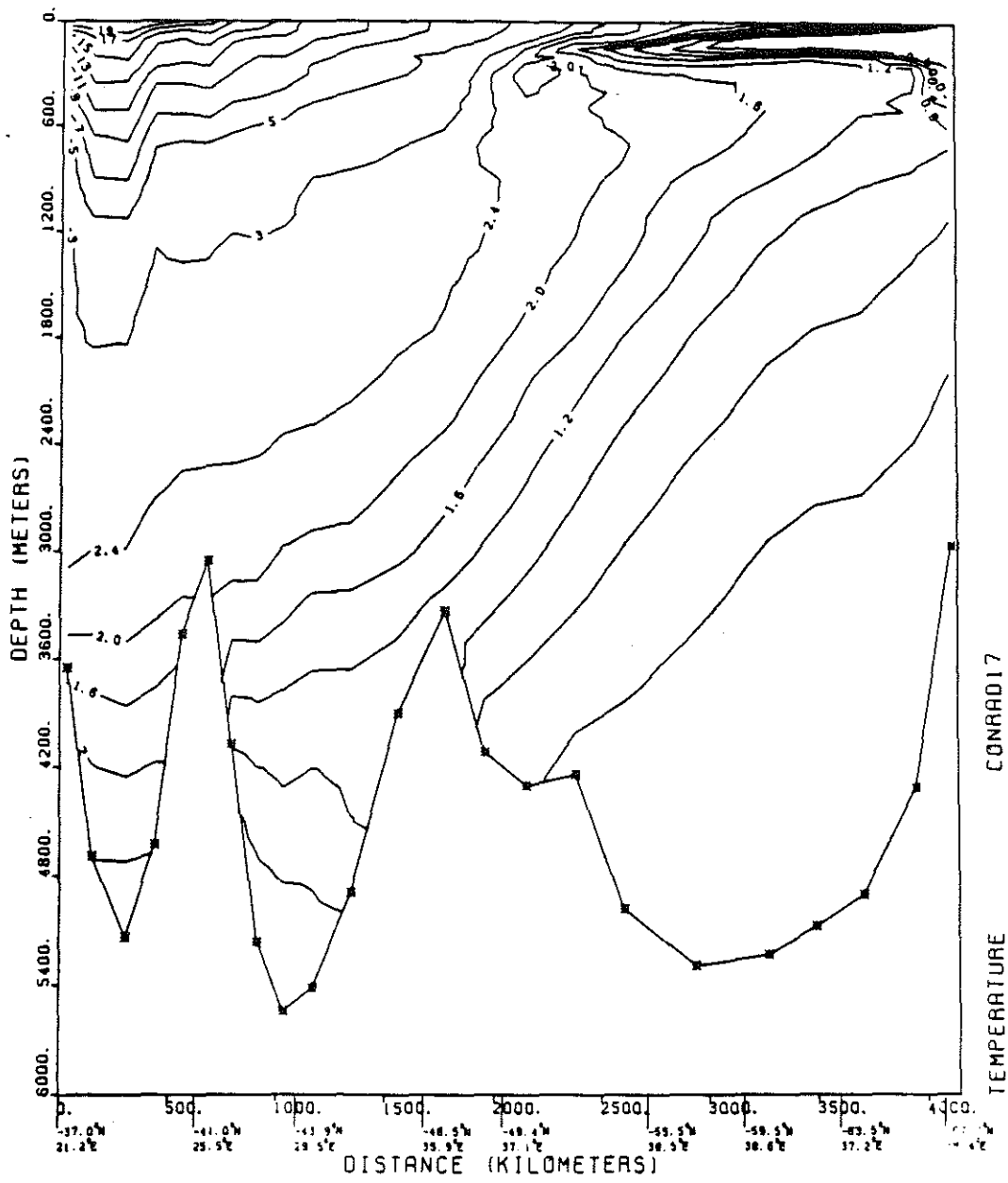


Fig. 2.5a Potential temperature at the Conrad section at 30°E.

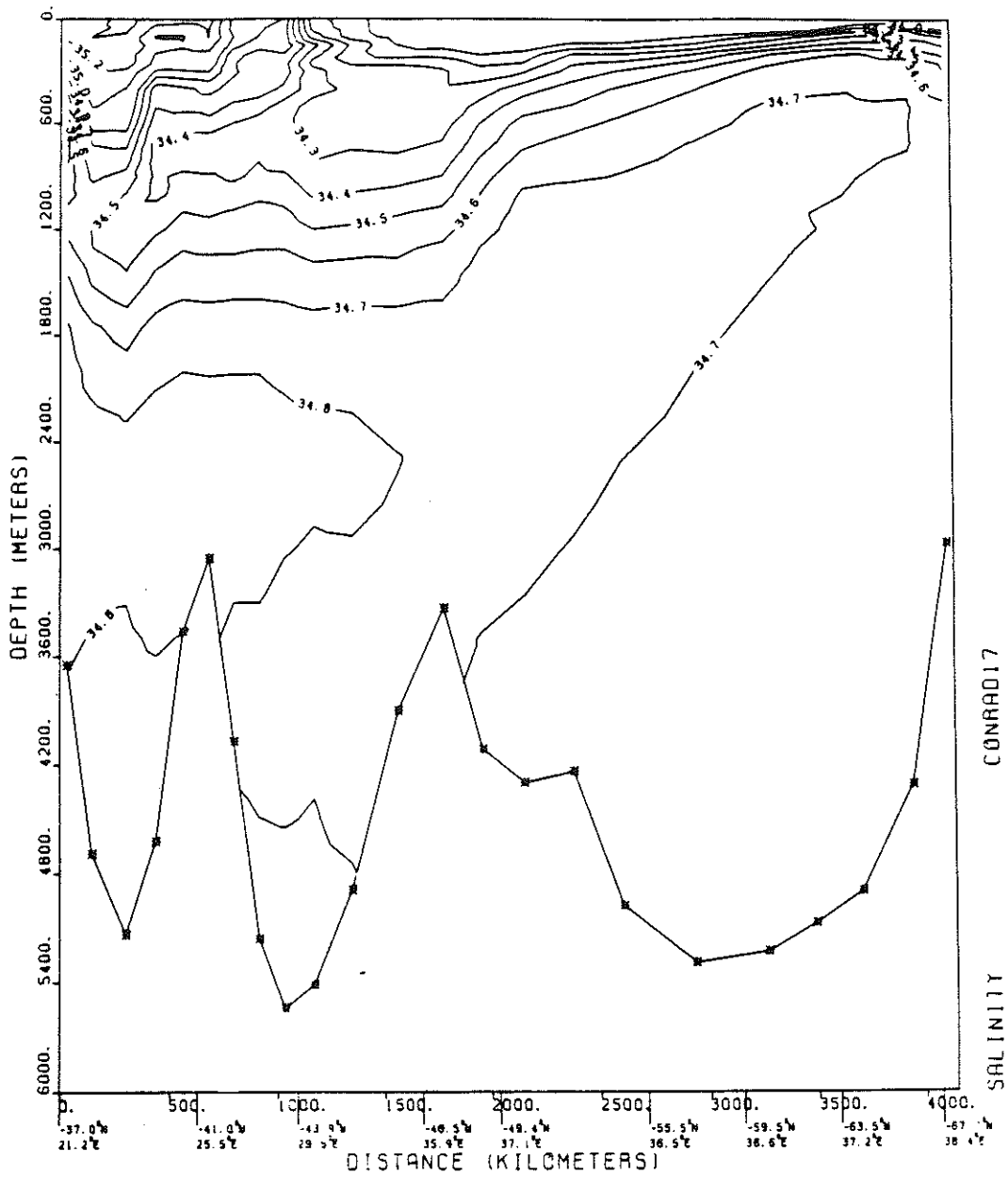


Fig. 2.5b Salinity at 30°E.

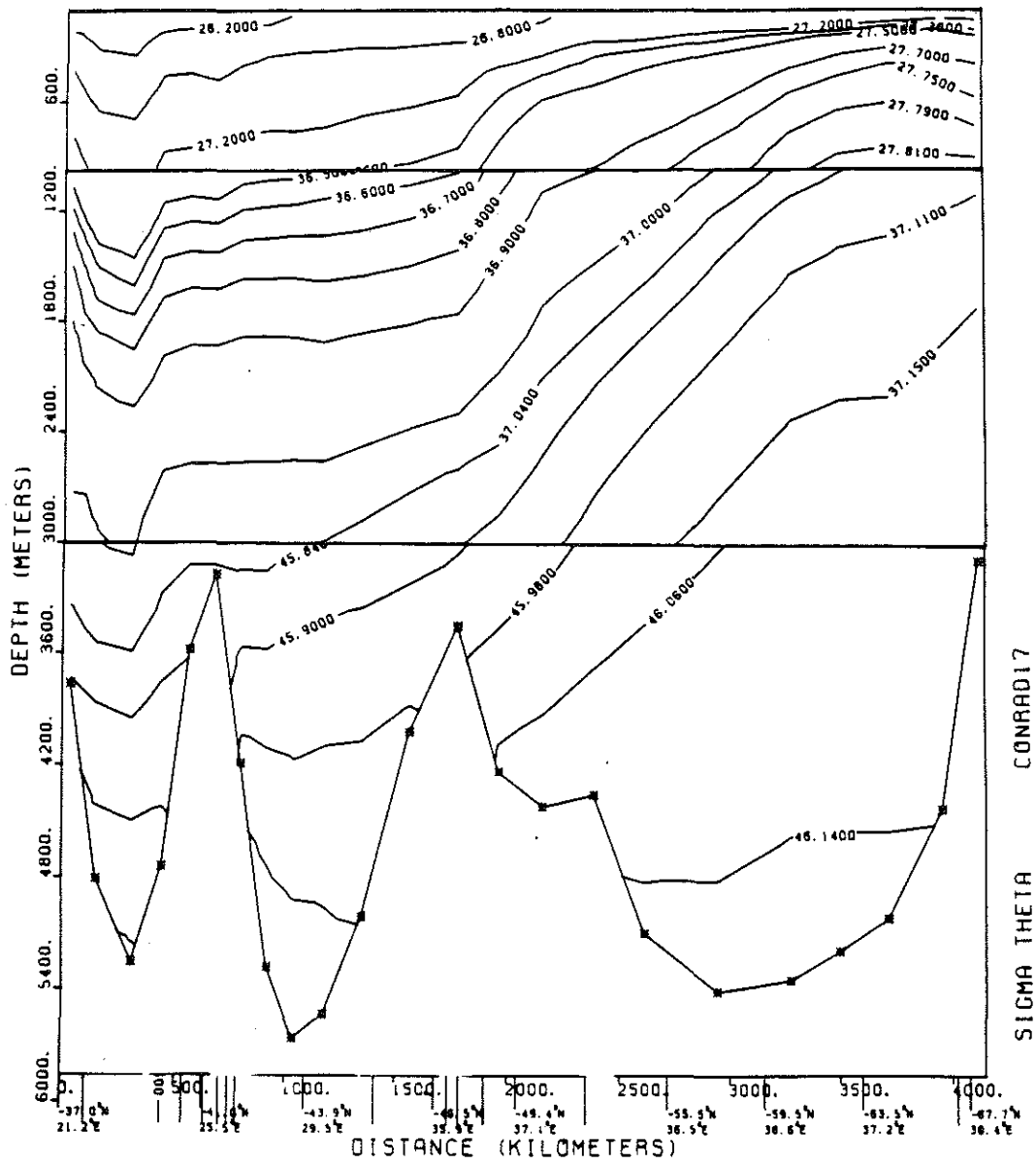


Fig. 2.5c Potential density anomaly at 30°E, as in Fig. 2.2c.

there are several strong eddies, some of which reach to significant depths. Along the eastern boundary, the northward-flowing Benguela Current is indicated by a shoaling of the isopleths toward the coast.

## 2.2 Design of a Standard Model

Within each region defined by these sections the water column was divided into 13 layers defined by density surfaces. The isopycnals plotted in Fig.'s 2.2c-2.6c correspond to the nominal layer boundaries, which are also listed in Table 2.1 along with the layer average temperature and salinity at each section. These layers were chosen to resolve the major water masses and for the most part correspond to the definitions of Reid *et al.*(1977). Experiments run with more than 13 layers gave similar results. The layer boundaries in Table 2.1 are "nominal" in that the reference pressure used to calculate the potential density is allowed to vary as the surface undergoes large vertical excursions, so that the "isopycnal" surface approximates a true neutral surface, as discussed in Chapter 1. Accounting for compressibility effects is particularly important in this problem, where the depth of the density surfaces may change by  $>2000$  m across the ACC.

As described in Chapter 1, we assume the flow is in thermal wind balance, that the sections are representative of the mean state of the ocean, and that mass is conserved in each layer in each region. The conservation statements form a set of linear equations to be solved for the reference level velocity at each station pair and the "cross-isopycnal transfer" across each interface.

The system of equations is solved using the singular value decomposition (SVD). Before doing the SVD, the rows and columns of the coefficient matrix are weighted. The columns are divided by their length to remove the bias introduced by variable station spacing and water depth. The rows are weighted by the expected error in each equation so that each equation has unit variance. The uncertainty in each conservation equation due to measurement and interpolation errors and errors introduced in extrapolating

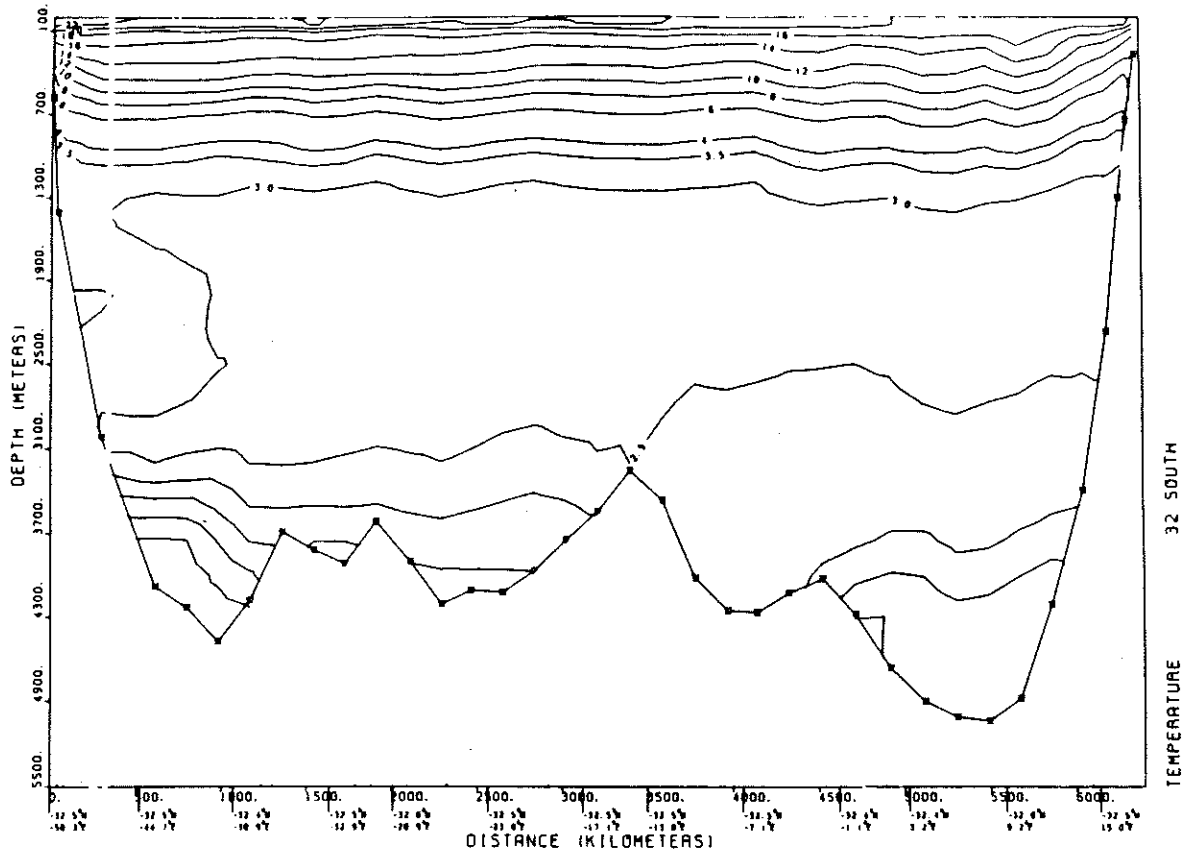


Fig. 2.6a Potential temperature at 32°S.

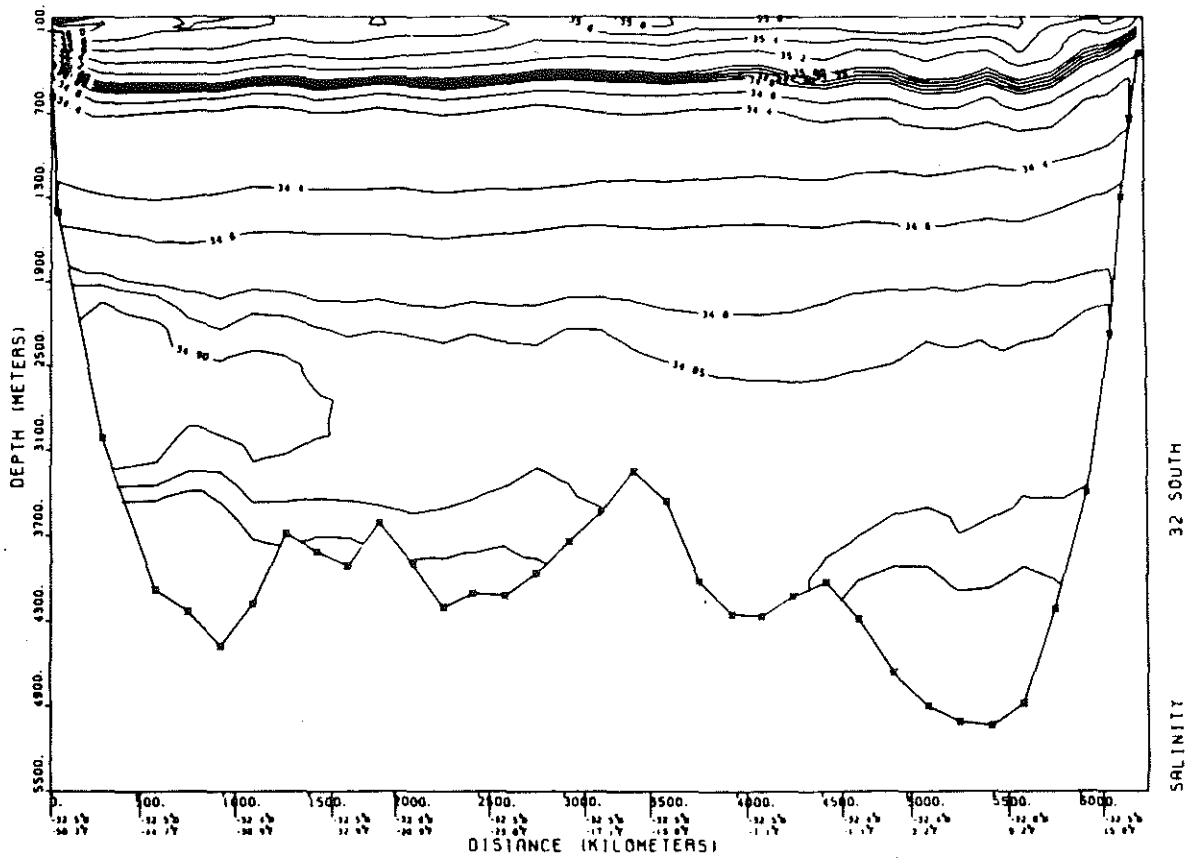


Fig. 2.6b Salinity at 32°S.

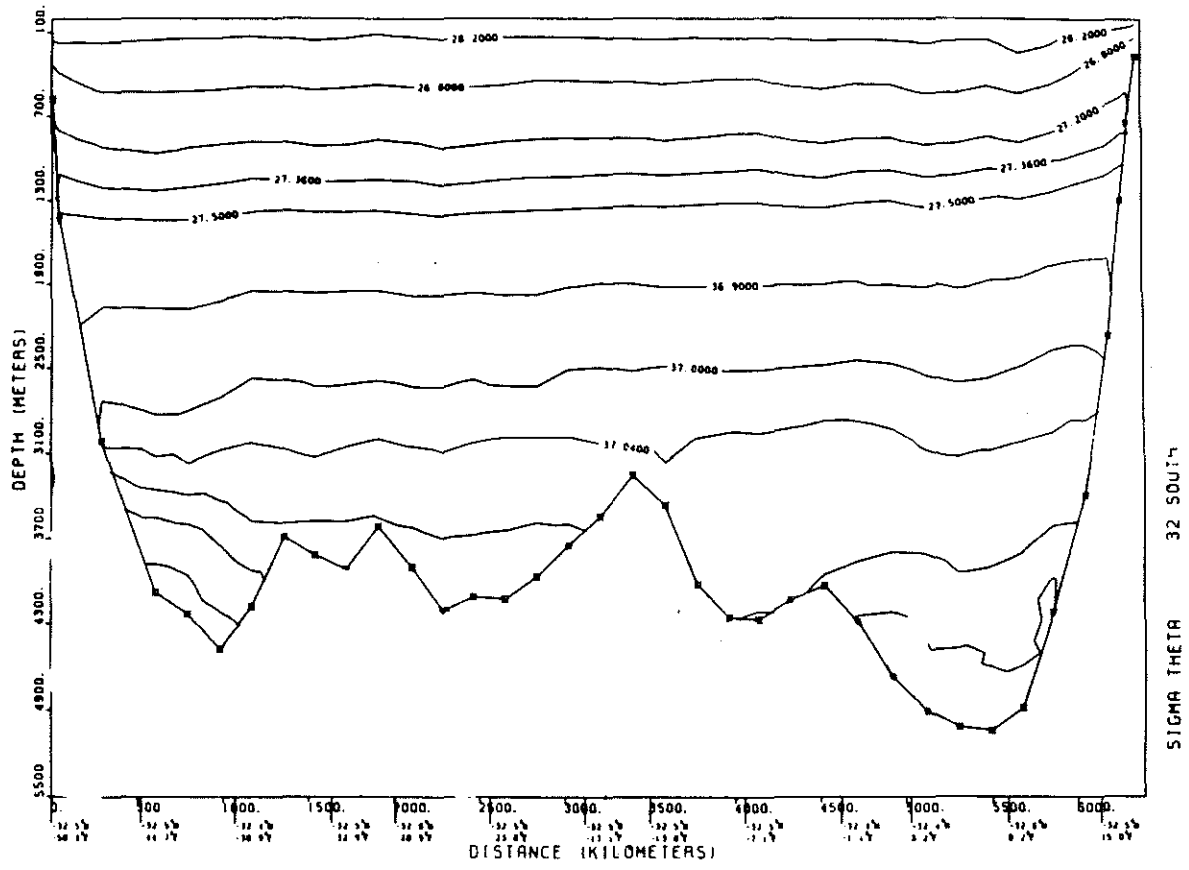


Fig. 2.6c Potential density anomaly at 32°S, as in Fig. 2.2c.



Table 2.1 Layer boundaries and layer average potential temperature (upper value, °C) and salinity (lower value, psu) at each section. "\*" indicates no water in this layer at this section.

| Layer | Upper bndy       | Lower bndy       | Drake  | 0°E    | 30°E   | W-S    | 32°S   |
|-------|------------------|------------------|--------|--------|--------|--------|--------|
| 1     | surface          | $\sigma_0=26.20$ | *      | 16.80  | 16.98  | *      | 18.27  |
|       |                  |                  | *      | 35.288 | 35.250 | *      | 35.661 |
| 2     | $\sigma_0=26.20$ | 26.80            | 6.82   | 10.21  | 10.37  | *      | 13.05  |
|       |                  |                  | 34.070 | 34.635 | 34.629 | *      | 35.227 |
| 3     | 26.80            | 27.20            | 4.18   | 5.85   | 5.66   | 1.93   | 6.73   |
|       |                  |                  | 34.137 | 34.332 | 34.319 | 33.918 | 34.489 |
| 4     | 27.20            | $\sigma_1=32.00$ | 2.72   | 3.02   | 3.18   | 1.00   | 3.54   |
|       |                  |                  | 34.220 | 34.245 | 34.286 | 34.038 | 34.321 |
| 5     | 32.00            | 32.16            | 2.39   | 2.45   | 2.46   | 0.48   | 2.91   |
|       |                  |                  | 34.392 | 34.403 | 34.407 | 34.160 | 34.454 |
| 6     | 32.16            | 32.36            | 2.10   | 2.26   | 2.14   | 0.57   | 2.76   |
|       |                  |                  | 34.583 | 34.603 | 34.589 | 34.394 | 34.648 |
| 7     | 32.36            | $\sigma_2=37.00$ | 1.80   | 2.21   | 2.05   | 1.15   | 2.67   |
|       |                  |                  | 34.698 | 34.766 | 34.745 | 34.566 | 34.832 |
| 8     | 37.00            | $\sigma_3=41.50$ | 1.50   | 1.87   | 1.80   | 0.83   | 2.32   |
|       |                  |                  | 34.724 | 34.799 | 34.785 | 34.548 | 34.876 |
| 9     | 41.50            | 41.54            | 1.23   | 1.49   | 1.39   | 0.90   | 1.91   |
|       |                  |                  | 34.726 | 34.780 | 34.759 | 34.585 | 34.859 |
| 10    | 41.54            | 41.60            | 0.85   | 0.92   | 0.98   | 0.93   | 1.32   |
|       |                  |                  | 34.719 | 34.734 | 34.732 | 34.661 | 34.804 |
| 11    | 41.60            | 41.66            | 0.37   | 0.40   | 0.40   | 0.33   | 0.66   |
|       |                  |                  | 34.705 | 34.696 | 34.700 | 34.678 | 34.736 |
| 12    | 41.66            | $\sigma_4=46.14$ | 0.06   | -.33   | -.26   | -.32   | -.09   |
|       |                  |                  | 34.687 | 34.661 | 34.668 | 34.660 | 34.674 |
| 13    | 46.14            | bottom           | *      | -.73   | -.64   | -.72   | *      |
|       |                  |                  | *      | 34.652 | 34.655 | 34.650 | *      |

the shear below the deepest common observed depth was roughly estimated to be  $\pm 2$  Sv in each layer, as described in Chapter 1.

An additional contribution to the net imbalance in the conservation equations arises from physics left out of the model. For example, at high latitude many of the

layers outcrop at the sea surface as the isopycnals shoal toward Antarctica. Air-sea interactions may result in a net loss or gain of buoyancy and hence a transfer of mass from one layer to another. Indeed, as mentioned in the Introduction, the South Atlantic is thought to be a region of active water mass modification.

The possibility of mass transfers between layers due to atmospheric interactions at the layer outcrops is allowed for in the model in two ways. First, by retaining the cross-isopycnal flux term  $w^* A_u$  in equation (1.1) we have explicitly included transfers across the layer interfaces. We will see in Section 3 that the net transfers due to this term are consistent with estimates of air-sea exchange.

The second way in which non-conservation of mass due to forcing by the atmosphere is reflected in the model is in the row weights. Specifically, layers that outcrop within a region receive lower weights than those that are not exposed to the atmosphere. In the Weddell Sea, where even the densest layers reach the sea surface and buoyancy loss to the atmosphere drives active AABW formation, all the layers are strongly downweighted. Only total mass is required to be conserved, thus allowing for unconstrained exchange between individual layers in region II. The weights chosen for the layers in regions I and III are roughly proportional to the outcrop area of each layer. The specific values listed in Table 2.2 are very rough guesses of the uncertainty in each conservation equation due to all sources of error. The results of several experiments testing different weights suggested that the solution was insensitive to small (1-2 Sv) changes in the estimated errors.

In addition to the conservation equations for mass, a variety of other information can be incorporated into the model in the form of linear constraints. The additional constraints used in the standard case are described next and are summarized in Table 2.2.

Table 2.2 Constraints for standard model. Estimated uncertainties used in weighting the equations are given in parentheses.

- 
- Total mass conserved in regions I,II and III ( $\pm 2$  Sv).
  - Mass conserved in 13 layers in I and III (layers 1-4:  $\pm 4$  Sv; 5-8:  $\pm 3$  Sv; 9-13:  $\pm 2$  Sv).
  - Total transport across Drake Passage,  $0^\circ$ E and  $30^\circ$ E =  $130 \pm 13$  Sv.
  - Zero net transport across  $32^\circ$ S and the Weddell-Scotia section.
  - Zero net transport across  $32^\circ$ S below sill depth east of Walvis Ridge.
  - Zero net transport between Africa and the Agulhas Plateau below sill depth.
  - Transport of bottom water across  $32^\circ$ S west of Mid-Atlantic Ridge =  $4 \pm 1.2$  Sv.
  - Heat flux across the Weddell-Scotia section =  $.1 \pm .05 \times 10^{15}$  W (see text).
- 

The model was first run with conservation statements for salt included as well as for mass, but the salt constraints were found to add little information independent of that in the mass equations. Since there is a computational advantage to working with a smaller system, the salt equations were removed for most of the models discussed here. Only temperature and salinity were measured on the  $32^\circ$ S section, so we cannot write box budgets for the nutrients or other chemical properties with this data set.

However, there is additional useful information available to include as constraints in the model. During the ISOS program several extensive current meter and pressure sensor arrays were deployed in Drake Passage to measure the transport of the ACC. Nowlin and Klinck (1986) have recently reviewed these estimates and report a mean transport of 130 Sv with an uncertainty of not more than 10%. Since the Atlantic basin is closed to the north except for a weak inflow from the Pacific (1 Sv; Aagard *et al.*, 1985), the net transport across the sections running from Africa to Antarctica at  $0^\circ$  and  $30^\circ$ E must equal the transport at Drake Passage. Therefore constraints were added requiring that the total transport across these three sections be  $130 \pm 13$  Sv. (For comparison to the standard model, several runs were made with total mass conserved but with no constraint on the ACC transport. With an initial reference level at 3500 db the resulting transport is 113 Sv, somewhat lower than the value given by Nowlin

and Klinck; however, when not constrained the ACC transport is very sensitive to the reference level chosen.)

The current meter observations of Hogg *et al.* (1982) in the Vema Channel also provide useful constraints on the flow. The Vema Channel is a narrow, deep passage through the Rio Grande Rise at 30°S which provides the only path for the exchange of bottom water between the Argentine and Brazil basins. (Whether the poorly-surveyed Hunter Channel to the east is also deep enough to permit some flow of bottom water between the basins is unknown, and its contribution is assumed to be small in this model.) The northward volume transport of AABW found by dynamic calculations and direct current measurements was  $4 \pm 1.2$  Sv. Therefore a constraint was added requiring that the net flux of AABW across 32°S west of the Mid-Atlantic Ridge be equal to the flux observed by Hogg *et al.*

Several more constraints are suggested by the basin geometry. The Walvis Ridge crosses the 32°S section at 5°W and continues to the northeast to the African coast, closing the Cape Basin to the north. Thus there can be little net flow of water below the sill depth (3500 m) of the Walvis Ridge across the eastern portion of the 32°S section. Similarly, the basin between the Agulhas Plateau and the African coast is closed to the east below 4000 m and the net flow below this depth across this part of the *Conrad* section must be small. There is a similar requirement that the total transport across the 32°S and Weddell-Scotia sections be close to zero, since the Atlantic as a whole is nearly closed to the north and the Weddell-Scotia section spans the Weddell Sea. The total transport includes both the geostrophic and Ekman transports. However, in this case the Ekman transports across each of the sections is small: the 32°S section is nearly coincident with the zero line of the wind stress, the winds are weak in the Weddell Sea, and the strong zonal winds over the ACC drive only a small flux across the three meridional sections.

The final constraint listed in Table 2.2 concerns the heat flux across the Weddell-Scotia section. As described in the Introduction, the Weddell Sea is thought to be the major source of AABW to the world's oceans. The details of the formation mechanisms are uncertain, but it is generally accepted that the water mass that is exported from the Weddell Sea is a mixture of CDW and dense waters formed on the continental shelf (and perhaps in the gyre interior) by cooling and brine released by the freezing of sea ice (Gill, 1973; Killworth, 1977; Carmack and Foster, 1975; Gordon, 1978). One expects, then, that the Atlantic as a whole should be a net producer of AABW, but estimates of the rate at which this water mass is produced vary over a wide range. Indeed, one of the original goals of this work was to see if by considering heat and mass budgets for the South Atlantic as a whole we could make a better estimate of the rate of AABW production.

The model was first run with the only constraint in region II being that there be no net flux of mass across this section, so that total mass was conserved. By not requiring conservation of mass in individual layers in the Weddell Sea, as much mass could be transferred between layers as necessary to provide the sink of CDW and the source of AABW required by the budgets in regions I and III. It was hoped that in this way the conversion rate of CDW to AABW within the Weddell Sea would be "forced" by the requirement that these density layers be approximately conservative outside the Weddell Sea formation region.

This strategy was not completely successful: many of the early model runs showed the Atlantic consuming, rather than producing, AABW. The net transport across the sections at 0° and 30°E in the densest layers was 5-10 Sv from the Indian to the Atlantic Ocean. To conserve mass in these layers, the flow of BW into region I was in turn balanced by an inflow of BW to the Weddell Sea. Since total mass was conserved, the poleward transport of dense water was accompanied by an equatorward transport of warmer water. The Weddell Sea, as a result, appeared to be *gaining* heat from

the atmosphere and converting dense water to lighter water, contrary to the evidence indicating the Weddell Sea to be a major source of BW.

These results suggested that the constraint that there be no net mass flux across this section by itself did not provide sufficient information to determine the BW formation rate. There are several ways in which the *a priori* information that the Weddell Sea should be a source of BW can be explicitly included in the model. For example, one could simply add constraints fixing the rate of BW formation, or the net transport of BW across the 0° and 30°E sections. Here I have chosen to force the heat flux across the Weddell-Scotia section to be equal to the heat lost by the ocean to the atmosphere in the Weddell Sea. Gordon (1981) estimated the net annual heat loss by the ocean between 60° and 70°S to be  $31 \text{ W m}^{-2}$ . This value integrated over the surface of region II implies a heat transport of .1 PW by the ocean across this section. Estimates of air-sea exchange in this region are poor, but still are perhaps better known than the transports of the deeper layers across each section. Moreover, in this way we can at least determine the bottom water production rates implied by different values of the heat flux. The impact of this constraint on the solution is considered in Section 3. (Note that I have assumed that the heat lost to the atmosphere is balanced by heat carried in by the geostrophic flow. Although eddies are thought to make an important contribution to the meridional heat flux across the Polar Front (Bryden, 1979; de Szoeke and Levine, 1981), the meridional temperature gradient in the Weddell Sea itself is small and the eddy contribution is unlikely to significantly alter the results.)

Having chosen the model physics to be included as constraints, and appropriate weights for the rows and columns of the coefficient matrix, the final step before doing the SVD is to define an initial model - in this case, to select an initial reference level. As discussed in Chapter I, the problem considered here is underdetermined and there are an infinite number of consistent solutions. The solution found by the SVD is the minimum correction to the initial model required to satisfy the constraints, and so is

of course sensitive to the initial state used. Therefore one tries to pick an initial model that is reasonably close to the (unknown) true state; comparing the results obtained using different initial models is, in turn, a useful way to examine the range of consistent solutions.

The geostrophic shear in the ACC fronts extends nearly to the bottom and the transport estimates in Drake Passage obtained by referencing dynamic calculations to direct current meter measurements confirm that the eastward flow of the ACC reaches to great depth. Therefore most investigators studying the ACC have chosen a deep reference level (Jacobs and Georgi, 1977; Georgi and Toole, 1982; Whitworth, 1983; Whitworth and Nowlin, 1987). A deep reference level also seems to be appropriate at 32°S. Wüst's (1955) choice of a mid-depth level (2000 m) at 28°S led to a poleward transport of AABW. Wright (1969) suggested that a kink in the  $\theta$ -S curve at  $\approx 2.0^\circ\text{C}$  marking the boundary between the AABW and NADW was a better reference level choice; this surface lies at 3400-3800 m at 32°S. Subsequent studies have also found that a deep level leads to a more consistent deep circulation pattern in the southwest Atlantic (Johnson *et al.*, 1976; Reid *et al.*, 1977; Georgi, 1981; Hogg *et al.*, 1982; Fu, 1981).

After some experimentation, an initial reference level of 3500 db was chosen for the standard case. For station pairs at which the bottom depth was less than 3500 db the reference level was taken to be at the deepest common sample depth. The transport across each of the sections relative to this level is close to satisfying the total transport constraints: 150, 134, and 114 Sv at Drake Passage, 0° and 30°E, respectively; 4 Sv across the Weddell-Scotia section and 20 Sv at 32°S.

There are a total of 190 unknowns (reference level velocities at 154 station pairs and 36 cross-interface transfers). The mass conservation statements and supplementary constraints described above result in 42 equations, not all of which are independent.

Thus the system is in fact underdetermined (more unknowns than independent equations) and the reference level velocities at individual station pairs are not very well resolved, as discussed below.

The results of the standard model are presented in the next section. Additional experiments run to test the sensitivity of the solution to the particular model assumptions made are also described.



### 3. Results of the standard model

The first step in analysing the results of an inverse procedure is determining the rank,  $k$ . The rank of the standard model was determined to be about  $k=32$  based on an inspection of the residual and solution norms and the solution variance as a function of  $k$ , as described in Chapter I. At larger values of  $k$  the residual norm is decreased further in magnitude, but at the cost of a rapid increase in the solution norm and variance as the smaller eigenvalues are included. The results are similar for choices of  $k$  between 30-34. At this rank the diagonal elements of the data resolution matrix  $UU^T$  indicate that the mass conservation equations for the deeper layers contribute nearly independent information, as do the net mass and heat flux constraints. The constraints fixing the flux of individual layers at certain locations contribute significant information, but are not entirely independent (diagonal elements of  $\approx .4-.6$ ).

Before presenting the solutions, it is worth commenting on the errors in the estimates. As discussed in Chapter I, there are two sources of uncertainty in the estimates of the reference level velocities: errors due to noise in the observations and errors due to the fact that we have insufficient information to fully resolve the velocities. The error due to noise can be estimated from the expression for the relative variance in equation (1.3) and the estimate of the problem variance based on the residuals in equation (1.4). In this case, this source of error is negligible:  $<.1 \text{ cm s}^{-1}$  at Drake Passage and  $<.01 \text{ cm s}^{-1}$  for most of the remaining  $b_i$ .

The uncertainty in the individual model parameters due to the lack of resolution is much larger than that due to data noise. Typically the diagonal elements of the resolution matrix are  $<0.2$ . For the standard model we found the number of independent equations (i.e. the rank) to be about 32, so that with the available information we are able to determine only 32 weighted averages of the 190 unknowns in the problem. The resolution, however, is compact: the solution at each station pair is generally a weighted

average of the (unknown) "true" velocity at physically adjacent pairs, not pairs from different sections, or distant parts of the same section. The solution found is thus a spatially smoothed version of the real reference level velocity field. The length scale of the smoothing varies along each section, as can be seen by examining the columns of the  $VV^T$  matrix. Several representative columns are shown in Fig. 3.1.

Fig. 3.1a shows the 16 columns corresponding to the 16 station pairs across Drake Passage. Each column has a broad peak centered on the particular model parameter which decays to small values within  $\pm 4$  station pairs ( $\pm 200$  km) of the maximum. As one moves across the section the "smoothing window" translates with little change in shape. The elements of each column are very small for station pairs on other sections demonstrating that the resolution is indeed compact on this section. Several of the columns show small sidelobes for parameters 130 to 141, corresponding to the cross-isopycnal transfers in region I, as expected since the  $w^*$  are not independent of the flow through each of the sections bounding region I.

Additional examples corresponding to station pairs along the  $0^\circ\text{E}$  and  $32^\circ\text{S}$  sections are shown in Fig. 3.1b-c. Each of the columns plotted is similar to several adjacent columns not shown here. At each section the reference level velocities tend to be resolved in groups or clusters, with horizontal scales of roughly 500-1000 km in the interior and 100-200 km near the boundaries. The scale of the resolution reflects the scales on which the hydrography shows significant variation. Station pairs are grouped together which have similar ratios of layer depths or, in other words, whose columns of the coefficient matrix  $A$  are nearly linearly dependent. The fact that the reference level velocities are resolved on very broad scales in the interior is a statement that the property fields and layer geometry contain little information on the scale of the station spacing.

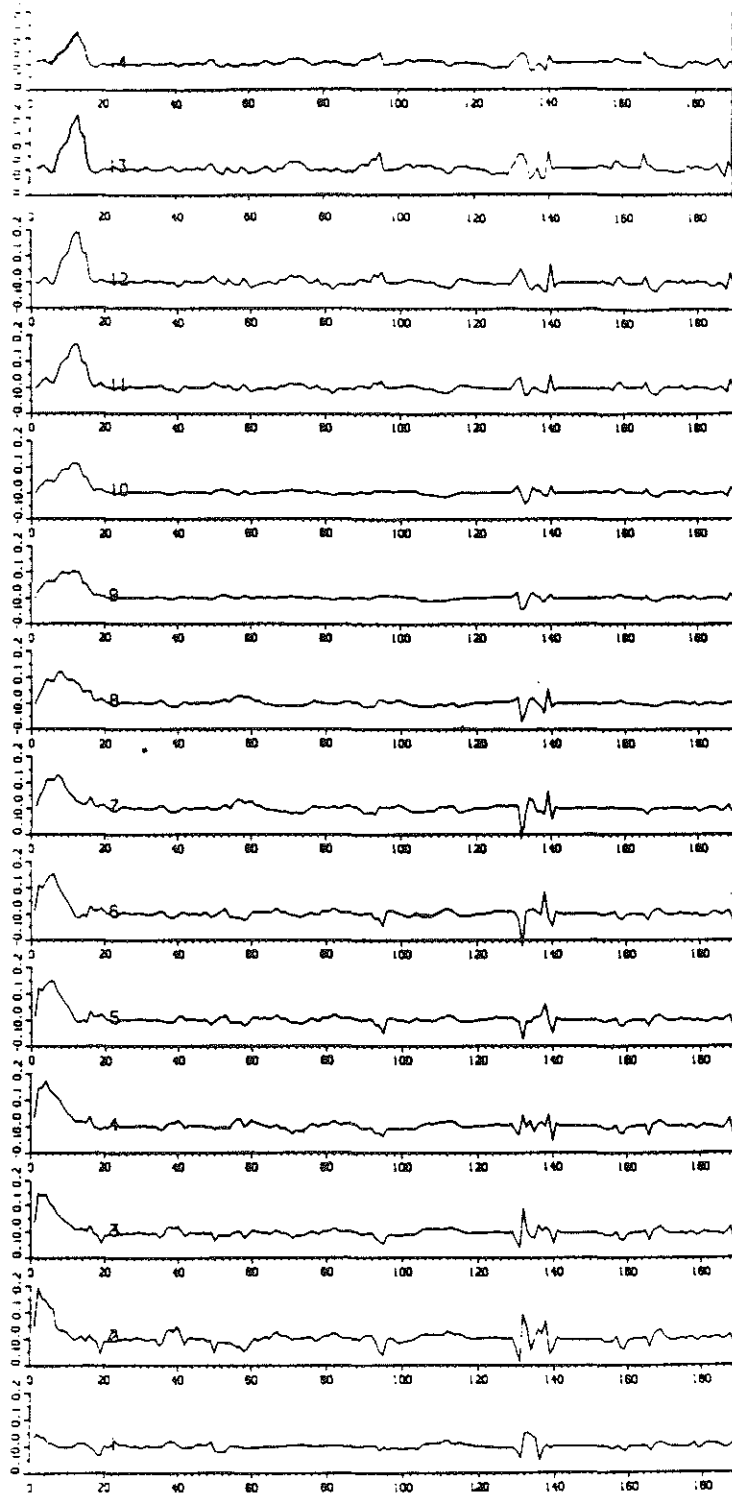


Fig. 3.1a First 14 columns of the resolution matrix, corresponding to the station pairs of the Drake Passage section. On abscissa is column, or station pair, number. Columns 1-16: Drake Passage station pairs; 17-53: 32°S; 54-93: Weddell-Scotia; 94-129: 0°E; 130-141:  $w_I^*$ ; 142-153:  $w_{II}^*$ ; 154-178: 30°E; 179-190:  $w_{III}^*$ .

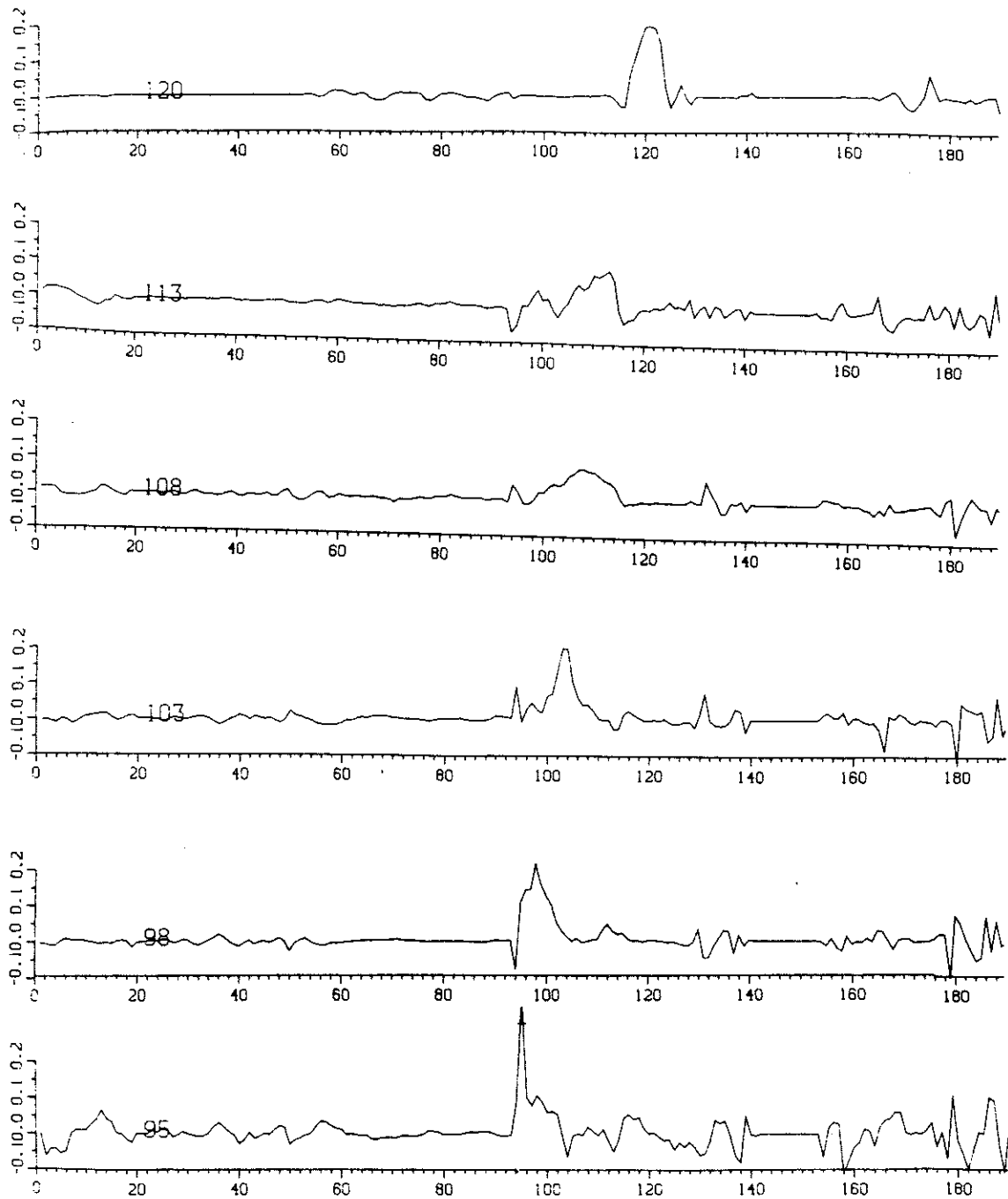


Fig. 3.1b As in Fig. 3.1a, for columns of the resolution matrix corresponding to several station pairs of the 0°E section.

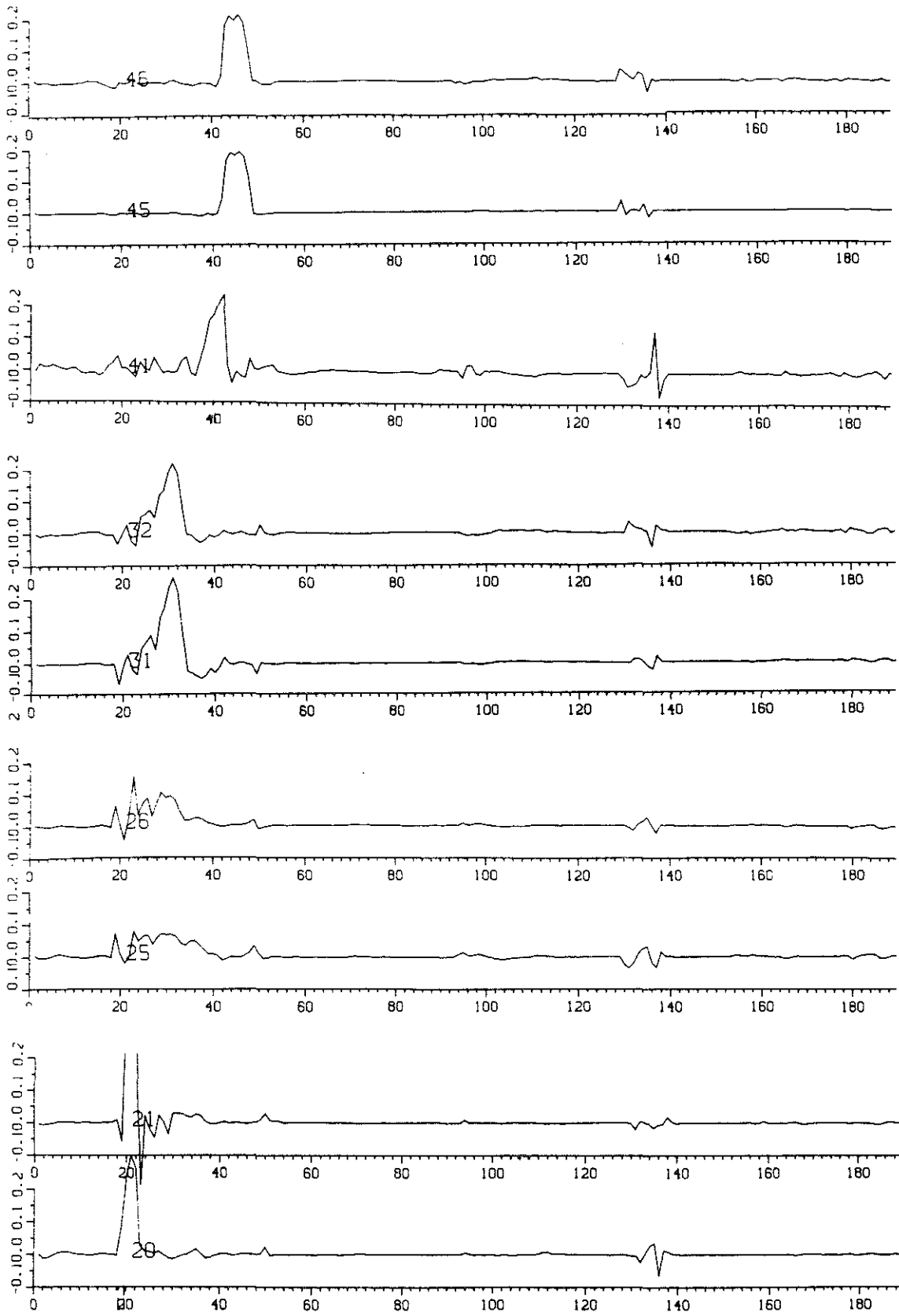


Fig. 3.1c As in Fig. 3.1a, for columns of the resolution matrix corresponding to several station pairs of the 32°S section.

The results of the standard model are presented in the remainder of this section. First the geostrophic velocity field at each section is described, followed by a discussion of the mass and heat transport results.

### 3.1 *The Velocity Field*

The geostrophic velocity at Drake Passage is shown in Fig. 3.2 for the standard model. The ACC appears as four deep jets with horizontal scales of  $O(100 \text{ km})$  and maximum velocities greater than  $25 \text{ cm s}^{-1}$ . The jets are separated by regions of slower eastward or even westward flow. The strongest velocities are found in the northernmost jet corresponding to the Subantarctic Front. The flow is to the west near the bottom in the northern portion of the section and over the continental slope at the southern end of the Passage.

The reference level velocity is shown at the top of the plot. Note that the solution varies smoothly across the section, as anticipated from the discussion of resolution above. At this section the initial transport relative to 3500 db is 150 Sv; to decrease this to 130 Sv and satisfy the mass conservation constraints the system introduces flow at the reference level to the west in the northern half of the Passage and weaker eastward flow in the southern half.

The velocity field at the AJAX section crossing the ACC at  $0^\circ\text{E}$  is shown in Fig. 3.2b. The initial reference level used gave a net transport equal to 134 Sv and little adjustment of the reference level velocity was required to satisfy the transport and mass conservation constraints. At this latitude most of the transport of the ACC occurs in two jets associated with the Subantarctic and Polar Fronts. Both the SAF and the PF are broader at  $0^\circ\text{E}$  than in Drake Passage and result in less intense flows. However, Whitworth and Nowlin (1987) have shown that at both longitudes the cross-frontal scale is roughly twice the local deformation radius. The ACC is found mostly to the north of the Mid-Ocean Ridge. Further south is a third jet of eastward flow, much

DRAKE PASSAGE

STANDARD ABS. VEL.

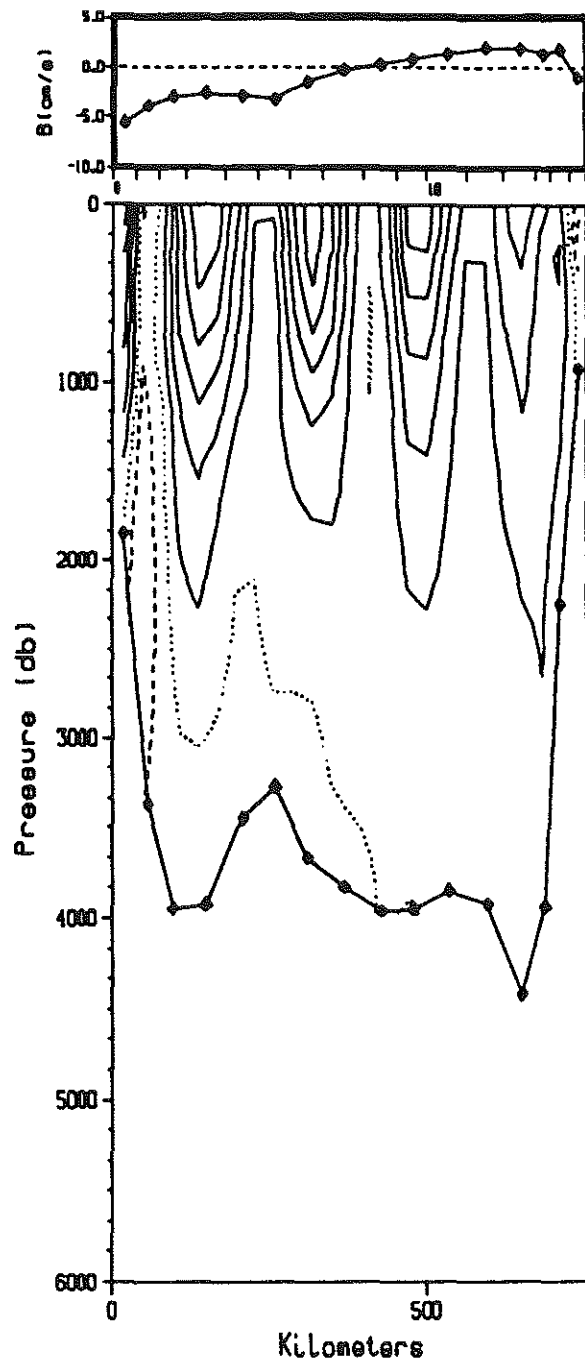


Fig. 3.2a Geostrophic velocity at Drake Passage for the standard model. Solid, dashed and dotted contours refer to eastward, westward and zero velocity, respectively. Contour interval is  $5 \text{ cm s}^{-1}$ . Upper plot is reference level velocity for this solution.

weaker than the SAF and PF, which corresponds to the boundary between the ACC and the cyclonic Weddell gyre to the south (Whitworth and Nowlin, 1987). Near the African coast there is a strong flow to the west (maximum speed  $>15 \text{ cm s}^{-1}$ ) over the continental slope. Further offshore the flow is weak and alternates in sign until the edge of the ACC is reached at the SAF at  $45^\circ\text{S}$ .

At  $30^\circ\text{E}$  (Fig. 3.2c) the ACC appears as a much broader and weaker flow than at  $0^\circ\text{E}$ , but this may be partially due to the wide station spacing along this section. Two distinct fronts or jets of eastward flow can still be seen, separated by a thin band of westward velocities. Toward Antarctica the sense of the flow reverses, reflecting the eastern extension of the weak nearly-barotropic circulation of the Weddell gyre. Nearer the coast the westward flow increases in strength in the Antarctic Coastal Current (Gill, 1973). By far the most intense flows at this section are the Agulhas and Agulhas Return Currents at the northern end of the section, with maximum speeds of  $>100 \text{ cm s}^{-1}$ . The Agulhas Current is separated from the African coast by a narrow but strong eastward flow, while offshore of the Current there is a strong ( $15 \text{ cm s}^{-1}$ ) eddy or meander reaching to the bottom over the Agulhas Plateau.

The geostrophic velocity field at  $32^\circ\text{S}$  is dominated by the boundary currents (Fig. 3.2d). The Brazil Current is very strong in this section and reaches speeds up to  $60 \text{ cm s}^{-1}$ . Southward flow extends to the bottom beneath and offshore of the surface expression of the boundary current, while in the upper 1000 db the current is bounded offshore by a counterflow to the north. The interior flow is characterized by columns of weak flow moving alternately to the north and south as the section crosses eddies, or possibly meanders of a mostly zonal flow. Further east the eddies are surface-intensified and have smaller horizontal scales. There is a substantial northward flow along the coast of Africa but it is difficult to distinguish between the Benguela Current and isolated eddies. Again the reference level velocity correction required to satisfy the constraints is small.



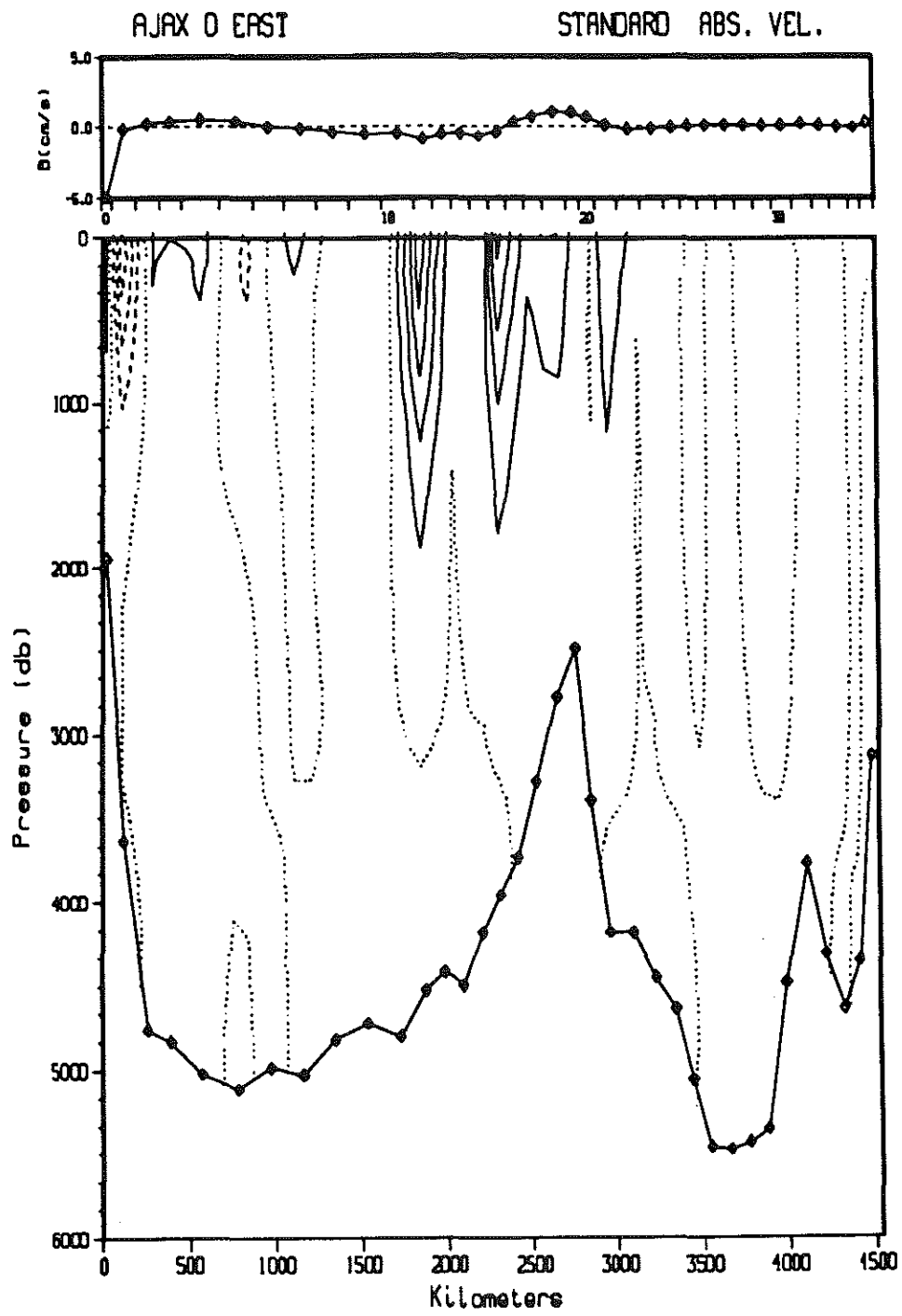


Fig. 3.2b Geostrophic velocity at 0°E for the standard model. Solid, dashed and dotted contours refer to eastward, westward and zero velocity, respectively. Contour interval is  $5 \text{ cm s}^{-1}$ . Upper plot is reference level velocity for this solution.

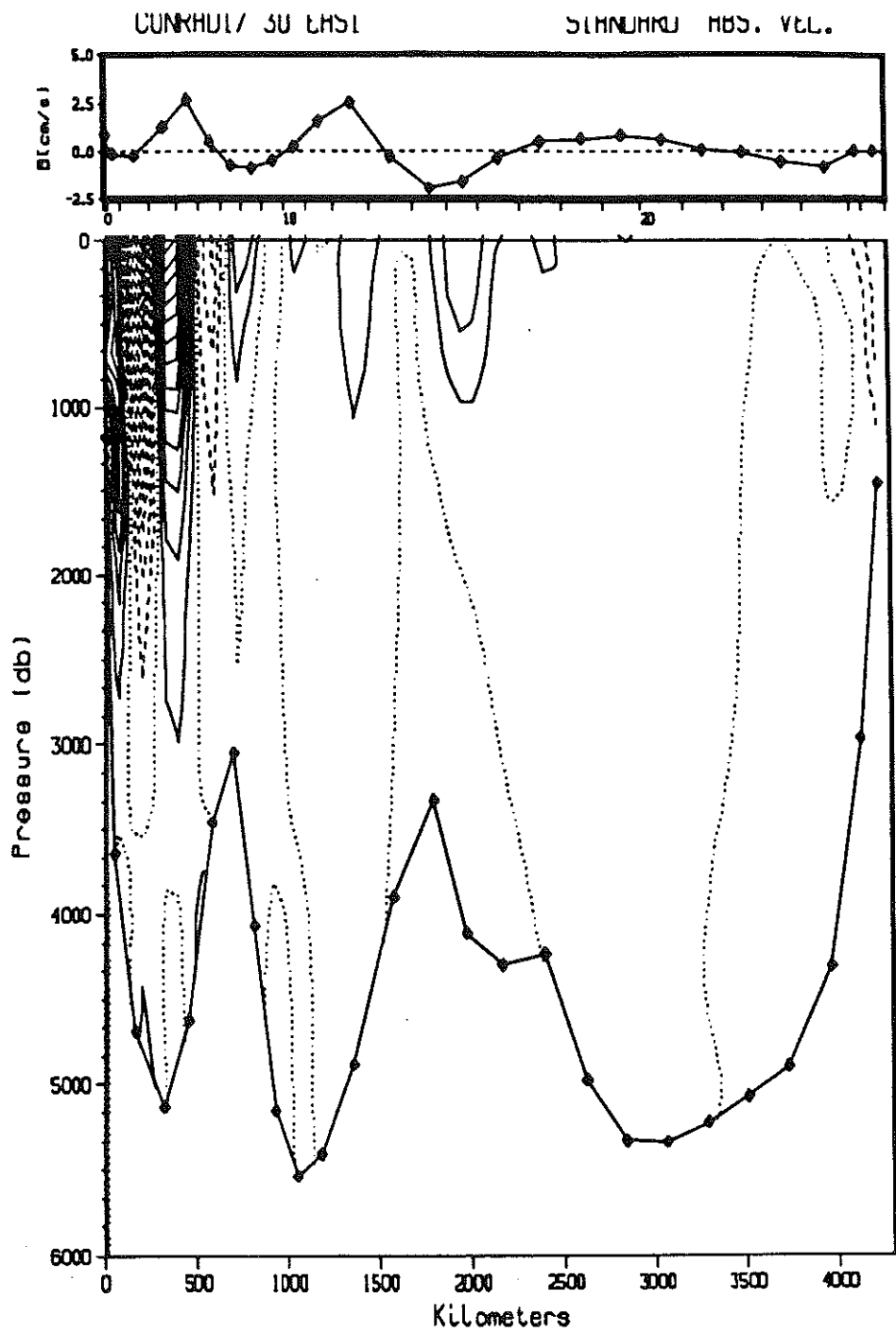


Fig. 3.2c Geostrophic velocity at 30°E for the standard model. Solid, dashed and dotted contours refer to eastward, westward and zero velocity, respectively. Contour interval is  $5 \text{ cm s}^{-1}$ . Upper plot is reference level velocity for this solution.

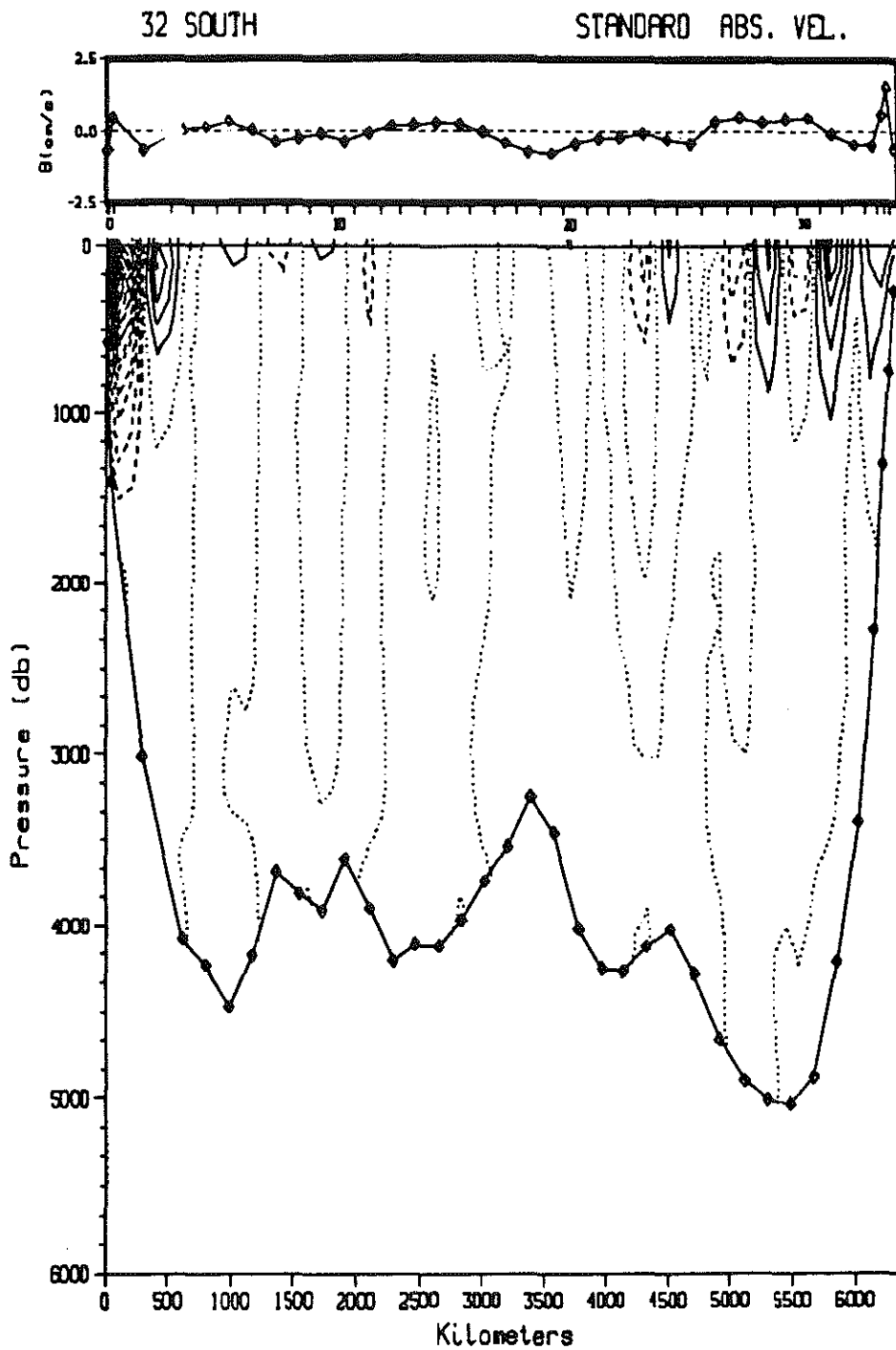


Fig. 3.2d Geostrophic velocity at 32°S for the standard model. Solid, dashed and dotted contours refer to eastward, westward and zero velocity, respectively. Contour interval is  $5 \text{ cm s}^{-1}$ . Upper plot is reference level velocity for this solution.

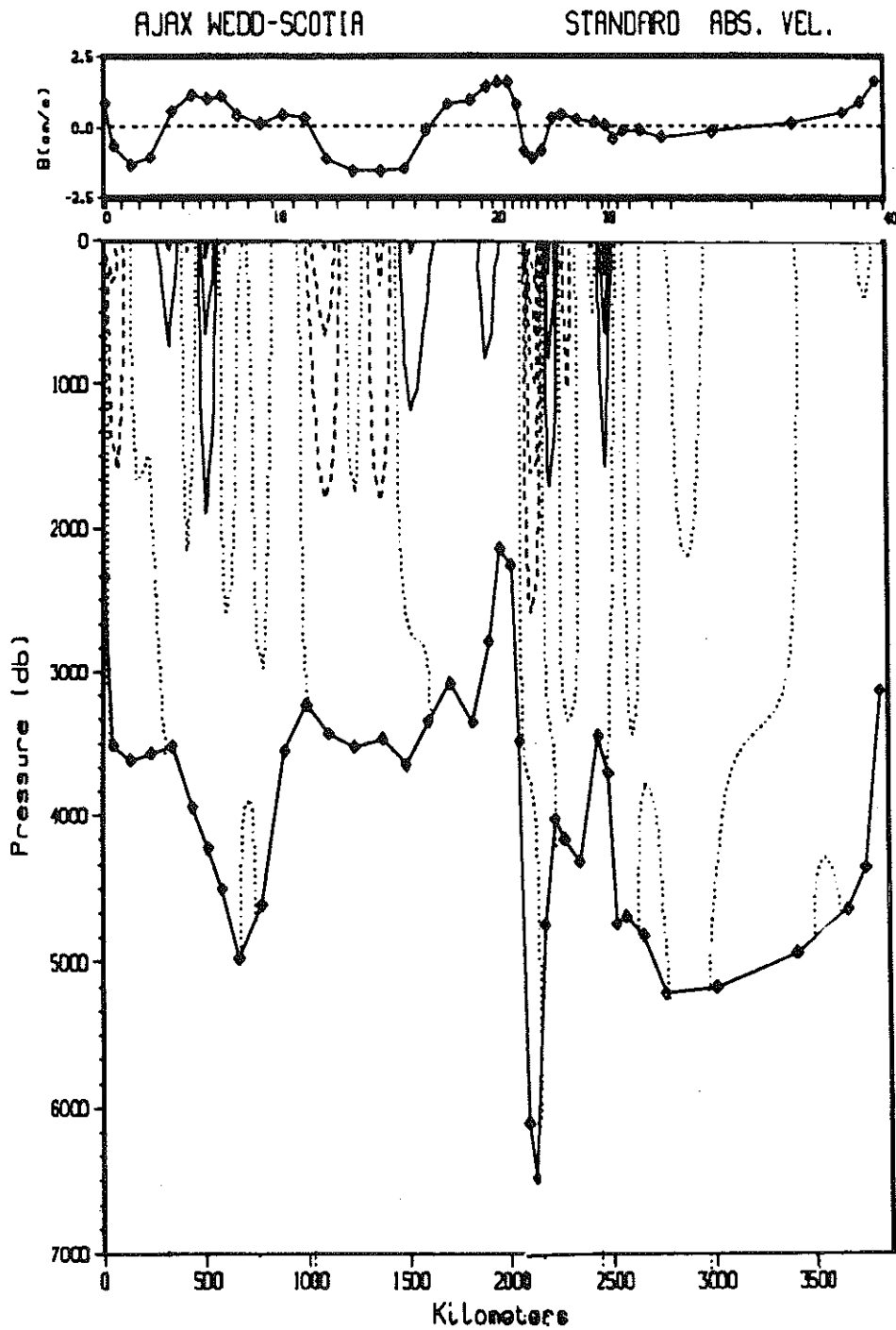


Fig. 3.2e Geostrophic velocity at the Weddell-Scotia section for the standard model. Solid, dashed and dotted contours refer to eastward, westward and zero velocity, respectively. Contour interval is  $5 \text{ cm s}^{-1}$ . Upper plot is reference level velocity for this solution.

The velocity field along the section crossing the Weddell and Scotia Seas is shown in Fig. 3.2e. As seen in the temperature and salinity plots, the Weddell gyre is not symmetric at this section: the broad westward flow in the interior of the basin returns to the east in a narrow jet near the northern boundary of the basin (stations 29-30). This jet is thought to be the open ocean expression of the western boundary current of the Weddell gyre (Gordon *et al.*, 1981). To the north there is a tightly-confined anticyclonic gyre of strong flow which reaches to the bottom and appears to be related to the topography of the South Sandwich Trench. Within the Scotia Sea the flow is strong and alternates in sign as the ship track runs from the South Scotia Ridge into the Scotia Sea and back again across the Weddell-Scotia Confluence (Gordon *et al.*, 1977).

The estimate of the absolute velocity field found in the standard case and presented in Fig. 3.2 is not unique, as discussed in Chapter I, and with the available information we have been able to resolve the reference level component of the velocity field only on broad scales. However, we are primarily interested in the net exchange of water masses between the ocean basins, and the net transports across each section are better determined than the details of the velocity field itself. One way to demonstrate this is to simply compare the results of different models, as done below. A more formal way to demonstrate the insensitivity of the section integral fluxes is shown in the Appendix and discussed more thoroughly in Section 4.

### 3.2 Mass and Heat Transport

In this section I will focus on the net transport across each section in each layer for the standard model. The transport per unit depth, or mass flux density, for the three sections crossing the ACC show a similar pattern in each case, as seen in Fig. 3.3. The net transport is to the east in all layers and strongest near the sea surface. Roughly two-thirds of the transport into the Atlantic through Drake Passage is intermediate water (layers 3-6).

Despite the similarity of the plots and the fact that the total transport across each section is constrained to be 130 Sv, the transport in individual layers is not the same across each section. The differences in transport are easier to see by plotting the difference between the mass flux in each layer at Drake Passage and at  $0^\circ$  and  $30^\circ\text{E}$  (Fig. 3.4). More intermediate water enters the Atlantic through Drake Passage than leaves south of Africa. To keep the total transport across each section equal, the deficit of intermediate water is made up by a surplus of deep and bottom water leaving the basin across  $0^\circ$  and  $30^\circ\text{E}$ . Thus the Atlantic as a whole converts intermediate water into deep and bottom water.

At  $32^\circ\text{S}$  the zonal integral of the circulation consists of northward flow of surface and intermediate water, southward flow of deep water, and northward flow of bottom water (Fig. 3.5). Note that although the synoptic velocity field shown in Fig. 3.2d bears little resemblance to the layered circulation described by Wüst (1935), the zonal integral of the velocity is consistent with the picture Wüst derived from analysis of the property fields. The integral of the flow across the Weddell-Scotia section also reveals an overturning cell: poleward flow of deep water into the Weddell Sea balanced by an equatorward transport of bottom water in layers 12 and 13.

These results can be summarized with the help of a "circulation cartoon" such as Fig. 3.6. In this figure the net transport across each section has been summed in

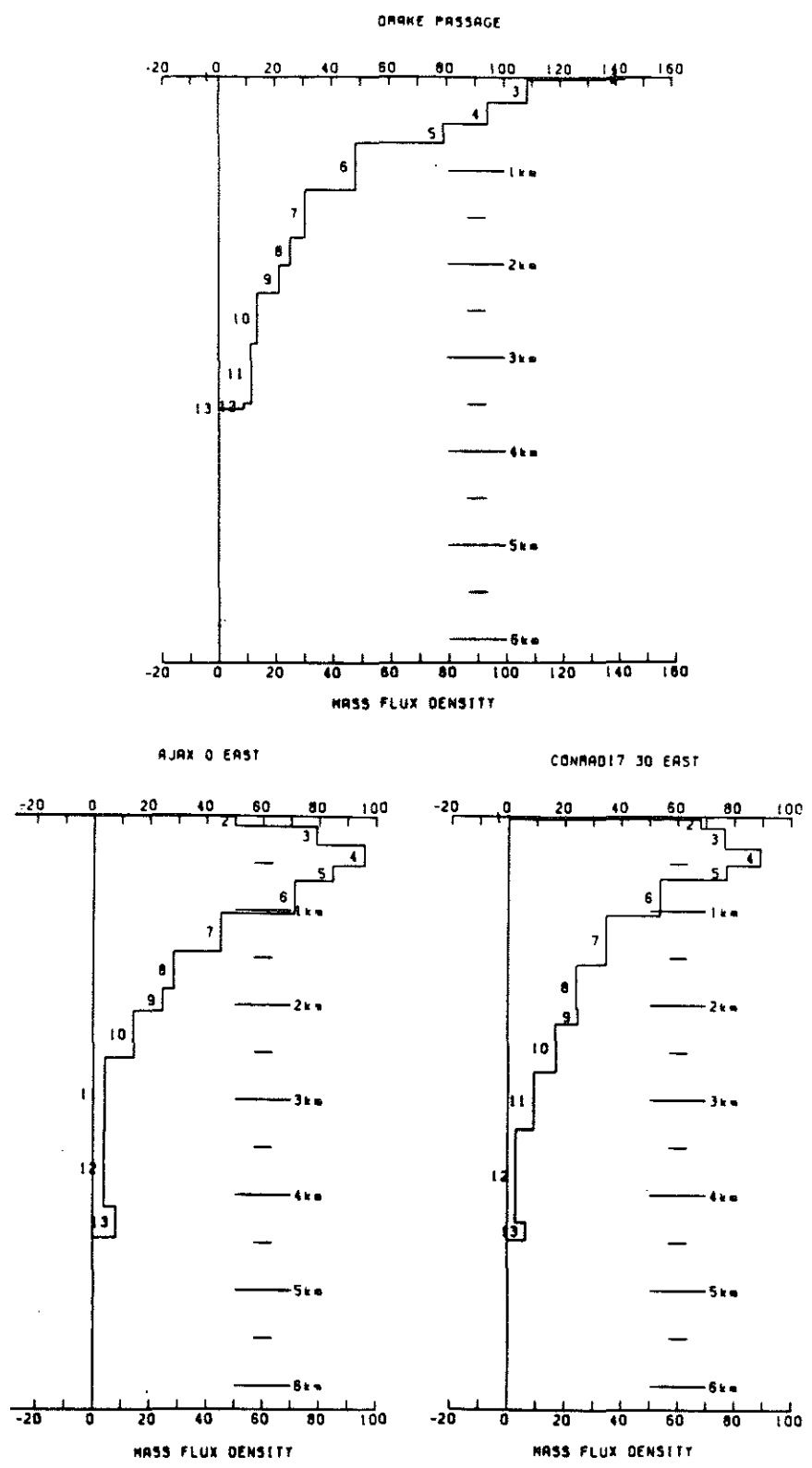


Fig. 3.3 Mass flux integrated across the section per unit depth, or mass flux density, at Drake Passage, 0°E and 30°E for the standard model (Sv/km). The thickness of each layer plotted is the average thickness of the layer at the section. The area between the curve and the axis equals the transport; positive fluxes are to the north or east.

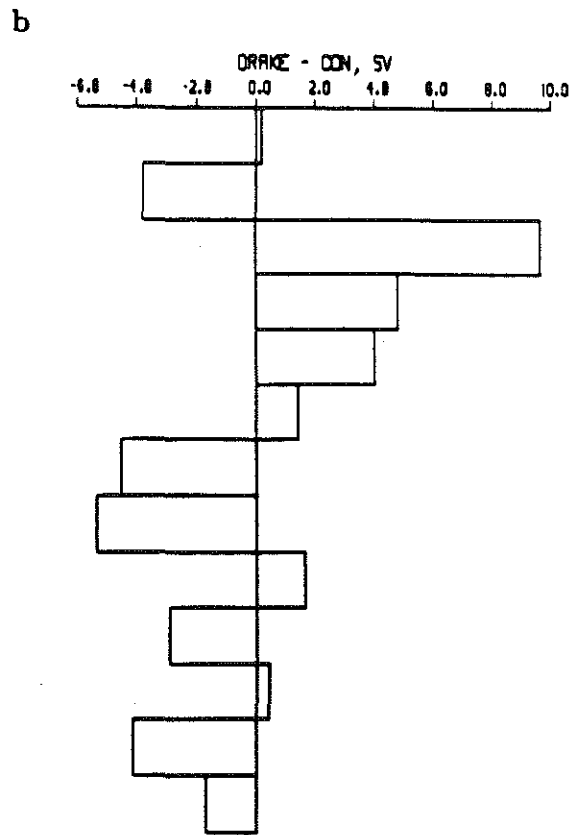
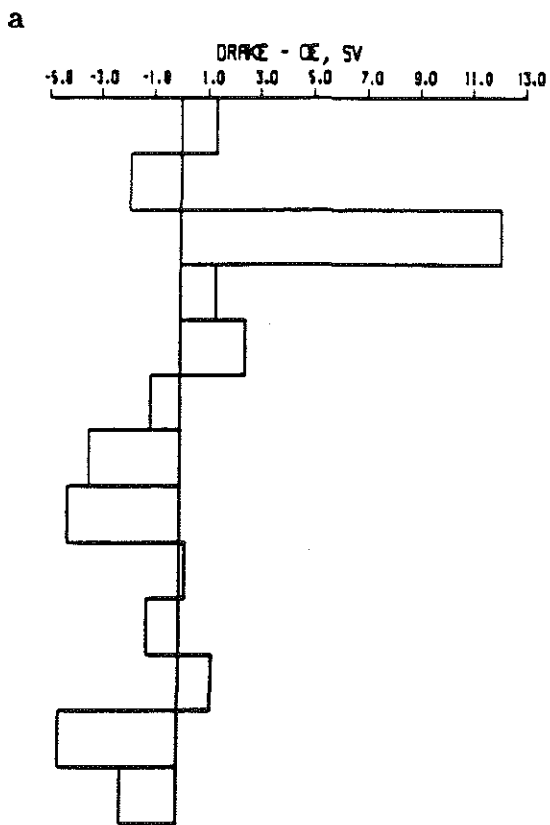


Fig. 3.4 Difference in transport in each layer between (a) Drake Passage and 0°E and (b) Drake Passage and 30°E.



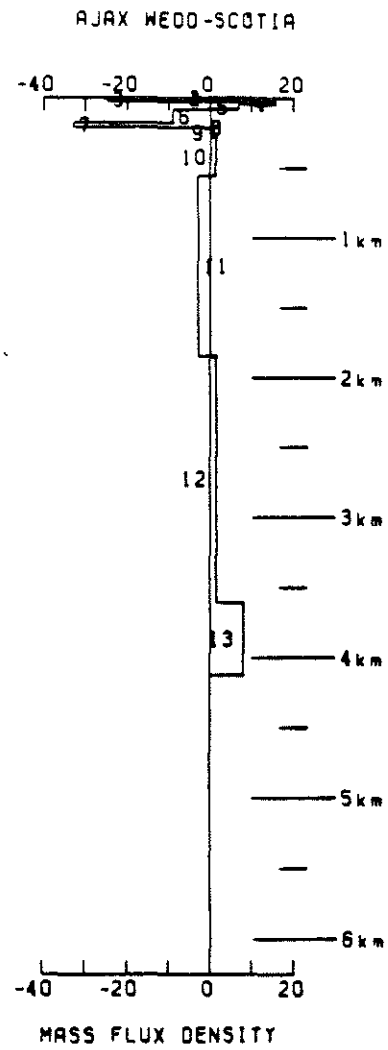
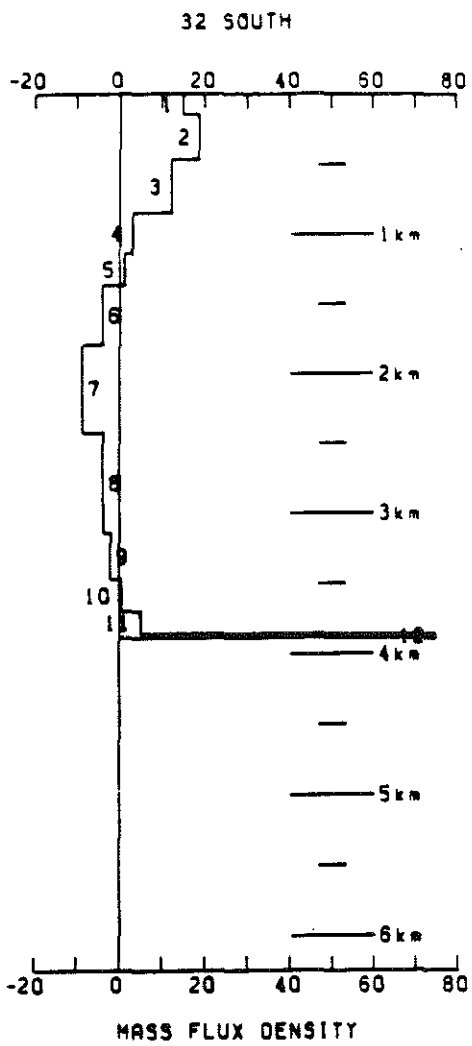


Fig. 3.5 Mass flux density across 32°S and the Weddell-Scotia section for the standard model.

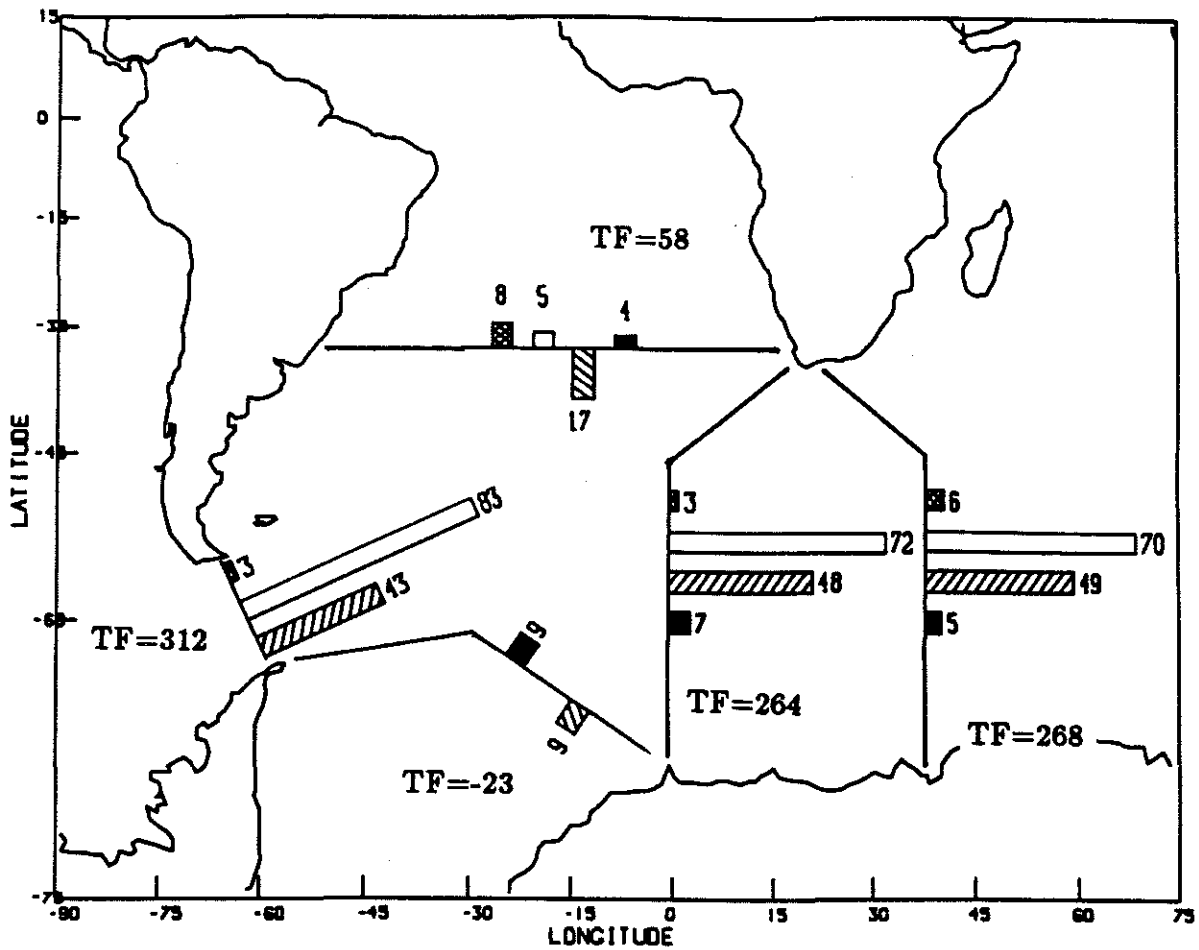
groups of layers corresponding to different water masses and plotted as a bar whose length is proportional to the transport.

Most of the ACC transport is in the intermediate layers at Drake Passage. The Passage is restricted in both latitudinal and vertical extent and prohibits inflow of very dense water from the Pacific. Furthermore, the most intense flow is in the northern part of the Passage, where the upper layers are thick relative to the deep water and so account for the majority of the transport. The same pattern is seen at 0° and 30°E, but the transport of intermediate water has decreased by about 10 Sv and the flux of deep and bottom water has increased by a similar amount. The net transport in layers 1 and 2 ( $\sigma_0 < 26.8$ ) at these sections is 4-6 Sv to the east.

Also presented in Fig. 3.6 are estimates of the net temperature flux across each section, relative to 0°C. The ACC loses  $\approx 50$  °C Sv, or .19 PW of heat, in crossing the Atlantic between Drake Passage and 0°E, while the net heat divergence between 0° and 30°E is roughly zero.

At 32°S the integrated flow consists of equatorward transport of surface and intermediate water, poleward flow of deep water, and an equatorward flux of bottom water. As discussed in the introduction, the equatorward flow of warm water and poleward flow of cooler deep water results in a net equatorward flux of heat. It will be shown in Section 4.2 that the magnitude of the heat flux is tightly tied to the vigor of this overturning cell; in this model, a cell carrying 17 Sv of NADW to the south across 32°S results in a heat flux of .25 PW.

The integrated flow across the Weddell-Scotia Sea section also consists of an overturning cell, and the transport results again reflect the tight coupling between the strength of the cell and the meridional heat flux. Recall that in this model the heat flux across this section was required to equal the heat lost to the atmosphere within the Weddell Sea. The constraint that the ocean carry .1 PW of heat into the Weddell



Standard Model

$$b^T b = 1200$$





- |   |   |
|---|---|
|  = surface water (layers 1-2)      |  = deep water (layers 7-11)    |
|  = intermediate water (layers 3-6) |  = bottom water (layers 12-13) |

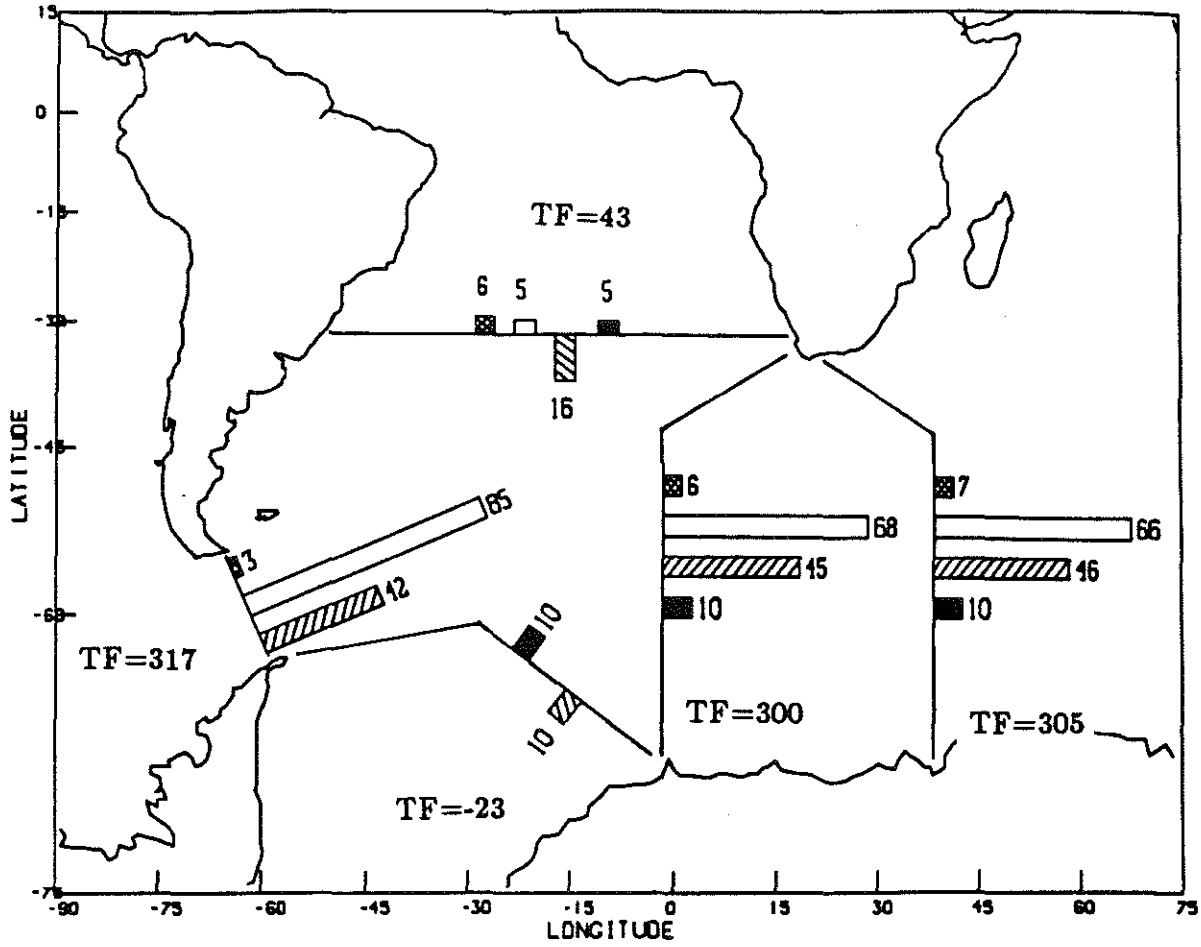
Fig. 3.6 Schematic circulation cartoon for the standard model. Length of each bar is proportional to the net transport across each section in sum of layers corresponding to each water mass (see legend). Numbers at end of each bar give transport in Sv. Also shown is the temperature flux across each section (relative to 0°C) in units of °C Sv.

Sea leads to a poleward transport of  $\approx 9$  Sv of CDW balanced by an export of cooler AABW from the Weddell Sea.

One way to get a feeling for the uncertainty in these transport estimates is to examine the sensitivity of the results to the initial model assumed. In Fig.'s 3.7 and 3.8 the results of running the model with initial reference levels at 700 db and the bottom, respectively, are summarized. The solution norm is increased significantly in both cases, as either choice leads to an initial state that is far from satisfying the constraints (e.g. with an initial reference level at 700 db the transport through Drake Passage is  $>100$  Sv to the west). However, the transports differ from the standard model by only a few Sverdrups. In particular, the main results discussed above are unchanged: a surplus of intermediate water enters the Atlantic in the ACC and is balanced by an increase in the transport of deep and bottom water leaving the basin; the ACC loses heat in crossing the Atlantic; and at  $32^\circ\text{S}$  there is an overturning cell of  $O(15$  Sv) which carries an equatorward heat flux of .13-.25 PW.

The export of BW from the Weddell Sea is also unchanged when different reference levels are used. In fact, the transport of CDW and BW across the Weddell-Scotia section varied by less than 1 Sv for all the models considered, demonstrating that fixing the heat flux places a strong constraint on the system. This section has particularly little freedom to partition the layer transports to carry this heat flux, since only the densest layers have a significant area at this latitude, and the temperature difference between them is small (Table 2.1, Fig. 2.4).

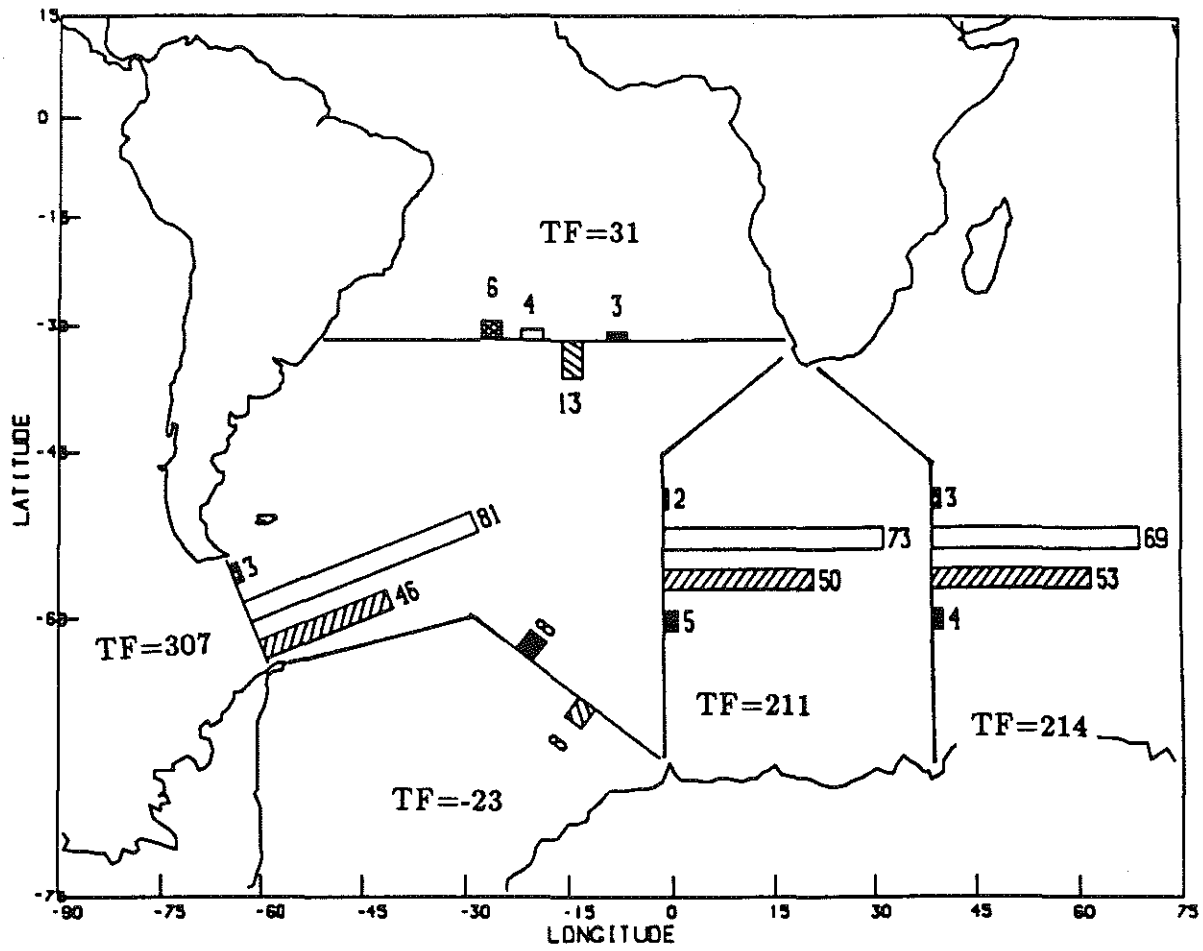
To test the sensitivity of the results to the value used, an experiment was run with the system forced to carry twice as much heat into the Weddell Sea. The results are shown in Fig. 3.9. The net export of bottom water is roughly doubled when the heat flux is doubled. The increased production of bottom water has relatively little effect on the transports in the rest of the basin, however. At Drake Passage and  $32^\circ\text{S}$  the transports are the same as in the standard case, while at  $0^\circ$  and  $30^\circ\text{E}$  the flux of deep



Reference Level = 700 db

$$b^T b = 10,480$$

Fig. 3.7 Circulation cartoon for model with initial reference level at 700 db.



Reference Level at the Bottom

$$b^T b = 2500$$

Fig. 3.8 Circulation cartoon for model with initial reference level at the bottom.

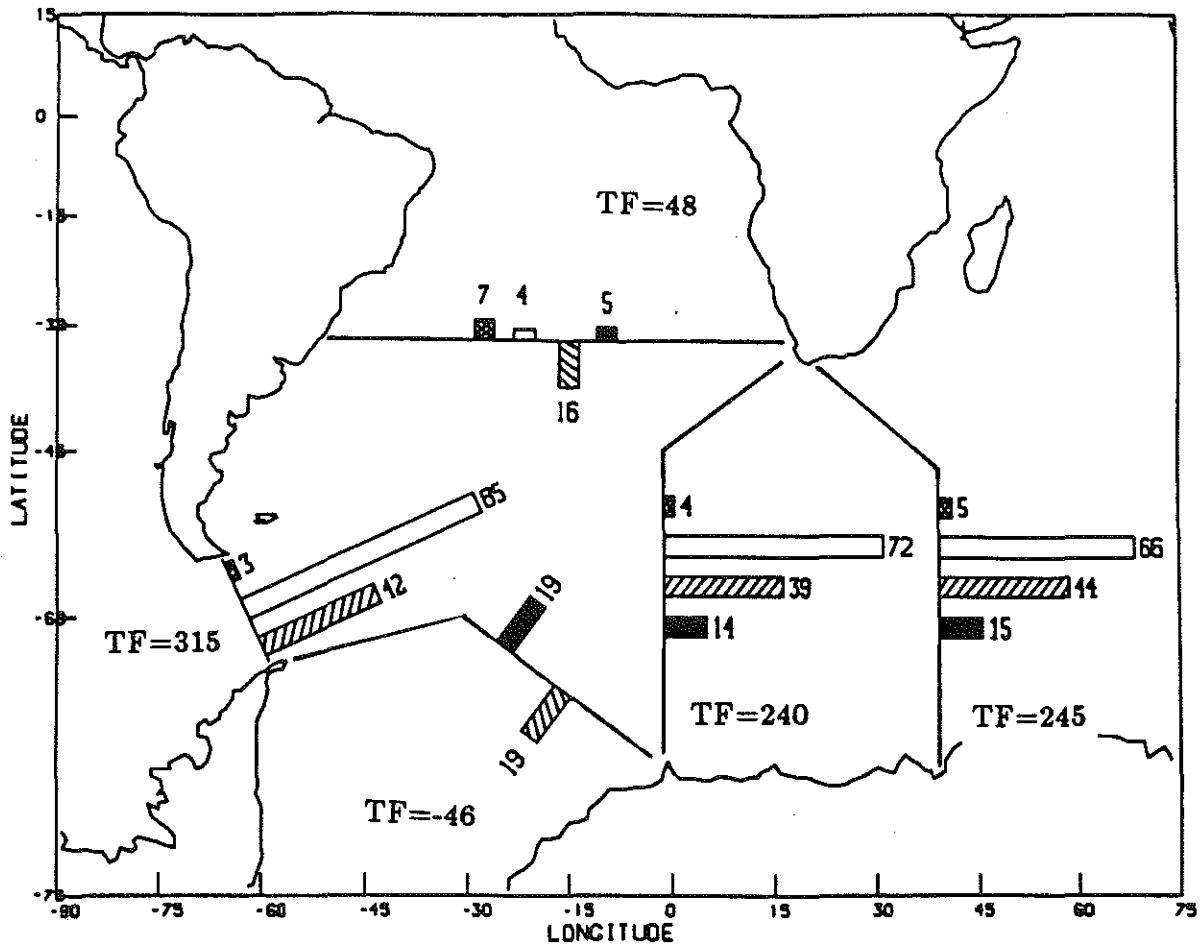
water is decreased to compensate for the increased export of bottom water, but the sum of the deep and bottom water transports is unchanged. The divergence of heat in the ACC is only slightly changed, since the temperature difference between the deep and bottom water layers south of Africa is small.

### 3.3 Interpretation of the Residuals

The stability of the solution to significant changes in the initial model assumed suggests that these results are relatively robust. Another important step in any inverse analysis is examination of the residuals. If the model is consistent with the data then the residuals should appear to be randomly distributed. If there is systematic structure to the residuals, it is an indication that the physical model used is inadequate. The residual structure itself can often be used to identify the important physics missing from the model.

The mass residuals in regions I and III are shown in Fig. 3.10. For each layer the residuals are small and appear randomly distributed, suggesting that the model is indeed sufficient to account for the observations. Also shown in Fig. 3.10 is a second set of residuals, which give the imbalance left in each layer by the “horizontal” advection terms alone. When the mass flux carried by the cross-isopycnal transfer term is removed, the deep layers are still roughly in balance but layers 2 and 3 show large residuals of opposite sign in region I. The “upwelling” across the interface between these two layers is the only  $w^*$  term that carries a significant mass flux (5 Sv). Indeed, allowing transfer across this isopycnal is essential to find a consistent solution: an experiment in which the  $w^*$  term was removed from the mass conservation equations resulted in a solution that could not balance mass without unreasonably large reference level velocities.

In Chapter 1 it was mentioned that although  $w^*$  enters the mass conservation equations as a velocity-like term, it is properly interpreted as a proxy for the net effect



Weddell Sea Heat Flux = .2 PW

Fig. 3.9 Circulation cartoon for the experiment with the heat flux into the Weddell Sea doubled to .2 PW.



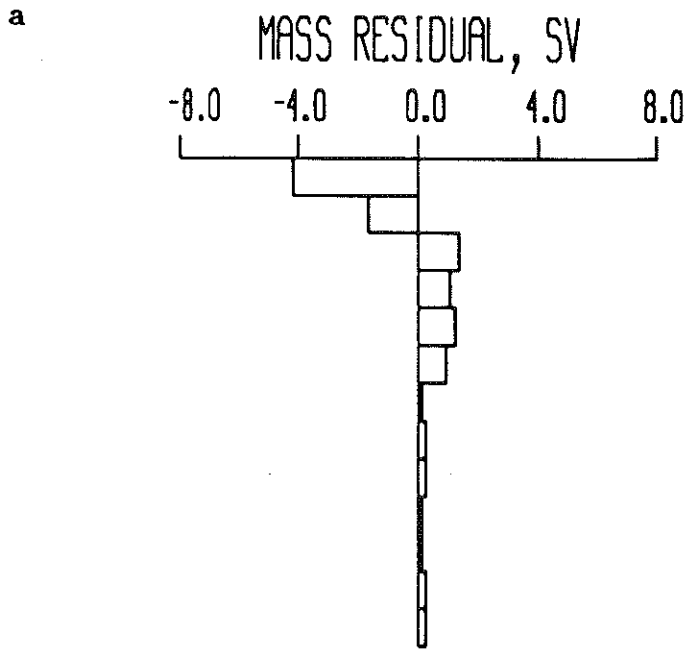


Fig. 3.10 (a) Mass residuals in each layer in region I for the standard model (Sv). (b) Mass residuals in region I from sum over "horizontal" advection terms alone.

of a variety of processes which may act to transfer mass across the layer boundaries. This transfer may be due to true upwelling in the ocean interior, or, for layers which outcrop within a box, it may be the result of air-sea interaction altering the density of water exposed at the sea surface. In this section I argue that the transfer from layer 3 to layer 2 found in this model reflects the latter of these two processes.

At first, the conversion of more dense water to less dense water in this part of the ocean seems counter to expectations: the South Atlantic has often been suggested to be a source region of intermediate water (Wüst, 1935; Taft, 1963; Kirwan, 1963), and one usually thinks of the ocean poleward of  $32^{\circ}$  to be an area where exchange with the atmosphere results in a net loss of buoyancy. However, there is some evidence that suggests this is not the case in the South Atlantic.

Bunker (1980) used ship meteorological observations and bulk formulae to estimate surface energy fluxes in the Atlantic. His map of net annual heat gain by the ocean is reproduced here in Fig. 3.11. Outside the narrow poleward extensions of the subtropical western boundary currents, the South Atlantic between  $30^{\circ}$  and  $60^{\circ}$ S is a region of net heat gain, in strong contrast to the North Atlantic. In particular, there is a broad, relatively weak maximum at  $50\text{-}55^{\circ}$ S,  $10^{\circ}$ W- $20^{\circ}$ E, and a stronger maximum related to the equatorward flowing Malvinas Current along the South American coast. Taylor *et al.* (1978) also found a region of oceanic heat gain between the Antarctic Divergence and the Polar Front.

The difference in the pattern of heat gain in the two basins is primarily due to the large volume of warm water carried to high latitudes by the near-surface currents in the North Atlantic. Although both oceans gain a similar amount of heat through radiation, the warmer North Atlantic evaporates more easily and experiences a much larger latent heat loss (Bunker, 1980). The larger land area in the Northern Hemisphere also contributes to the high latent heat loss through outbreaks of cold, dry continental air over the North Atlantic.

Annual Heat Gain  
by the Ocean  
 $W m^{-2}$

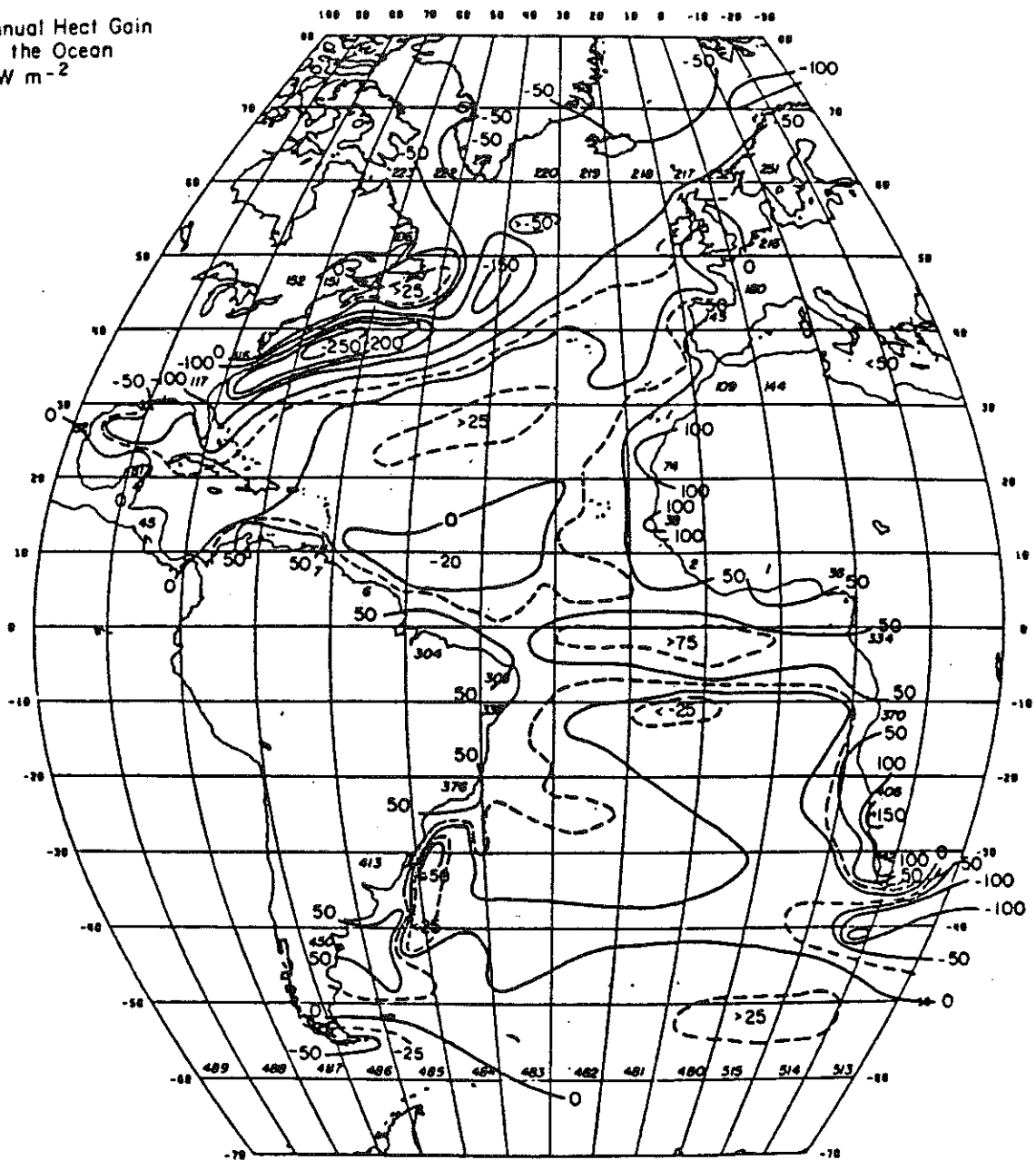


Fig. 3.11 Net annual heat gain for the Atlantic Ocean, from Bunker (1982) ( $W m^{-2}$ ).

In Fig. 3.12 I have roughly indicated the extent of the outcrop area of layer 3 by highlighting the bounding isopycnals on the map of potential density at 100 m from Gordon and Molinelli (1982). Comparison of the two figures shows that layer 3 outcrops over a large area that corresponds closely to the area of heat gain on Bunker's map, including the strong maximum near South America. Moreover, the strong westerly winds in this region (Fig. 3.13, also from Bunker (1980)) drive an equatorward Ekman flow near the surface. Note that the maxima in the wind stress and the heat gain maps occupy the same longitude band but that the heat gain extremum is displaced to the south: south of the wind stress maximum the net divergence of mass in the Ekman layer causes upwelling of cooler water to the surface, which in turn results in a larger heat gain by the ocean.

The fact that the ocean south of the wind stress maximum is a region of net heat gain is not surprising. If the pattern of annual mean near-surface temperature is to remain steady despite Ekman suction of colder waters from below, and equatorward transport of these waters in the Ekman layer, there must be a source of heat. In the North Atlantic it appears that the heat is supplied by horizontal advection of relatively warm waters from the south; that is, the near-surface flow, consisting of the sum of the Ekman and geostrophic flow, has a significant poleward component. In the South Atlantic the poleward penetration of warm water is blocked by the strong zonal flow of the ACC and the necessary heat must be supplied by the atmosphere.

Thus, the (admittedly scarce) meteorological evidence supports the notion that in this density range the net effect of air-sea interactions is to warm the surface waters and drive them to the north. While this is not a demonstration of the existence of such a water mass modification mechanism, a rough calculation shows that the numbers are reasonable. To warm 5 Sv of water entering the South Atlantic through Drake Passage at an average temperature of  $4.2^{\circ}\text{C}$  in layer 3 to layer 2 water with an average temperature of  $10.2^{\circ}\text{C}$  (the average temperature of the isopycnal bounding layers 2 and

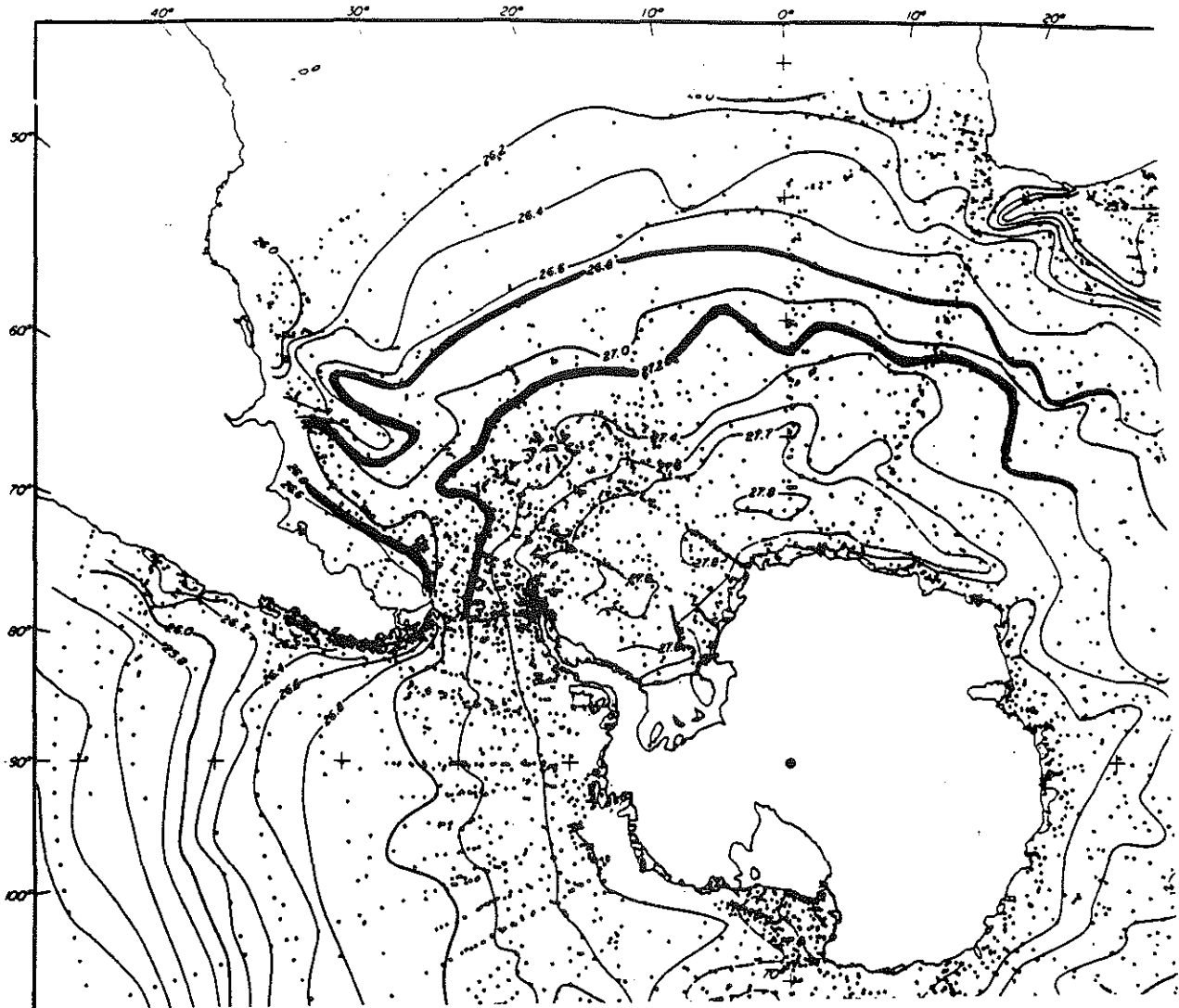


Fig. 3.12 Potential density at 100 m from Gordon and Molinelli (1982). Isopycnals bounding the outcrop area of layer 3 ( $26.8 < \sigma_0 < 27.2$ ) are highlighted.

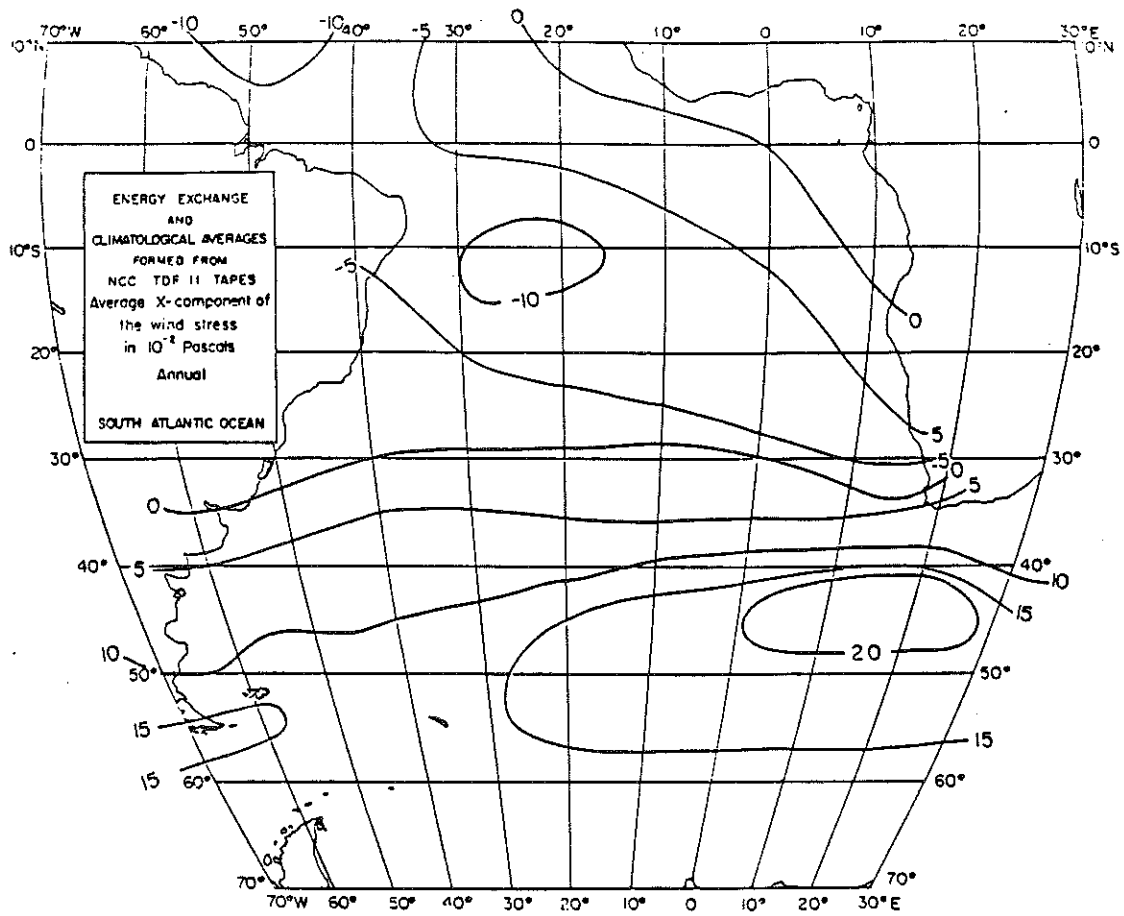


Fig. 3.13 Annual average x-component of the wind stress ( $10^{-2}$  Pascals) from Bunker (1982).

3 at 32°S) requires .12 PW, or about  $19 \text{ W m}^{-2}$  over the outcrop area of layer 3. This value is of the same order of magnitude as the estimates of Bunker and Taylor *et al.* for this region.

Another possibility is that water with the properties of layer 2 is produced by cooling water in layer 1. McCartney (1982), Gordon (1981) and others have suggested that the Brazil-Malvinas confluence is a region of active subtropical mode water formation. Warm core rings spawned by meanders of the Brazil Current undergo strong cooling in the winter, and the resulting deep convection produces a water mass with properties close to the average properties of layer 2 at 32°S. A similar process seems to be an important thermocline ventilation mechanism in the North Atlantic, where Schmitt and Olson (1985) estimated that winter cooling of warm core rings could result in 1/5-3/4 of the ventilation of the  $\sigma_\theta=26.5\text{-}27.0$  surface due to Ekman pumping. However, the volume of modified South Atlantic Central Water produced is not known, and depends on the number of warm core rings present each winter. Moreover, this mechanism does not explain the structure of the residuals, as there is no excess layer 1 water from which to produce denser mode water, and the deficit in layer 3 is still unaccounted for.

The suggestion, then, is that the surplus of upper thermocline water leaving region I across 32°S over that entering through Drake Passage is locally produced through interaction with the atmosphere. The strong westerly winds along  $\approx 50^\circ\text{S}$  in the South Atlantic drive an equatorward Ekman drift and divergence in the surface layers. Cool water brought to the surface by Ekman suction is warmed by the atmosphere and made less dense as it moves to the north. A second mechanism, involving strong cooling of warm water carried poleward by the western boundary current, may also play a role but does not explain the structure of the residuals. A verification of the importance of this mechanism will have to await better estimates of the wind stress and the air-sea heat flux based on many more observations.

## 4. Discussion

In this section the results of the standard model are compared to the results of other investigators. Since the problem is underdetermined, the standard model represents only one of an infinite set of consistent solutions. We will see that one of the advantages of the inverse machinery is that the range of possible solutions can be explored by varying the model assumptions, and by explicitly testing whether specific hypotheses are consistent with the data. This is particularly useful in this case to gain insight into the mechanisms responsible for the meridional heat flux at 32°S, and to study the global thermohaline cell associated with the formation of NADW.

### 4.1 *Water Mass Transports*

The results of the standard model presented in the last section show that although the total transport at each crossing of the ACC is the same, the flux of individual water masses across each of these sections is not equal. A surplus of intermediate water enters the Atlantic through Drake Passage which is balanced by a larger flux of deep and bottom water out of the basin south of Africa. The CDW occupies a large area of each of the meridional sections and is the principal water mass of the ACC by volume (Whitworth and Nowlin, 1987). For this reason, the relatively thin intermediate water layers have generally received less attention. However, because the strongest flows are concentrated in the upper layers at the northern edge of the current, the IW is actually the dominant water mass in terms of transport. At Drake Passage, for example, the transport of IW is nearly twice that of the CDW.

The shift in transport in the ACC from intermediate to cooler deep and bottom water layers results in a smaller heat transport at 0° and 30°E than at Drake Passage, and a net heat divergence of  $\approx .25$  PW in the Atlantic. Note, however, that this heat divergence is not due to local cooling of waters in the ACC. In fact, summing the heat flux across each of the four sections bounding region I implies that the ocean gains a



small amount of heat (.1 PW) from the atmosphere in this area. The heat divergence caused by the increased flux of deep and bottom water relative to the warmer layers actually reflects the heat lost by the ocean in the deep water formation regions at high latitude.

The uncertainty in the heat divergence can be estimated in various ways. One statement of the error is the difference between models with different initial reference levels. The range of values found using reference levels from 700 db to the bottom was .06 - .40 PW. These numbers do not represent real extremes - one could start with an initial state even further out of balance and perhaps find a divergence outside this range - but they suggest that the heat divergence has been determined to within  $\pm(.15-.20)$  PW.

As discussed in Section 3, with the available information we have not fully resolved the velocity field. To the extent that the unresolved components of the flow make a significant contribution to the heat flux, our estimates will be in error. An estimate of the resulting uncertainty can be made by considering the projection of the total heat content onto the vectors of the null-space, as shown by Wunsch *et al.* (1983). The details are shown in the Appendix. In this case, as for most of the sections considered in this study, the projection onto the null-space is small. In other words, the depth-integrated temperature varies along each section primarily on the broad scales we have resolved. A  $1 \text{ cm s}^{-1}$  rms increase in the reference level velocity at Drake Passage,  $0^\circ$  and  $30^\circ\text{E}$  would result in a change in the heat flux across the section of .010, .012 and .013 PW, respectively.

A more difficult source of error to evaluate is that due to the aliasing of time variability by combining hydrographic sections taken in different years. (Due to the harsh working conditions in the Southern Ocean, each of the sections used was collected during the same season: austral summer.) Given the significant variability described in the Introduction, this might be particularly important in the ACC. However, the work

of Whitworth (1980), Wearn and Baker (1980) and the analytical model of Clarke (1982) suggests that the baroclinic field varies on long time scales. Georgi and Toole (1982) noted that the standard deviation of the volume-transport-weighted mean potential temperature and salinity for seven sections across Drake Passage was only  $.07^{\circ}\text{C}$  and  $.012 \text{ ‰}$ , also suggesting that the baroclinic field was stable on the time scale of 5-10 years. The barotropic component of the transport varies on much shorter time scales (Whitworth, 1980; Wearn and Baker, 1980) but the capacity of the barotropic flow to contribute to the heat divergence is limited, since the temperature difference between each section is fairly small. For example, the volume-transport-weighted temperature is  $\approx .6^{\circ}\text{C}$  lower at  $0^{\circ}\text{E}$  than at Drake Passage. A change in transport of the ACC by 80 Sv is thus required to change the heat divergence by .2 PW.

The flux of BW out of the Weddell Sea was effectively set in this model by imposing the net heat flux across the Weddell-Scotia section. Without this constraint some of the solutions showed features that were believed to be unrealistic (e.g. BW was consumed rather than produced in the Weddell Sea). Setting the heat flux was chosen to be the least restrictive way to include the *a priori* information that the Atlantic should be a net producer of BW. A heat loss of .1 PW results in an export of 9 Sv of BW ( $\Theta < 0^{\circ}\text{C}$ ) in the standard case; doubling the heat loss roughly doubles the transport.

This estimate lies between the large values suggested by the box budgets and a few velocity observations, and the much smaller numbers implied by the dynamical bottom water formation models. Carmack and Foster (1975) estimated the transport across a transect of the Weddell Sea just to the west of this section by referencing geostrophic calculations to several short-term (.97 - 354 hours) current meter observations across the gyre. They found a total outflow of 97 Sv from the Weddell Sea, with 16 Sv of water colder than  $-0.7^{\circ}\text{C}$ . It is difficult to know how much confidence to put in estimates based on records of such short duration, however. A significant fraction of the total transport in fact relies on a bottom velocity measurement of  $2.9 \text{ cm s}^{-1}$  from the .97

hour record in the center of the gyre. Heat and salt budgets using box models also tend to support large (20-50 Sv, Gordon, 1975) fluxes of BW out of the Weddell Sea. The models of Gill (1973), Killworth (1973) and Foster and Carmack (1974), on the other hand, suggest that only a small flux of very dense water can leave the continental shelf to mix with less dense water in the interior and form the water mass that actually leaves the Weddell Sea. How much entrainment, and hence net outflow, to expect in this case is unknown, but it is unlikely to be as large as the box model estimates.

The surplus intermediate water entering through Drake Passage leaves region I to the north across 32°S. However, the results suggest that some of the intermediate water is modified by interaction with the atmosphere before reaching 32°S, as discussed in the end of Section 3. Roughly 5-6 Sv of layer 3 water is converted to layer 2 water, apparently by heating of cool water carried to the north in an Ekman flow driven by the strong zonal winds.

The northward flow of intermediate and thermocline water, and a small flux of BW, across 32°S balances the export of NADW. The return flow is roughly equally partitioned between the upper layers and the IW and BW layers in each of the models considered. The general pattern of the surface and mid-depth circulation is known from maps of dynamic topography constructed from historical data to consist of an anticyclonic gyre with poleward flow along the western boundary, mostly zonal flow along 32°S in the interior and equatorward flow near the eastern boundary (Defant, 1941; Montgomery and Pollock, 1942; Buscaglia, 1971; Reid *et al.*, 1977; Tsuchiya, 1985). These maps also show a return flow or recirculation just offshore of the western boundary current, analogous to the recirculation gyre of the Gulf Stream system (Tsuchiya, 1985; Worthington, 1976). Reid *et al.* (1977) suggest that the anticyclonic gyre is reflected in the dynamic topography field to depths of 3000-3500 m.

The velocity section in Fig. 3.2d is consistent with this picture, showing strong boundary currents in the east and west and weak alternating flows in the interior.

(The more recent maps included the section used here so the consistency is expected.) The poleward flow extending from the sea surface to the bottom along the western boundary has traditionally (and arbitrarily) been divided into two currents: the Brazil Current in the upper layers, corresponding to the western boundary current of the wind-driven subtropical gyre, and a deep western boundary current resulting from the thermohaline circulation. Reid *et al.* (1977) call the flow above 1000 m the Brazil Current, while Gordon and Greengrove (1985) used 1400 m as the lower boundary. In the standard model, the total top-to-bottom transport in the western boundary current is 63 Sv; of this, 33 Sv is returned to the north in the counterflow offshore. Above 1400 m (layers 1-5) the transport is 44 Sv in the Brazil Current with 22 Sv returned in the return current. Gordon and Greengrove (1985) found somewhat smaller values at 38°S: 19 Sv of poleward flow which was nearly compensated by equatorward flow in the return current. The Sverdrup calculation of Hellerman and Rosenstein (1983) suggests, however, that the maximum poleward transport should be at about 30°S, which may in part explain the larger values found here.

The current system along the eastern boundary is more difficult to define than that in the west. Lutjeharms and Stockton (1987) describe the region off the southwest coast of Africa as an "extensive field of upwelling filaments, streamers, etc., establishing a cold water archipelago with an abundance of long frontal lines and eddies." Hart and Currie (1960) distinguish between a narrow coastal current and a broad offshore oceanic current flowing in the same direction. In addition to making a distinction between the near-shore and open ocean components of the northward flow, it is common to refer to only the flow in the upper layers as the Benguela Current. Wooster and Reid (1963), for example, defined the northward flow above 1000 m and within 1000 km of the coast to be the Benguela Current and estimated a transport of 15.7 Sv at 28.5°S using the *Meteor* data.

The velocity section at 32°S (Fig. 3.2d) shows strong equatorward flow in several narrow jets reaching to near the bottom, separated from each other by bands of poleward flow. For comparison to the Wooster and Reid estimate, the transport above 1000 m and within 1000 km of the coast is 28.7 Sv; the top-to-bottom transport through this part of the section is 40.3 Sv to the north.

As mentioned in the Introduction, the path by which the intermediate water enters the Atlantic from the Southern Ocean has been a topic of debate for several decades. The early view was that the northward flow of AAIW was concentrated along the western boundary (e.g. Wüst, 1935). Later, several investigators concluded on the basis of maps of dynamic topography that the AAIW followed the coast only as far as the Brazil-Malvinas Confluence at 40°S, there turning to the east and following the path of the anticyclonic subtropical gyre into the South Atlantic (Martineau, 1953; Reid, 1965; Buscaglia, 1971). The first direct velocity measurements (Evans and Signorini, 1985), however, showed northward flow of AAIW near the coast at 23°S, supporting the earlier ideas of Wüst at least at this latitude.

The results of this model suggest that both paths may be important. As mentioned above, immediately adjacent to the western boundary poleward flow extends to the bottom in the Brazil Current and deep western boundary current. However, just offshore there is a return flow to the north above 1200 m. Of the 24 Sv carried to the south in layers 3-5 in the Brazil Current, half is compensated by this return flow. The most intense salinity minimum signal of the AAIW is in fact found just offshore of the Brazil Current (Fuglister, 1960). The net flux of water in this density range in the interior is weakly to the north (1 Sv). Further east, 16 Sv of IW is carried to the north by the strong flows near the eastern boundary, resulting in a net flux of 5 Sv to the north across the section. Note that the net flux across the section is a relatively small residual of the strong flows in the opposing boundary currents. The minimum salinity values found in the equatorward flow in the east are .1 ‰ higher than in the western

part of the section. This may be indicative of mixing with the more saline waters above and below this layer as the intermediate water crosses the Atlantic from Drake Passage south of 32°S. Thus the transport of IW across 32°S occurs primarily in narrow flows near the boundaries, with the northward flow near the western boundary found just seaward of the Brazil Current, rather than as a counterflow beneath the core of the surface current.

The deep poleward flow along the western boundary is broader and weaker than the Brazil Current itself and accounts for most of the net NADW transport. The limits of the current are not easy to define, but the transport in layers 6-10 in the band of poleward flow near the coast is 19 Sv. The weak eddies in the interior of the western basin result in a small flux (2 Sv) to the north. In the eastern basin there is predominantly southward flow of deep water ( $\approx 11$  Sv) above and to the east of the Mid-Atlantic Ridge, which is compensated by a northward flow within 1000 km of the African coast. At abyssal depths in the Cape Basin there is a cyclonic gyre carrying  $\approx 3$  Sv.

#### 4.2 *The Meridional Flux of Heat across 32°S*

The overturning cell at 32°S discussed above results in an equatorward heat flux of .25 PW in the standard model. This estimate can be compared to the estimates of other investigators in Table 1.1 and Fig. 4.1. The range of values is very broad, from a minimum of .04 PW (Hsiung, 1985) to a maximum of 1.15 PW (Hastenrath, 1980). (Interestingly enough, both of the extreme values are calculated by similar bulk-formula integrations of air-sea exchange estimates.) The heat flux found in the standard case falls toward the low end of this range. The projection of the total heat content onto the null-space vectors for this section is small (<2%) suggesting that the potential contribution of the unresolved components of the flow to the heat flux is also small. Experiments run with different initial reference levels confirmed this point: using 700 db and the bottom as initial levels resulted in slightly smaller heat fluxes, showing that the heat flux estimate is stable in the sense of not being sensitive to the choice of initial model. Alternatively, one can use the inverse machinery to explore the consequences of forcing the system to accommodate a larger equatorward heat flux.

The model was run again with the addition of constraints forcing the system to carry a specified heat flux across 32°S. The constraint requiring that there be no net mass flux across this latitude was upweighted slightly to ensure that the system did not satisfy the heat flux constraint by simply carrying a net flux of mass to the north. All other constraints were as in the standard model.

The results obtained when the heat flux is set equal to Hastenrath's (1982) estimate of .69 PW are shown in Fig. 4.2. Satisfying the heat flux constraint requires an increase in energy of the reference level velocity by a factor of five. In particular, increasing the heat flux to .69 PW requires a much more vigorous overturning cell at 32°S, and the export of NADW is increased from 17 to 27 Sv. The compensating equatorward flow is still roughly evenly split between the thermocline and intermediate layers.

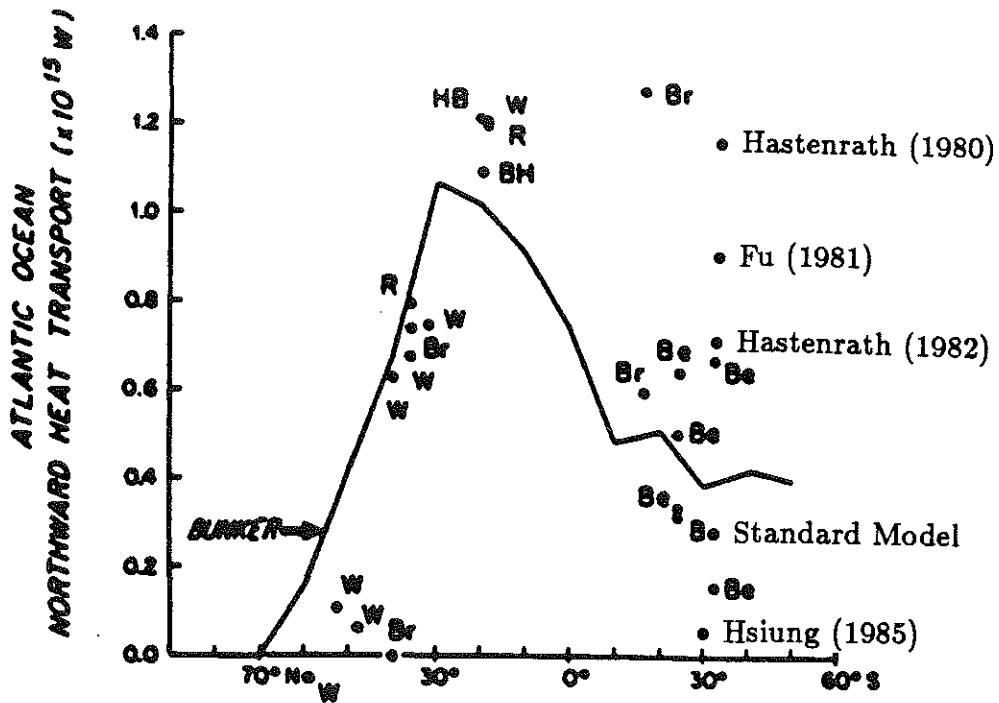
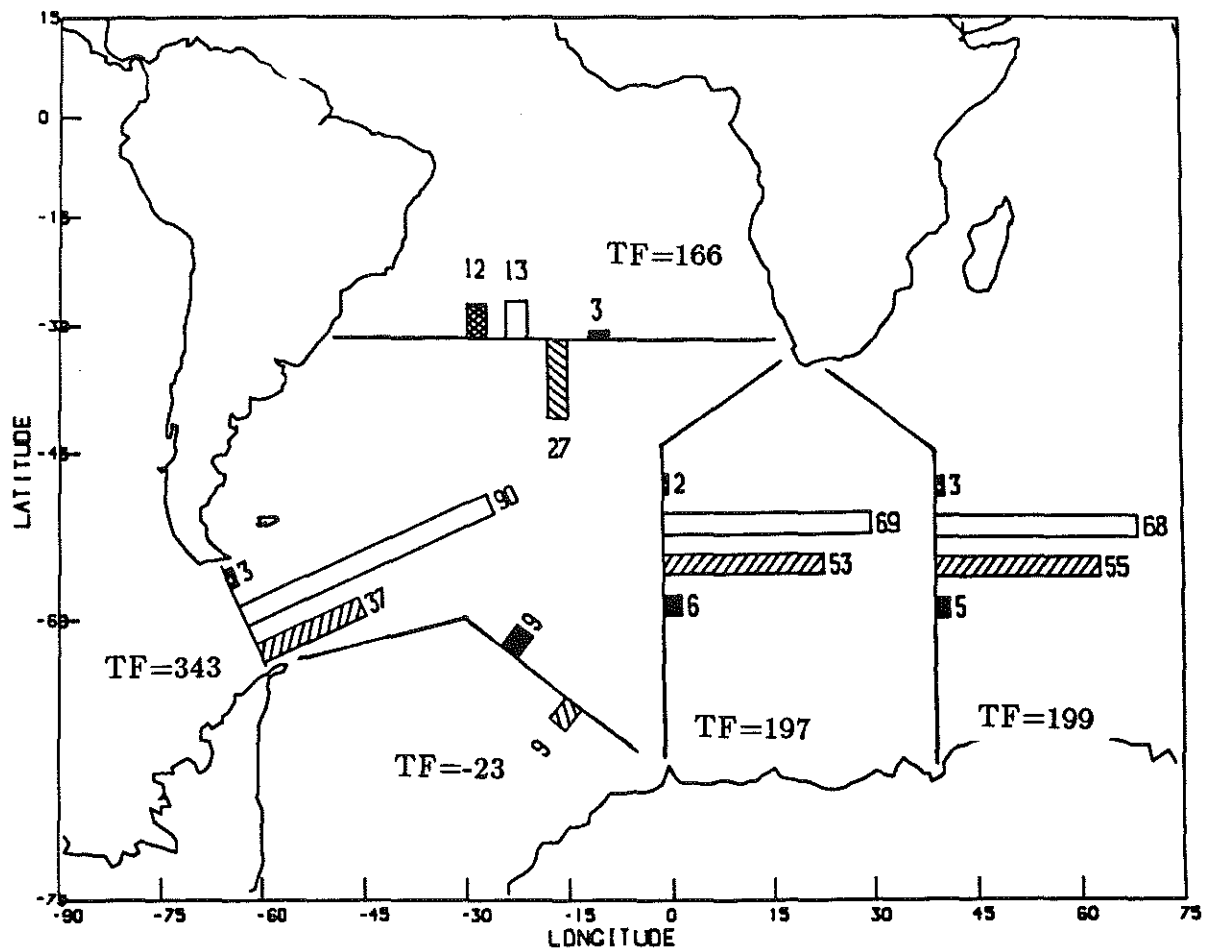


Fig. 7. Northward ocean heat transport ( $\times 10^{15}W$ ) in the Atlantic Ocean, derived from integrating BUNKER'S (1980) air-sea exchange values (see Fig. 2). Single points are values obtained by authors using the direct method: Be, BENNETT; Br, BRYAN; BH, BRYDEN and HALL; HB, HALL and BRYDEN; R, ROEMMICH; W, WUNSCH.

Fig. 4.1 Meridional heat transport, based on Fig. 7 of Hall and Bryden (1981).





32°S Heat Flux = .69 PW

$$b^T b = 6300$$

Fig. 4.2 Circulation cartoon for the experiment with the heat flux across 32°S fixed at .69 PW (Hastenrath, 1982).

The transports at the sections crossing the ACC reflect the increased production rate of NADW implied by the stronger overturning cell. The divergence of IW in the ACC between Drake Passage and  $0^{\circ}\text{E}$  is increased to 21 Sv, 11 Sv of which must be converted to surface or thermocline water before leaving the box to the north across  $32^{\circ}\text{S}$ . Thus increasing the export of heat across  $32^{\circ}\text{S}$  requires an increase of  $\approx .1$  PW in the net heating of the ocean by the atmosphere in region I. The large flux of NADW entering region I at  $32^{\circ}\text{S}$  turns to the east and leaves the basin as part of the ACC. In the upper layers, the net flow is slightly decreased in magnitude at  $0^{\circ}$  and  $30^{\circ}\text{E}$  but is still to the east.

These changes in the pattern of mass transport divergences in various water masses alter the heat fluxes as well. To support the large flux of heat to the north across  $32^{\circ}\text{S}$  more heat is carried into the basin at Drake Passage and less is removed south of Africa. The difference in heat carried in and out of the basin by the ACC is thus increased to .6 PW from .2 PW in the standard case.

Further insight into how the system responds to the requirement for a larger heat flux can be gained by comparing the mass flux density at  $32^{\circ}\text{S}$  for the standard model and for the Hastenrath (1982) heat flux case. Fig. 4.3 makes the tight coupling between the magnitude of the heat flux and the strength of the overturning cell very clear. Note, however, that the relative contribution made by each water mass to the total transport remains roughly the same. The layer geometry evidently imposes strong limits on the response of the system to the requirement for an increased heat flux: the strength of the whole cell must be increased, rather than, for example, keeping the volume unchanged but maximizing the temperature difference by concentrating the flow in the warmest and coldest layers.

Another useful way to examine how the heat flux constraint is met is to compare the total mass transport integrated from west to east along the  $32^{\circ}\text{S}$  section (Fig. 4.4). The integrated transports differ substantially in the western basin. Specifically,

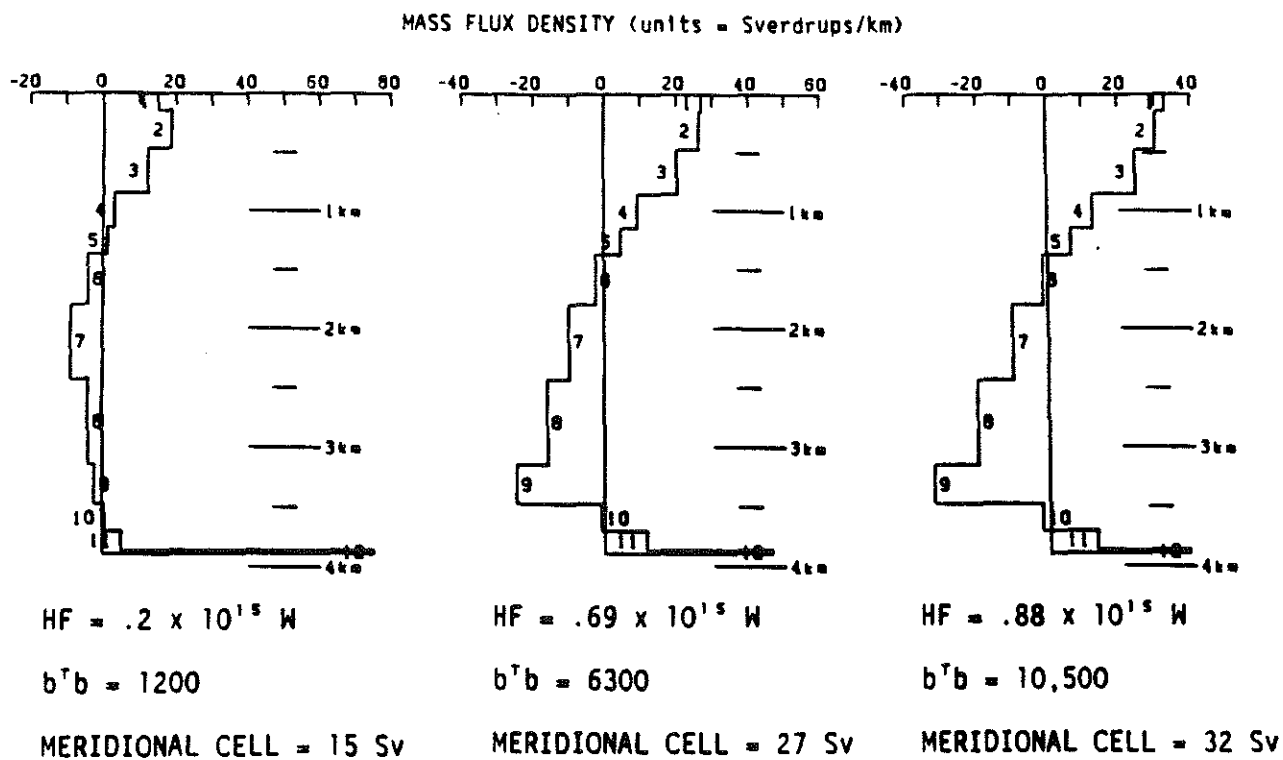


Fig. 4.3 Mass flux density at 32°S for (a) the standard case, (b) the .69 PW case and (c) the .88 PW case.

to satisfy the requirement for an increased equatorward heat flux, strong northward velocities at the reference level are introduced near the western boundary, decreasing the poleward flow of warm water in the Brazil Current. In the .69 PW case the net transport by the Brazil Current and the deep western boundary current is reduced by a factor of three. East of where the Walvis Ridge crosses the section the solutions are nearly identical because the constraint requiring no net flux of deep water across this portion of the section largely fixes the reference level velocities there. To balance the northward flow near the eastern boundary and keep the total transport equal to zero, the model including the heat flux constraint introduces strong southward flows between the Mid-Atlantic Ridge and the Walvis Ridge, where the depth-averaged temperature is low relative to that in the west. For this model, then, the primary path by which NADW leaves to the south is not along the western boundary, where the most intense salinity maximum water is found, but just east of the Mid-Atlantic Ridge.

Driving the meridional heat flux to the larger value of Hastenrath (1982) thus leads to dramatic changes in the circulation at  $32^{\circ}\text{S}$ . Satisfying the heat flux constraint requires a large increase in the solution norm and a much more vigorous overturning cell: a heat flux of .69 PW requires an export of NADW of 27 Sv. However, in both cases the return flow balancing the outflow of NADW is half surface water and half intermediate and bottom water.

Fu (1981) also found significantly higher heat transports across  $32^{\circ}\text{S}$  in his inverse calculation in the subtropical South Atlantic: .66 and .88 PW for initial reference levels at 2000 and 4000 db, respectively. Since both this model and that of Fu use the same IGY section at  $32^{\circ}\text{S}$ , and similar methods, the discrepancy at first seems surprisingly large. However, despite using the same section at this latitude and a similar inverse method, there are several important differences between the calculations. Fu's heat flux estimate includes an Ekman contribution of .28 PW, due to an equatorward mass transport of 5 Sv. Fu realized that this value was probably very uncertain, and

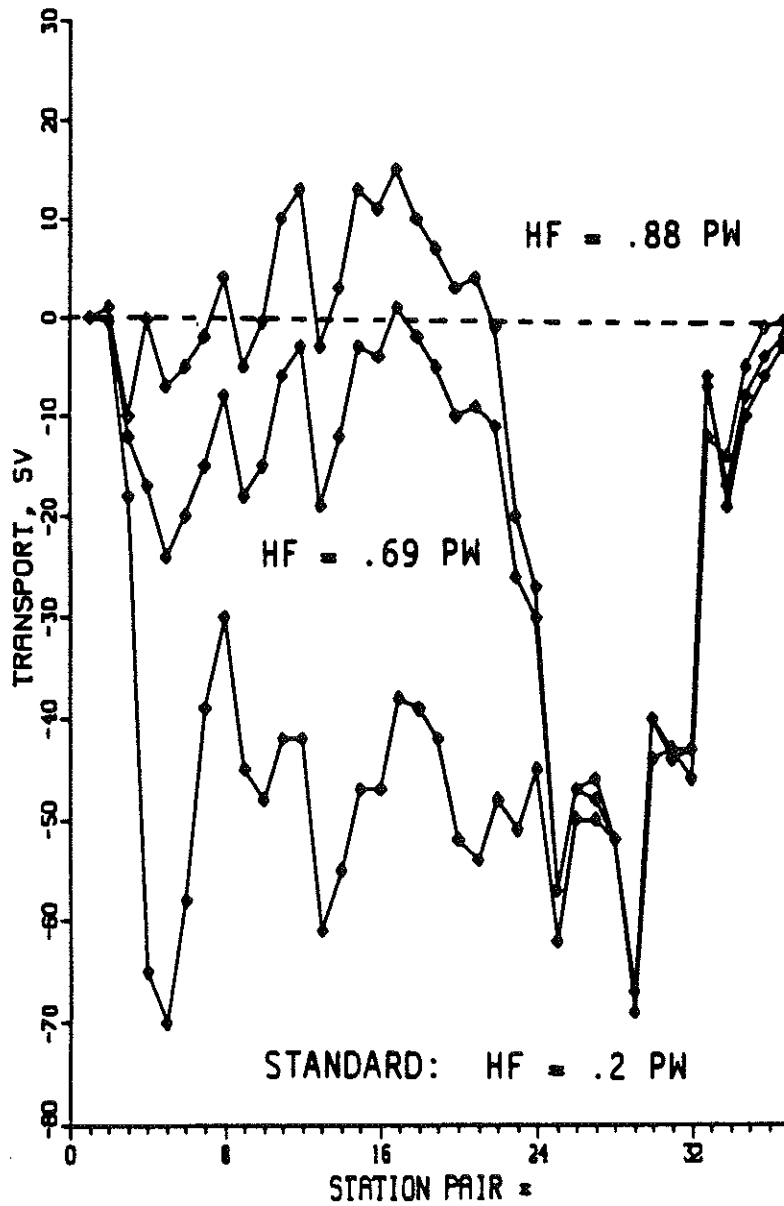


Fig. 4.4 Total mass transport integrated along 32°S from west to east for the standard case and the .69 PW case.

suggested it be taken as an upper bound, since it was based on the wind stress values of Hellerman (1967) which were thought to be overestimated (Saunders, 1976). The more recent compilations of Han and Lee (1981) and Hellerman and Rosenstein (1983) in fact suggest that the Ekman transport is less than 1 Sv to the north at 32°S.

A second way in which the standard model differs from that of Fu is in the addition in this case of a constraint forcing the net equatorward flux of BW across 32°S to be  $4 \pm 1$  Sv, as estimated by Hogg *et al.* (1982) from direct current observations. Fu found the net transport of BW to be about 1 Sv. By shifting a larger fraction of the equatorward flow to the relatively cold BW layers, the BW constraint effectively decreases the equatorward heat flux in the standard model. When the present model was run with this constraint removed the BW flux was reduced to 1 Sv and the heat flux was increased to .4 PW, close to the value Fu obtained for the geostrophic component of the heat transport (.38 PW, with the 4000 db reference level). Thus, the difference in the heat flux estimates of Fu (1981) and the standard model are due to Fu's overestimate of the Ekman contribution, and the addition of a constraint in the present model forcing the BW flow to be consistent with the Hogg *et al.* current meter results at 32°S.

### 4.3 North Atlantic Deep Water and the Thermohaline Circulation

Traditionally studies of the thermohaline circulation have focused on the process and rate of deep water formation. And yet the way in which this deep water returns to the upper ocean to close the global thermohaline cell is also an important part of the problem, as this may play a role in determining the rate at which the thermohaline "mill" grinds. If the ocean is in nearly steady-state, then deep water must upwell into the layers above at the same rate that new deep water is formed. This upwelling has generally been assumed to occur uniformly over the ocean basins, although there is no direct evidence that this is true, as the flow is too weak ( $O(10^{-5}) \text{ cm s}^{-1}$ ) to be observed with present technology. The bias toward emphasizing the sinking branch of the thermohaline cell has in part been due to these observational difficulties: at least one had some hope of measuring the transport at the overflows or in the deep western boundary currents. The recent work of Gordon (1985,1986), however, has rekindled interest in the path taken by the upwelled water as it returns to the North Atlantic to balance the export of NADW.

Gordon (1986) has proposed that this return flow occurs primarily within the warm upper layers of the ocean. In this scheme NADW reaching the Pacific upwells into the thermocline, flows westward through the Indonesian passages and across the tropical Indian Ocean, where it is joined by NADW upwelled into the Indian Ocean thermocline, and ultimately reenters the Atlantic via a branch of the Agulhas Current that does not complete the retroflexion. He suggested that the alternative "cold water path," in which the flow of NADW out of the Atlantic is balanced by water entering from the Pacific through Drake Passage, could account for no more than 25% of the return flow. Gordon's picture of the global thermohaline circulation is shown schematically in Fig. 4.5.

The idea of a "warm water path" did not originate with Gordon (Taft (1963), for example, suggested a similar circulation scheme) but he was evidently the first to

GORDON: INTEROCEAN EXCHANGE OF THERMOCLINE WATER

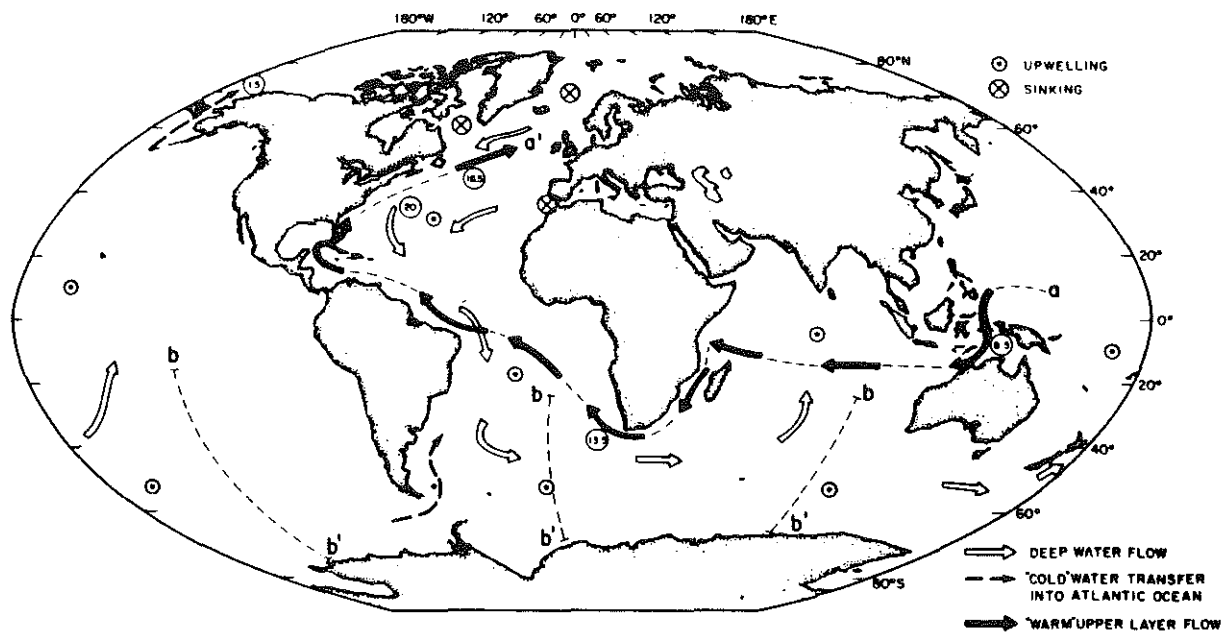


Fig. 2a. Global structure of the thermohaline circulation cell associated with NADW production. The warm water route, shown by the solid arrows, marks the proposed path for return of upper layer water to the northern North Atlantic as is required to maintain continuity with the formation and export of NADW. The circled values are volume flux in  $10^6$   $m^3/s$  which are expected for uniform upwelling of NADW with a production rate of  $20 \times 10^6$   $m^3/s$ . These values assume that the return within the cold water route, via the Drake Passage, is of minor significance.

Fig. 4.5 Fig. 2a. from Gordon (1986) showing schematic of warm water path.



appreciate the climatic implications. If the global cell associated with NADW formation is closed by a warm water return flow, then the thermoclines of the world's oceans may be more tightly coupled than anticipated. Gordon (1985) suggested that the "anomalous" equatorward heat flux in the South Atlantic was likely to be due to the injection of warm Indian Ocean water at the southeastern corner of the basin. Moreover, since key links in the warm water path (such as the Indonesian throughflow and the Agulhas leak) may be vulnerable to a range of local and basin-scale variability in the wind and other forcing fields, distant changes in the forcing may cause variations in the deep water formation rate.

Gordon called on a variety of evidence to support this hypothesis. The linchpin in his argument was a demonstration that the mean temperature of the water moving to the north to balance the export of NADW across 30°S was too warm to have come through Drake Passage. The temperature of the northward return flow was determined using the equations for the mass and heat flux across 30°S:

$$V_R = V_{BZ} + V_{NADW} - V_{BS}$$

$$V_R T_R = V_{BZ} T_{BZ} + V_{NADW} T_{NADW} + Q$$

where  $V$  and  $T$  are the mass flux and average temperature, respectively, of each component, denoted by the subscripts 'BZ' for the Brazil Current (10 Sv, 18°C); 'NADW' for the NADW outflow (16 Sv, 2°C); 'BS' for the Bering Strait inflow (1.5 Sv, 0°C); and 'R' for the northward return flow.  $Q$  is the equatorward oceanic heat flux.

Assuming these values for the transport and temperature of each water mass and Hastenrath's (1982) estimate of the heat flux (.69 PW), he found the mean temperature of the northward flow to be 15.4°C. Since the warmest water in Drake Passage is about 8°C (Gordon and Molinelli, 1982), he concluded "the bulk of the upper layer return

flow must reside within the thermocline. The only source for such water south of 30°S is the Indian Ocean thermocline water within the Agulhas Current.”

Although this argument seems feasible at first, a closer look makes it clear that there is an inconsistency somewhere. There is ample evidence both from the present study and those of earlier investigators that AAIW and AABW flow northward from their source regions and ultimately enter the North Atlantic (e.g. Wüst, 1936; Hogg *et al.*, 1982; Wright, 1970; Georgi, 1981; Buscaglia, 1971). Part of the southward flow of NADW is clearly balanced, then, by the northward flow of Antarctic water lying above and below the NADW layer. If we explicitly include reasonable estimates of the transport and temperature of these water masses and recalculate the mean temperature of the thermocline return flow, it is clear that something is wrong. Assuming a transport of 6 Sv of AAIW at a mean temperature of 3.5°C (Georgi, 1981) and 4 Sv of AABW at a mean temperature of 0°C (Hogg *et al.*, 1982), the mean temperature of the warm water return flow is 24.6°C. It is difficult to find water this warm south of 30°S, even in the Agulhas Current. If the mean temperature of the AAIW is pushed to an upper bound of 8.0°C the temperature of the warm return flow is still 22.7°C.

Of course, the fact that the temperature of the rest of the return flow is increased when the relatively cold intermediate water and bottom water are included in the calculation comes as no surprise: since some of the return flow occurs at depth, there is a smaller volume of water returning in the upper layers; as the transport decreases, the temperature must increase to carry the same heat flux. That the calculation in this case leads to such an impossibly high value for the mean temperature indicates that the case for the warm water path needs to be reexamined.

The results of the inverse models discussed above show where the inconsistency lies. In particular, the heat flux experiments showed that the heat flux across 32°S is tightly tied to the strength of the meridional cell. As a result, the magnitude of the heat flux and the transport of NADW cannot be specified independently. The flaw

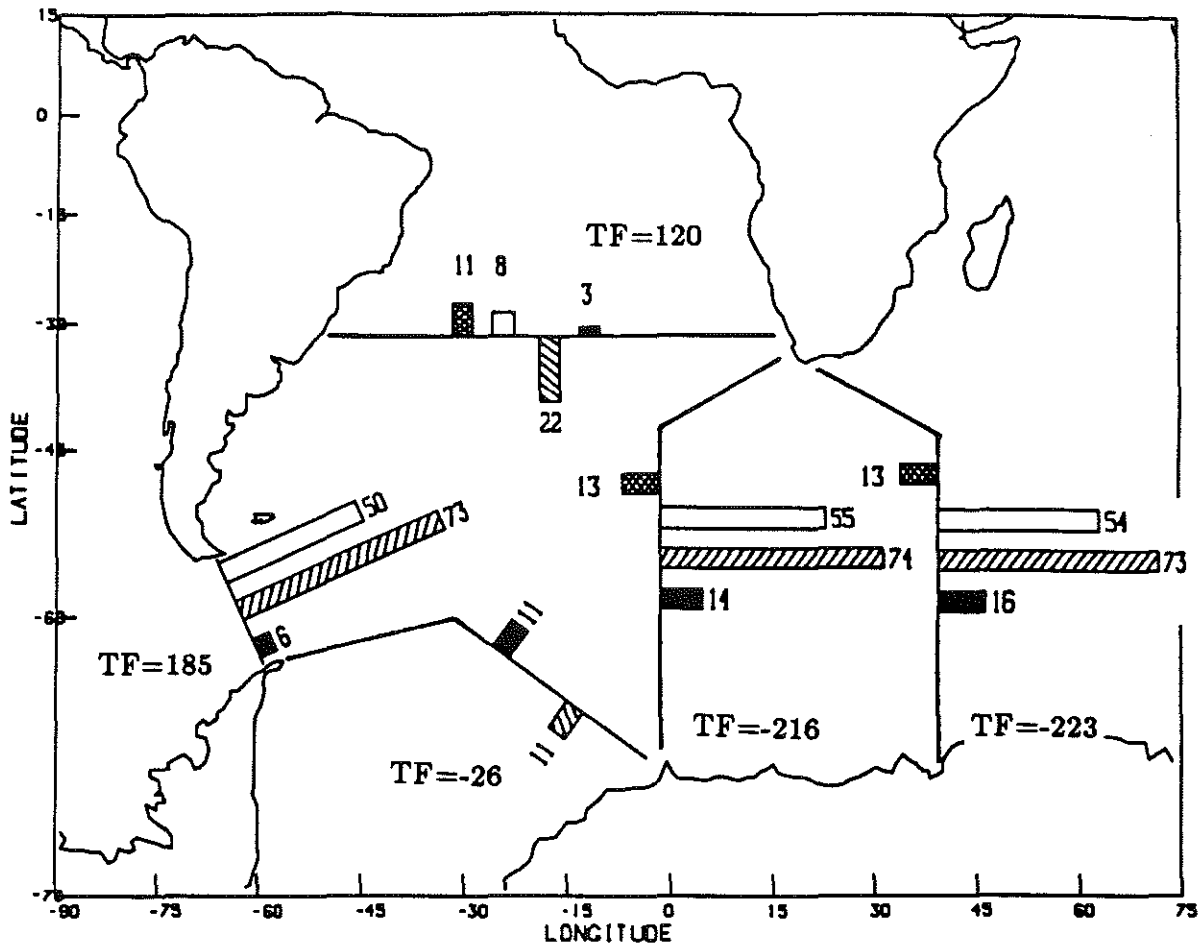
in the above box-model argument is that the values assumed for the heat flux and the NADW transport are not consistent with each other: if one insists that a weak meridional circulation carry a large heat flux, an unreasonably high temperature for the warm return flow is required.

The inversion results also showed that the northward flow of intermediate and bottom water from the Antarctic plays an important role in closing the meridional circulation: independent of the strength of the overturning cell, one half of the NADW leaving the Atlantic across 32°S returns at depth in these layers. None of the models showed a net import of warm Indian Ocean water into the Atlantic. Even when the system was forced to carry an equatorward heat flux four times that of the standard model the system responded by increasing the vigor of the overturning cell, not by boosting the influx of warm thermocline water from the Indian Ocean. In contrast, Gordon was led to formulate the “warm water path” hypothesis in part by his observation in 1983 of 13.5 Sv of Agulhas water entering the Atlantic between the coast and an Agulhas ring offshore (Gordon, 1985). To test directly whether the data set used here was consistent with a large inflow of Indian Ocean thermocline water, the model was run again with a constraint added forcing a net flux of 13 Sv to the west of warm water ( $\sigma_\theta < 26.8$ ; layers 1 and 2) across the 0° and 30°E sections.

The results of the warm water path experiment are summarized in Fig. 4.6. Forcing the system to carry a large flux of warm water into the South Atlantic requires an increase in the solution norm by an order of magnitude, and reference level velocities  $> 35 \text{ cm s}^{-1}$  near the African coast. To maintain a total transport across 0° and 30°E of 130 Sv, despite a net westward flow of warm water, requires an increase in the flux of deep and bottom water carried by the ACC of  $\approx 35$  Sv. These changes in the circulation lead to large changes in the heat flux, as well. Across 0° and 30°E the heat flux is reversed in sign, leading to a net convergence of  $> 1$  PW in region I in contrast to the small divergence found in the standard case. Such a large convergence of heat

is difficult to reconcile with the estimates of air-sea exchange discussed in Section 3 showing this part of the South Atlantic to be a region of weak heat gain. Furthermore, the residuals suggest that  $\approx 13$  Sv of deep water must be converted to intermediate water within region I, which requires a *gain* of heat from the atmosphere, not a large heat loss.

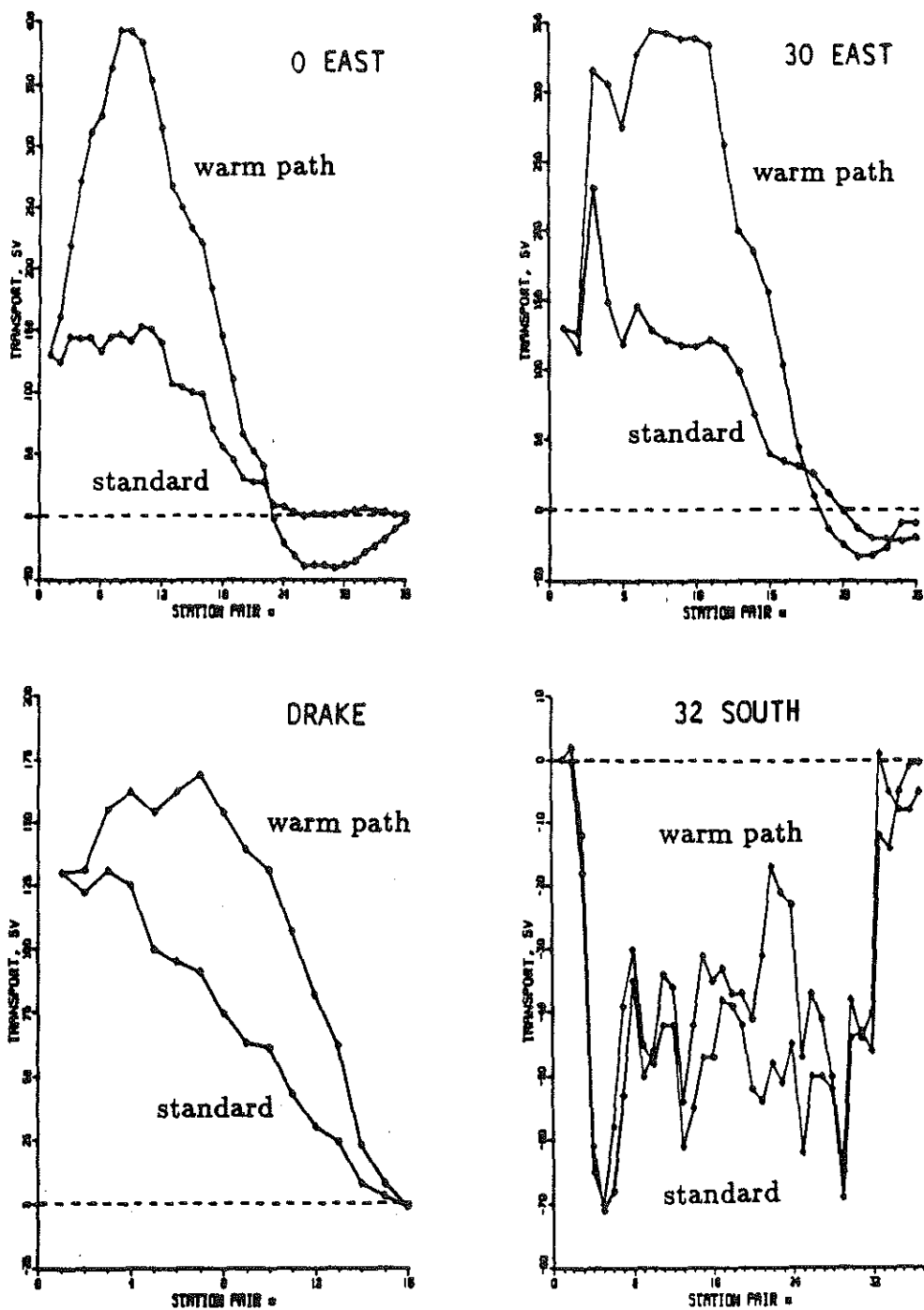
An even more dramatic illustration of the large changes in the flow field required to satisfy the constraint is provided by comparing the total mass transport integrated along each section in this model to the standard case (Fig. 4.7). To carry more warm water into the Atlantic across  $0^\circ$  and  $30^\circ$ E the system introduces reference level velocities to the west in the northern end of the sections, where these layers are thickest. In turn, eastward velocities are required in the southern half of the section to keep the total transport equal to 130 Sv. However, the upper layers are relatively thin and occupy only a small fraction of the water column (Fig.'s 2.3,2.5); reference level velocities sufficient to reverse the 4-6 Sv of eastward flow in these layers found in the standard case to a westward flow of 13 Sv carry an even larger transport of deep and bottom water to the west. The effect on the circulation is to introduce a recirculation of very large transport with westward flow in the north and eastward flow in the southern part of each section crossing the ACC. At Drake Passage, for example, the velocities are large enough to nearly reverse the transport of the strong jet associated with the Subantarctic Front. The transport across the first 8 station pairs of the  $0^\circ$ E section is more than 200 Sv to the west in this model, compared to roughly zero net transport for these pairs in the standard case. And at  $30^\circ$ E a reference level velocity of  $10 \text{ cm s}^{-1}$  to the west at the Agulhas and Agulhas Return Currents is sufficient to increase the transport of the former and decrease that of the latter by 70 Sv, leading to a net flux from these 3 station pairs alone of 150 Sv into the Atlantic. The pattern of total transport at  $32^\circ$ S is comparatively little changed.



Warm Water Path

$$b^T b = 17,400$$

Fig. 4.6 Circulation cartoon for the warm water path experiment.



### TEST OF WARM WATER PATH

Fig. 4.7 Total mass transport integrated from south to north along each section crossing the ACC for the warm water path experiment.

Imposing a large net transfer of thermocline water from the Indian to the Atlantic Ocean thus leads to unreasonable changes in the circulation, and the present data set appears to be incompatible with an interocean exchange of the magnitude required by the warm water path hypothesis. This does not mean, of course, that Indian Ocean water does not enter the South Atlantic. The constraint required that there be a net flux of warm water across the sections south of Africa: an arbitrarily large amount of warm water could enter the South Atlantic and return to the Indian Ocean within the same density range and not affect the constraint imposed. That is, the data are not inconsistent with the thermoclines of the two oceans being connected, as suggested by the similar  $\Theta$ - $S$  relation in each basin (McCartney, 1977; Gordon, 1981) and some numerical model results (de Ruijter, 1982; de Ruijter and Boudra, 1985). In fact, the velocity field found at 0°E in the standard case showed a strong jet of westward flow along the African coast with a top-to-bottom transport of 20 Sv. Whitworth and Nowlin (1987) found a similar flow in their dynamic calculations using this section and suggested that this was evidence supporting the warm water path. However, although 9 Sv are carried to the west in layers 1 and 2 in this jet, an even larger flux of water in these layers flows to the east south of this station pair, so that the net flux of thermocline water across the section is 4 Sv from the Atlantic into the Indian Ocean.

Furthermore, these results do not rule out intermittent exchange. Indeed, there is good evidence that some Indian Ocean water enters the Atlantic, but the magnitude and steadiness of the exchange is uncertain. Lutjeharms and Stockton (1987) in a recent review of the flow off Southern Africa claim that advection of Agulhas water into the South Atlantic occurs by two main mechanisms: in rings pinched off from the Agulhas Retroflexion, and in filaments apparently formed by shear-edge interaction along the inshore edge of the Agulhas Current. Chapman *et al.* (1986) concluded from oxygen and nutrient observations that the filaments did not penetrate below 50-200 m, and thus that their contribution to the total volume transport must be small. In

addition, Shannon (1985) showed that the "Agulhas water" apparently being advected into the Atlantic around the Agulhas Bank was not pure Indian Ocean water but rather contained a significant fraction of Atlantic water.

Eddies formed in the Agulhas Retroflexion region have frequently been observed to enter the South Atlantic using satellite data and satellite-tracked drifters (Harris *et al.*, 1977; Gordon, 1985; Lutjeharms, 1981; Olson and Evans, 1986). Olson and Evans (1986) estimate that one ring per year amounts to a transport of less than .5 Sv. Lutjeharms and van Ballegooyen (1987) concluded from a study of four years of daily satellite imagery that rings are shed from the Agulhas retroflexion loop at intervals of 1.5-2 months. If all rings formed enter the South Atlantic, this formation rate implies a transport of 3-4 Sv.

The impact of these eddies on the heat budget of the South Atlantic is not clear. Gordon (1985) described a ring found northwest of the retroflexion in 1983 (the "Cape Town Eddy") which had apparently formed at an earlier date and drifted toward the Atlantic. The core of the eddy was well-mixed and 100% oxygen saturated down to 250 m, suggesting that convection forced by strong winter cooling had reached to this depth. The resulting mode had the same  $\Theta$ -S properties as the South Atlantic thermocline waters. If the Indian Ocean water carried by rings can be effectively converted into South Atlantic water by air-sea exchange within the Retroflexion region, then the injection of Agulhas rings may not be as important to the South Atlantic heat and salt budget as anticipated from the characteristics of the eddies when formed.

The results discussed above demonstrate that a net exchange of thermocline water from the Indian Ocean to the South Atlantic is inconsistent with the present data set, at least of the magnitude suggested by Gordon (1986). Clearly, forcing the system to carry a smaller flux would result in less drastic changes to the system and perhaps a "reasonable" circulation could be found that included a net flux opposite in sign to that found in the standard case. I have not attempted to find an upper bound on



the net interocean exchange of warm water. In any case, the inverse models presented do show that a large import of warm water is not necessary to explain the observed "anomalous" equatorward heat transport in the South Atlantic. In the remainder of this section I present some additional (somewhat more circumstantial) evidence of the essential role played by the cold water path in the global thermohaline circulation.

The budget of freshwater in the Atlantic apparently requires a significant equatorward transport of intermediate water across 32°S, following an argument of Stommel (1980). Stommel noted that the shape of the  $\Theta$ -S relation imposed certain constraints on the meridional flux of heat and freshwater in the ocean. The mean  $\Theta$ -S curve for the subtropical South Atlantic is shown in Fig. 4.8. It is clear that, provided the  $\Theta$ -S curve is relatively tight, the transports of heat and freshwater carried by an overturning meridional cell are coupled. If the volume-transport weighted temperature of the equatorward return flow is warmer than about 10°C, then a line on the  $\Theta$ -S curve connecting this water with the poleward flow of NADW has a positive slope, implying that the meridional flux of freshwater is poleward. If the transport-weighted temperature of the return flow is  $\approx 15^\circ\text{C}$ , as suggested by Gordon (1986), then the transport-weighted salinity is much greater than that of the poleward flow, resulting in a large poleward flux of freshwater. Estimates of the net freshwater balance of the Atlantic using bulk formulae, on the other hand, suggest that the Atlantic as a whole *loses* freshwater to the atmosphere (Baumgartner and Reichel, 1975). To carry freshwater into the Atlantic across 32°S and balance the water budget the return flow must be sufficiently cold, and hence the contribution of the sub-thermocline water must be significant.

Broecker and Peng (1982) have also argued that the nutrient balance of the North Atlantic requires a contribution from the AAIW. Since there is no large source or sink of nutrients in the northern North Atlantic, the upper layer water feeding the NADW formation regions must have about the same nutrient concentrations as the NADW leaving. Broecker and Peng suggested that "the most likely candidate for the feed

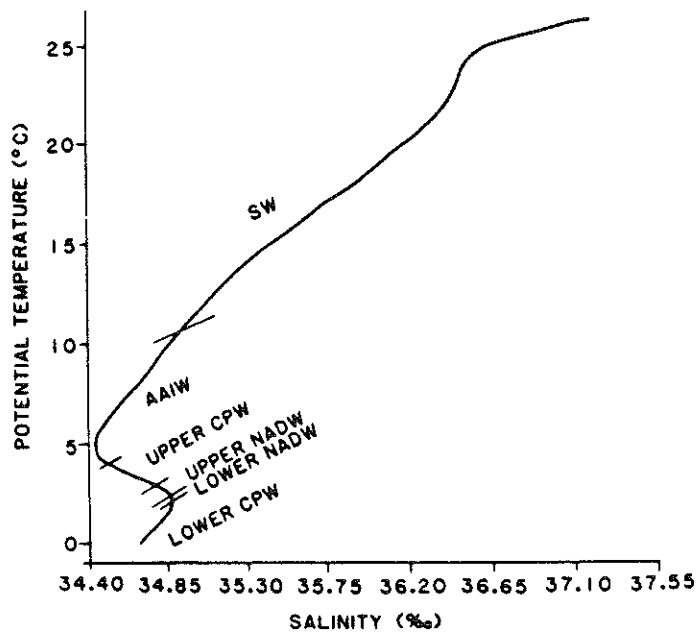


FIG. 2. Potential temperature-salinity diagram constructed from the station data of both the IGY and the METEOR sections. The six water types defined in Table 2 are divided by constant potential density lines and labeled.

Fig. 4.8 Potential temperature-salinity diagram for the South Atlantic, from Fu (1981).

water is the silicate maximum water . . . found at about one kilometer depth. This feature is likely generated by the isopycnal transport of silicate rich water all the way from the Antarctic Ocean!" (p. 346). A source of feed water to the formation region at this depth is also supported by the radiocarbon data, they continued, as the observed  $\delta^{14}\text{C}$  of NADW is low relative to that of the near-surface water in the North Atlantic.

The distribution of AAIW in the ocean is also suggestive of a link between the intermediate water and the global cell associated with NADW formation. As Jacobs and Georgi (1977) noted, the distribution of intermediate water is not uniform in the three oceans: the 34.4 ‰ isohaline reaches to 40°S in the Indian Ocean, and to 35-45°S in the Pacific, while in the Atlantic the same isohaline extends to 5°S. They suggested that the disparity in the degree of penetration of AAIW in each ocean might be due to the presence of an additional source of AAIW within the South Atlantic, or to topographic control. Alternatively, these results suggest that the AAIW is drawn into the Atlantic by the formation of NADW: the AAIW tongue extends further into the Atlantic than the other oceans because the Atlantic is the only ocean with a significant northern source of deep water. Broecker and Takahashi (1981) were led to a similar hypothesis in their study of the intermediate waters in the central Atlantic.

## 5. Summary and Conclusions

In this chapter I have used an inverse method and historical hydrographic data to estimate the absolute velocity field and property transports in the South Atlantic poleward of  $32^{\circ}\text{S}$ . The particular focus has been on the exchange of mass and heat between the South Atlantic and the neighboring ocean basins. In addition to constructing a "standard model," which represents my best estimate of the circulation, several additional experiments were run to test specific hypotheses. In this way much can be learned about the circulation, despite the fact that the problem is underdetermined and the solution non-unique.

The reference level velocity required to satisfy the constraints was generally small and consequently the estimate of the absolute velocity field obtained is similar to that obtained by earlier investigators based on dynamic calculations relative to a deep level (e.g. Nowlin *et al.*, 1977; Georgi, 1981; Georgi and Toole, 1982; Whitworth and Nowlin, 1987). At each section crossing the ACC the flow is concentrated in narrow but deep-reaching jets or fronts, which account for the majority of the transport. Poleward of the ACC, the  $0^{\circ}\text{E}$  and Weddell-Scotia sections cross the cyclonic Weddell gyre; at the latter section the center of the gyre is displaced nearly to the northern edge of the basin. Within the Scotia Sea the ship track makes several crossings of the Weddell-Scotia Confluence. The flow at  $32^{\circ}\text{S}$  is characterized by strong, deep boundary currents on both the eastern and western sides of the basin, with a substantial counterflow or recirculation offshore of the Brazil Current, and weak flow in the interior consistent with the predominantly zonal flow seen in maps of dynamic topography at this latitude (e.g. Defant, 1941; Buscaglia, 1971; Reid *et al.*, 1977; Tsuchiya, 1985).

Individual features of the velocity field are somewhat sensitive to the model assumptions. The transport of the boundary currents, for example, depends on the initial reference level chosen. Study of the resolution matrix showed that the reference level

velocity at individual station pairs was not very well resolved . However, the resolution is compact: we have determined local spatial averages of the reference level velocity, with the length scale of the smoothing varying from a few hundreds of kilometers near the boundaries to 500-1000 kilometers in the interior. To some extent the broad scale of the resolution is a desirable aspect of the solution, since it implies that our estimate of the velocity field is determined by the large-scale features in the data, which are assumed to be more nearly time-independent than the shorter scales.

The large scale features of the flow are also primarily responsible for the net flux of mass and heat across each section, and the net transports in each layer were found to be relatively insensitive to the modelling assumptions made. This was shown by comparing the results of a series of models with different choices of initial reference level, constraints and weighting, and by considering the potential contribution made by the unresolved components of the flow lying in the null space. Generally the volume transports and divergences of each water mass varied by a few Sverdrups or less.

In particular, all the models show a divergence of intermediate water and a convergence of deep and bottom water in the ACC during its transit of region I. The surplus IW carried into the Atlantic leaves the box to the north across 32°S, with 5 Sv first gaining heat from the atmosphere over the broad outcrop area of layer 3 ( $26.8 < \sigma_0 < 27.2$ ).

The equatorward flow of thermocline and intermediate water across 32°S balances a poleward flow of 17 Sv of NADW in the standard case. Most of the NADW transport is concentrated in the deep western boundary current. Poleward of 32°S, the western-intensified NADW flow meets the ACC and turns to the east. The injection of NADW into the ACC increases the transport of deep water in the current and provides a source of heat and salt to the CDW. Part of the CDW entering the basin through Drake Passage is incorporated into the Weddell gyre and carried into the Weddell Sea from the east to be converted to denser bottom water. An average heat loss of 31

$W m^{-2}$  (Gordon, 1981) over the area of the Weddell Sea in region II results in a net conversion of 9 Sv of CDW to bottom water. A consistent circulation can also be found when the heat loss, and hence the production rate of bottom water, is doubled, with the additional BW in this case joining the ACC and flowing to the east to enter the Indian Ocean.

The shift in transport from intermediate to deep layers in the ACC also results in a net divergence of heat carried by the current. The magnitude of the divergence,  $.25 \pm .20$  PW, is similar to that found by Georgi and Toole (1982). The "loss" of heat is not due to local cooling of the waters in the ACC, however, but rather reflects the heat lost in the high latitude regions in the formation of deep and bottom water.

The results of the standard model also confirm that the meridional heat flux at  $32^{\circ}S$  is equatorward. As found by earlier investigators, the primary mechanism responsible for the meridional heat transport is the overturning cell in which equatorward flow of thermocline and intermediate water balances the poleward flow of NADW. The heat flux found in the standard case, .25 PW, falls toward the low end of the range of values found by other authors (Fig. 4.1). To see if the data were compatible with a larger heat flux, the model was run again with a constraint added fixing the heat transport at  $32^{\circ}S$ . Imposing the estimates of Hastenrath (1982) and Fu (1981) led to dramatic changes in the solution: a large increase in the solution norm; a near-reversal of the western boundary current; and a doubling in strength of the meridional cell. These changes were considered to be unrealistic and the hypothesis that the heat flux across  $32^{\circ}S$  was as large as .69 PW was rejected.

Even when the system is forced to carry an unreasonably large heat flux across  $32^{\circ}S$ , however, the water mass transports show the same pattern as in the standard model. The equatorward return flow balancing the export of NADW at  $32^{\circ}S$  is evenly split between the thermocline and the intermediate and bottom water layers, and the surplus of intermediate water entering the basin in the ACC is balanced by a net export

of deep water. Thus both the standard model and the heat flux tests support the notion that the Atlantic as a whole converts intermediate water entering the basin through Drake Passage into deep and bottom water leaving the basin south of Africa.

These results are in conflict with Gordon's (1986) recent suggestion that the global thermohaline circulation associated with the formation of NADW is closed primarily by a "warm water path," in which the export of NADW is compensated by an inflow of warm Indian Ocean thermocline water south of Africa. He suggested that the injection of warm water in the southeastern corner of the basin may be responsible for the "anomalous" sign of the meridional heat flux in the South Atlantic. However, the results of these models demonstrate that such an inflow is not necessary to account for the observed heat flux. Furthermore, even when the system is forced to accommodate a large equatorward heat flux across 32°S the net flux of warm water is from the Atlantic to the Indian Ocean.

To test directly whether the data set used here was consistent with the warm water path, the model was run with a constraint added requiring a net flux of 13 Sv (Gordon, 1985,1986) of warm water from the Indian to the Atlantic. Satisfying this constraint requires drastic changes in the circulation: the solution norm is increased by an order of magnitude; there is a net *convergence* of heat of >1 PW in region I, inconsistent with estimates of air-sea exchange in this region; and a horizontal recirculation of >150 Sv is introduced at the 0° and 30°E sections. The shear results in a net flux of warm water to the east south of Africa, relative to a reference level below 500 m. To reverse the sense of this flux with a barotropic reference level velocity leads to huge transports of deep water in addition to the required 13 Sv of warm water, since the deep layers occupy a much larger fraction of the water column. The present data set is thus apparently inconsistent with a net transfer of warm water of this magnitude from the Indian Ocean to the South Atlantic. This does not mean that warm Indian Ocean water never enters the South Atlantic – flow from the Indian to the Atlantic and back *within* a density

layer is not restricted by this model – but rather suggests that the import of Indian Ocean thermocline water does not play a major part in the global overturning cell associated with the formation of NADW.

Taken together, the results of the inverse models discussed in this chapter make a strong case for the cold water path playing a dominant role in closing the thermohaline circulation. Such a role is also apparently required by the freshwater and nutrient budgets of the Atlantic and may account for the greater degree of northward penetration of the fresh intermediate water tongue in the Atlantic relative to the other ocean basins.

Inverse methods have proved to be particularly useful in this study of interbasin exchange in several ways. By considering budgets for a set of density layers we have been able to make the first estimates of the transports and transport divergences of individual water masses in the ACC. These budgets in turn revealed the important role played by the intermediate water in the global thermohaline circulation. Since the eigenvectors in the range and null space of  $\mathbf{A}$  form a complete set, the inverse machinery provides a way to formally estimate the uncertainty in the property fluxes due to components of the flow that remain unresolved by the available information. The flexibility of the method was also used to advantage in this case, enabling us to include a variety of *a priori* information in the model, including, for example, estimates of mass and heat transports based on direct velocity measurements, or imposed by the basin geometry. The inverse method also allows specific hypotheses to be tested for consistency with the observations in an explicit and straightforward manner. This provided additional insight into the mechanisms responsible for the equatorward meridonal heat flux at 32°S and into the possible role played by the exchange of thermocline water from the Indian Ocean in the NADW cell.

Perhaps the weakest link in this study is the fact that the sections used are far from synoptic: the IGY section at 32°S, for example, was occupied 25 years before the AJAX lines, and the errors due to aliasing of interannual variability are difficult to estimate.



The 32°S section is also poorly suited to this study in several other ways: the station spacing is very wide, especially in the crucial western boundary region; the salinity values in the eastern basin required editing; and the vertical resolution of the bottle data is also poor relative to the CTD data used on the other sections. Moreover, there is no reliable oxygen, nutrient or other chemical data. A calculation using the recent high resolution sections at 23°S and 11°S in place of the 32°S section would provide a valuable check on the results found here. The hydrographic and chemical observations currently being collected as part of the SAVE program will provide further data to fill the large gaps in the existing data set in the South Atlantic. These results suggest, furthermore, that much could be learned about the global thermohaline circulation by applying similar methods to study the circulation at high latitudes of the South Indian and South Pacific Oceans (although the data are relatively sparse in these areas as well). In particular, one may hope to shed some light on the poorly understood upwelling branch of the circulation, in which the NADW that has left the Atlantic is modified to become intermediate water before reentering the basin.

## Chapter 3

### Mass, Heat and Nutrient Fluxes in the North Atlantic

#### 1. Introduction

The North Atlantic has received more attention from oceanographers than any other ocean basin and an extensive collection of both physical and chemical observations now exists. However, these two types of data have rarely been considered together in a quantitative way. In this section of the thesis I reconsider the circulation of the subtropical North Atlantic, with a special focus on the distribution and transport of the nutrients (nitrate, phosphate and silicate). There are two complementary goals of this work. The first is to use the information contained in the nutrient fields to constrain our estimate of the velocity field. The second goal is to use a physically realistic model to determine the nutrient fluxes themselves, in order to gain some insight into the processes controlling the basin-scale nitrogen and silica cycles in the North Atlantic.

When sea water is exposed to sunlight at the sea surface, nutrients and carbon dioxide are taken up by the phytoplankton during photosynthesis. Nutrient concentrations thus tend to be depleted in the surface waters; in fact, the lack of nitrate and phosphate in the surface ocean is thought to be the primary factor limiting productivity in most of the world ocean (Redfield *et al.*, 1963).

Nitrate and phosphate are required by all marine organisms, while silica is an important nutrient only for silicious organisms such as diatoms and radiolarians (Sverdrup *et al.*, 1942). We will see that the different way in which silicate is used by the biota results in a significantly different pattern of sources and sinks, and hence distribution, of silicate. In Section 4 it will be shown explicitly that the silicate field contains substantial information independent of nitrate and phosphate, and can provide valuable constraints on the circulation.

The growth of phytoplankton provides a source of food for the herbivores, which in turn are preyed upon by other organisms. Most of the total nutrient pool is thought to be recycled within the euphotic zone, as organic matter eaten by animals is consumed and the products of this "combustion" are returned to the sea in ionic form (Riley, 1951). A fraction of the organic matter, however, settles out of the surface layers, representing a net loss of nitrogen, phosphorous and silica from the euphotic zone. This fraction of the total primary production is referred to as the net "new" production.

As the organic matter sinks through the water column it is decomposed by bacteria and by chemical dissolution. In the process, oxygen is consumed and nutrients are returned to the sea water, or regenerated. Thus biological processes result in a net downward transport of nutrients in the water column (Redfield, 1942). To complete the cycle, physical processes, such as upwelling or mixing, must return nutrient-rich deep water to the surface layers.

Understanding the nutrient cycles in the ocean is an important step toward understanding the processes controlling production in the ocean. The global new production, in turn, has implications for the earth's climate and carbon cycle since a primary path by which carbon taken up by the surface ocean from the atmosphere reaches the deep ocean is by the fixation of carbon dioxide by the phytoplankton, and the subsequent settling of particles (Sundquist, 1985).

Oxygen enters the ocean when sea water equilibrates with the atmosphere at the sea surface, and is consumed at depth in the process of metabolising organic matter (Sverdrup, 1938). As a result, the oxygen and nutrient distributions in the ocean tend to be roughly anti-correlated. This can be seen, for example, in the sections of oxygen and nitrate concentration at 24°N shown in Figure 2.2.

In addition to these overall trends, the plots show a variety of other structures in the distributions. For example, the nitrate and phosphate distributions have a maximum at mid-depth and generally higher concentrations in the eastern basin, while

silicate has a weaker mid-depth maximum, and increases rapidly in the deep water. These details of the distribution depend both on the biological processes of oxygen consumption and nutrient regeneration discussed above, and on the physical processes of advection and mixing. Indeed, the oxygen and nutrient distributions have frequently been used as tracers to follow the spreading paths of water masses. Wüst (1935) used the oxygen maximum at 2000 m depth to trace what he referred to as the Middle North Atlantic Deep Water (NADW) as it flowed southward from its source region in the Labrador Sea. Mann *et al.* (1973) showed how extrema in vertical profiles of silicate in the western Atlantic Ocean could be used to identify the spreading of silica-rich Antarctic Intermediate (AAIW) and Bottom Water (AABW) northward into the Atlantic, and the southward movement of silica-poor Norwegian Sea Water. Other early studies in which the nutrients have been used as water mass tracers include Cooper (1952), Richards (1958), Edmond and Anderson (1971) and Stefansson and Atkinson (1971).

More recently, several authors have used the information in the nutrient distributions to identify the role of various processes at work in the ocean, as well as to trace water masses. Broecker and co-workers have used "mixing-diagram" arguments to roughly quantify the contribution of different source waters or end-members to the water masses observed, and to infer the relative importance of physical and biological processes in determining the property distributions (Broecker and Ostlund, 1979; Broecker *et al.*, 1976, 1980; Broecker and Takahashi, 1980).

Kawase and Sarmiento (1985, 1986) produced maps of nutrient distributions on isopycnal surfaces in the North and tropical Atlantic Ocean. From these maps they were able to identify the primary source regions for the waters in the Atlantic thermocline, and to determine the relative contributions made by *in situ* regeneration and cross-isopycnal mixing and advection to the observed property distributions. The authors also found a correspondence between the pattern of the property fields and features

expected from recent theoretical models of the subtropical gyre, including the poorly-ventilated "shadow zone" of the ventilated thermocline theory (Luyten, Pedlosky and Stommel, 1983) and an homogenized region in the recirculating regime in the western portion of the gyre (Rhines and Young, 1982).

The analysis of nutrient distributions, as in the studies discussed above, has become a standard and useful tool in oceanography, but there have been few attempts to estimate nutrient *fluxes* or to include these properties in quantitative budget calculations. One notable exception is the pioneering work of Riley (1951). Riley divided the Atlantic from 60°S to 60°N into 76 boxes, and used the dynamic method and salinity conservation statements for each box to estimate the velocity field and the horizontal and vertical eddy diffusion coefficients. He then used the distributions of the non-conservative properties (oxygen and nitrate) to estimate the rate of oxygen consumption and nutrient regeneration as a function of depth.

Riley was limited by both the data and mathematical methods available to him, but his effort to use the physical and chemical data to construct a consistent, quantitative model of the ocean laid the foundation for a series of models to follow, based on better data sets and optimization techniques such as inverse methods. The work presented in this paper is in a sense the latest descendant of Riley's work.

Riley, however, did not discuss the fluxes of oxygen, phosphate or nitrate implied by his box balances. The first estimates of nutrient fluxes of which I am aware were those presented by Wunsch *et al.* (1983) for the South Pacific. Using an inverse method similar to the one used here, they found that the net meridional fluxes of phosphate, oxygen and silicate were indistinguishable from zero across 28 and 43°S. They also concluded that the nutrients did contribute independent information useful in constraining the velocity field.

In the Atlantic, the first calculation of nutrient fluxes was that of Brewer and Dyrssen (1987, unpublished manuscript) in an informal discussion paper prepared for

a Global Ocean Flux Study (GOFs) planning meeting. They took estimates of the net meridional transport across 24°N from Hall and Bryden (1982), calculated average property values in each depth class and multiplied the two to get the net flux across this latitude.

Brewer and Dyrssen concluded from this simple calculation that there is a net export of oxygen from the North Atlantic, which they interpreted as a signature of the large-scale ventilation of the deep ocean by newly-formed NADW; that the Gulf Stream plays a primary role in supplying nutrients to the North Atlantic, contrary to the conventional view that deep winter mixing could replenish the nutrient concentrations near the surface with no need for an "external" source; and, most surprising, that the North Atlantic basin is a very strong source of silica to the world ocean ( $340 \text{ kmol s}^{-1}$ ) and a weaker but still significant source of nitrate ( $100 \text{ kmol s}^{-1}$ ).

Estimates of the rate at which nutrients are supplied to the North Atlantic by rivers, glacial run-off and inflow originating in the Bering Sea are roughly  $30\text{-}60 \text{ kmol s}^{-1}$  for silicate (Anderson and Dyrssen, 1981; Anderson *et al.*, 1983) and  $10 \text{ kmol s}^{-1}$  for nitrate (Brewer and Dyrssen, 1987). Thus there is a large discrepancy between the estimated input rates of these properties and the net fluxes calculated by Brewer and Dyrssen.

One purpose of the present work is to examine the physical and chemical fluxes in the subtropical North Atlantic more thoroughly using inverse methods, in part to see if the oceanic fluxes can be reconciled with the source strength estimates. We would also like to identify the specific physical mechanisms responsible for the transport of each property, in order to better understand the processes controlling the mass, heat and nutrient budgets in the North Atlantic.

A second objective is to explore the extent to which the nutrients contain information independent of temperature and salinity. Nutrient observations are relatively cheap and easy to collect and so are generally made as a matter of course on hydrographic

cruises, but they are rarely used by physical oceanographers except as an additional "tag" with which to identify water masses. Inverse methods provide a straightforward way to explicitly determine the extent to which different properties are independent (Wunsch, 1978; Wunsch, Hu and Grant, 1983). The second goal, then, is to address the questions: what do we really learn about the circulation from the nutrient distributions? Do the nutrients help to resolve the velocity field better than can be done using the mass and salt fields alone?

In Section 2 the property distributions are presented and the main features of the subtropical North Atlantic circulation as revealed by the property extrema are discussed. To go beyond classical "core-layer" analysis requires additional model assumptions; section 3 describes the construction of a set of inverse models designed to use both physical and chemical data to resolve the absolute velocity field. A progression of models were considered in the process of developing a "best estimate" of the circulation; the results of these experiments are presented in Section 4. The discussion in Section 5 focuses in more detail on the flow field and property fluxes of this optimal model, and the chemical and biological implications of the nutrient transport results are addressed. The main conclusions are summarized in Section 6.

## 2. The data

The data used in this study consist of two transatlantic sections at  $24.5^{\circ}\text{N}$  and  $36.25^{\circ}\text{N}$  occupied by the *Atlantis II* in the summer of 1981 (Figure 2.1). Roemmich and Wunsch (1985) (RW, hereafter) have described the data collection and processing procedures. The sections have very high spatial resolution, with a nominal station spacing of 80 km over abyssal plains and 50 km or less elsewhere. Roemmich and Wunsch examined horizontal wavenumber spectra of temperature for these sections and concluded that most of the eddy energy had been resolved. The mesoscale resolution of these sections, and the fact that they are separated in time by less than two months, make them probably the best existing data for this type of study.

Roemmich and Wunsch (1985) presented sections of temperature, potential temperature, salinity, nitrate, phosphate, oxygen and silicate, but did not discuss the nutrient distributions, focusing instead on the zonally integrated meridional mass and heat transport. In this section I briefly discuss the structure of the property fields, both to review the hydrography of the subtropical North Atlantic and to point out features of importance for the discussion of the circulation and nutrient fluxes in the next section. As in RW, the  $24^{\circ}\text{N}$  section will be discussed in two parts: a section across the Florida Straits and an "interior" section from the Bahamas to Morocco.



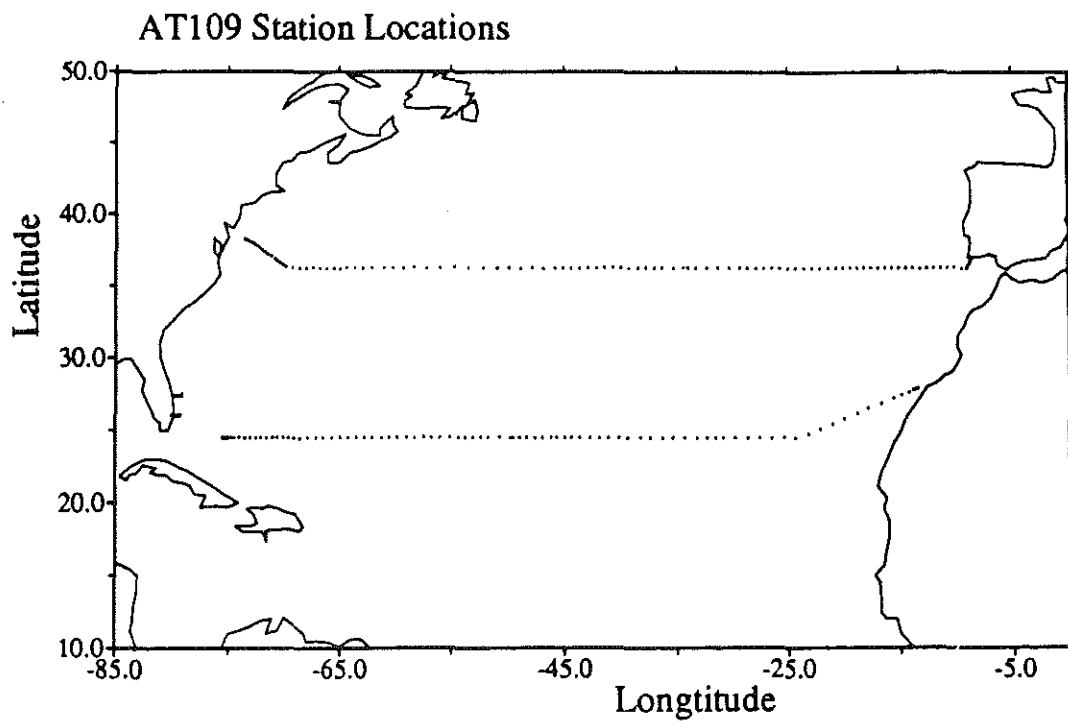


Fig. 2.1 Station locations from *Atlantis II* cruise 109.

## 2.1 The 36°N section

*Potential Temperature and Salinity.* The section at 36°N cuts through the northern portion of the subtropical gyre. Several characteristic features can be seen in the plots of potential temperature and salinity in Fig. 2.2. In the west, the Gulf Stream appears as a region of steeply-sloping isopleths extending to the bottom, which separates the cold, fresh slope water from a thick homogeneous pool of subtropical mode water, the "18°water", to the east (McCartney, 1982; Worthington, 1959). Inshore of the Gulf Stream the Western Boundary Undercurrent (WBUC) can be identified along the continental slope, where the isopleths slope down to the west between 1000 and 3000 m, corresponding to southward flow relative to a deeper level (Barrett, 1965; Richardson, 1977). Embedded in the mode water pool is an intense cold core Gulf Stream Ring or meander, at stations 25-27. The isopleths continue to shoal to the east in the upper 600 m, resulting in the characteristic "bowl" shape of the anticyclonic wind-driven gyre. Superimposed on this trend are several weak, but deep-reaching eddies. Near the eastern boundary, the nearly-isothermal ( $\approx 11^\circ\text{C}$ ) salinity maximum between 600 m and 1200 m depth indicates the presence of Mediterranean Outflow Water (Wright and Worthington, 1970). Below 4000 m the water west of the Mid-Atlantic Ridge is colder and fresher than east of the ridge, reflecting the stronger influence of the AABW in the western basin (Wüst and Defant, 1936).

*Oxygen.* The dominant feature in the oxygen distribution is a prominent minimum at 700-1000 m depth (Sverdrup, 1938). Early investigators (Wüst, 1935; Wyrki, 1962) believed that the oxygen minimum indicated a relatively "stagnant" layer, characterized by minimal horizontal and/or vertical advection. More recently the  $\text{O}_2$  minimum has been described as an advective feature. Broecker and Takahashi (1980) noted that the  $\text{O}_2$  minimum was coincident with maxima of silicate, alkalinity,  $^{226}\text{Ra}$  and barium and could be traced through the South Atlantic to the thermocline waters in the circumpolar

belt. Menzel and Ryther (1968) and Kawase and Sarmiento (1986) suggested that the oxygen minimum layer in the North Atlantic was primarily formed beneath the upwelling area near the African coast, where large amounts of oxygen were consumed in the respiration of organic material sinking out of the highly-productive surface waters. Once formed, the low oxygen, high nutrient water was thought to spread throughout the basin through a combination of advective and diffusive processes. The minimum at a particular point is probably due to a combination of local consumption, and low oxygen water carried from southern and northern sources.

The minimum is strongest in the western basin, beneath the pool of 18° water. The 18° water is characterized by high, uniform oxygen values, as expected for a water mass recently renewed by deep convection. The Mediterranean Outflow Water, also a relatively young water mass, has slightly higher oxygen concentrations than found at the same depth further west. The highest concentrations (6.0-6.5 ml l<sup>-1</sup>) are found below 2000 m in the western basin, in the NADW core; in particular, the WBUC shows up very clearly as a thin oxygen maximum banked up along the continental slope between 2000 and 3500 m depth (Barrett, 1965). The fact that the NADW has higher oxygen concentrations than the near-surface layers at this latitude reflects the temperature dependence of the solubility of oxygen in sea water: the solubility increases with decreasing temperature, so that water exposed to the atmosphere at high latitude receives more oxygen than water exposed at more temperate latitudes (Broecker and Peng, 1982).

*Nitrate and Phosphate.* Nitrate and phosphate co-vary in the ocean and will be discussed together. (In a later section it will be shown explicitly that phosphate contributes essentially no information independent of nitrate.)

The distributions of nitrate and phosphate tend to vary inversely with the oxygen distribution, as discussed in the Introduction. The concentration of nitrate and phosphate is depleted to near-zero concentrations in the surface ocean due to uptake

by phytoplankton in the euphotic zone. The relatively well-oxygenated subtropical mode water also has very low nutrient concentrations. Since nutrients are regenerated as oxygen is consumed in the respiration of organic matter, the  $O_2$  minimum discussed above coincides with a nutrient maximum layer between 700-1000 m. The nutrient maximum is found only west of the Mid-Atlantic Ridge, while to the east, the Mediterranean Outflow Water has low nutrient concentrations at these depths. The Mediterranean water is low in nutrients because the water feeding the Mediterranean inflow is nutrient-depleted Atlantic surface water (Thomsen, 1931).

In the western basin the deep water (below 1300 m) has very uniform, relatively high concentrations of nitrate and phosphate ( $\approx 20 \mu\text{g-at. l}^{-1}$  and  $1.2 \mu\text{g-at. l}^{-1}$ , respectively). Below 2000 m the water east of the ridge is richer in nutrients than that to the west, with the highest concentrations near the bottom. The higher nutrient and lower oxygen concentrations found at depth in the eastern basin reflect the longer residence time for the deep waters in this basin (Wüst, 1935; Metcalf, 1969).

*Silicate.* Silicate is also utilized by organisms in the euphotic zone, and has near-zero concentration in the surface water. However, the distribution of silicate differs significantly from that of nitrate and phosphate. There is only a very weak silicate maximum at the depth of the oxygen minimum, overlying a weak but thick silicate minimum layer with a temperature of  $\approx 4-6^\circ\text{C}$ . This low silicate water corresponds to Wüst's (1935) Upper NADW, formed in the Labrador Basin (Metcalf, 1969). In contrast to phosphate and nitrate, there is significant structure in the silicate distribution at depth. In particular, the concentration of silicate increases steadily to the bottom, and below 2500 m is significantly greater east of the Mid-Atlantic Ridge than to the west at any given depth. There is also a sharp silicate front coincident with the Gulf Stream extending from the surface to the sea floor.

The nutrient concentration of a particular water parcel is the sum of the concentration of the water when it left the sea surface in the source region (the "preformed"

nutrient concentration, Redfield (1942)) plus nutrient regenerated by the decomposition of organic matter. The differences between the nitrate and silicate distributions reflect both different water mass source characteristics and the fact that nitrate and phosphate are generally found in the soft parts of organisms, which are relatively easy to decompose, and so tend to be regenerated higher in the water column than silicate, which is incorporated into the hard parts or shells of organisms such as diatoms and is less labile (Redfield *et al.*, 1963).

## 2.2 The 24°N section

*Potential Temperature and Salinity.* The most notable characteristic of the potential temperature and salinity sections on the part of the 24°N line from the Bahamas to Morocco is the general lack of structure (Fig. 2.3). Over most of the water column the isopleths of all fields are nearly flat. This result, again, is consistent with expectations for a slice through the quiet interior regime of the subtropical gyre, away from the energetic western boundary current and recirculation regimes.

Still, several features can be identified. The subtropical mode water appears as a weak 18°C thermostad which is isolated from the sea surface by a shallow thermocline at this latitude. At 1000 m along the eastern boundary there is a salinity minimum, which RW interpreted as the signature of AAIW flowing north in an eastern boundary current fed by eastward flow in the tropics. The salinity field contains two other extrema: a salinity minimum "layer", consisting of several isolated low salinity blobs, at 1000 m in the interior of the section, again marking the presence of the AAIW; and a strong salinity maximum at the surface in the eastern portion of the section due to the Subtropical Underwater, a water mass formed by strong evaporation in the center of the gyre (Wüst, 1964).

In the deep water the deep western boundary current is still visible as a narrow region of sloping isopleths against the continental slope. The presence of AABW is

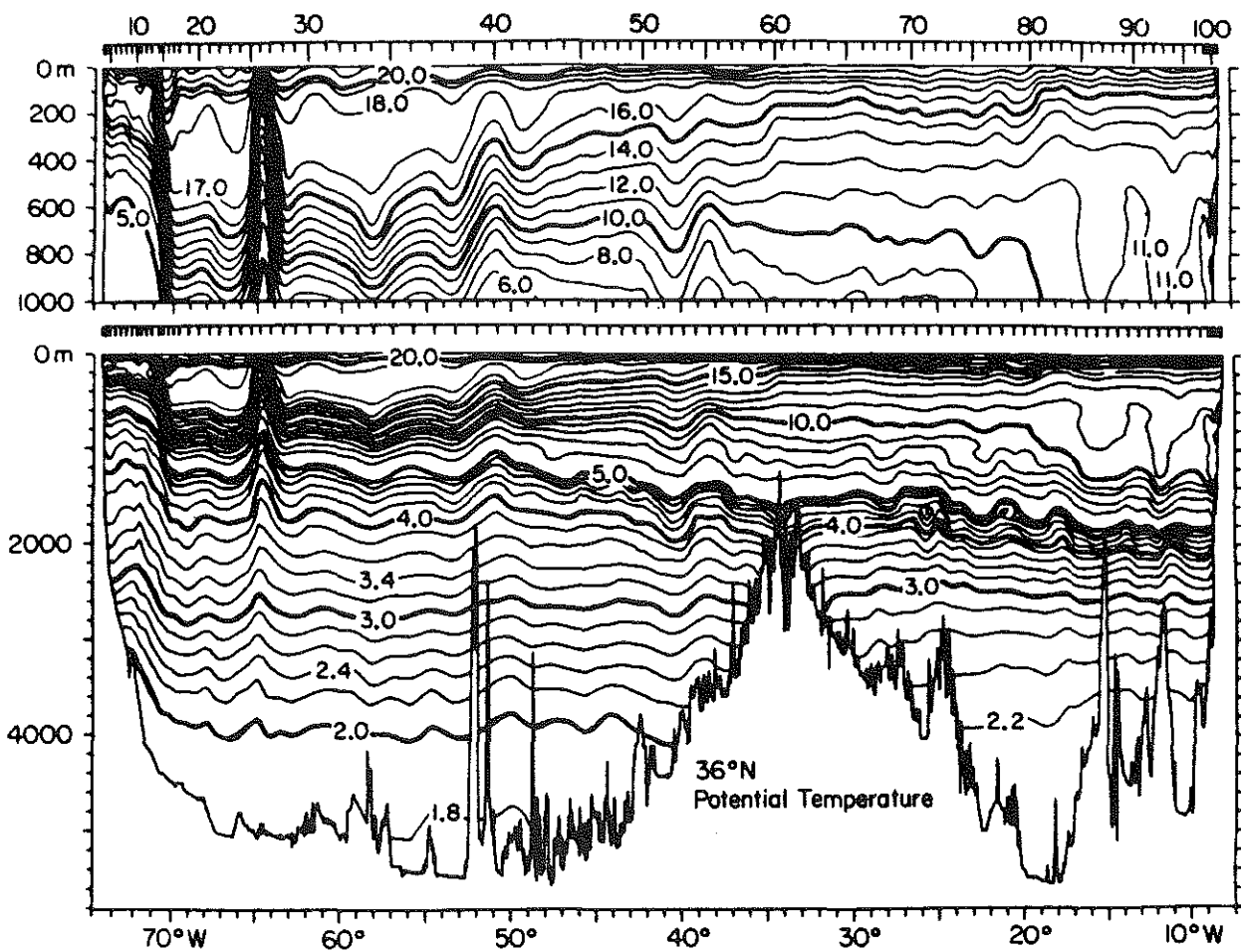


Fig. 2.2 Property distributions at 36°N, from Roemmich and Wunsch (1985). (a) potential temperature (°C).

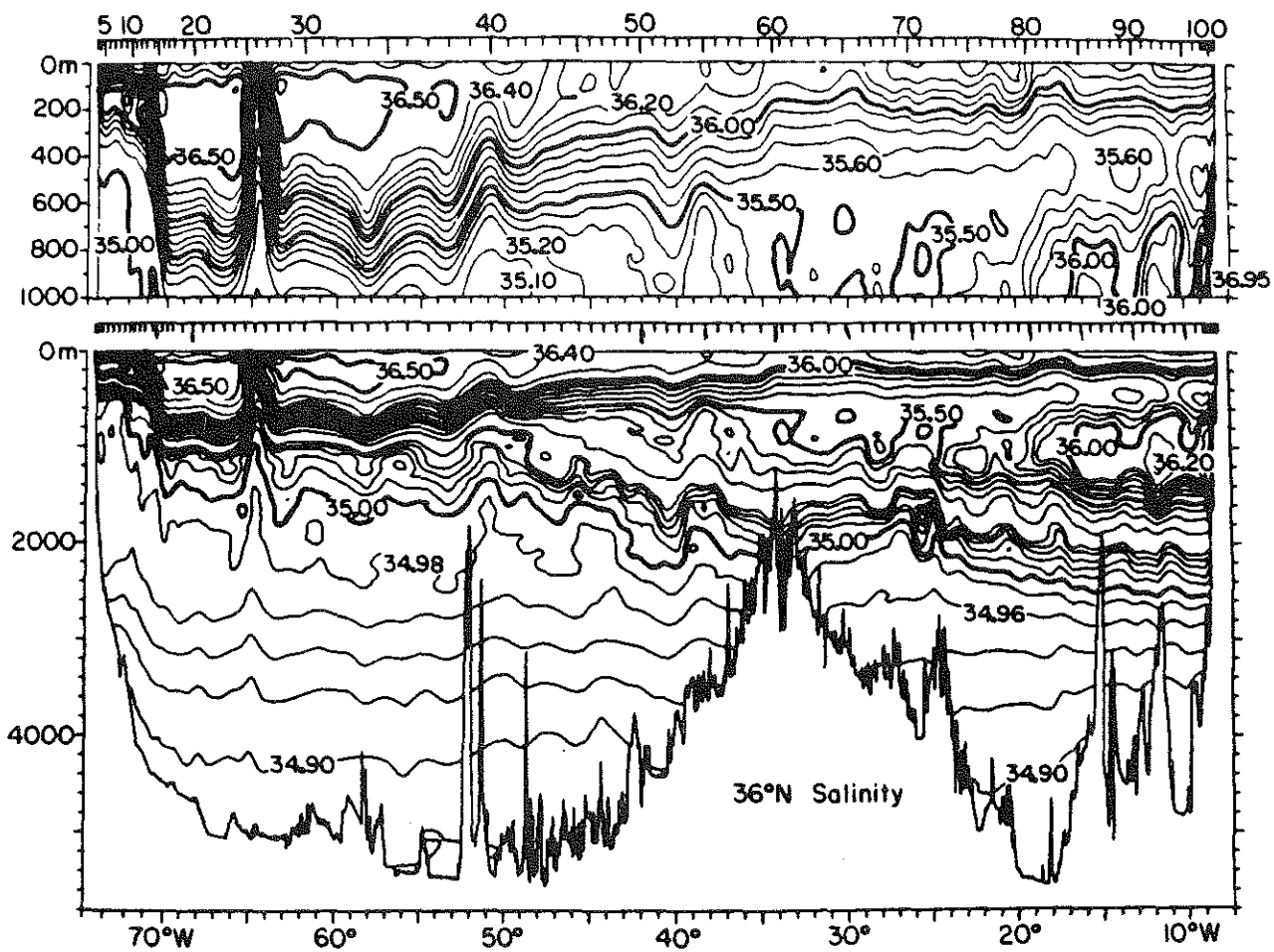


Fig. 2.2 (b) salinity (practical salinity units).

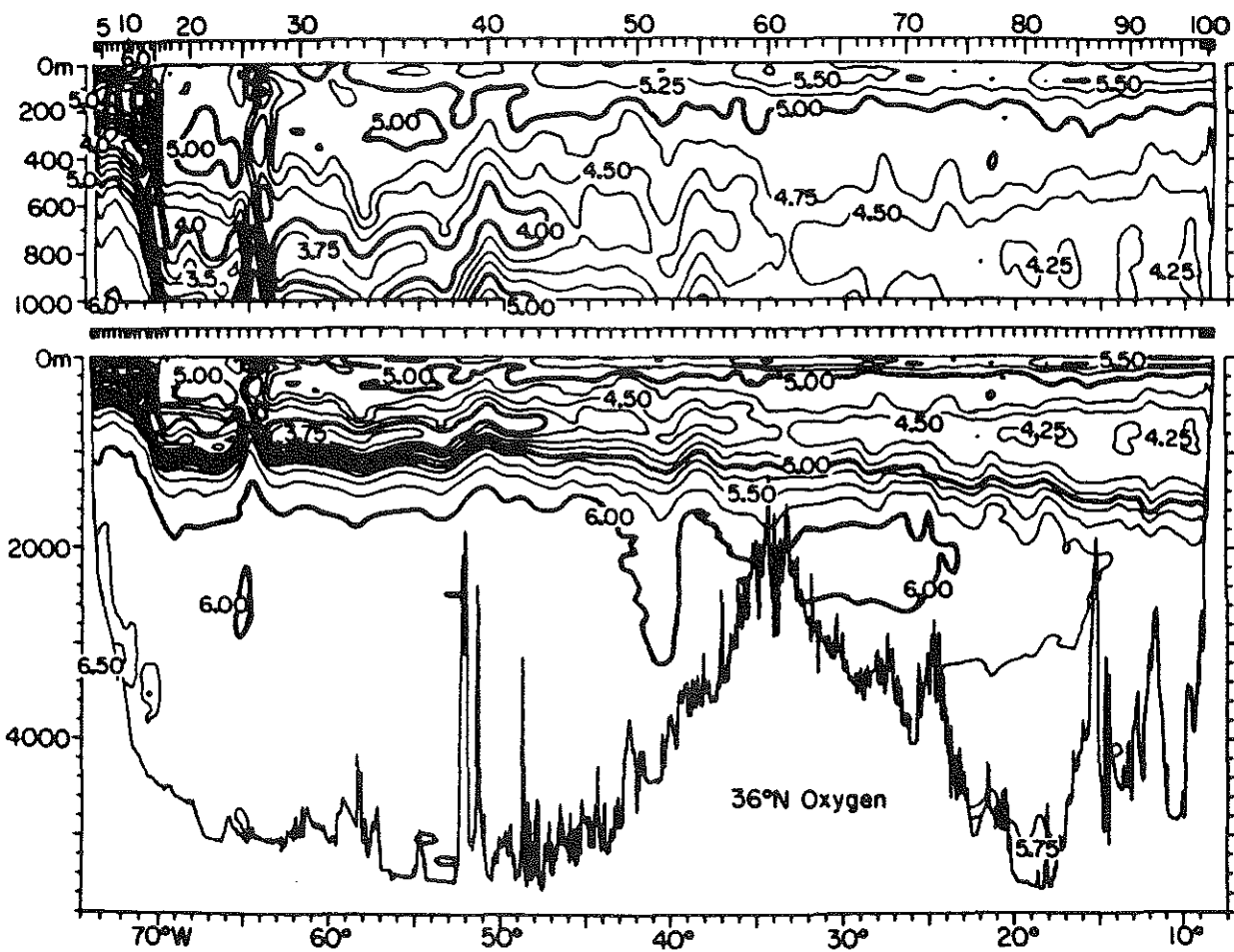


Fig. 2.2 (c) oxygen ( $ml\ l^{-1}$ ).



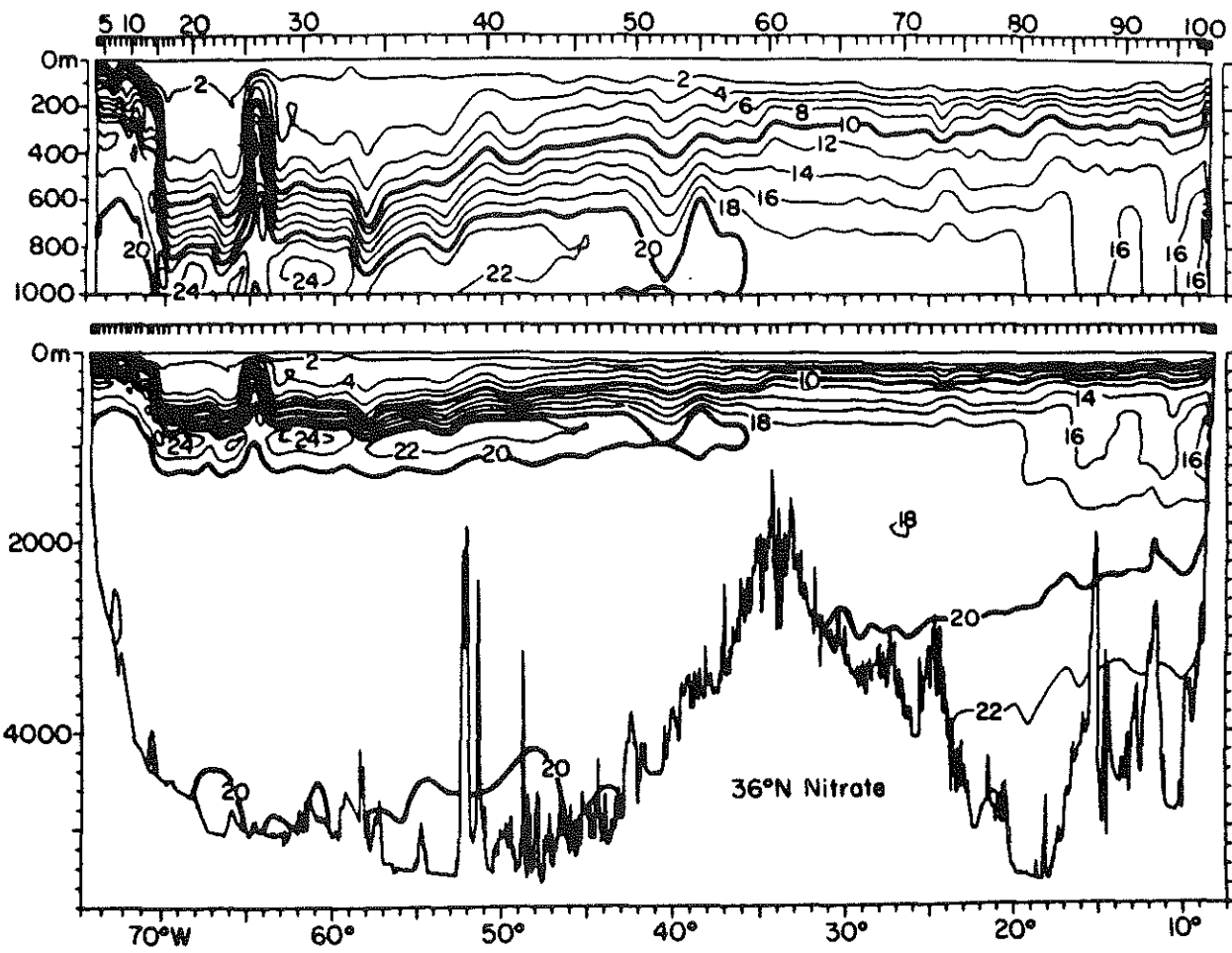


Fig. 2.2 (d) nitrate ( $\mu\text{g-at. l}^{-1}$ ).

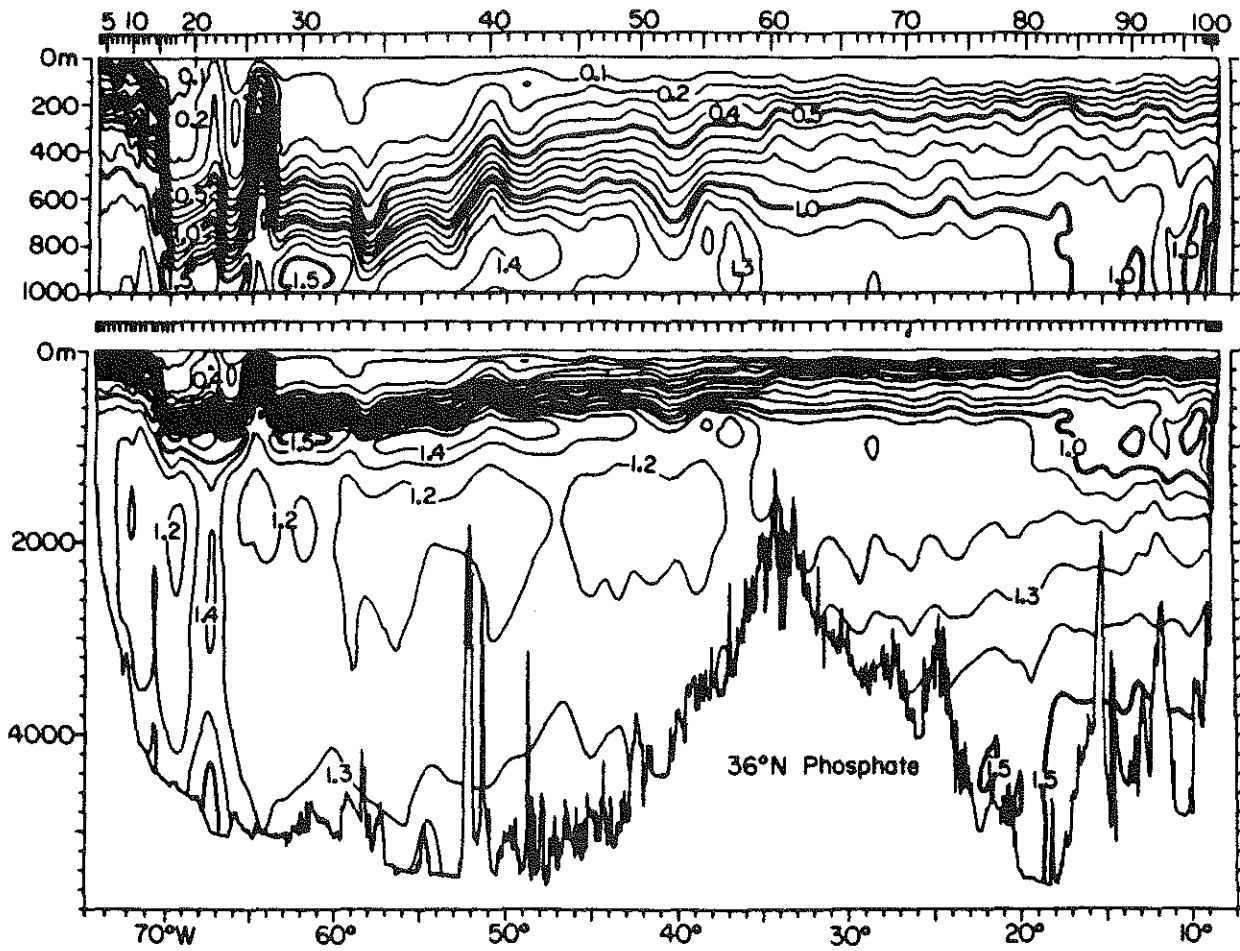


Fig. 2.2 (e) phosphate ( $\mu\text{g-at. l}^{-1}$ ).

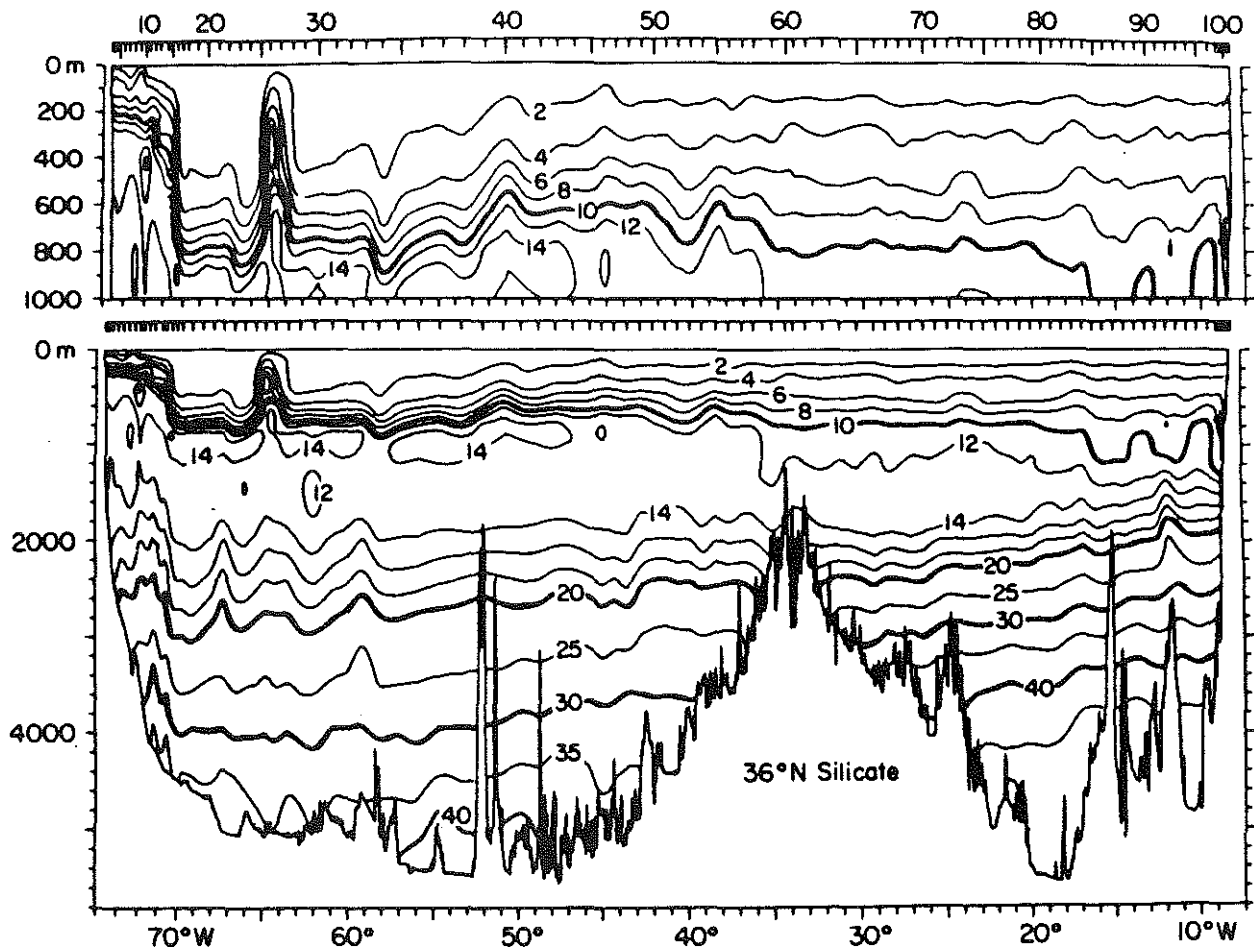


Fig. 2.2 (f) silicate ( $\mu\text{g-at. l}^{-1}$ ).

much stronger at 24°N than at 36°N in the western basin and is seen as a pool of cold, fresh water banked up on the western flank of the Mid-Atlantic Ridge (Warren,1981). *Oxygen.* Oxygen shows the same general features at 24°N as at 36°N. Oxygen concentrations are high near the surface, low from 600-1000 m depth, and reach a maximum in the NADW below 2000 m in the western part of the section. The oxygen minimum layer is more intense at 24°N, especially in the eastern basin, with values below 3.0  $ml\ l^{-1}$ . In contrast, the  $O_2$  maximum associated with the southward flowing NADW has decreased both in strength and extent at this latitude. The distinction between the "young" NADW to the west and the less well-oxygenated AABW against the Mid-Atlantic Ridge is also clear from the oxygen distribution in the deep waters of the western basin. The oxygen concentration of the deep water in the eastern basin is nearly uniform and lower than that west of the ridge.

*Nitrate and Phosphate .* The nitrate and phosphate distributions again mirror the oxygen distribution: low values near the surface, a maximum at mid-depth, and a deep minimum in the NADW. The nutrient maximum coincides with the  $O_2$  minimum and increases in strength to the east. At depth, the lowest values are found along the western boundary in the core of the NADW; the high oxygen and low nutrient concentrations of this water mass reflect its relatively recent formation at the sea surface. The AABW core can also be distinguished from the NADW by its high nitrate and phosphate content. In the eastern basin there is a weak minimum layer between 1500-3500 m depth.

*Silicate.* As at 36°N, the silicate distribution at 24°N differs significantly from that of nitrate and phosphate. There is no silicate maximum layer at mid-depth; in fact, there is a weak silicate *minimum* between 1000-2000 m in the western basin. The NADW has low to intermediate silicate concentrations, in strong contrast to the silicate maximum against the Mid-Atlantic Ridge due to the AABW. As a result, the silicate concentration

at a given depth is higher in the eastern basin than to the west for depths between 2000 m and 4500 m, while the reverse is true below 4500 m.

Silicate concentrations in the deep water are much higher at 24°N than at 36°N. Worthington (1976) took this as evidence that the deep Gulf Stream recirculation must occur in a narrow gyre confined in latitude, since flow passing through the high silicate water to the south would have to lose silicate again before rejoining the Gulf Stream. Note that at both latitudes, the silicate field has much more structure at depth than any of the other physical or chemical properties discussed. This "orthogonality" of silicate with respect to the other variables will be exploited in the inverse models discussed below, where we will see that silicate does contribute significant independent information.

### 2.3 *The Florida Straits Section*

*Potential Temperature and Salinity.* At 24°N the western boundary current is mostly confined to the Florida Straits (Fig. 2.4). This strong flow is reflected in the steep plunging of the isotherms and isohalines to the east, corresponding to northward flow relative to the bottom. The thermostad of 18° water is apparently recirculating subtropical mode water, while the salinity maximum layer between 100-200 m is evidence of the incorporation of the Subtropical Underwater into the Gulf Stream at this latitude. The AAIW appears as a salinity minimum layer below 600 m, with a temperature of  $\approx 6-7^\circ\text{C}$ .

*Oxygen.* There are two extrema in the oxygen distribution in the Florida Straits. The maximum centered at 300 m depth coincides with the 18°C thermostad and reflects the presence of convectively-renewed subtropical mode water. The weak oxygen minimum layer, sloping from 200 m in the west to 600 m in the east, lies just above the sharp halocline marking the boundary between saline North Atlantic Central Water and the fresh AAIW below.

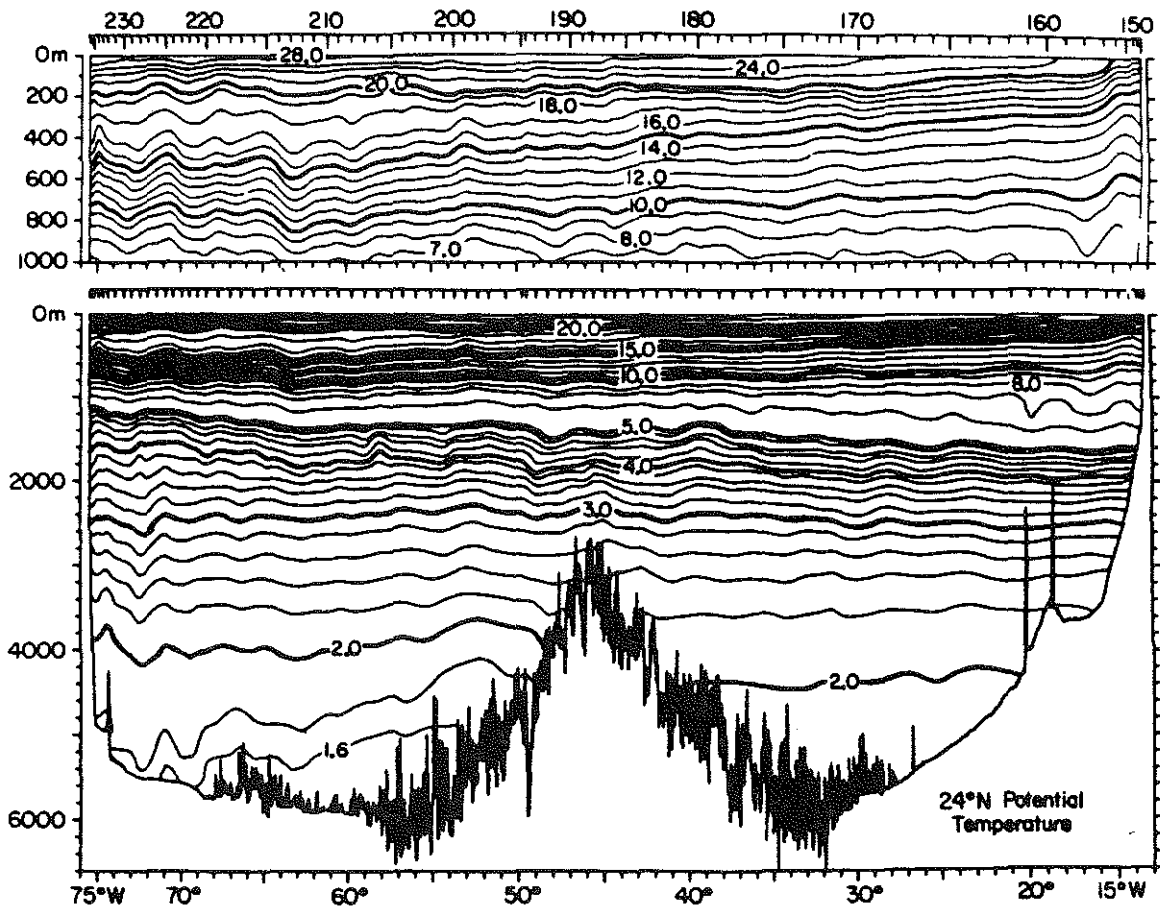


Fig. 2.3 Property distributions at 24°N, from Roemmich and Wunsch (1985). (a) potential temperature (°C).

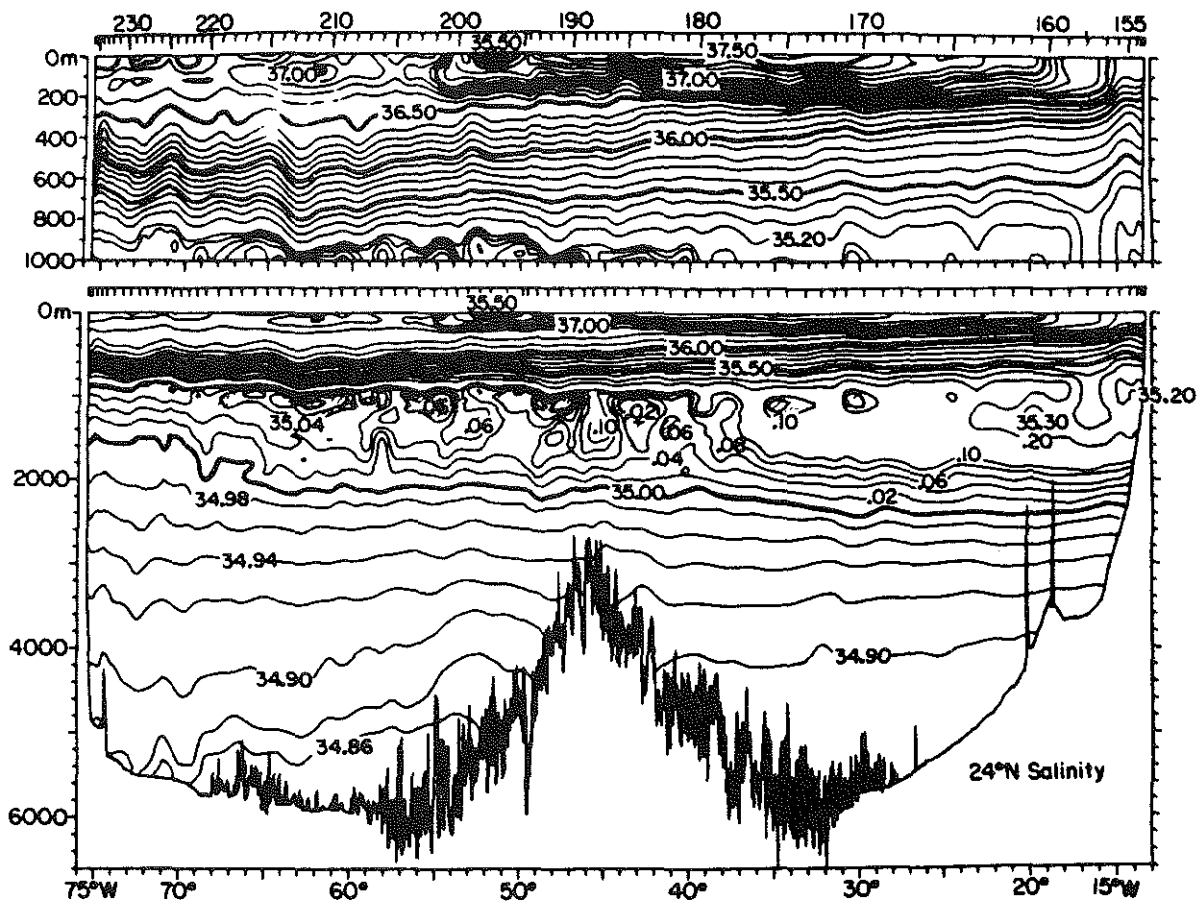


Fig. 2.3 (b) salinity (practical salinity units).

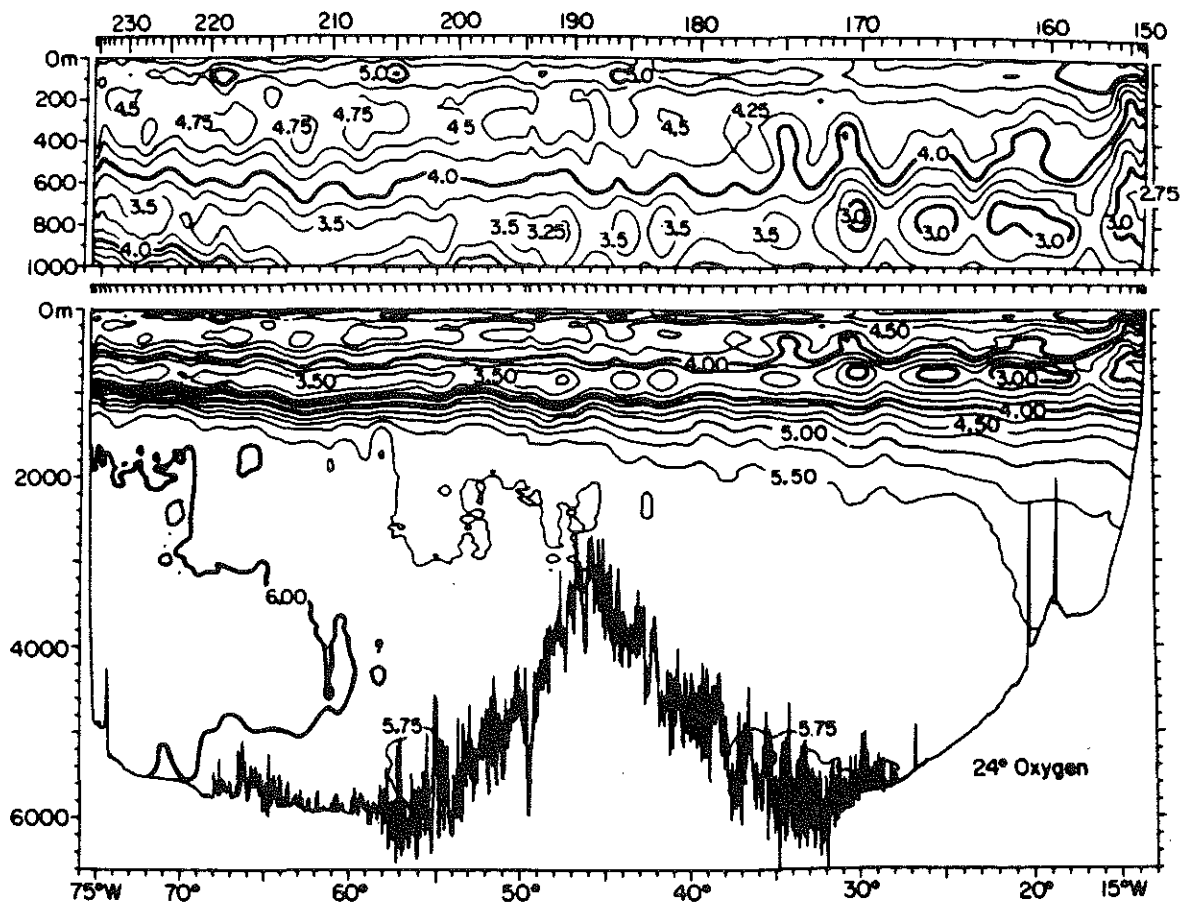


Fig. 2.3 (c) oxygen ( $ml\ l^{-1}$ ).



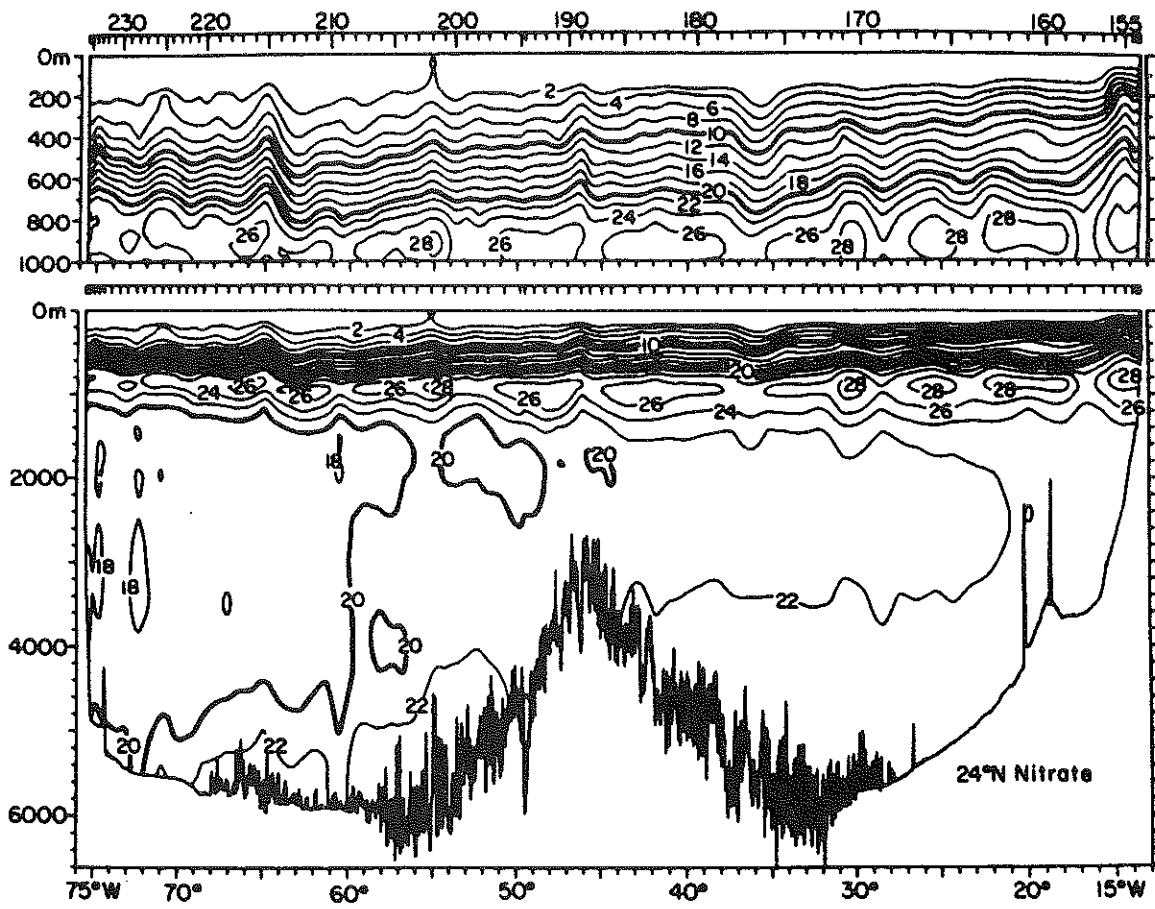


Fig. 2.3 (d) nitrate ( $\mu\text{g-at. l}^{-1}$ ).

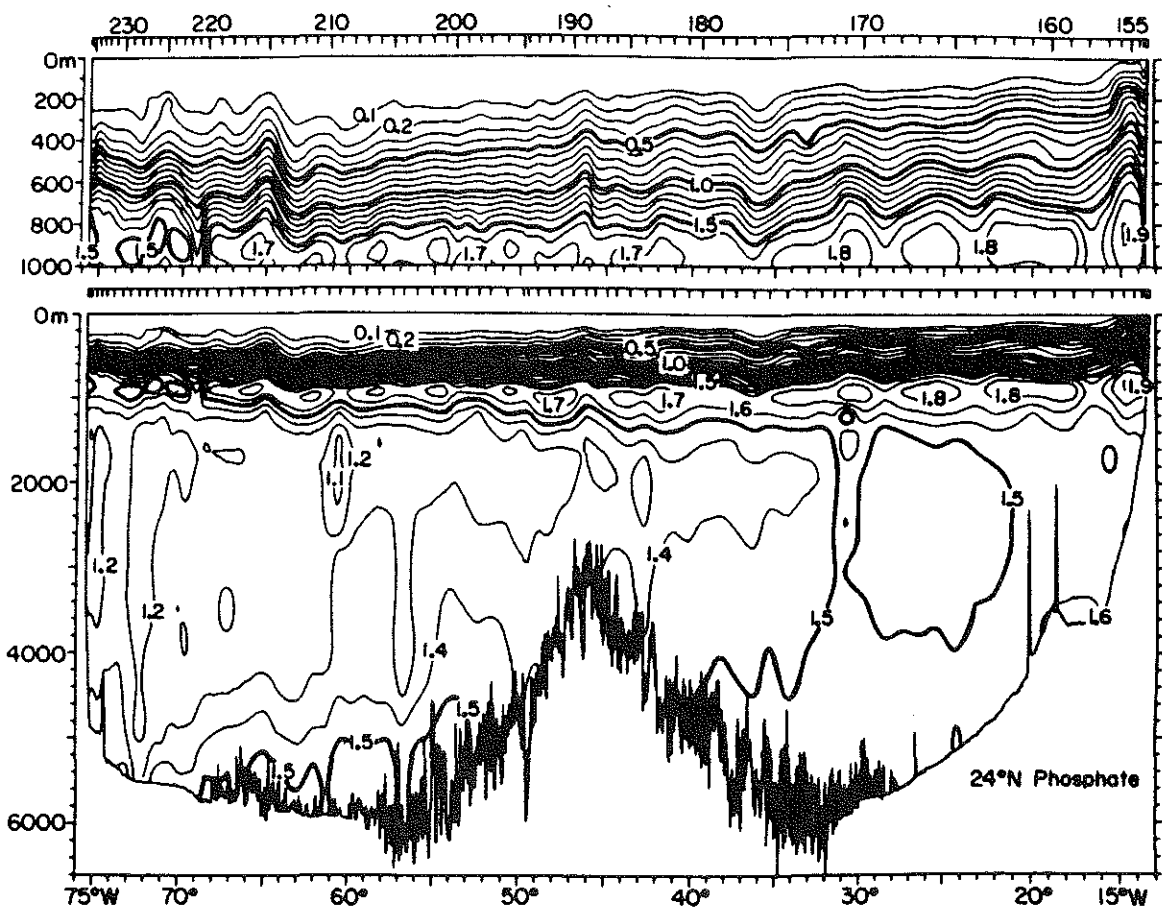


Fig. 2.3 (e) phosphate ( $\mu\text{g-at. l}^{-1}$ ).

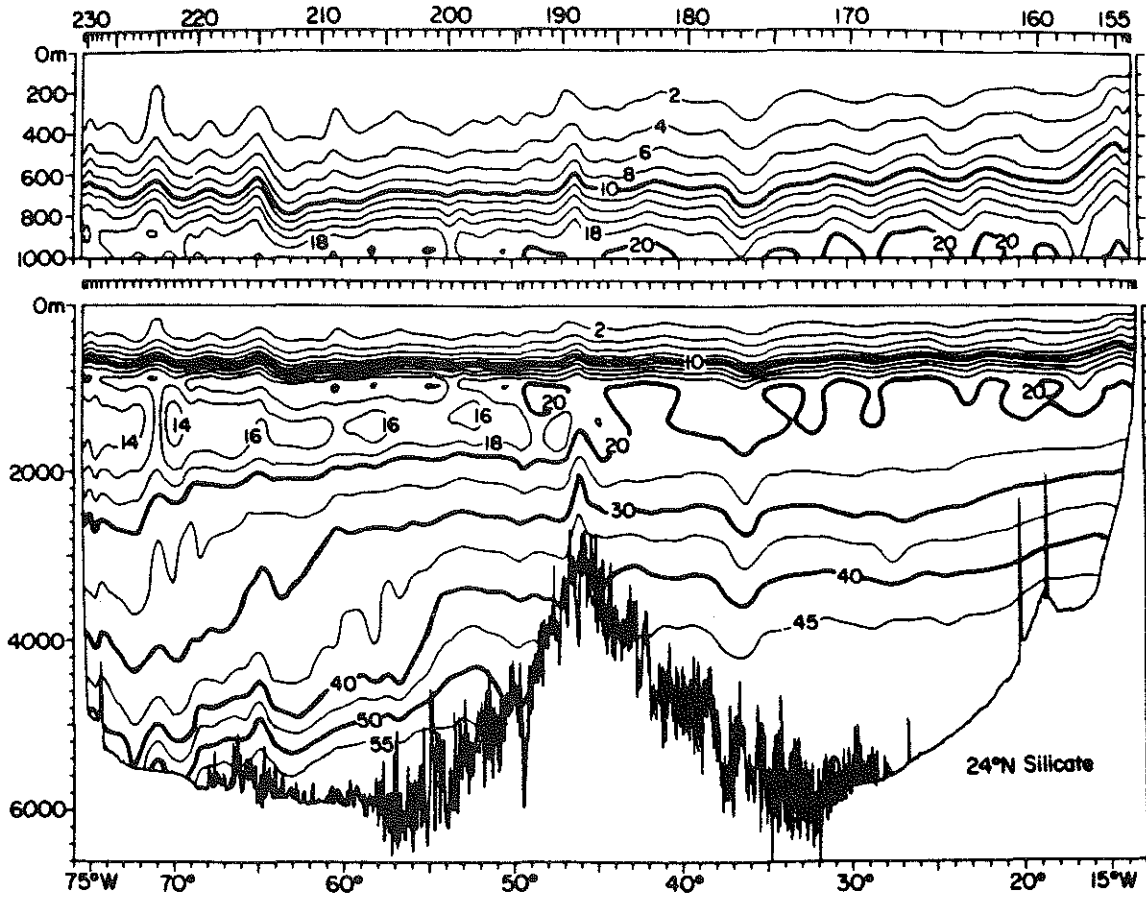


Fig. 2.3 (f) silicate ( $\mu\text{g-at. l}^{-1}$ ).

*Nitrate, Phosphate and Silicate.* In contrast to the sections in the gyre interior, the oxygen minimum does not coincide with a nutrient maximum: nitrate, phosphate and silicate all increase monotonically to the bottom in the Florida Straits. Indeed, the cold, fresh AAIW lying below the oxygen minimum layer has the highest nutrient concentrations seen on any of these sections.

#### 2.4 *Summary of Circulation and Core Layers*

Following Wüst (1935), one can use the property extrema discussed above to construct a picture of the general circulation of the subtropical North Atlantic. The dominant signal in the upper 1000 m is the bowl-shaped anticyclonic gyre, made up of a strong northward flow in the Gulf Stream and a broad return flow to the south in the interior. Within the "bowl" is a pool of well-mixed water with high oxygen and low nutrient concentrations, the convectively-renewed subtropical mode water.

There is another oxygen maximum banked up against the continental slope in the western part of the 36°N section. This is the signature of relatively recently-formed NADW flowing south in the deep western boundary current away from the source region. At 24°N this extrema is still present but is more diffuse, presumably the result of mixing with less well-oxygenated water offshore as it flows south.

The lowest oxygen values and highest nutrient concentrations observed in the interior are found at 800 m off the coast of Africa at 24°N. This may reflect northward flow of water from the intensely productive upwelling region to the south. Broecker *et al.* (1976) and Kawase and Sarmiento (1985) have suggested that in the high productivity region off the west coast of Africa a large amount of organic material sinks out of the euphotic zone, resulting in extensive oxygen consumption and nutrient regeneration as this material is decomposed in the water column.

A second source for high nutrient water at this depth is AAIW entering the basin from the south, as mentioned by RW. This low oxygen, high nutrient water lies just

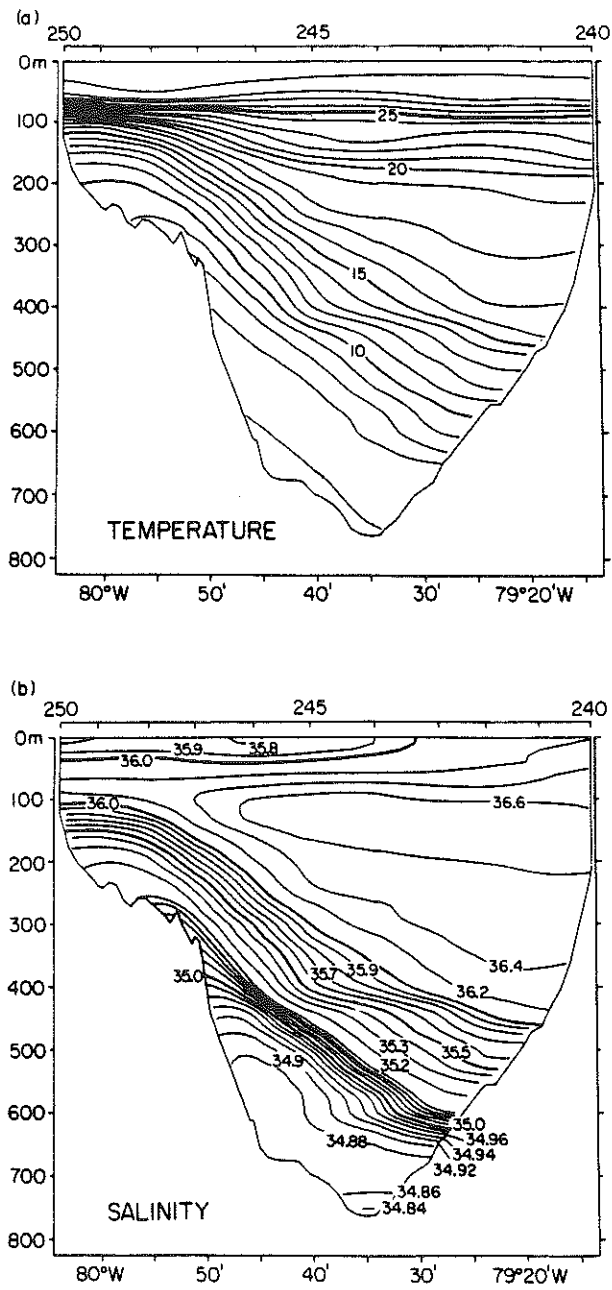


Fig. 2.4 Property distributions at the Florida Straits section, from Roemmich and Wunsch (1985). (a) potential temperature ( $^{\circ}\text{C}$ ). (b) salinity (psu).

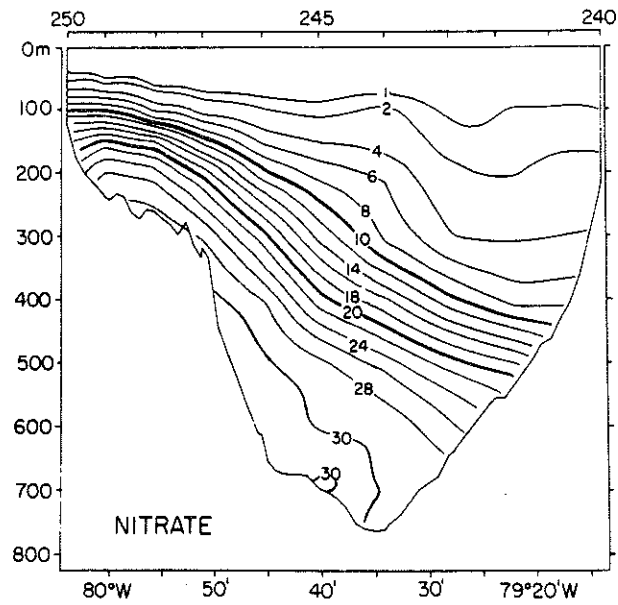
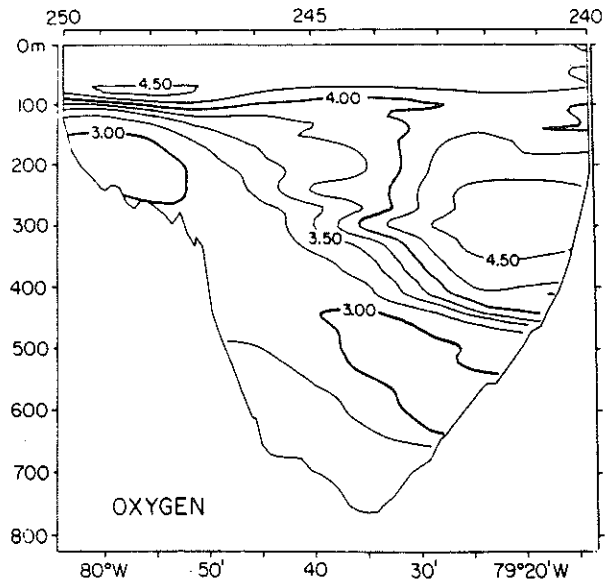


Fig. 2.4 (c) oxygen ( $ml\ l^{-1}$ ). (d) nitrate ( $\mu g\text{-}at.\ l^{-1}$ ).

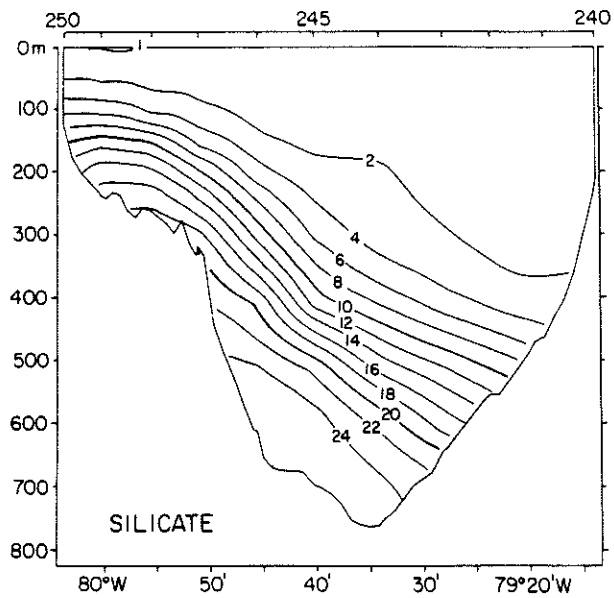
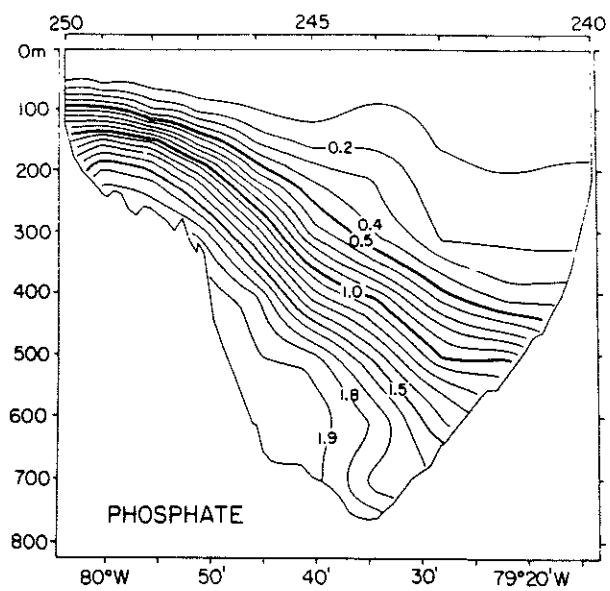


Fig. 2.4 (e) phosphate ( $\mu\text{g-at. l}^{-1}$ ). (f) silicate ( $\mu\text{g-at. l}^{-1}$ ).

above a weak salinity minimum. RW suggested that this feature might be interpreted as a northward flowing eastern boundary current fed by an eastward flow of AAIW in the tropics.

The strongest signal of the AAIW is found in the Florida Straits. The AAIW core enters the North Atlantic along the western boundary, flows into the Caribbean Sea, and is incorporated into the Gulf Stream at the Florida Straits (Iselin, 1936). The influence of the AAIW can still be seen at  $36^{\circ}\text{N}$ , where there is a high nutrient, low salinity layer within the Gulf Stream at intermediate depths. We will see below that the relatively high nutrient concentrations in the Gulf Stream play an important role in the North Atlantic nutrient cycle.

The AABW core is also easily identified by the property extrema, particularly at  $24^{\circ}\text{N}$ . Here the AABW appears as a cold, fresh, very high silica water mass along the west flank of the Mid-Atlantic Ridge. At  $36^{\circ}\text{N}$  the highest silica values are also found near the bottom, but the concentrations are significantly lower. Evidently the AABW at this latitude has been strongly diluted.

The property extrema can thus be used to synthesize a picture of the main features of the circulation, and to identify different flow regimes. We have been able to recognize the western boundary current and gyre interior flows, the deep western boundary current, the transposed AABW boundary current, and smaller scale features such as an intermediate depth eastern boundary current at  $24^{\circ}\text{N}$ . However, classical "core-layer" analysis such as this provides no information on rates or fluxes of properties. To determine the absolute velocity field, and the transports of physical and chemical properties, requires additional modelling assumptions. Inverse methods provide one way to combine the techniques of core-layer or isopycnal analysis with dynamical information to develop a consistent model of the circulation. The next section describes the modelling strategy adopted here.



### 3. The Model

The inverse method was reviewed in Chapter 1. In this section I will focus on the features specific to the series of models considered here.

The three hydrographic sections at 36°N, 24°N and the Florida Straits and the land connecting these sections define a closed volume of ocean (Fig. 2.1). Within this region the water column is divided vertically into 18 layers defined by isopycnal surfaces. The nominal layer boundaries are given in Table 3.1, along with the layer average property values at each section. The bounding isopycnals at each section are plotted in Figure 3.1. These layers were chosen to resolve the main water masses in the North Atlantic and correspond to those of RW.

(The correspondence is not exact: as in Chapter 1, the reference pressure used to calculate the potential density of the layer boundary is allowed to vary as the surface undergoes large vertical excursions, so that the "isopycnal" surface approximates a true neutral surface. Neglecting compressibility effects and using a single density parameter to define each layer boundary, as done by RW, is not as serious for these mid-latitude zonal sections as it was for the meridional lines used in Chapter 2. Nevertheless, for a few layers there is a significant difference between the two definitions (Table 3.2). In the most severe case, the area of layer 7 at 36°N is more than a factor of two larger when the nonlinearity of the equation of state is not accounted for, equivalent to an increase in average thickness from 165 m to 340 m. This layer, with a mean depth of about 1000 m, intersects the slope water in the west and the Mediterranean Outflow Water in the east; consequently, the range of temperature and salinity in this layer is very large. As McDougall (1987) has shown, the discrepancy between a true neutral surface and a potential density surface referenced to a single reference pressure is proportional to the salinity difference on the surface as well as the displacement of the surface from

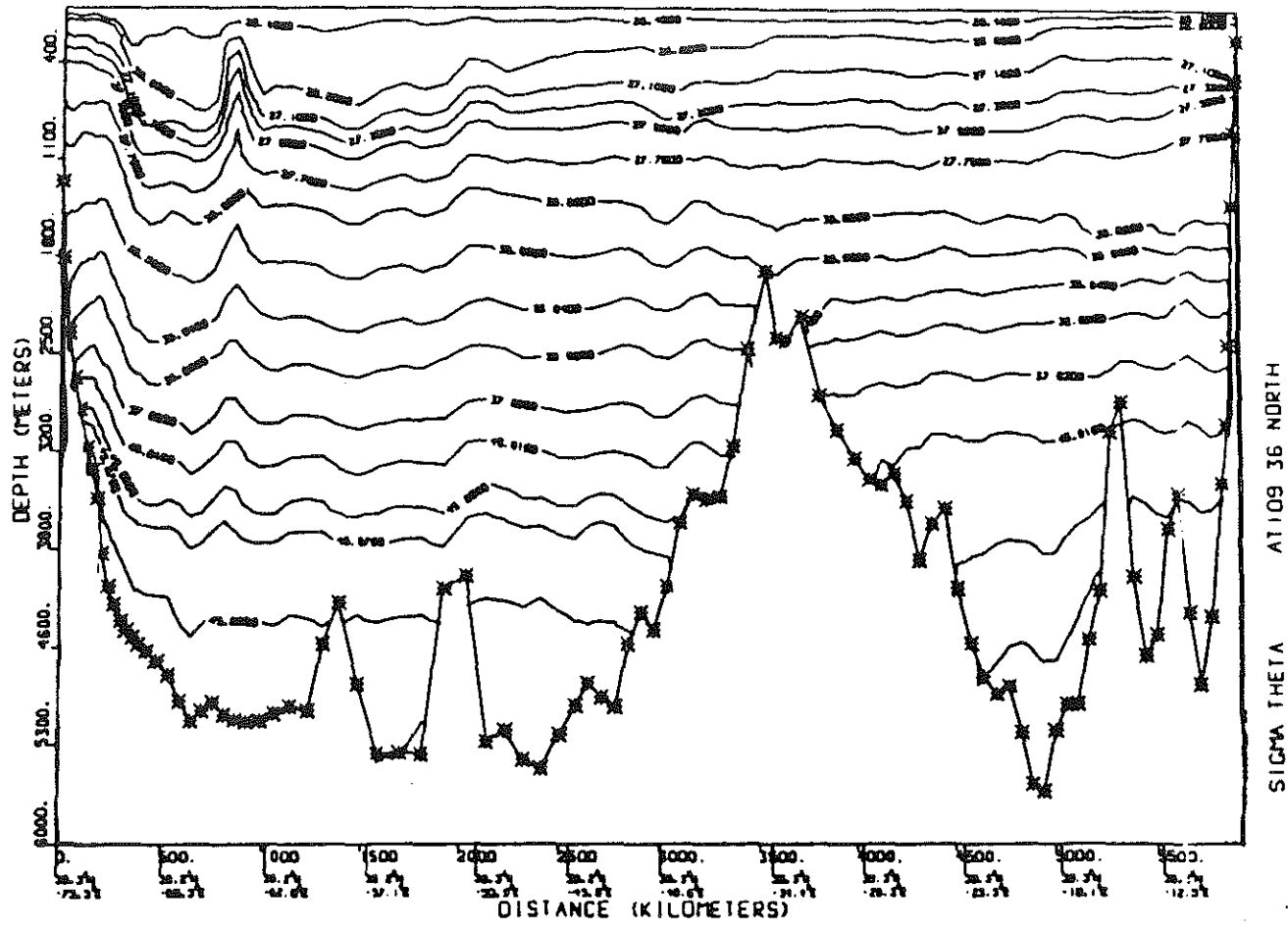


Fig. 3.1 (a) Potential density layers at 36°N.

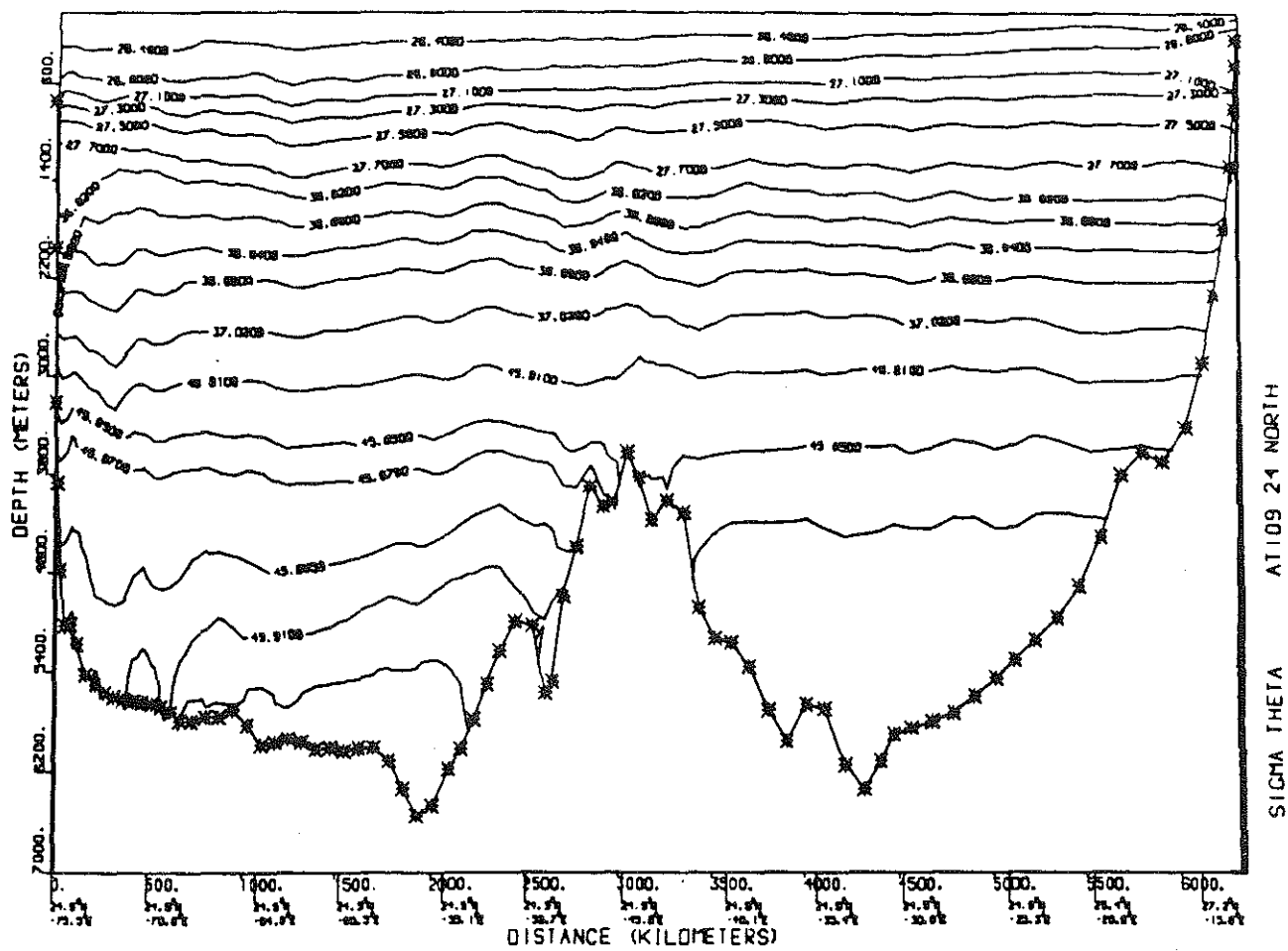


Fig. 3.1 (b) Potential density at 24°N.

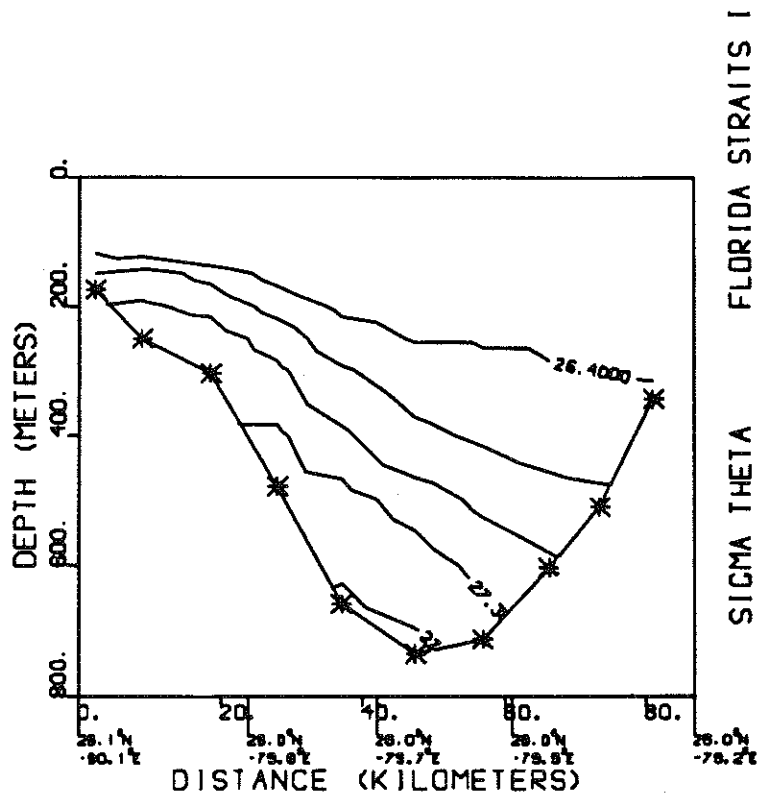


Fig. 3.1 (c) Potential density at the Florida Straits.

Table 3.1 Layer boundaries and layer average potential temperature (upper value, °C) and salinity (lower value, psu) at each section. "\*" indicates no water in this layer at this section.

| Layer | Upper bndy       | Lower bndy       | 36°N            | 24°N            | Florida Straits |
|-------|------------------|------------------|-----------------|-----------------|-----------------|
| 1     | surface          | $\sigma_0=26.40$ | 19.52<br>36.297 | 22.06<br>36.895 | 23.37<br>36.375 |
| 2     | $\sigma_0=26.40$ | 26.80            | 16.53<br>36.278 | 16.69<br>36.328 | 16.20<br>36.165 |
| 3     | 26.80            | 27.10            | 13.00<br>35.753 | 13.15<br>35.786 | 12.18<br>35.542 |
| 4     | 27.10            | 27.30            | 10.69<br>35.496 | 10.43<br>35.436 | 8.97<br>35.114  |
| 5     | 27.30            | 27.50            | 9.28<br>35.479  | 8.00<br>35.180  | 6.48<br>34.897  |
| 6     | 27.50            | 27.70            | 7.48<br>35.428  | 6.14<br>35.106  | 5.33<br>34.837  |
| 7     | 27.70            | $\sigma_2=36.82$ | 5.70<br>35.227  | 5.15<br>35.105  | *<br>*          |
| 8     | 36.82            | 36.89            | 4.78<br>35.127  | 4.53<br>35.079  | *<br>*          |
| 9     | 36.89            | 36.94            | 3.87<br>35.024  | 3.98<br>35.047  | *<br>*          |
| 10    | 36.94            | 36.98            | 3.44<br>34.998  | 3.54<br>35.018  | *<br>*          |
| 11    | 36.98            | 37.02            | 3.04<br>34.973  | 3.08<br>34.983  | *<br>*          |
| 12    | 37.02            | $\sigma_4=45.81$ | 2.67<br>34.950  | 2.68<br>34.952  | *<br>*          |
| 13    | 45.81            | 45.85            | 2.38<br>34.931  | 2.36<br>34.927  | *<br>*          |
| 14    | 45.85            | 45.87            | 2.14<br>34.911  | 2.12<br>34.908  | *<br>*          |
| 15    | 45.87            | 45.89            | 1.98<br>34.903  | 1.96<br>34.894  | *<br>*          |
| 16    | 45.89            | 45.91            | 1.85<br>34.893  | 1.81<br>34.885  | *<br>*          |
| 17    | 45.91            | 45.93            | 1.73<br>34.878  | 1.63<br>34.862  | *<br>*          |
| 18    | 45.93            | bottom           | *<br>*          | 1.49<br>34.844  | *<br>*          |

Table 3.2 Comparison of layer areas at 36°N for layers defined by variable and constant reference pressures. Units = km<sup>2</sup>.

| Layer | Constant<br>$P_{ref}$ | Variable<br>$P_{ref}$ | Diff. | % Diff. |
|-------|-----------------------|-----------------------|-------|---------|
| 1     | 550                   | 550                   | 0     | 0       |
| 2     | 1405                  | 1388                  | -17   | -1.2    |
| 3     | 1300                  | 1416                  | 117   | 9.0     |
| 4     | 1000                  | 981                   | -18   | -1.8    |
| 5     | 899                   | 1040                  | 141   | 15.7    |
| 6     | 1450                  | 1824                  | 374   | 25.8    |
| 7     | 2016                  | 976                   | -1040 | -51.6   |
| 8     | 1990                  | 2391                  | 401   | 20.1    |
| 9     | 1937                  | 1962                  | 24    | 1.3     |
| 10    | 1705                  | 1709                  | 4     | 0.2     |
| 11    | 2061                  | 2161                  | 100   | 4.8     |
| 12    | 1900                  | 1778                  | -122  | -6.4    |
| 13    | 2061                  | 2110                  | 49    | 2.4     |
| 14    | 1454                  | 1474                  | 20    | 1.4     |
| 15    | 1836                  | 1856                  | 20    | 1.1     |
| 16    | 1640                  | 1588                  | -52   | -3.2    |
| 17    | 38                    | 37                    | -1    | -2.6    |
| 18    | *                     | *                     | *     | *       |

the reference pressure. Thus the effect is most pronounced in the North Atlantic in the core of the Mediterranean Outflow.)

The model is constructed as in Chapter 1. Assuming the flow is in thermal wind balance and that the circulation has not changed significantly between the occupations of the three sections (a good assumption for these nearly synoptic sections), conservation equations are written for mass and other properties in each isopycnal layer. The conservation statements, and a variety of additional constraints written in similar form, result in a set of linear equations to be solved for the reference level velocity at each station pair and the "cross-isopycnal transfer" across each interface.

The system of equations is solved using the singular value decomposition (SVD). The columns of the coefficient matrix are weighted by their length, to remove the bias introduced by variable station depth and spacing (see Chapter 1). The rows of the matrix are also weighted, in two stages: first, to non-dimensionalize the equations so that all coefficients are of  $O(1)$ ; second, to account for the expected error in each equation, such that equations with large uncertainties receive low weights. For example, the top three layers, which may be in direct contact with the atmosphere were downweighted in all of the models considered. The particular values used vary from model to model and are discussed along with the results in Section 4.

There are a total of 216 unknowns (199 reference level velocities and 17 cross-interface transfers). Even with a large number of layers and properties for which to write conservation equations the system is still underdetermined and the reference level velocities at individual station pairs are not very well resolved. The structure of the resolution of the reference level velocities and of the net property fluxes will be discussed below.

A discussion of the constraints imposed in each model is also deferred to the presentation of the model results. Several constraints, however, are common to all the models. Total mass is conserved in each case to within  $\pm 2$  Sv. The Ekman flux across each section was estimated to be  $2 \pm 2$  Sv to the south across  $36^\circ\text{N}$  and  $6 \pm 2$  Sv to the north across  $24^\circ\text{N}$ , using the annual mean wind stress estimates of Hellerman and Rosenstein (1983), with the error bar based on seasonal variations. As in Wunsch and Grant (1982), the Ekman transports are included in the total mass conservation constraint, so that the Ekman convergence is balanced by a net geostrophic divergence of the same magnitude. By including the Ekman flux in the total mass constraint, the system is allowed to distribute the required divergent geostrophic flow "where it wants." This seems most appropriate given the uncertainty in how Ekman transports are balanced by geostrophic flows in the ocean. Since the Atlantic is closed to the

north except for a small inflow from the Pacific (1 Sv; Aagard *et al.*, 1985), the net (geostrophic + Ekman) flux across both latitudes must be approximately equal to zero. As in Bryden and Hall (1982) and RW, the transport through the Florida Straits is required to equal 30 Sv, as estimated by Niiler and Richardson (1973) from direct current measurements. To keep the total transport across 24°N equal to zero, there must then be a net southward transport of 30 Sv across the interior section at 24°N.

The modelling strategy adopted is to seek the simplest model consistent with the observations. In this spirit, the results of a series of models is presented in the next section, starting with the basic model described above. For each model, the sensitivity of the results to the initial model assumed is examined by considering several initial reference levels. By starting with the most basic model and gradually adding constraints, one can also obtain a clear picture of how each type of information affects the solution.



#### 4. Model development results

In this section a variety of constraints are considered in the course of developing a "best estimate" of the circulation, defined in this case to be the simplest model consistent with the observations. The consistency of each set of model assumptions is evaluated by considering the residuals and zonally-integrated transports of each property. The horizontal and vertical structure of the velocity field and property fluxes for the best estimate model will be considered in detail in Section 5.

##### 4.1 Model 1: Total mass conservation

The lowest order model requires only that the basic constraints listed at the end of section 3 be satisfied, with no constraints written for individual layers. This simplest model is equivalent to the Brewer and Dyrssen calculation, with the addition of the 36°N section. The initial reference level was chosen to be at 1300 db. As noted by RW, a reference level at this depth results in a northward flow of surface and intermediate water and a southward flow of deep water, consistent with the salinity and nutrient distributions (Broecker *et al.*, 1976; W'ust, 1935). A 1300 db reference level also gives approximately zero total transport across each latitude.

With an initial reference level at 1300 db, only a small uniform correction to the reference level velocity is necessary at each section to satisfy the total mass constraint:  $b_{36N} = .06 \text{ cm s}^{-1}$ ,  $b_{24N} = -.06 \text{ cm s}^{-1}$ , and  $b_{FS} = 9.48 \text{ cm s}^{-1}$ . The net flux of temperature, oxygen, silicate and nitrate across each of the three sections is summarized in Table 4.1 along with the results of Brewer and Dyrssen. These transports include the Ekman contribution (see Table 4.2 for the values used).

At 24°N the net flux of oxygen, silicate and nitrate is strongly to the south, similar in sign and magnitude to the results of BD. At 36°N, the net transport of oxygen and silicate is also to the south, but of larger magnitude, while the transport of nitrate is to the north. As a result there is a large convergence of oxygen and silica within the

Table 4.1 Net flux results for total mass conservation model. Units of temperature flux = °C Sv; units of oxygen and nutrient fluxes = kmol s<sup>-1</sup>. Positive flux is northward; 'BD' are results of Brewer and Dyrssen (1987).

|           | Temp | Oxygen<br>BD |       | Silicate<br>BD |      | Nitrate<br>BD |      |
|-----------|------|--------------|-------|----------------|------|---------------|------|
| 24°N      | -312 | -7113        | -6970 | -477           | -525 | -374          | -392 |
| FS        | 570  | 5089         | 4890  | 171            | 187  | 280           | 292  |
| 24°N+FS   | 258  | -2024        | -2080 | -306           | -338 | -94           | -100 |
| 36°N      | 288  | -3473        |       | -439           |      | 96            |      |
| net conv. | -30  | 1449         |       | 133            |      | -190          |      |

Table 4.2 Transport of each property across each section carried by the Ekman transport. Estimates made by multiplying the mass transports from the Hellerman and Rosenstein (1983) wind stress values (2 Sv to the south at 36°N; 6 Sv to the north at 24°N) by the average concentration of each property at the sea surface. Units of temperature flux are °C Sv; units of chemical fluxes are kmol s<sup>-1</sup>. Negative transports are southward.

| Section | Temp | Oxygen | Silicate | Nitrate |
|---------|------|--------|----------|---------|
| 24°N    | 161. | 1235.  | 5.2      | 1.0     |
| 36°N    | -43. | -455.  | -1.6     | -.3     |

box bounded by 24°N and 36°N, and a large divergence of nitrate. The temperature flux across 24°N and 36°N shown in Table 4.1 corresponds to a heat flux of  $1.1 \times 10^{15}$  W and  $1.2 \times 10^{15}$  W, respectively, across each latitude.

This pattern of convergence/divergence of oxygen and nutrients would imply a large net consumption of oxygen and silicate within the box, and a net production of nitrate. However, this simple model results in a flow field that leaves large mass imbalances in individual layers, as shown in Fig. 4.1. This suggests constructing a more highly constrained model, in which mass is required to be conserved in density layers.

#### 4.2 Model 2: Mass conserved in isopycnal layers

##### *Velocity field and mass transport*

For this next-order model the constraints on total transport were supplemented by statements requiring approximate mass conservation in layers 4 to 18, which are not in contact with the atmosphere between 24°N and 36°N. The uncertainty in the mass balance in each layer was estimated to be  $\pm 1$  Sv due to the potential sources of error described in Chapter 1. The first experiment to be discussed has an initial reference level at 1300 db. This model is the same as that considered by RW, with two exceptions: the data in this case have not been objectively smoothed, and a variable reference pressure has been used to define the isopycnal surfaces bounding each layer (see section 3.1).

To satisfy the mass conservation equation in each layer to  $\pm 1$  Sv requires a modest increase in the reference level velocity, as seen in Fig. 4.2. The reference level velocities are no longer uniform across the 24°N and 36°N sections, but their magnitude is small, generally  $< 1 \text{ cm s}^{-1}$ . Note that the structure of the reference level velocity tends to mirror that of the bottom topography, particularly at 24 °N, with larger velocities over steeply-sloping topographic features such as the Mid-Atlantic Ridge and the continental slope. This tendency reflects the fact that the most "efficient" way, in a least squares sense, to eliminate the layer imbalances is to introduce a velocity correction at those station pairs at which the change in the ratio of layer depths is the greatest. If one

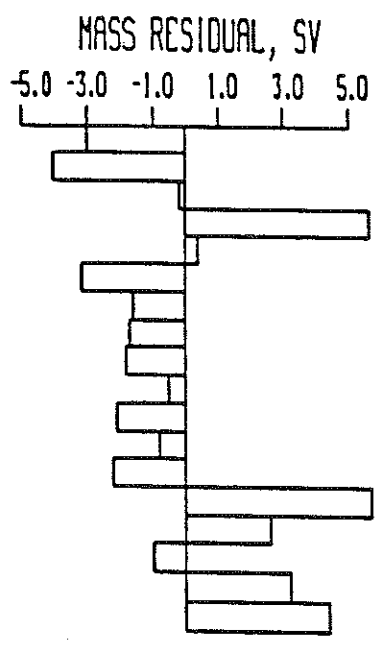


Fig. 4.1 Mass residuals in each layer (Sv) for model conserving total mass only.

considers this to be an undesirable feature of the solution, the weighting matrix  $W$  can be altered to remove some of the dependence on the bottom slope.

The zonally-integrated geostrophic transport per unit depth across each section is shown in Fig. 4.3. At  $36^\circ\text{N}$  there is a net northward flow of surface and intermediate water balanced by a southward flow of deep water, consistent with the water mass characteristics discussed in Section 2. The pattern of the meridional circulation is similar to that found by RW, as expected given similar model assumptions, with the NADW southward flow concentrated in the deepest layers. However, there is a small northward flow at depth in this case, splitting the upper and lower NADW. The net transport of 3 Sv to the south in layer 4 also differs from the RW results. Reasons for the differences between these results and those of RW are discussed in detail in Section 5.

The meridional transport of the upper water across the sections at  $24^\circ\text{N}$  consists of poleward flow in the western boundary current and an equatorward return flow in the interior. The sum of the transports through the Florida Straits and the interior section shows the same pattern as at  $36^\circ\text{N}$ .

Since the problem is still not highly constrained and, as discussed in Chapter I, does not have a unique solution, it is important to consider how sensitive a particular solution is to the model assumptions made. In particular, the results may depend on the choice of initial reference level. The choice of 1300 db was based in part on water mass characteristics: this depth approximately marks the boundary between the AAIW flowing to the north and the NADW flowing to the south. However, the zonally-integrated meridional transport in Fig. 4.3 has several zero crossings. Each depth of zero net meridional motion may represent a reasonable reference level choice.

In Fig. 4.4 the transport per unit depth at  $36^\circ\text{N}$  for models with initial reference levels at 1300 db, 3000 db and 4750 db are compared. The 3000 db level was chosen to roughly correspond to the level of the deep northward flow splitting the two primary

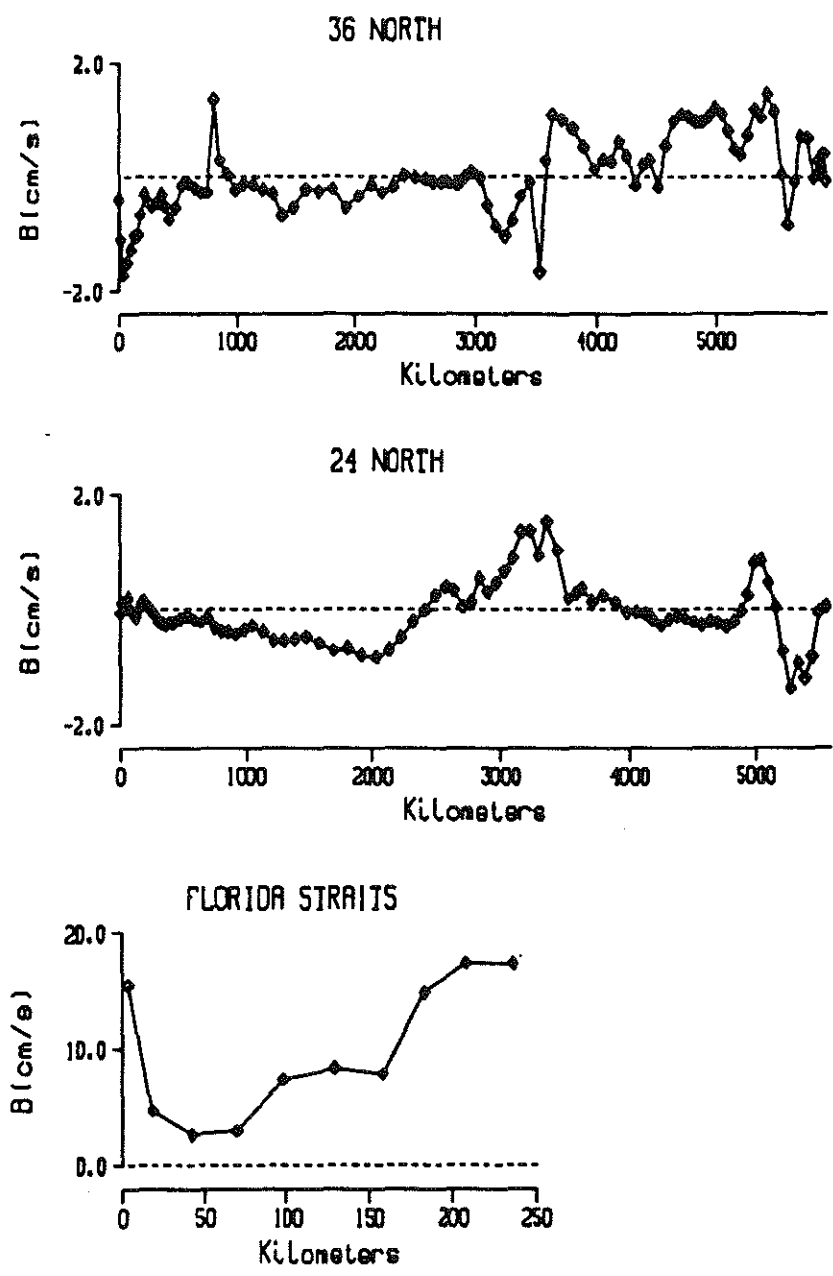


Fig. 4.2 Reference level velocity for model with mass conserved in isopycnal layers. Initial reference level = 1300 db.

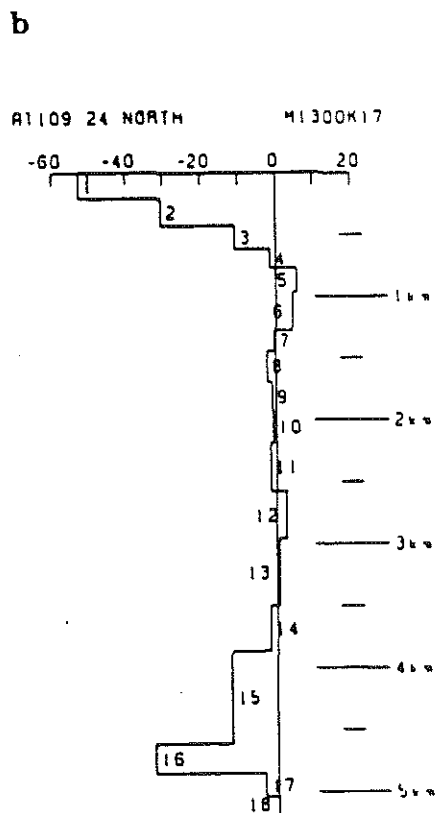
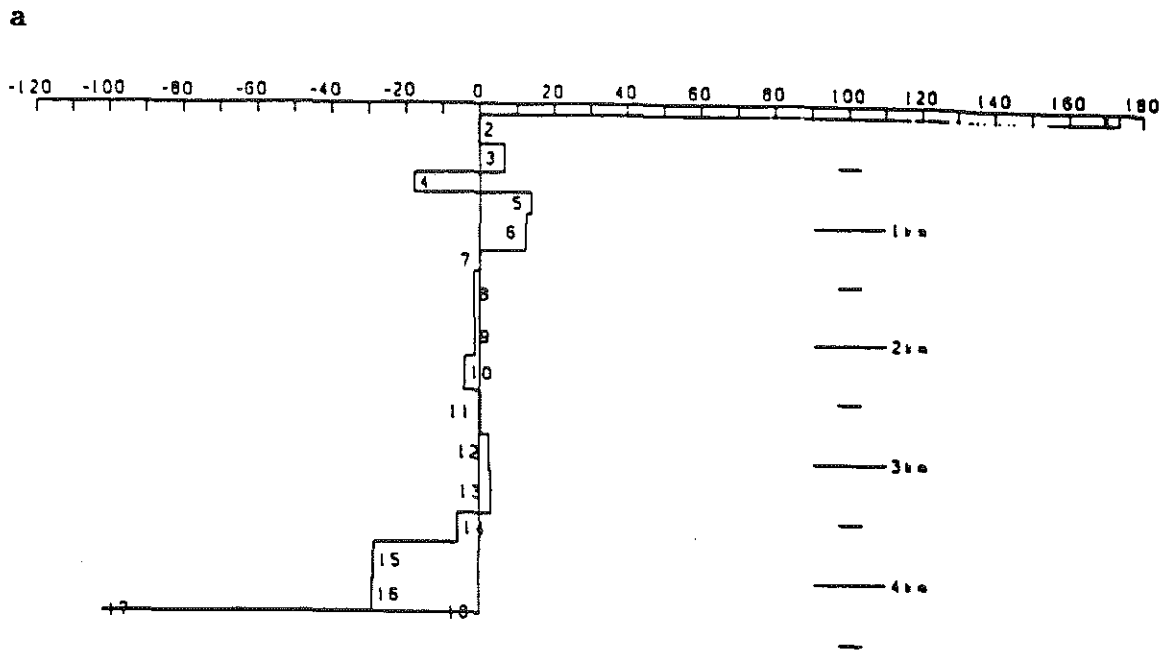


Fig. 4.3 Zonally-integrated volume transport per unit depth (Sv/km) for model with mass conserved in isopycnal layers; initial reference level = 1300 db. (a) 36°N; (b) 24°N; (c) Florida Straits.

branches of the NADW. The 4750 db level was also chosen to lie between water masses moving in opposing directions, in this case the northward flowing AABW and the NADW moving to the south.

There is relatively little difference between the 3000 db and 4750 db reference level cases, but there is a significant shift in the pattern of meridional transport between the 1300 db model and the models with deep levels. The net transport of surface and intermediate water is about the same, but with a deep reference level the southward flow of NADW occurs in two lobes of roughly equal strength, as opposed to the concentrated flow at depth in the 1300 db case. The deep northward flow in layer 13 between the upper and lower NADW branches is still present but weak in the deep reference level case.

The residuals for the mass conservation equations in each layer are shown in Fig. 4.5. For layers 4-18 the residuals are all much smaller than the estimated error of 1 Sv in each equation, showing that only a modest reference level velocity correction is required to satisfy the mass constraints nearly exactly. Thus, on the basis of the velocity field and mass transports, and the pattern of residuals, there is apparently no reason to favor one of these solutions over another. The meridional circulation below 1500 db is sensitive to the choice of initial reference level, and constraints on conservation of mass alone do not provide sufficient information to decide which of the two is more like the "true" flow.

In Table 4.3 the zonally-integrated transport in each layer at 36°N for the 1300 db and 3000 db reference level models are compared to the results of RW for these sections and for the IGY. RW assumed an initial reference level at 1300 db in both cases. RW had concluded, based on the difference between the IGY and the 1981 results, that there had been a significant shift in the meridional circulation in the North Atlantic between 1957 and 1981. This conclusion was supported by evidence that the structure of the property fields had also changed over the 24 years between the occupations of



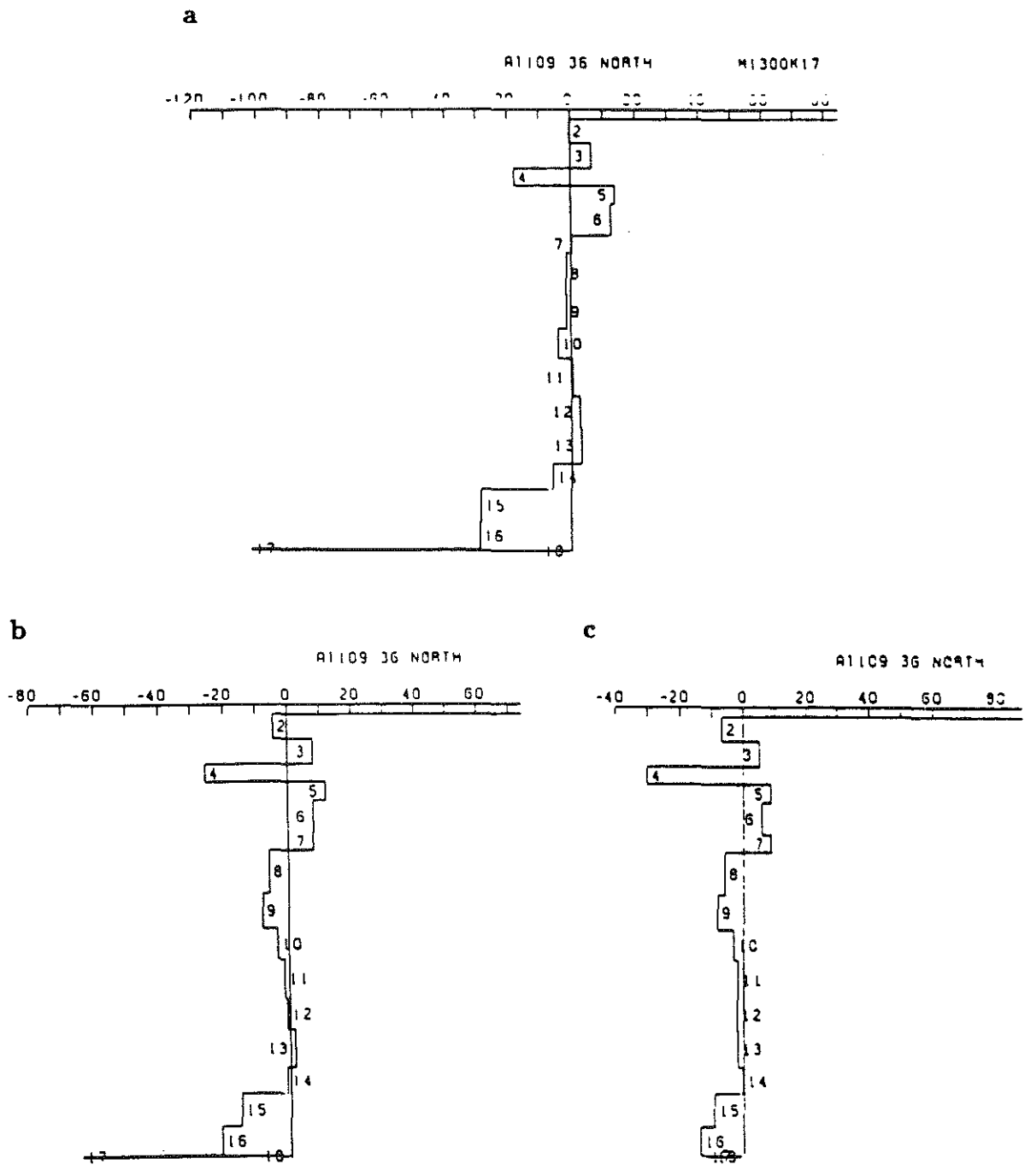


Fig. 4.4 Zonally-integrated volume transport per unit depth at 36°N for models conserving mass in isopycnal layers for different choices of initial reference level (Sv/km). (a) reference level = 1300 db; (b) reference level = 3000 db; (c) reference level = 4750 db.

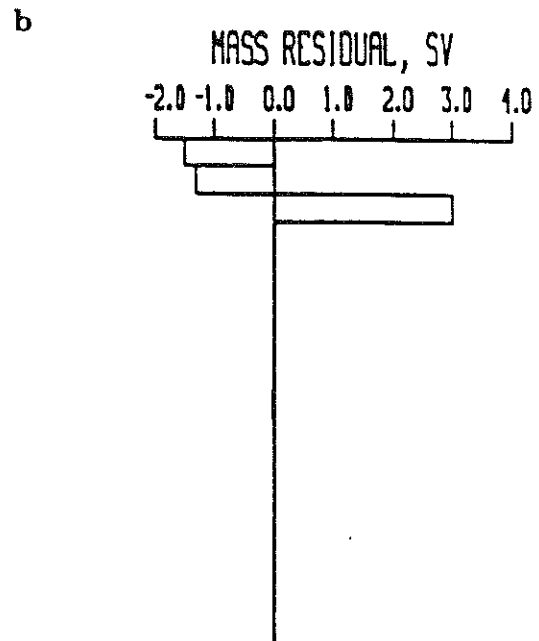
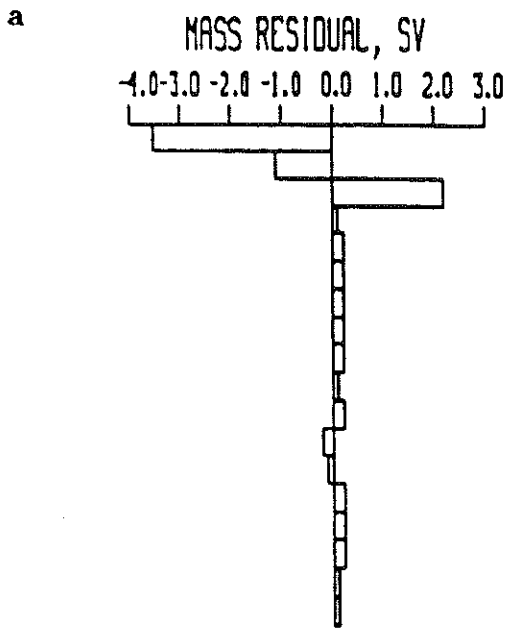


Fig. 4.5 Mass residuals for models conserving mass in isopycnal layers (Sv). (a) initial reference level = 1300 db; (b) initial reference level = 3000 db.

the two sections (Wunsch and Roemmich, 1984). However, using the same 1981 data and a deep reference level in this model results in a circulation more similar to that RW estimated for the IGY sections, using a shallow reference level. Without additional information allowing one to choose which of these solutions is a better representation of the actual flow, it is difficult to determine to what extent the circulation has changed over this period. Note also that the transports in some layers differ by several Sv between the 1300 db model and the RW results. Despite using the same data and a similar inverse technique, the two models differ in several important aspects. The differences will be addressed in detail in the discussion of the "best estimate" solution in Section 5.

#### *Physical and Chemical Fluxes*

We have seen that the velocity field, and in turn the mass transport, is sensitive to the initial model. In this section the temperature, oxygen and nutrient fluxes for each model are considered. The net flux results are summarized in Table 4.4 for each choice of initial reference level.

Table 4.3 Layer transports at 36°N for models with mass conserved in density layers, compared to results of RW for the 1981 data and the IGY data (Sv). The initial reference level is given at the head of each column.

| Layer | rl=1300<br>RW, IGY | rl=1300<br>RW, 1981 | rl=1300 | rl=3000 |
|-------|--------------------|---------------------|---------|---------|
| 1     | 13.4               | 11.2                | 13.8    | 15.0    |
| 2     | -2.6               | -1.7                | -1.2    | -2.3    |
| 3     | -0.6               | 1.4                 | 1.5     | 2.1     |
| 4     | 1.0                | 1.9                 | -2.5    | -3.7    |
| 5     | 2.1                | 1.6                 | 2.7     | 2.5     |
| 6     | 1.8                | 2.9                 | 4.1     | 2.8     |
| 7     | 1.4                | 1.8                 | 0.0     | 1.3     |
| 8     | -1.0               | -0.6                | -0.6    | -2.5    |
| 9     | -2.5               | -0.5                | -0.6    | -2.8    |
| 10    | -2.7               | -1.2                | -1.3    | -1.1    |
| 11    | -2.8               | -0.4                | 0.3     | -0.4    |
| 12    | -2.4               | -0.3                | 1.2     | 0.2     |
| 13    | -1.7               | -1.5                | 1.9     | 1.7     |
| 14    | -0.3               | -1.5                | 0.7     | 0.4     |
| 15    | -2.7               | -8.3                | -9.5    | -5.6    |
| 16    | -2.4               | -5.4                | -8.6    | -7.0    |
| 17    | 1.8                | 0.3                 | -0.7    | -0.5    |
| 18    | *                  | *                   | *       | *       |

There is little change in the temperature flux with reference level. In the previous section we saw that the primary difference between the shallow and deep reference level results was in the deep circulation: since below 1500 db there is relatively little change in temperature with depth, a redistribution of transport in the deep layers has little effect on the net temperature transport.

The oxygen flux is also not sensitive to the choice of reference level; the distribution of oxygen is even more uniform than temperature in the deep water (Fig. 2.1, 2.2), and changes in the deep circulation have little effect on the net flux. At both latitudes there is a significant net flux of oxygen to the south. As BD pointed out, this is a signal of

Table 4.4a *Temperature flux results for models with mass conserved in isopycnal layers ( $^{\circ}\text{C Sv}$ ).*

|           | rl=1300 | rl=3000 | rl=4750 |
|-----------|---------|---------|---------|
| 24°N      | -264    | -318    | -336    |
| FS        | 580     | 576     | 579     |
| 24°N+FS   | 316     | 258     | 250     |
| 36°N      | 305     | 310     | 288     |
| net conv. | 11      | -52     | -38     |

Table 4.4b *Oxygen flux results for models with mass conserved in isopycnal layers ( $\text{kmol s}^{-1}$ ). 'BD' are results of Brewer and Dyrssen (1987).*

|           | rl=1300 | rl=3000 | rl=4750 | BD    |
|-----------|---------|---------|---------|-------|
| 24°N      | -7560   | -7694   | -7247   | -6970 |
| FS        | 5134    | 5134    | 5134    | 4890  |
| 24°N+FS   | -2426   | -2560   | -2113   | -2080 |
| 36°N      | -2938   | -2849   | -2536   |       |
| net conv. | 512     | 289     | 423     |       |

the large-scale ventilation of the deep ocean through the formation of NADW; indeed, at both sections the highest observed oxygen concentrations are found in the NADW core in the deep western boundary current.

Table 4.4c *Silicate flux results for models with mass conserved in isopycnal layers ( $\text{kmol s}^{-1}$ ).*

|           | rl=1300 | rl=3000 | rl=4750 | BD   |
|-----------|---------|---------|---------|------|
| 24°N      | -649    | -239    | -295    | -525 |
| FS        | 164     | 167     | 169     | 187  |
| 24°N+FS   | -485    | -72     | -126    | -338 |
| 36°N      | -140    | -93     | -80     |      |
| net conv. | -345    | 21      | -46     |      |

Table 4.4d *Nitrate flux results for models with mass conserved in isopycnal layers ( $\text{kmol s}^{-1}$ ).*

|           | rl=1300 | rl=3000 | rl=4750 | BD   |
|-----------|---------|---------|---------|------|
| 24°N      | -361    | -260    | -313    | -392 |
| FS        | 270     | 275     | 277     | 292  |
| 24°N+FS   | -91     | 15      | -36     | -100 |
| 36°N      | 135     | 129     | 133     |      |
| net conv. | -226    | -114    | -169    |      |

In contrast to heat and oxygen, the flux of nutrients is very sensitive to the choice of initial reference level, particularly at 24°N. Both models result in a southward flux of silicate across each latitude. However, the 1300 db reference level results in a much

larger flux at 24°N than the 3000 db level,  $-485 \text{ kmol s}^{-1}$  vs.  $-72 \text{ kmol s}^{-1}$ , while BD's estimate is in the middle of this range. At 36°N, the 1300 db reference level also results in a larger transport, although the difference between the models is not as great at this latitude.

The net divergence of silicate within the box is also very different for the two models. With the 1300 db reference level, much more silicate leaves the box across the 24°N section than enters across 36°N and through the Florida Straits, requiring an apparent net production of more than  $300 \text{ kmol s}^{-1}$  of silica within the box. The 3000 db reference level, on the other hand, leads to essentially no net divergence of silicate.

The pattern of silicate divergences in individual layers (Fig. 4.6a) is another indication of the sensitivity of the silicate fluxes to the reference level used, particularly in the deep water. While in the 3000 db case the residuals are all fairly small, in the 1300 db case there are large ( $50 - 140 \text{ kmol s}^{-1}$ ) divergences in the deep layers.

The flux of nitrate at 24°N is also sensitive to the reference level used. In the 1300 db case the net flux of nitrate across 24°N is  $-91 \text{ kmol s}^{-1}$  (to the south), similar to that found by BD. The 3000 db case, however, gives a small net northward transport at 24°N of  $15 \text{ kmol s}^{-1}$ . In contrast, the nitrate flux at 36°N does not depend on the choice of reference level, with all models showing a net northward flux of more than  $100 \text{ kmol s}^{-1}$ . In each case there is a significant divergence of nitrate, apparently requiring a strong source between 24°N and 36°N.

The nitrate residuals in individual layers are compared in Fig. 4.6b. The two models both show a similar pattern, with fairly small residuals at depth, but strong divergence in the upper layers. This feature is considered in more detail below.

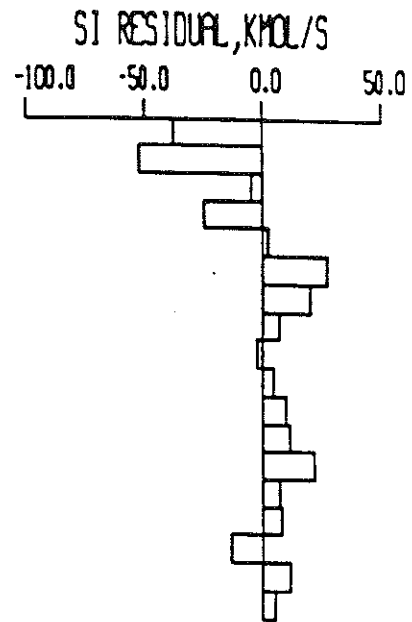
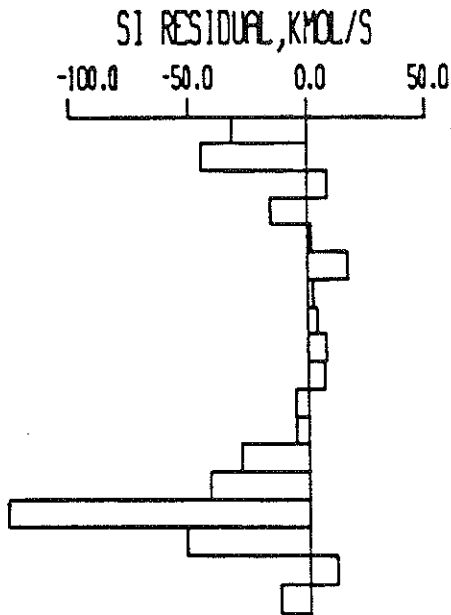
#### *Conclusions from mass-conserving models*

We have seen that for models in which the only constraints imposed are those on total transport and mass conservation in density layers, the results are very sensitive to

RL = 1300 db

RL = 3000 db

a



b

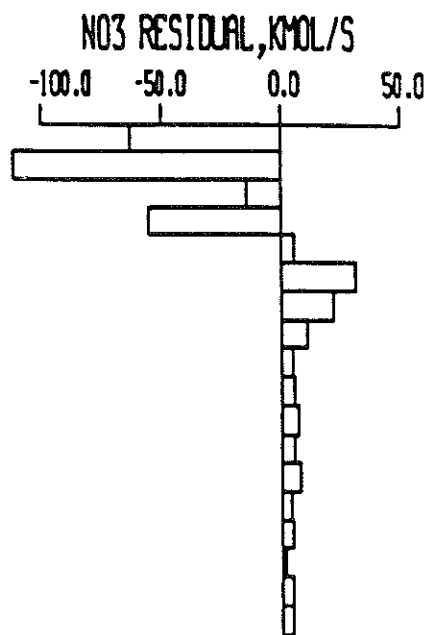
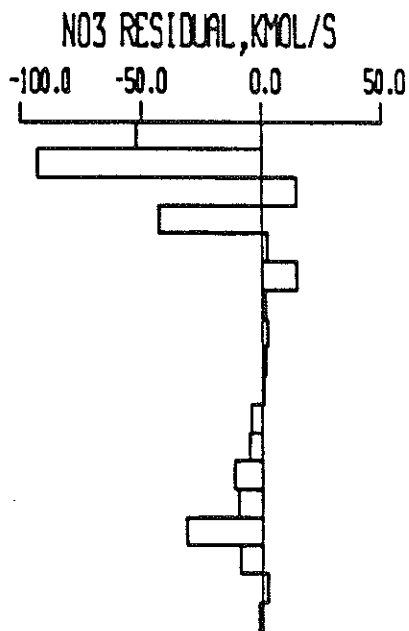


Fig. 4.6 Nutrient residuals in each layer for models conserving mass in isopycnal layers ( $\text{kmol s}^{-1}$ ). (a) silicate; (b) nitrate.



the choice of initial reference level. Both shallow and deep reference levels result in consistent solutions that give "reasonable" circulations: the flow of water masses is consistent with the property fields in being away from their source regions, the pattern and magnitude of the residuals in the mass conservation equations are similar, and the reference level velocities are sensible. The mass constraints alone do not provide enough information to determine which of the solutions is a better representation of the true mean flow.

However, there are substantial differences between the two circulation patterns, especially in the deep water. Changes in the deep circulation have a small effect on the heat and oxygen fluxes, since there is relatively little structure in the temperature and oxygen fields at depth. The nutrients do vary significantly in the deep water and the transport of silicate, in particular, is extremely sensitive to changes in the deep flow, and hence to the reference level chosen.

This sensitivity of the nutrient fluxes to the reference level choice means that given mass conservation statements alone we are not able to resolve the nutrient fluxes. On the other hand, it also suggests that there is information contained in the nutrient distributions that might be exploited to better resolve the circulation. The models discussed below explore the extent to which the nutrients contribute information independent of mass by including explicit constraints on the nutrient fluxes.

### 4.3 Model 3: Total silicate conserved

The 1300 db reference level model discussed in the previous section resulted in a large silicate divergence of  $>300 \text{ kmol s}^{-1}$  between  $24^\circ\text{N}$  and  $36^\circ\text{N}$ . The rate of silicate production implied by this divergence far exceeds estimates of the rate at which silicate is supplied. Within the subtropical North Atlantic the sediments are low in opal and dissolution is a negligible source of silicate (Broecker and Peng, 1982). The total input to the North Atlantic from rivers, glacial run-off and inflow of Pacific water was estimated to be between 30 and  $60 \text{ kmol s}^{-1}$  by Anderson *et al.* (1983), 5-10 times smaller than the silicate source required to balance this divergence. Moreover, there are no large rivers entering the Atlantic between  $24^\circ\text{N}$  and  $36^\circ\text{N}$  so the silica input is probably even smaller within this latitude band. The Mediterranean Outflow Water is also low in silicate (Metcalf, 1969).

Therefore the large imbalances in silicate found in the 1300 db model are incompatible with present understanding of the silica cycle in the Atlantic. A constraint requiring that total silicate be approximately conserved was next added to this model to see if a circulation could be found consistent with there being no net source or sink of silicate within the box.

The solution at each section for this model is shown in Fig. 4.7. Satisfying the constraint on total silicate conservation requires only a small change in the reference level velocities (the solution norm increases from 500 to 605). The rank is increased by one, indicating that the silicate constraint is independent of the mass constraints.

The new flux results are summarized and compared to the results of the mass-conserving models in Table 4.6. The net temperature flux is little changed by the addition of the silicate constraint. The equatorward flux of oxygen across  $24^\circ\text{N}$  is increased and is now roughly equal to that at  $36^\circ\text{N}$ , so that there is almost zero net convergence of oxygen in the box for this model. The changes in the nutrient transports are more dramatic at  $24^\circ\text{N}$  than at  $36^\circ\text{N}$ . The southward flux of silicate and nitrate at

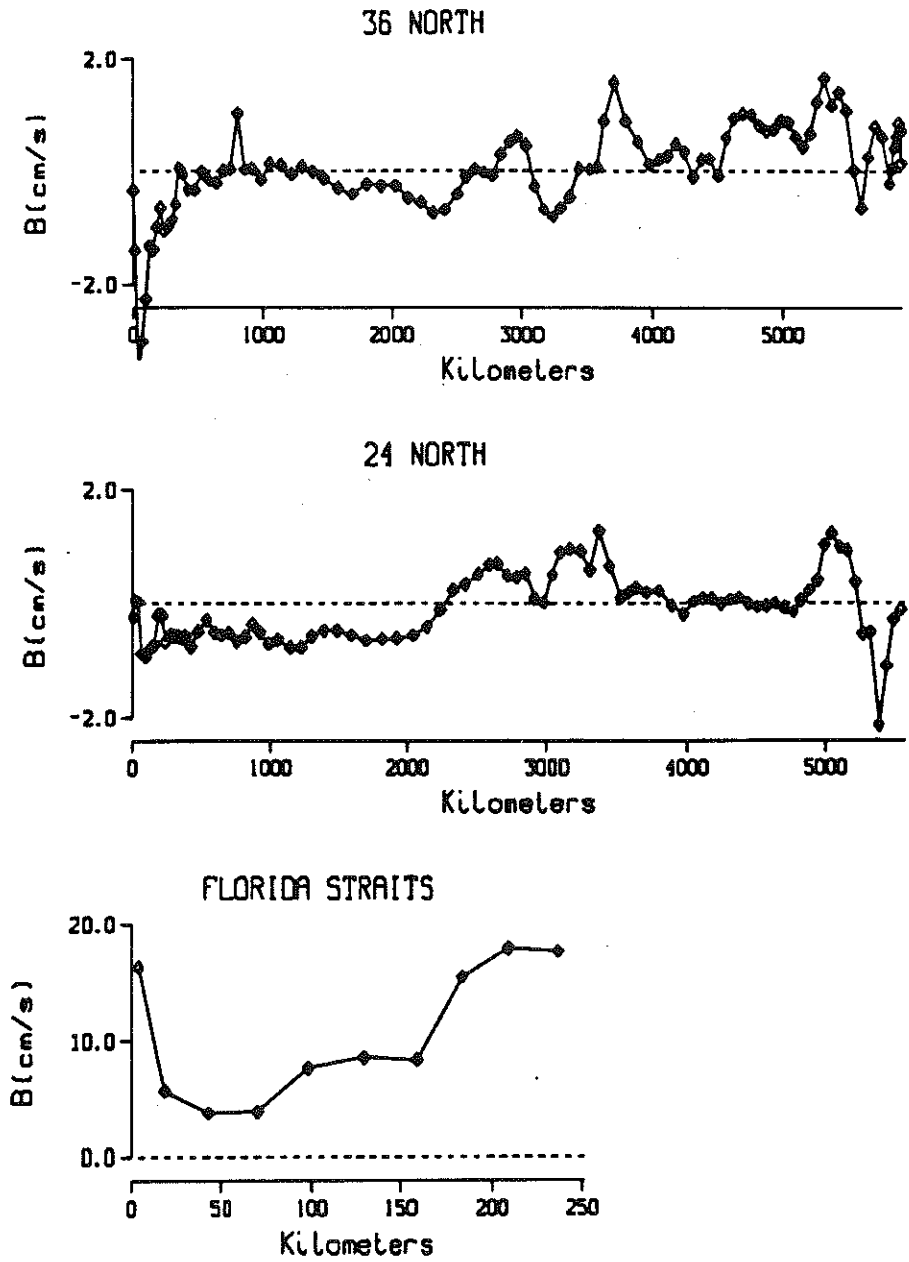


Fig. 4.7 : Reference level velocity for model conserving total silicate. Initial reference level = 1300 db.

Table 4.6a *Temperature flux results for model conserving total silicate ( $^{\circ}C Sv$ ). Initial reference level at 1300 db. Columns labeled 'rl=1300' and 'rl=3000' are results from models conserving mass only.*

|           | tot Si cons. | rl=1300 | rl=3000 |
|-----------|--------------|---------|---------|
| 24°N      | -288         | -264    | -318    |
| FS        | 583          | 580     | 576     |
| 24°N+FS   | 295          | 316     | 258     |
| 36°N      | 340          | 305     | 310     |
| net conv. | 45           | 11      | -38     |

24°N are both decreased when total silicate is conserved, to values closer to those found in the 3000 db reference level, mass-conserving case. The silicate flux at this latitude, however, is still more than four times as large as in the 3000 db model. At 36°N the southward silicate flux is increased by 40%. In other words, the system responds to the requirement that total silicate be conserved by bringing more silicate into the box from the north and removing less to the south at 24°N. The nitrate flux at 24°N is close to the 3000 db mass-only case, while at 36°N the transport is decreased slightly in magnitude but still to the north. Thus there is again a significant divergence of nitrate within the box.

Table 4.6b Oxygen flux results for model conserving total silicate ( $kmol s^{-1}$ ).

|           | tot. Si cons. | rl=1300 | rl=3000 | BD    |
|-----------|---------------|---------|---------|-------|
| 24°N      | -8125         | -7560   | -7694   | -6970 |
| FS        | 5130          | 5134    | 5134    | 4890  |
| 24°N+FS   | -2995         | -2426   | -2560   | -2080 |
| 36°N      | -3075         | -2938   | -2849   |       |
| net conv. | 80            | 512     | 289     |       |

Table 4.6c Silicate flux results for model conserving total silicate ( $kmol s^{-1}$ ).

|           | tot. Si cons. | rl=1300 | rl=3000 | BD   |
|-----------|---------------|---------|---------|------|
| 24°N      | -466          | -649    | -239    | -525 |
| FS        | 164           | 164     | 167     | 187  |
| 24°N+FS   | -297          | -485    | -72     | -338 |
| 36°N      | -290          | -140    | -93     |      |
| net conv. | -7            | -345    | 21      |      |

The property fluxes for a shallow reference level model which conserves total silicate are thus closer to the deep reference level mass-only results. However, as shown in Fig. 4.8, the pattern of the mass transport per unit depth still differs substantially from the 3000 db mass-conserving model (see Fig. 4.4b). In fact, the southward flow

Table 4.6d Nitrate flux results for model conserving total silicate ( $\text{kmol s}^{-1}$ ).

|           | tot. Si cons. | rl=1300 | rl=3000 | BD   |
|-----------|---------------|---------|---------|------|
| 24°N      | -297          | -361    | -260    | -392 |
| FS        | 277           | 270     | 275     | 292  |
| 24°N+FS   | -20           | -91     | 15      | -100 |
| 36°N      | 90            | 135     | 129     |      |
| net conv. | -110          | -226    | -114    |      |

of NADW is even more concentrated in the deepest layers in this case. The northward flow of AAIW is also slightly increased. But most notable, perhaps, is the fact that only slight shifts in the meridional circulation are required to drive the large silicate divergence to zero.

Different initial reference levels still lead to different meridional circulations, even with the additional constraint that total silicate be conserved. The silicate transport, in particular, is sensitive to changes in the deep circulation and differs substantially for the two models. Moreover, the 1300 db model results in large silicate residuals within density layers, as seen in Fig. 4.9. Several authors have suggested that regeneration of silica within the water column is insignificant in the North Atlantic. Menzel and Ryther (1968) found no evidence for respiration occurring below 300 m, and concluded that the nutrient maximum layer was due to spreading of nutrient rich water along density surfaces rather than local regeneration. Broecker and Takahashi (1980) concluded that the decomposition of particles was insignificant within the NADW complex, defined to lie between the 2°C discontinuity and the silicate minimum at  $\approx 1$  km depth. As mentioned in the Introduction, the relative nutrient enrichment of the deep water in

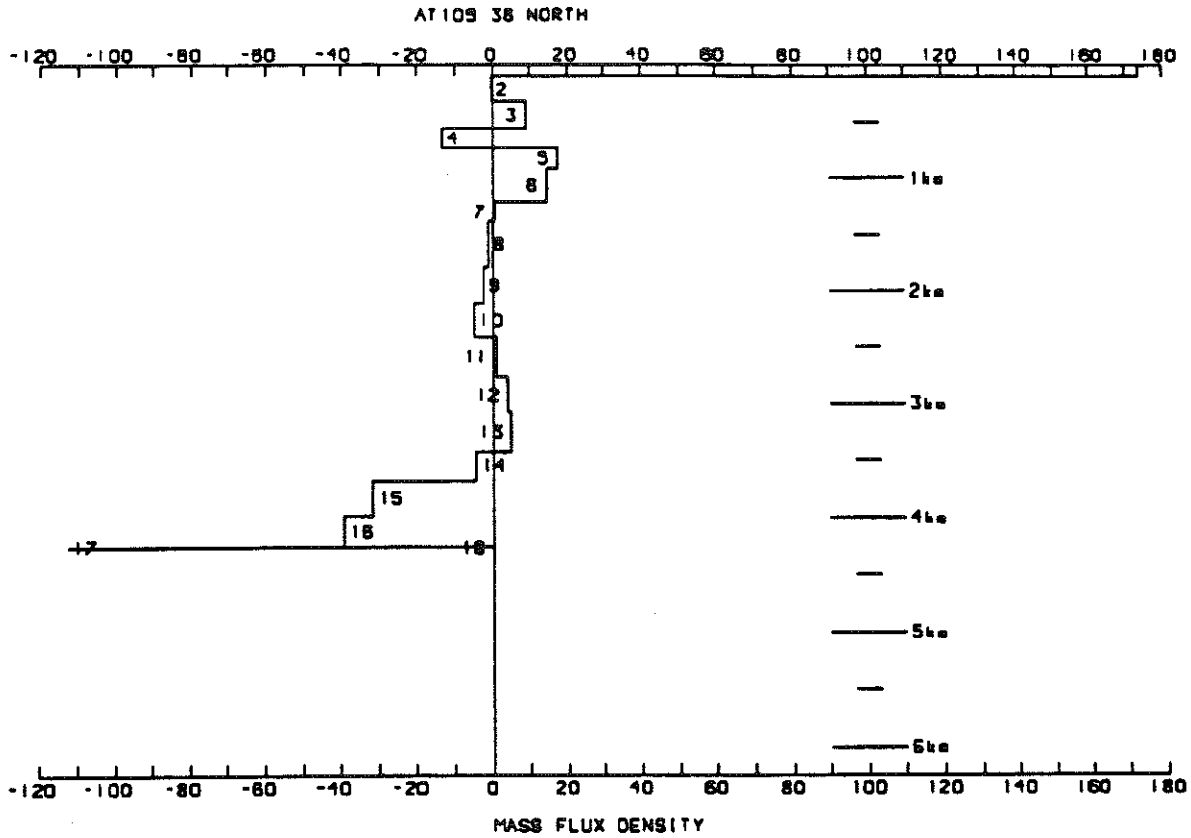


Fig. 4.8 Zonally-integrated volume transport at 36°N (Sv/km) for model conserving mass and total silicate; initial reference level = 1300 db.

the eastern basin has been taken as evidence of nutrient regeneration, but the contribution is apparently small relative to the fluxes calculated here. Broecker *et al.*(1980) estimated the oxygen respiration rate below the 2° discontinuity in the eastern basin to be  $.12 \pm .06$  moles  $m^{-2} yr^{-1}$ . Using the nitrate-oxygen and silicate-oxygen ratios they observed, the regeneration rate of nitrate and silicate implied by this value is  $.012$  moles  $m^{-2} yr^{-1}$  and  $.10$  moles  $m^{-2} yr^{-1}$ , respectively. Over the area of the eastern basin between 24 and 36°N this results in a net source of  $1 kmol s^{-1}$  and  $8 kmol s^{-1}$ , respectively, which is negligible relative to the flux through each section in the deep water. Broecker *et al.*(1976) and Kawase and Sarmiento (1986) also concluded that the nutrient distribution in the eastern basin could be most easily explained by assuming that the major source of nutrients was the rain of opal and organic debris beneath the upwelling area along the African coast, and subsequent spreading of high nutrient water to the north and south. These observations suggest constructing a next set of models, in which silica is conserved in isopycnal layers.



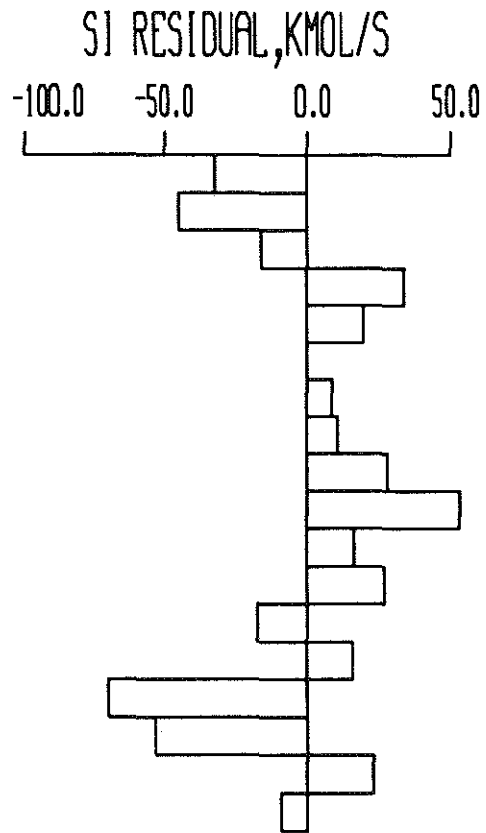


Fig. 4.9 Silicate residuals in each layer for model conserving mass and total silicate.

#### 4.4 Model 4: Mass and silicate conserved in isopycnal layers

Silicate conservation constraints for layers 4-18 were added to the mass conservation and total silicate constraints of the previous models, again considering initial reference levels at 1300 db and 3000 db. The equations were weighted by the mean silicate concentration for the sections multiplied by the estimated uncertainty in the mass balance for each layer.

The reference level velocities for both models are shown in Fig. 4.10. The solutions are both of "reasonable" magnitude, suggesting that the data are consistent with the assumption that silica is conserved in density layers. In the models discussed so far, a deep reference level led to relatively small silicate residuals, particularly in the deep water. It is not surprising, then, that satisfying the silicate conservation constraints introduces more structure in  $\mathbf{b}$  in the 1300 db case, and a larger increase in the solution norm. The increase is still modest, however:  $\mathbf{b}^t\mathbf{b}$  is increased from 400 to 654, corresponding to an rms increase in dimensional units of  $.22 \text{ cm s}^{-1}$  at  $24^\circ$  and  $36^\circ\text{N}$ . (The use of an rms value here is meant only to give a rough measure of the correction required, not to suggest that the structure of  $\mathbf{b}$  resembles that of a "white" process.) At both latitudes the largest changes in the solution occur in the center of the sections, on the west flank of the Mid-Atlantic Ridge, and stronger, more structured flow near the western boundaries. The flow through the Florida Straits is unchanged. For the 3000 db reference level, for which silicate was already nearly balanced in the mass conserving case, the reference level velocity correction required is even smaller ( $<.1 \text{ cm s}^{-1}$ , rms).

The net flux results are given in Table 4.7. For all properties the results are very similar for the two choices of initial reference level. The temperature and oxygen transports are only slightly changed by the addition of the silica constraints. Across both latitudes there is a poleward meridional heat flux of  $\approx 1.3 \text{ PW}$  and an equatorward flux of oxygen of  $\approx 3000 \text{ kmol s}^{-1}$ .

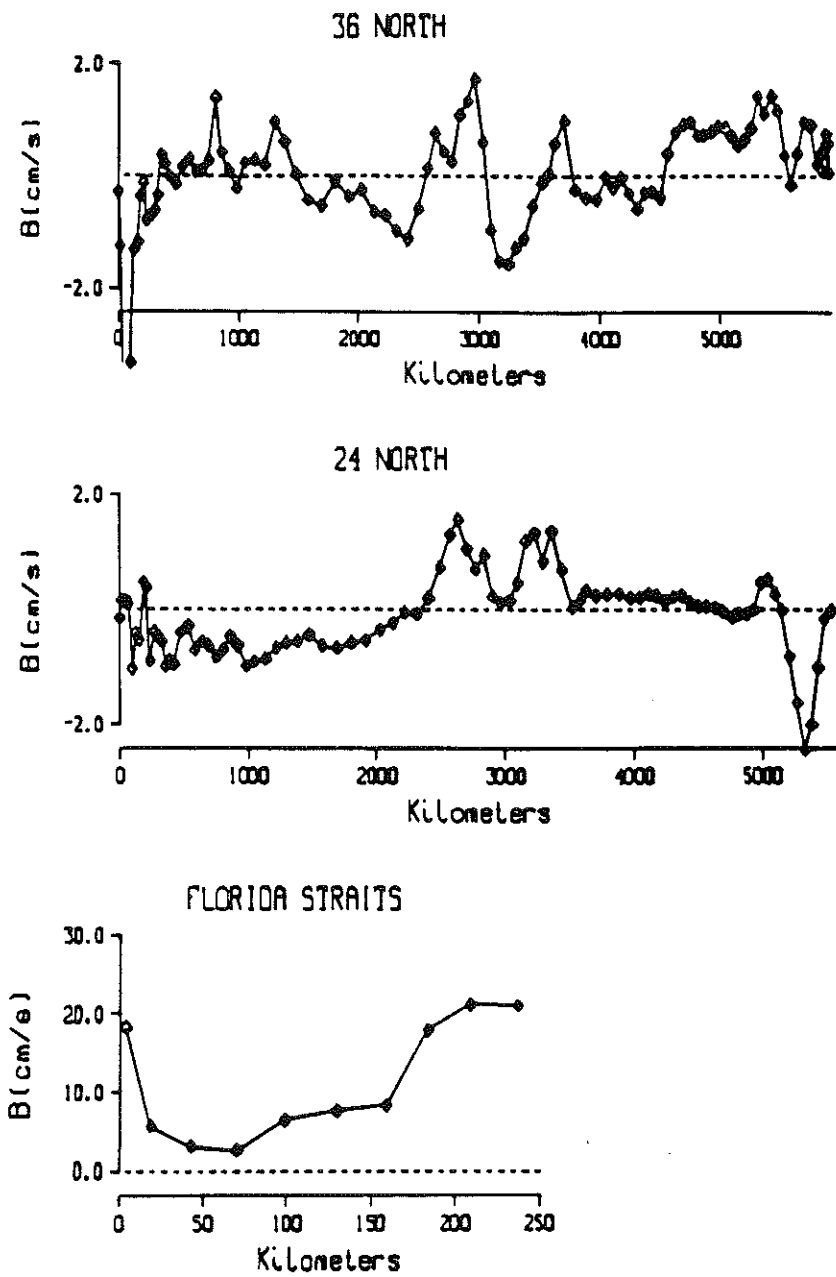


Fig. 4.10a Reference level velocity for model conserving silicate in isopycnal layers with initial reference levels at 1300 db.

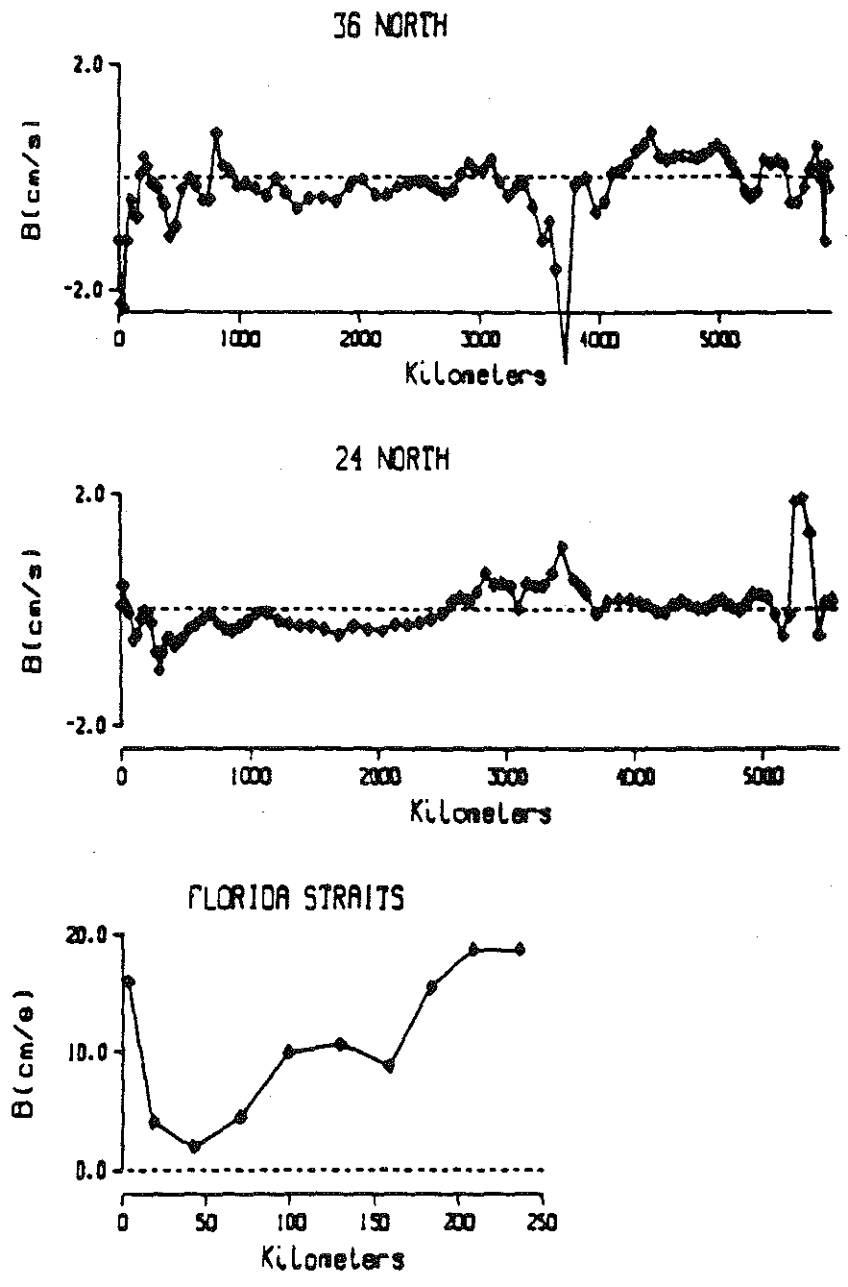


Fig. 4.10b Reference level velocity for model conserving silicate in isopycnal layers with initial reference levels at 3000 db.

Table 4.7a Temperature flux results for models conserving mass and silicate in layers 4-19 ( $^{\circ}\text{C Sv}$ ). Columns labeled 'noise', 'null', and 'Ekman' are estimates of error due to data noise, unresolved components of flow in the null-space, and errors in the wind stress. See the Appendix for details of error analysis.

|                    | rl=1300 | rl=3000 | noise | null | Ekman |
|--------------------|---------|---------|-------|------|-------|
| 24 $^{\circ}$ N    | -290    | -306    | 3     | 3    | 43    |
| FS                 | 600     | 596     |       |      |       |
| 24 $^{\circ}$ N+FS | 310     | 290     |       |      |       |
| 36 $^{\circ}$ N    | 312     | 328     | 4     | 4    | 31    |
| net conv.          | -2      | -48.    |       |      |       |

Table 4.7b Oxygen flux results for models conserving mass and silicate in layers 4-19 ( $\text{kmol s}^{-1}$ ).

|                    | rl=1300 | rl=3000 | noise | null | Ekman |
|--------------------|---------|---------|-------|------|-------|
| 24 $^{\circ}$ N    | -7872   | -7828   | 89    | 134  | 63    |
| FS                 | 5179    | 5223    |       |      |       |
| 24 $^{\circ}$ N+FS | -2693   | -2605   |       |      |       |
| 36 $^{\circ}$ N    | -3116   | -2938   | 134   | 179  | 45    |
| net conv.          | 423     | 333     |       |      |       |

The sensitivity of the silica transport to the choice of reference level is dramatically reduced by the additional constraint that silica be conserved. For example, at 24 $^{\circ}$ N the

Table 4.7c *Silicate flux results for models conserving mass and silicate in layers 4-19 ( $kmol s^{-1}$ ).*

|           | rl=1300 | rl=3000 | noise | null | Ekman |
|-----------|---------|---------|-------|------|-------|
| 24°N      | -336    | -321    | 14    | 20   | 56    |
| FS        | 164     | 169     |       |      |       |
| 24°N+FS   | -172    | -152    |       |      |       |
| 36°N      | -159    | -138    | 14    | 13   | 38    |
| net conv. | -13     | -14     |       |      |       |

Table 4.7d *Nitrate flux results for mass and silicate conserved in layers 4-19 ( $kmol s^{-1}$ ).*

|           | rl=1300 | rl=3000 | noise | null | Ekman |
|-----------|---------|---------|-------|------|-------|
| 24°N      | -305    | -286    | 5     | 12   | 39    |
| FS        | 271     | 278     |       |      |       |
| 24°N+FS   | -34     | -8      |       |      |       |
| 36°N      | 114     | 119     | 4     | 11   | 35    |
| net conv. | -135    | -127    |       |      |       |

range of transports is reduced from 410 to 15  $kmol s^{-1}$ . The net flux at both latitudes is again to the south. The mean value of -155  $kmol s^{-1}$  is slightly less than half that estimated by Brewer and Dyrssen, but still several times larger than the estimated silicate input to the North Atlantic.

The addition of constraints on silicate has also made the nitrate transport results independent of the choice of reference level. At 24°N the range is cut from 106 to 16  $kmol s^{-1}$ . For both reference levels the net flux across 24°N is to the south but small, about 10-30% of the 100  $kmol s^{-1}$  estimated by BD. At 36°N the flux of nitrate is still strongly to the north at 115  $kmol s^{-1}$ . Consequently, the silica conserving models also show a large divergence of nitrate between 24° and 36°N.

The addition of silica conservation constraints has effectively removed the sensitivity of the nutrient transports to the choice of initial model. Has this additional information reduced the indeterminacy in the flow field as well?

The zonally-integrated transport across 36°N is shown in Fig. 4.11. The transport in individual layers is not identical in the two cases, but the net flux of each water mass is now more similar for the two reference levels than in the less-constrained models. The flow is essentially unchanged for the deep reference level. For the 1300 db model, the meridional cell at 36°N is the same strength when silicate is conserved, but the southward flow of NADW is more evenly distributed with depth: in this case 5 Sv, or 25% of the NADW flow, occurs in layers 7-11, as opposed to 2 Sv when only mass is conserved. This is still less broadly distributed than the deep reference level case, however, in which 45% of the southward flow occurs in the upper NADW branch. The models also differ in the deeper layers, where the shallow reference level leads to a stronger northward flow in layers 12-14.

The meridional property flux results suggest that silica provides information independent of mass conservation that is useful in reducing the sensitivity of the transports to the choice of initial reference level. This is particularly true for the nutrients. The pattern of net meridional mass transport is also found to be less dependent on the reference level when silicate is conserved, but some differences still remain.

Given that silica has proved useful in resolving the velocity field and transports, a logical next step is to ask whether there are any additional observations available to

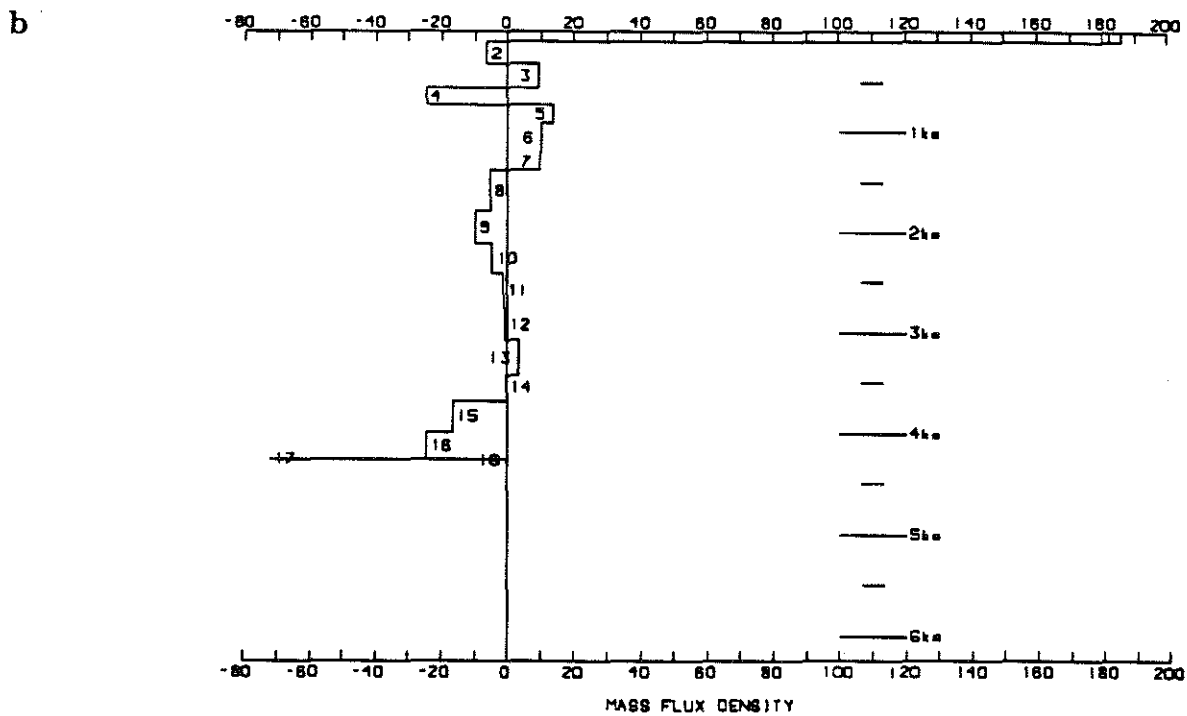
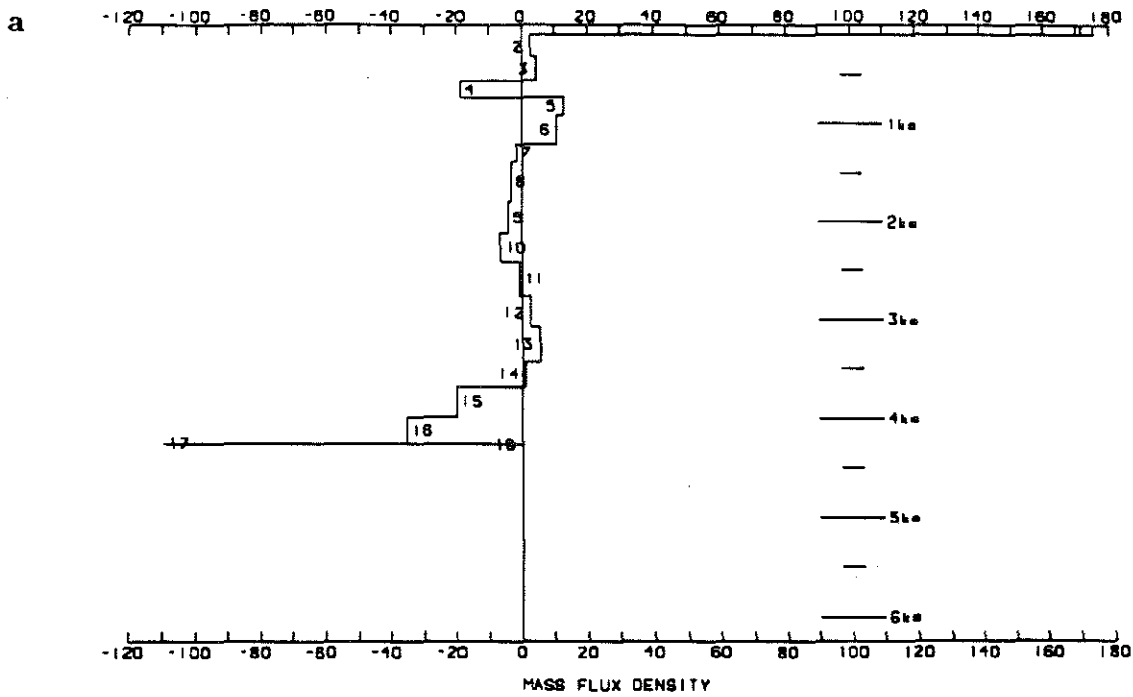


Fig. 4.11 : Zonally-integrated mass transport across  $36^{\circ}\text{N}$  for models conserving silicate in isopycnal layers with initial reference level at (a) 1300 db and (b) 3000 db.



further constrain the system. The nitrate, oxygen and 'PO' residuals in each density layer are shown in Fig. 4.12 and Fig. 4.13 for the silica conserving models. ('PO' is an approximately conservative tracer obtained from the linear combination of the phosphate and oxygen concentrations weighted by the Redfield ratio:  $'PO' = 135PO_4 + O_2$ ; Broecker, 1974). Although only mass and silicate were required to be conserved, the imbalances for the other properties are all equal to zero to within estimated errors below the top three layers. In other words, a flow field that conserves mass and silicate also approximately conserves 'PO' and salt, as well as nitrate and oxygen, which might be expected to be non-conservative due to biological activity in the water column. The conclusion, then, is that the other property fields contain little information independent of that contained in the mass and silicate distributions. (A possible exception is the large divergence of nitrate in the upper layers, which is discussed in more detail in Section 5.)

The purpose of this section has been to find the simplest model consistent with the physical and chemical observations. The strategy adopted has been to consider a progression of models, gradually adding constraints and evaluating the consistency of the model results and the data by considering the residuals and the zonally-integrated property transports. By these criteria we have found that a model that conserves mass and silicate in density layers is consistent with the data, starting with either a shallow or a deep initial reference level.

In the next section the horizontal and vertical structure of the circulation and the mechanisms responsible for the property transports are discussed more thoroughly for the silicate-conserving models. We will see that despite the similarity of the flux results, the details of the flow still differ substantially in the two models. Although the property fields do not provide the information required to select one of the solutions as preferable to the other, other observations including direct velocity measurements can be used as diagnostics to determine which features of the solutions are most realistic.

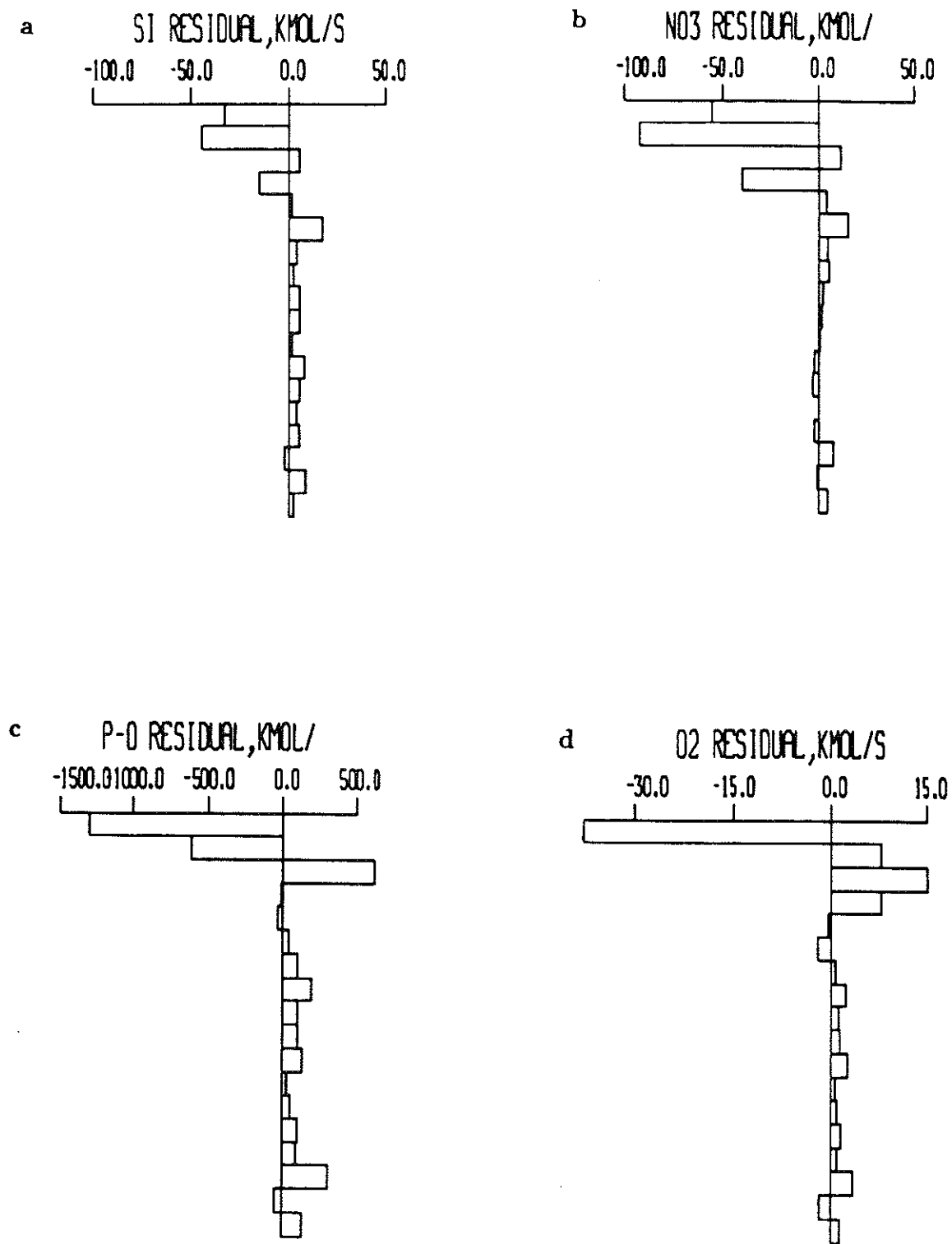


Fig. 4.12 Residuals in each layer for silicate-conserving models with initial reference level at 1300 db: (a) silicate; (b) nitrate; (c) 'PO'; (d) oxygen.

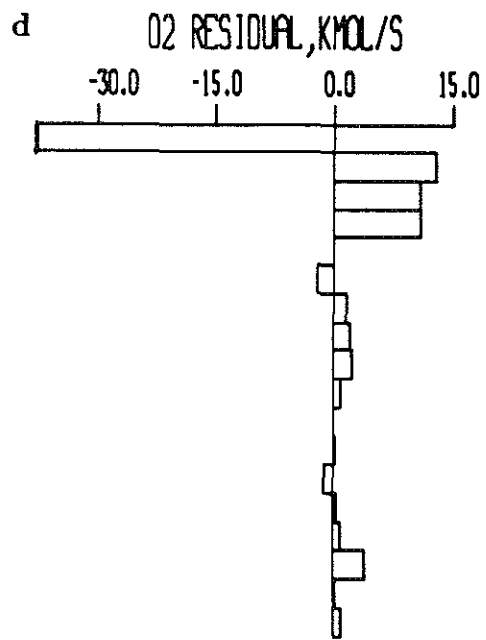
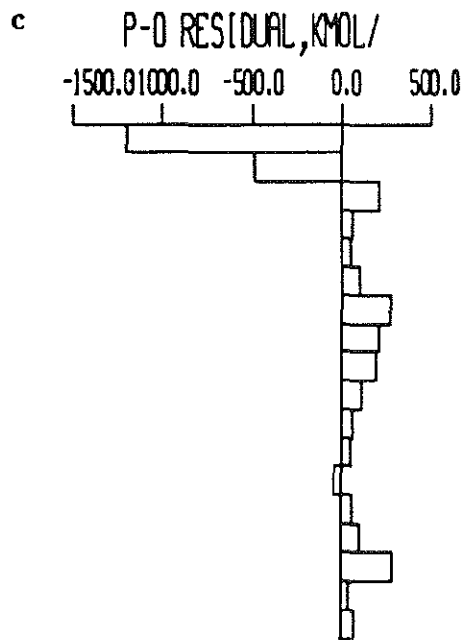
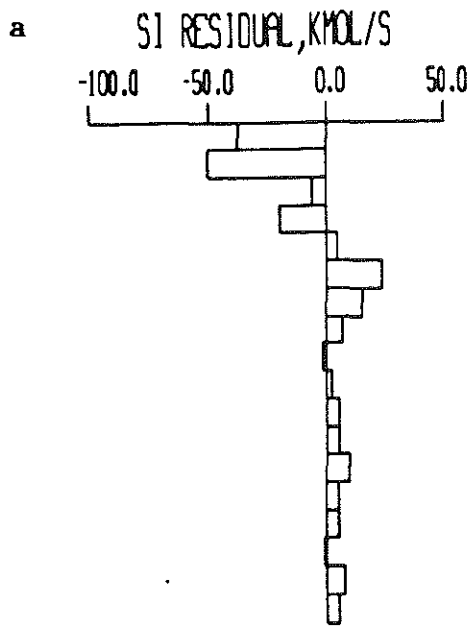


Fig. 4.13 Residuals in each layer for silicate-conserving models with initial reference level at 3000 db: (a) silicate; (b) nitrate; (c) 'PO'; (d) oxygen.

## 5. Discussion

In this section the flow field and transports for the mass and silicate conserving models are examined in more detail. Each property is considered in turn, starting with the velocity field and mass transport. For the property transports, estimates of the uncertainty are presented, and the implications of the oxygen and nutrient flux results for the North Atlantic biological and chemical cycles are addressed.

### 5.1 *The Velocity Field*

*Initial reference level = 3000 db.* The absolute velocity field at each section is shown in Fig. 5.1 for the model conserving mass and silicate with an initial reference level at 3000 db. Visually the field at both latitudes is dominated by alternating flows or eddies with horizontal scales of  $O(100 \text{ km})$  which are intensified in the upper 1000 db. There is still a suggestion of the initial level of no motion at 3000 db, particularly at  $24^\circ\text{N}$ . Since the shear is monotonic with depth at almost all stations, an initial reference level above the bottom leads to fluxes of opposite sign above and below this level. In this case the reference level velocity required to satisfy the constraints is sufficiently small that this trend remains in the final solution.

Note that the columnar nature of the circulation, seen also in the results of several other inverse calculations (e.g. Wunsch and Grant, 1983; Fu, 1981), is due to the relative velocity, not to the particular reference level velocity found here. These coherent bands of alternating flow were considered by some to be a weakness of the inverse solutions, because it did not correspond to conventional notions of a layered meridional circulation (Veronis, 19). However, any estimate of the flow based on geostrophy and synoptic, mesoscale-resolving hydrography will contain such features. Synoptically, the ocean does not appear as a stack of layers moving alternately to the north and south.

At  $36^\circ\text{N}$  the Gulf Stream appears as a narrow intense jet with maximum speeds of  $>150 \text{ cm s}^{-1}$ . Beneath the surface expression of the Gulf Stream there is northward

flow to 3000 db, embedded in a weaker southward flow in the Slope Water and the deep water beneath and offshore of the Gulf Stream. Although the velocity oscillates in sign throughout the section, the sub-thermocline flow is generally to the south in the western basin and to the north in the east.

The velocity field at 24°N is also dominated by mesoscale features that are most energetic in the thermocline and above. The Antilles Current can be seen against the western boundary, with a maximum speed of  $25 \text{ cm s}^{-1}$  to the north. The DWBC appears to be more concentrated at 24°N than at 36°N and has a maximum speed at the bottom of  $6 \text{ cm s}^{-1}$ . As at 36°N, the tendency in the deep water is for southward flow in the western basin and northward flow in the east. The flow over the Mid-Atlantic Ridge itself is mostly to the north.

Also shown in Fig. 5.1 is the reference level velocity for this solution. Most of the individual  $b_i$  are small ( $< 1 \text{ cm s}^{-1}$ ). As discussed in Chapter 1, there are two sources of uncertainty in the determination of  $b$ : errors due to noise in the data, and errors due to the fact that we have insufficient information to fully resolve the individual  $b_i$ . In this case the latter is easily the dominant source of error. The error due to noise is  $< .05 \text{ cm s}^{-1}$  for all the  $b_i$ , using the expressions for the relative variance and problem variance based on the residuals in equations (1.3) and (1.4) (see Chapter 1).

In contrast, none of the  $b_i$  are individually well resolved. Typically the diagonal elements of the resolution matrix are  $< 0.1$ . Thus with the information available we have resolved less than 10% of the variance of  $b$ . For this model the rank was estimated to be  $k=20$ , so that we have determined only 20 weighted averages of the 217 unknowns in the problem.

The resolution, however, is relatively compact: the solution at each station pair is generally a weighted average of the "true" solution at physically adjacent pairs, not pairs from different sections, or distant parts of the same section. The solution is thus a spatially smoothed version of the real reference level velocity field. The length scale

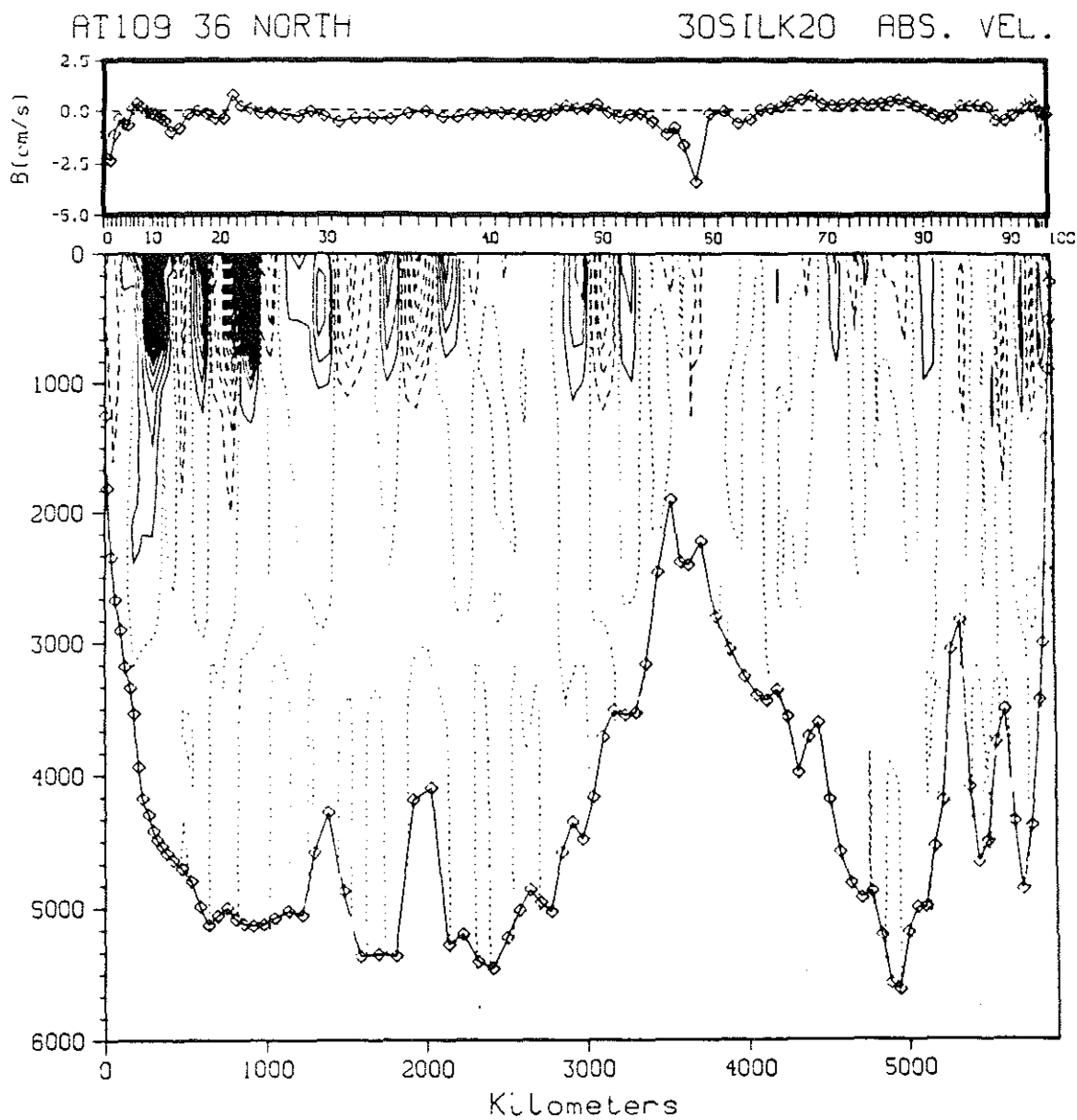


Fig. 5.1 Geostrophic velocity for the model conserving mass and silicate in density layers with initial reference level at 3000 db at (a)  $36^\circ\text{N}$ . Solid contours indicate northward velocity; dashed contours indicate southward velocity. Contour interval is  $5 \text{ cm s}^{-1}$ . Upper plot is of reference level velocity for this solution.

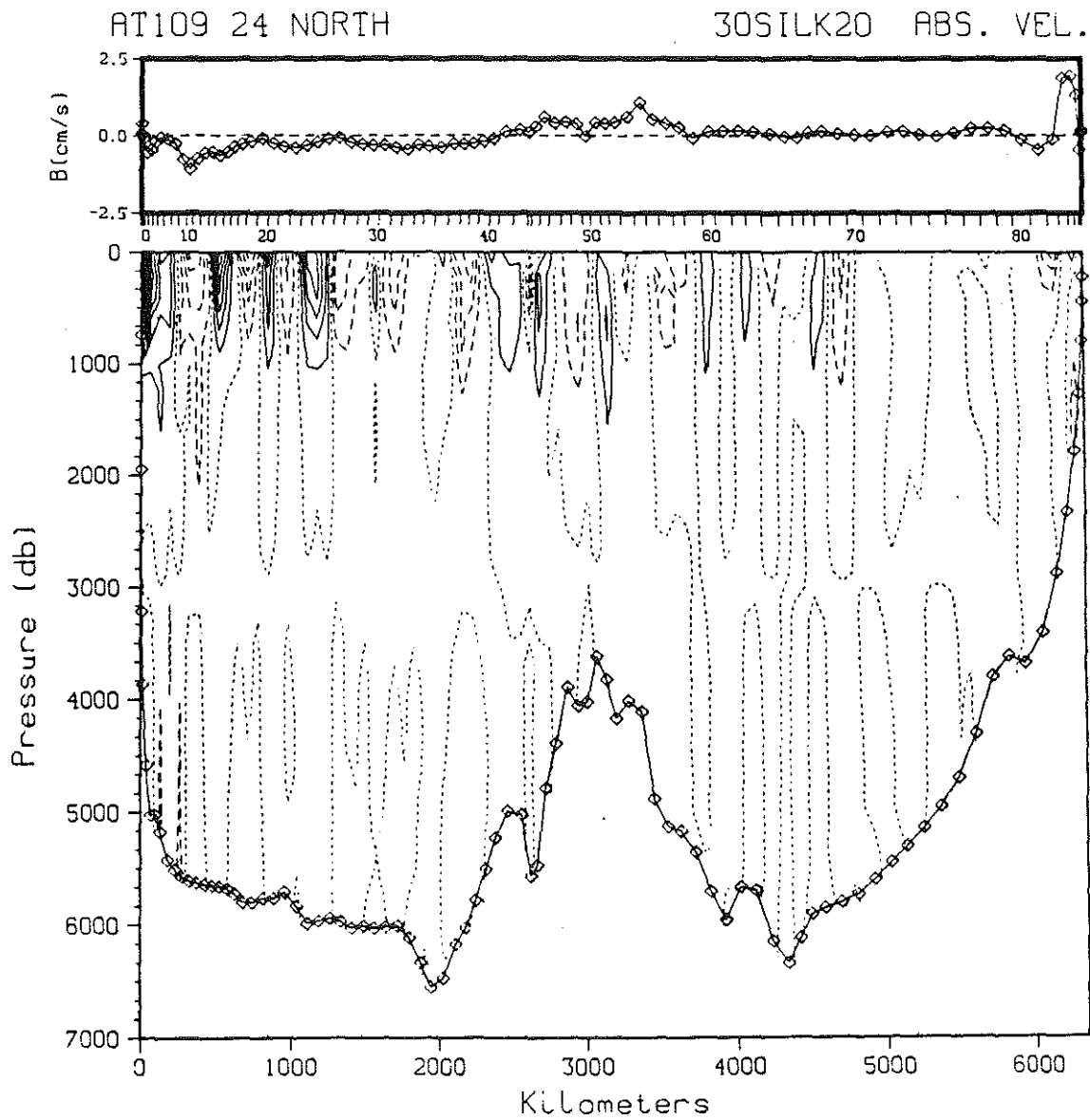


Fig. 5.1 (b) Geostrophic velocity at 24°N.

FLORIDA STRAITS 1 30SILK20 ABS. VEL.

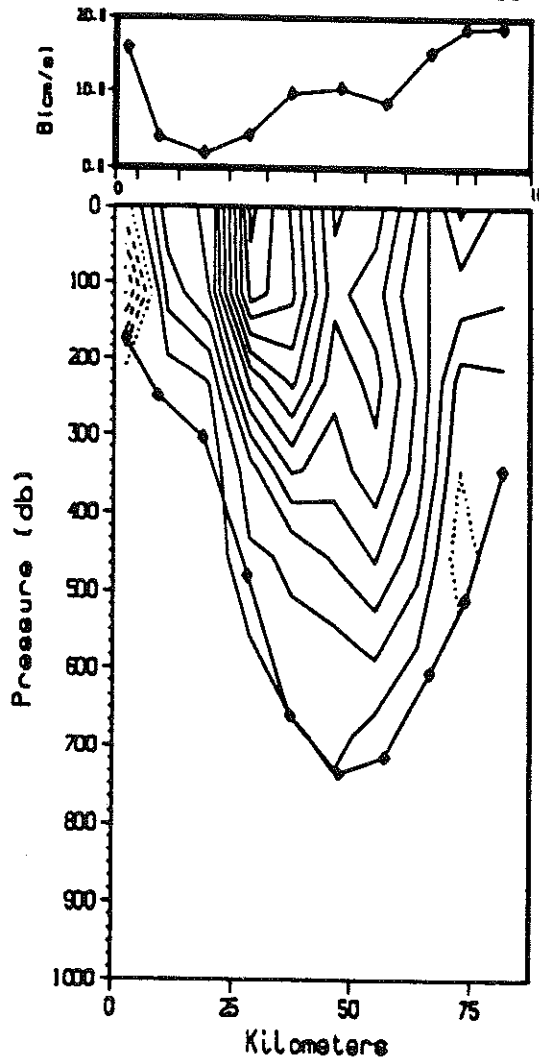


Fig. 5.1 (c) Geostrophic velocity at the Florida Straits. Contour interval = 20  $cm\ s^{-1}$ .



of the smoothing varies along the section, as can be seen by examining the columns of the  $\mathbf{V}\mathbf{V}^T$  matrix. Several representative columns are shown in Fig. 5.2.

Columns 44-46 are examples of station pairs with particularly low resolution. There is no defined peak and the solution at these pairs is smoothed over the entire Hatteras Abyssal Plain in the western basin at  $36^\circ\text{N}$ . Recall from Chapter 1 that the  $j$ 'th column of  $\mathbf{V}\mathbf{V}^T$  can be thought of as the estimate that would be obtained from the model if the "true", perfectly resolved solution was  $=1$  at the  $j$ 'th station pair and  $=0$  elsewhere. The fact that these station pairs are grouped together in the solution is an indication that the system contains no information with which to distinguish one station from the other, or that these columns of the  $\mathbf{A}$  matrix are nearly linearly dependent.

Column 41 is an example of a station pair that is better resolved, with a well-defined peak that decays relatively quickly. Note also that in this case there is a small side-lobe at stations 41-43 of the  $24^\circ\text{N}$  section. These two groups of station pairs, 41-43 (columns 142-144) at  $24^\circ\text{N}$  and 40-42 (columns 40-42) at  $36^\circ\text{N}$ , are both on the west flank of the Mid-Atlantic Ridge and have similar ratios of layer depths, and so are grouped together by the solution.

The resolution matrix suggests that we have succeeded in determining only the broadest scale structure of the reference level velocity. However, we will see below that because the property fields generally vary on similarly large scales, the integrated property fluxes across each section are well determined.

*Initial reference level = 1300 db.* The absolute velocity field for the 1300 db reference level model is similar to that of the 3000 db model for the most part (Fig. 5.3). The reference level velocity is larger than in the previous model but still fairly small, and remnants of the initial level of no motion can still be seen, especially in the eastern basin at  $24^\circ\text{N}$ . The most striking difference between the two solutions is in the deep

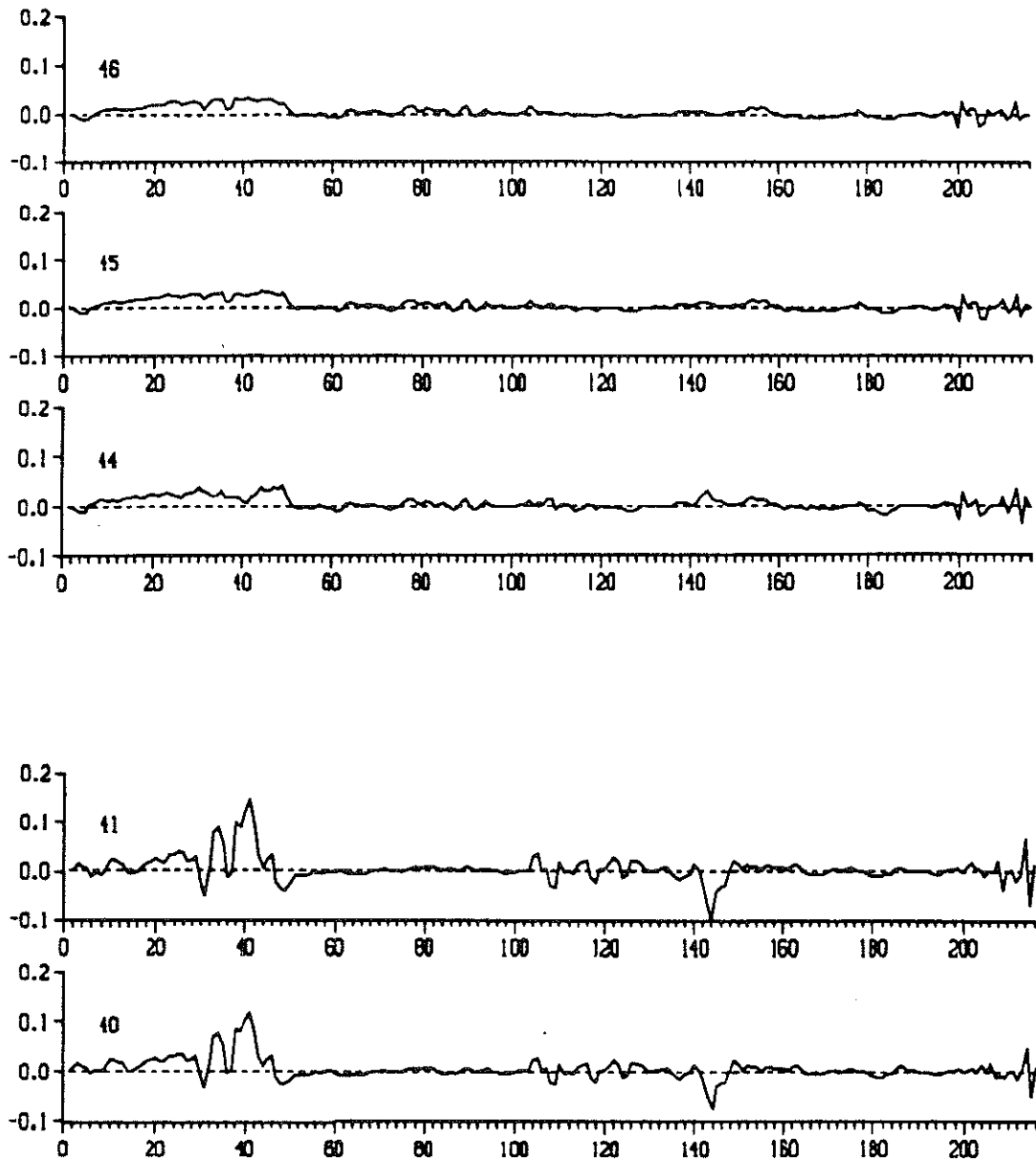


Fig. 5.2 Representative columns of the resolution matrix, plotted vs. column number (1-100: station pairs at 36°N; 101-190: pairs at 24°N; 191-201: Florida Straits; 202-219:  $w^*$ ).

circulation of the western basin. Since the shear is monotonic with depth, a shallow reference level leads to stronger deep flows of opposite sign to those in the surface layers. At  $36^{\circ}\text{N}$ , there is strong southward flow beneath the surface Gulf Stream at speeds up to  $14 \text{ cm s}^{-1}$ , and a deep counter-rotating flow below the cyclonic cold core ring, with bottom velocities as high as  $15 \text{ cm s}^{-1}$ . The Antilles Current is also shallower in this model, and the DWBC at  $24^{\circ}\text{N}$  is much more intense (maximum speed =  $12 \text{ cm s}^{-1}$ ).

In summary, the velocity field for both models, at both latitudes, is dominated by energetic western boundary currents and mesoscale variability in the interior. The flow in the interior consists of fluid moving alternately to the north and south, with the most intense circulation in the upper 1000 db. With only two zonal sections, it is not possible to determine if these features are isolated eddies, transient features such as Rossby waves, or meanders of a primarily zonal current such as Hogg (1983) has hypothesized for the deep flow at  $36^{\circ}\text{N}$ . A different picture of the same shear field relative to 1300 db was given by RW. They used a horizontal filter with a decay scale of 500 km to remove mesoscale eddies, and somewhat different model assumptions. Their Fig. 9, reproduced here as Fig. 5.4, gives a feeling for the large-scale structure of the geostrophic shear field underlying the eddy-dominated pictures presented here. In both model solutions the reference level velocity makes a relatively small contribution to the absolute velocity field and remnants of the initial level of no motion remain in parts of the sections. Further insight into the differences between the two models can be gained by considering the distribution of transport across each section in each layer.

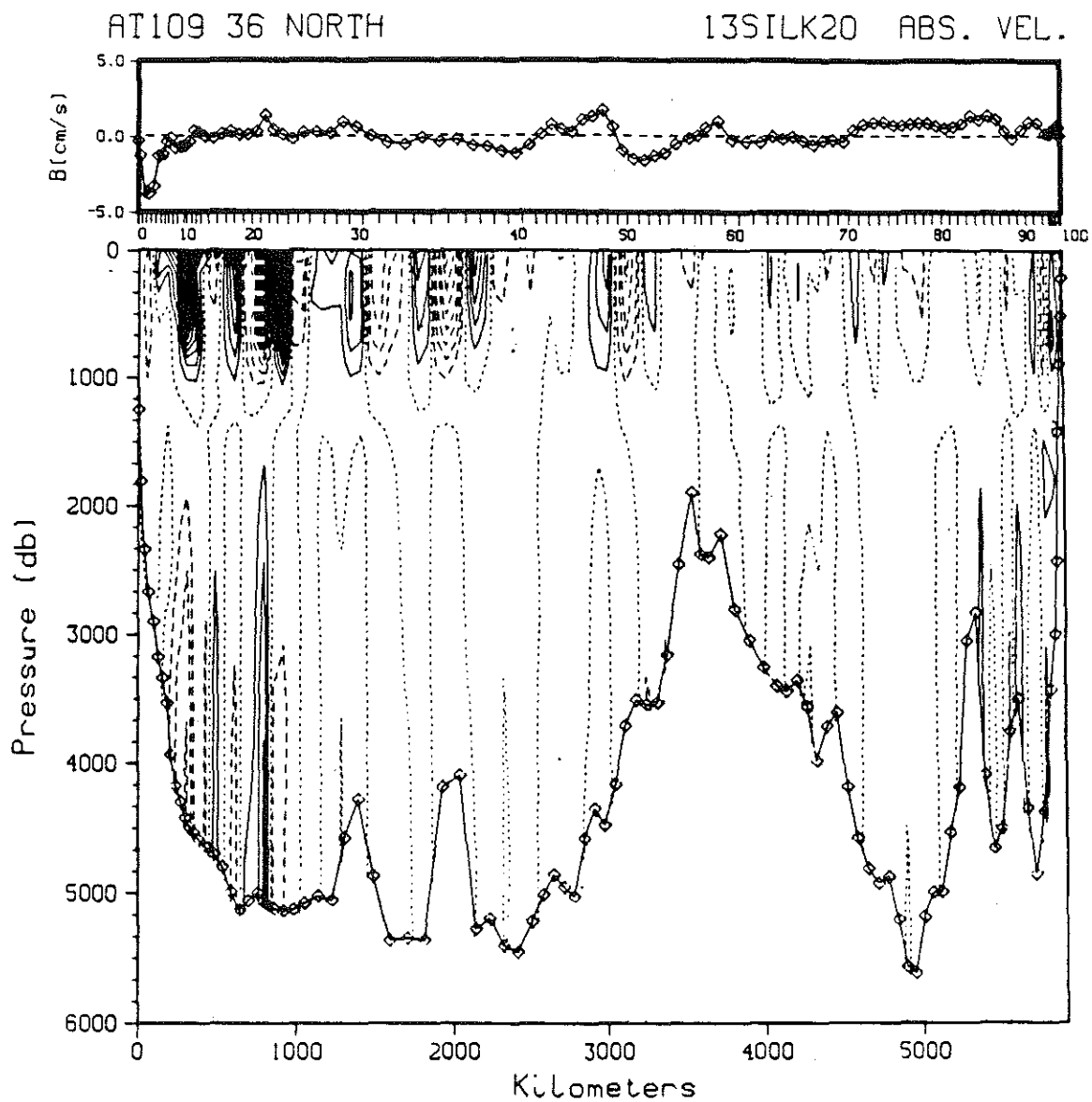


Fig. 5.3 Absolute velocity for the model conserving mass and silicate in density layers with initial reference level at 1300 db. Solid contours indicate northward velocity; dashed contours indicate southward velocity. Contour interval is  $5 \text{ cm s}^{-1}$ . Upper plot is of reference level velocity for this solution. (a)  $36^\circ\text{N}$ .

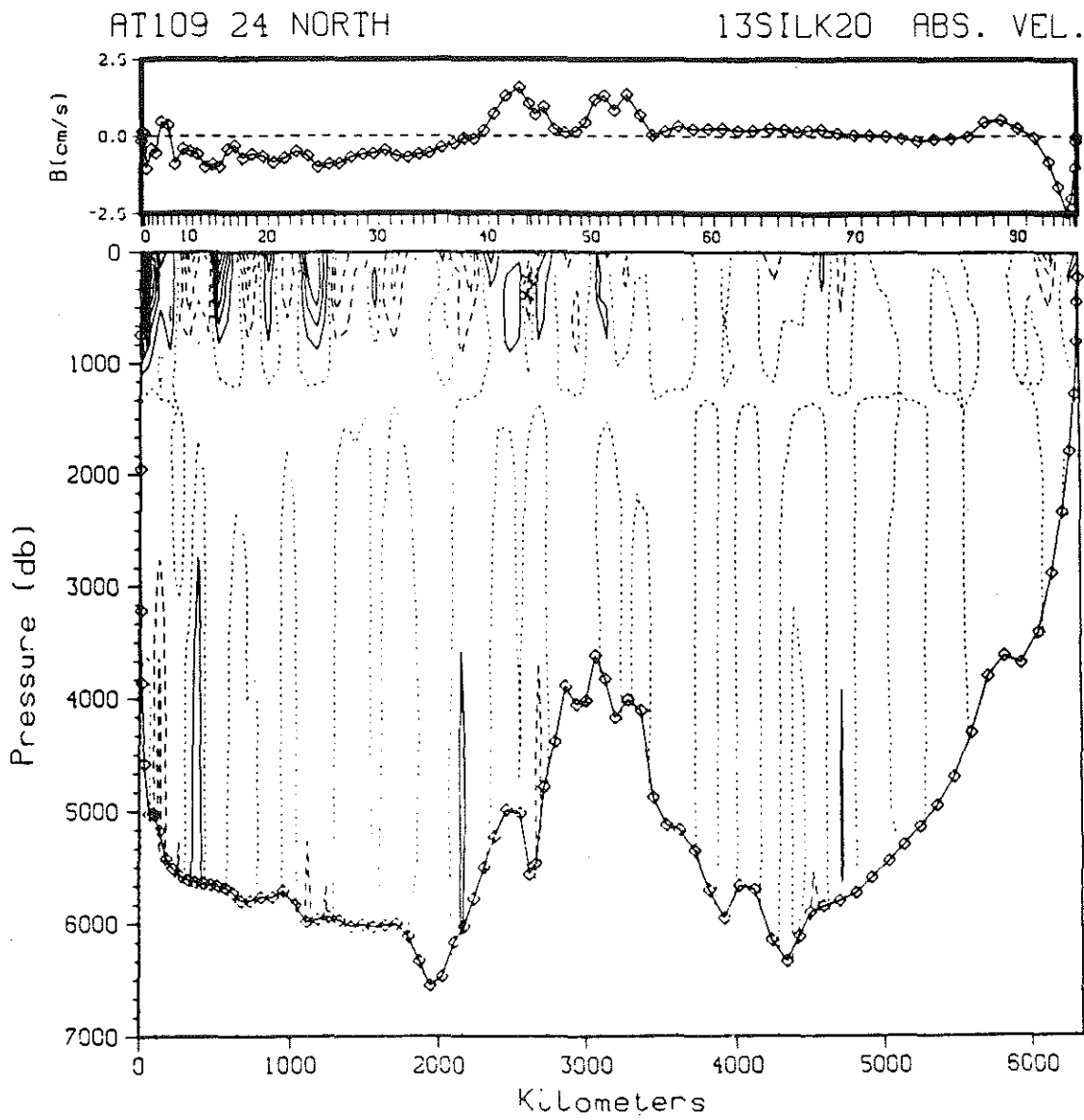


Fig. 5.3 (b) Geostrophic velocity at 24°N.

FLORIDA STRAITS 1

13SILK20 ABS. VEL.

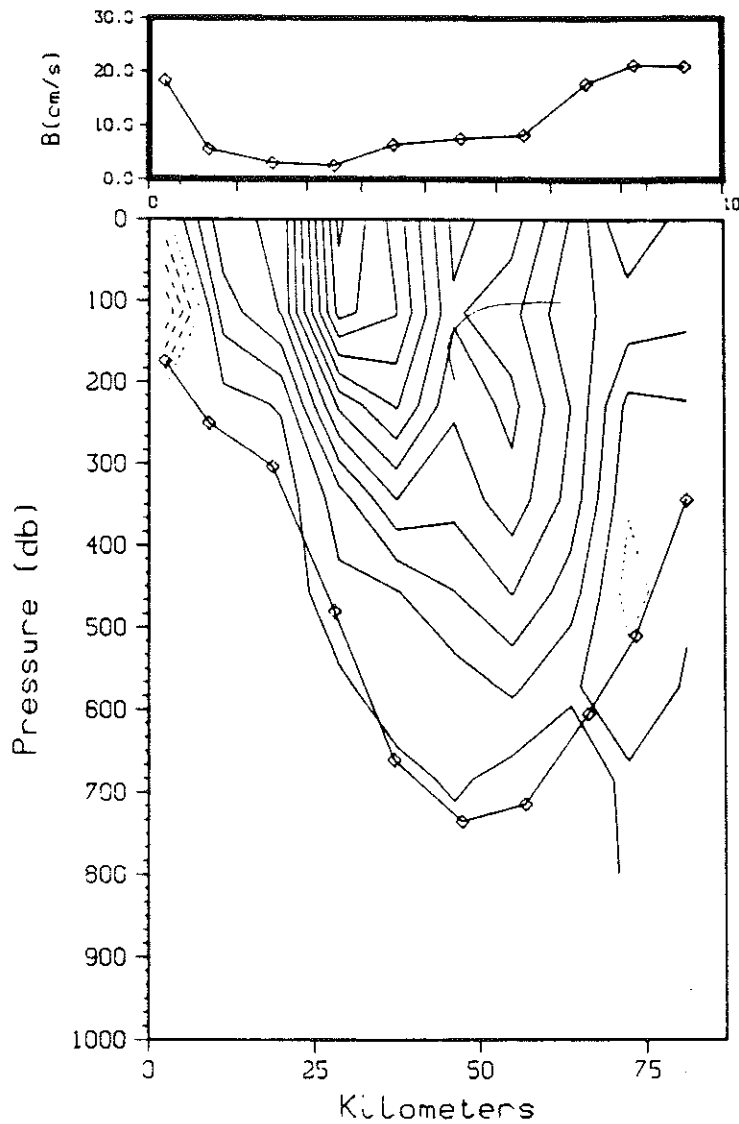


Fig. 5.3 (c) Geostrophic velocity at the Florida Straits. Contour interval is  $20 \text{ cm s}^{-1}$ .

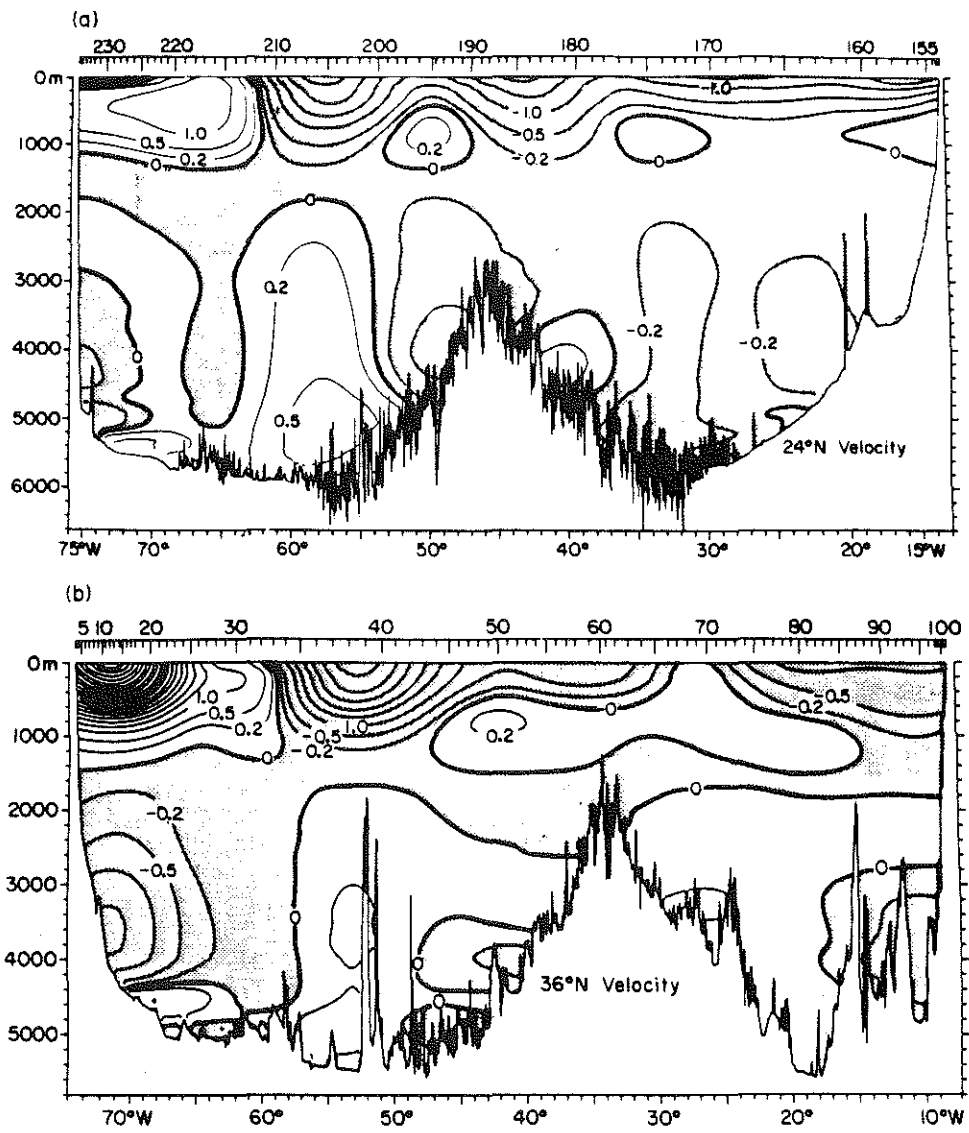


Fig. 9. (a) Horizontally smoothed geostrophic velocity ( $cm\ s^{-1}$ ) at  $24^{\circ}N$  from 1981 data, based on the reference level calculation with constraints on total transport only. Southward velocities are shaded. The western end is on the left. (b) Same as (a) for  $36^{\circ}N$ .

Fig. 5.4 Horizontally smoothed geostrophic velocity ( $cm\ s^{-1}$ ) at (a)  $24^{\circ}N$  and (b)  $36^{\circ}N$  from Roemmich and Wunsch (1985). Southward velocities are shaded.

## 5.2 Comparison of Mass Transport Results for 3000 db and 1300 db Models

The horizontal structure of the mass transport will be discussed using maps of the transport at each station pair along the hydrographic sections, as shown in Fig. 5.5. In these plots the transport at each pair is shown as a stick whose length is proportional to the transport; the scale is given in the lower left hand corner and changes for each plot. In addition, the sum of the transport through certain groups of station pairs is shown. The transport patterns for the 3000 db model are shown in the upper panel of each figure, and will be discussed first.

### *Transport Results for the 3000 db Model*

The mass flux in layers 1-4 for the 3000 db reference level model is shown in Fig. 5.5. The flow is dominated by strong eddies, particularly in the western basin at  $36^{\circ}\text{N}$ . The cold core ring or Gulf Stream meander noted above recirculates nearly 50 Sv in these three layers alone. The other striking feature at  $36^{\circ}\text{N}$  is the Gulf Stream itself, with a transport of 54 Sv in layers 1-4. (The limits of the Gulf Stream are defined here to be the points where the top to bottom transport changes sign, as in Halkin and Rossby, 1985.) Of this northward flow of warm water, 38 Sv is returned to the south in the interior, primarily in the western basin. However, any sense of a coherent tight recirculation gyre is masked by the eddy field.

The mass flux through the Florida Straits in the top three layers is 27 Sv, half of the observed Gulf Stream transport at  $36^{\circ}\text{N}$ . Knauss (1969) also found that the transport of the Gulf Stream roughly doubled between the Florida Straits and Cape Hatteras, based on geostrophic calculations referenced to neutrally bouyant floats. In the interior at  $24^{\circ}\text{N}$  the flow is more energetic in the western basin than in the east, as at  $36^{\circ}\text{N}$ , but the eddies appear significantly weaker at this latitude. The Antilles Current does not appear as a well-defined boundary current. Rather, the flow near the western boundary consists of several eddies embedded in a general northward drift



which carries a net mass flux of 18 Sv in these layers west of 63°W. Further to the east the flow is generally to the south with a transport of 34 Sv, so that the net flux of warm water across this section is to the south.

Figure 5.6 shows the mass transport for layers 5-8 for this model (note the change in scale from the previous plot). The flow field at intermediate depths is also dominated by the eddy field, with the cold core ring at 36°N being particularly striking, but several coherent patterns emerge. At 36°N the Western Boundary Undercurrent (WBUC) appears as a well-defined flow carrying 7 Sv to the south inshore of the Gulf Stream. The Gulf Stream transports 23 Sv of intermediate water to the north. This northward flow is balanced in part by a net southward flow of 12 Sv west of the Mid-Atlantic Ridge.

In the eastern basin there is a net northward flow of 9 Sv between the coast of Europe and 20°W, and a southward flow of equal magnitude between 20 °W and the crest of the Mid-Atlantic Ridge. Reid (1979,1981) showed that the oxygen, nutrient and geostrophic shear fields implied a similar circulation, with poleward flow near the eastern boundary and equatorward flow further offshore. Note that the net meridional flux of mass in these layers (5 Sv) is much smaller than the individual flows to the north and south in different parts of the basin. Also notable is a strong northward flow at a single station pair near the coast of Portugal. This flow corresponds to a small bubble of very warm and saline water banked up along the coast (see Figure 2.1), and is apparently a lens of Mediterranean Outflow Water flowing along the continental slope to the north.

At 24°N the intermediate depth circulation alternates in sign in the interior and the net flux summed over layers 5-8 is .5 Sv.

Layers 9-11 lie near the depth of the initial reference level, where the shear is also weak; as a result, the reference level velocity tends to dominate the transport pattern, which is seen to be more smoothly-varying and weaker than in the layers above (Fig.

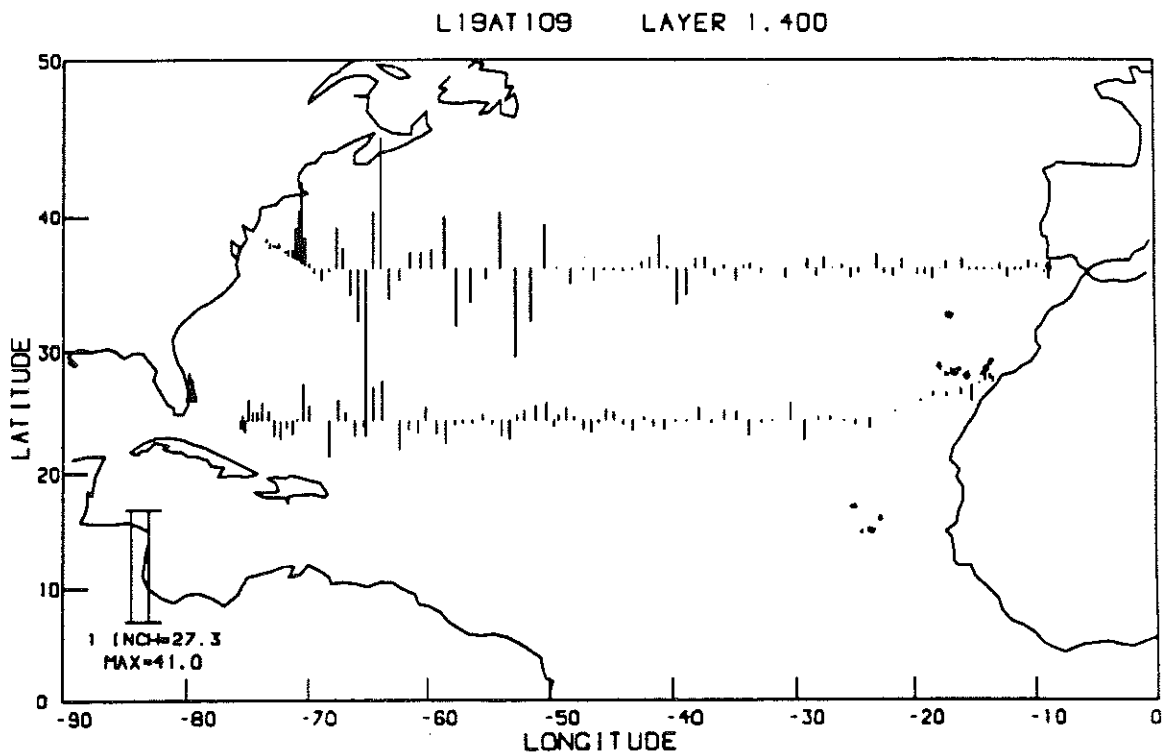
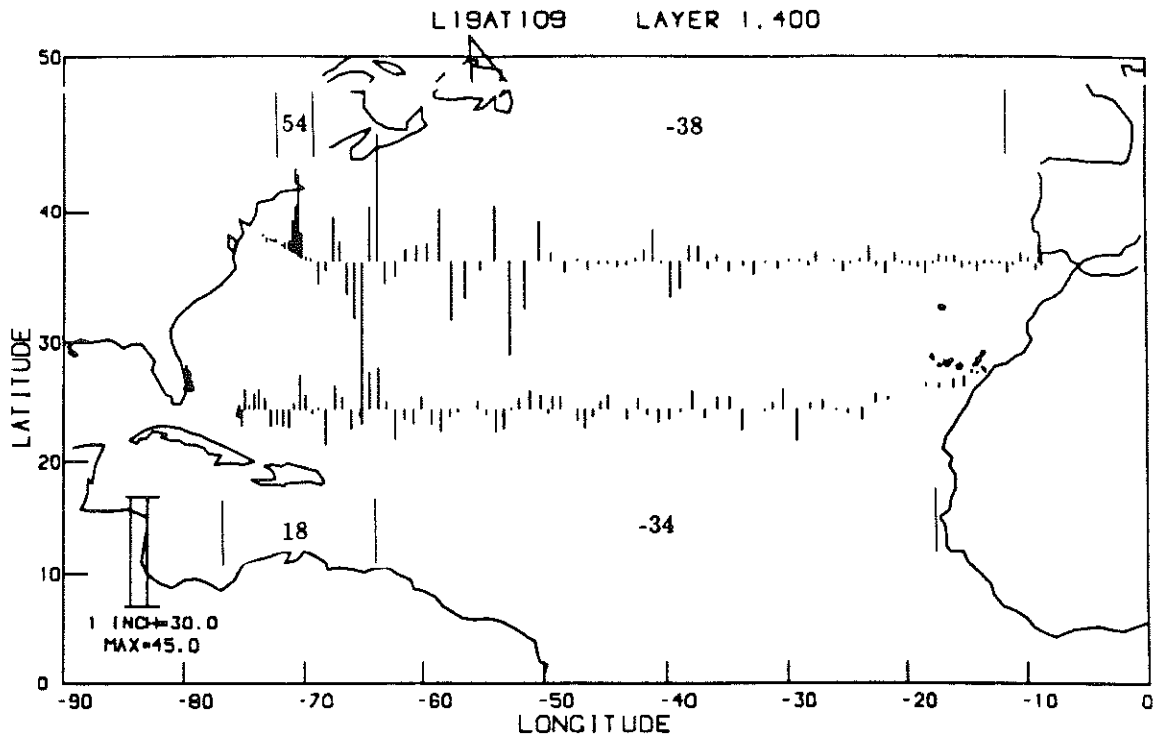


Fig. 5.5 Mass transport in layers 1-4 at each station pair for the mass and silicate conserving models. Scale is given in the lower left corner of plot. Numbers between square brackets give sum of transport (Sv) for groups of station pairs. (a) initial reference level at 3000 db (b) initial reference level at 1300 db.

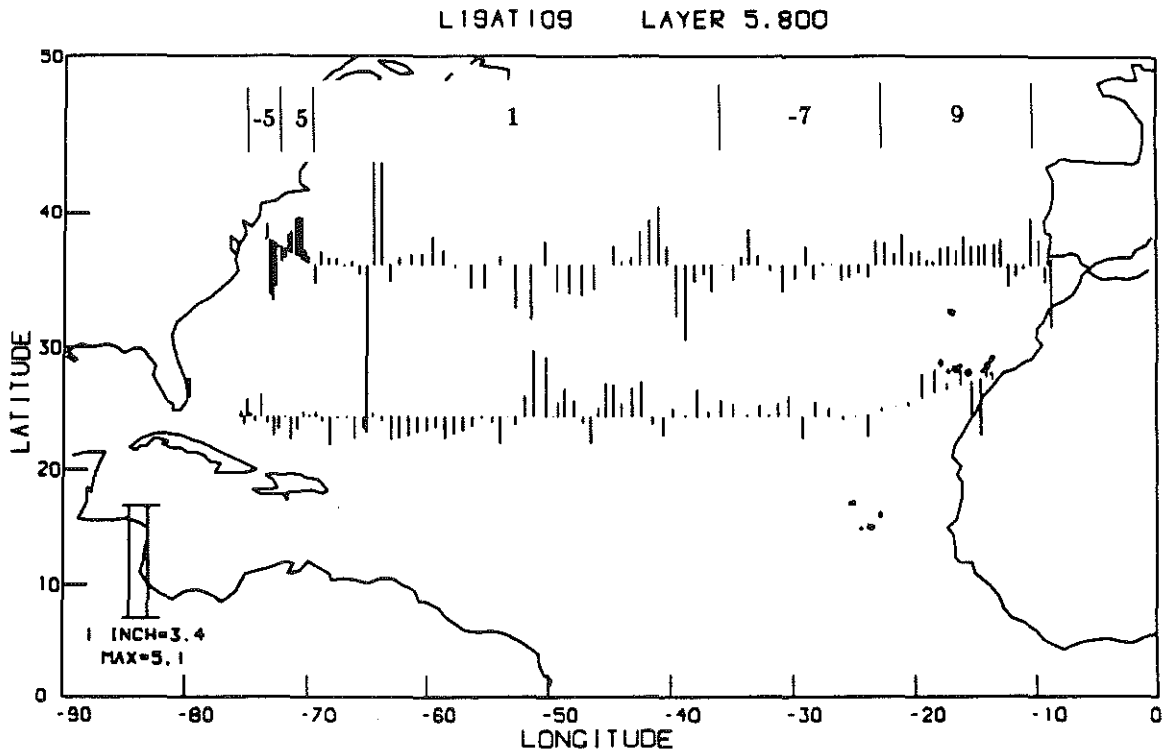
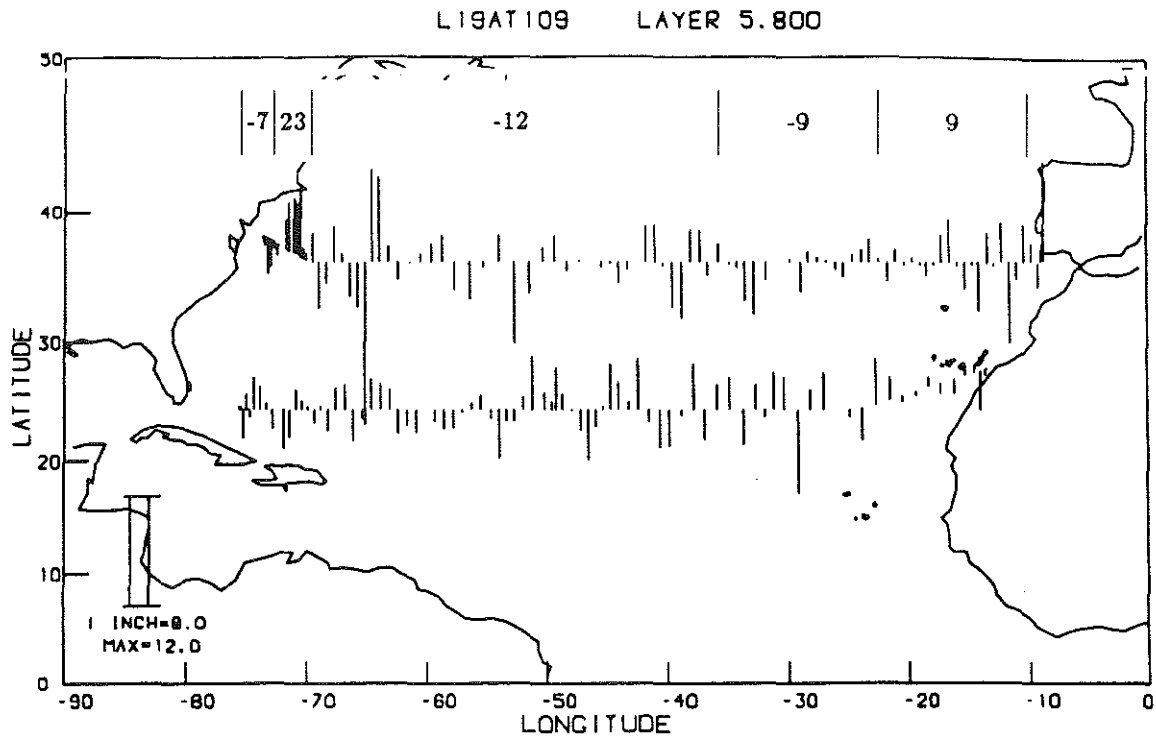


Fig. 5.6 Same as Fig. 5.5 for layers 5-8.

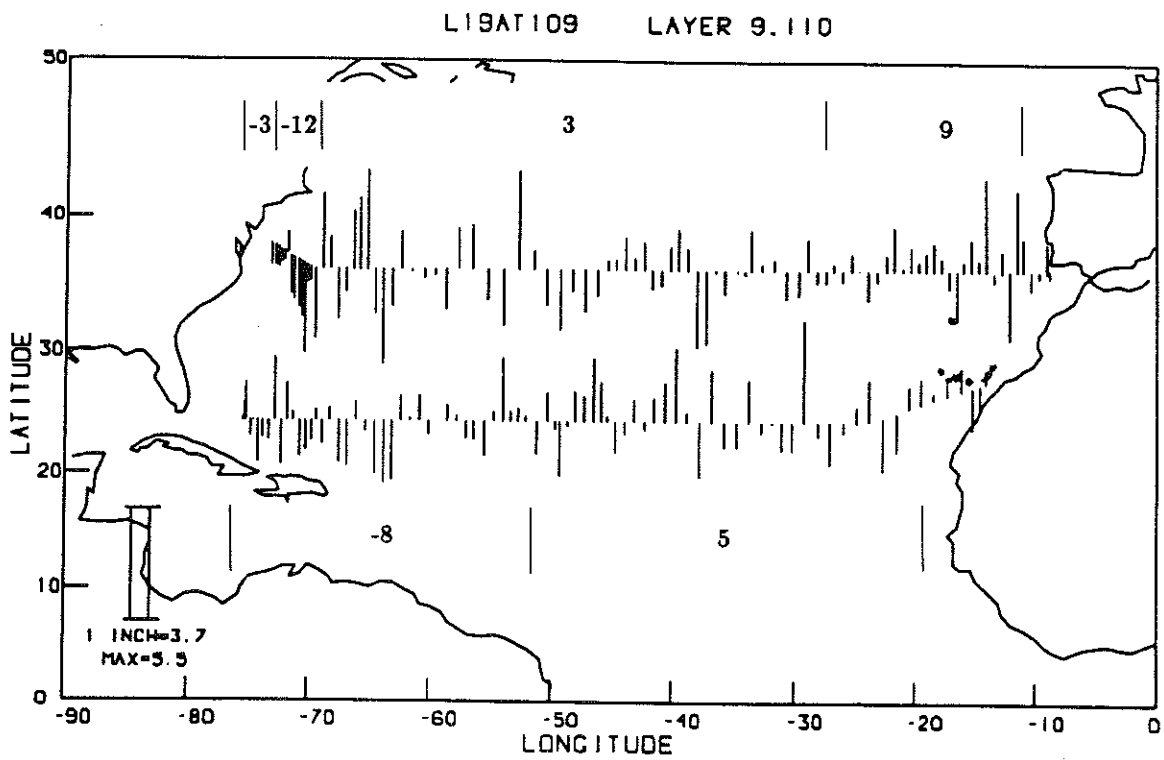
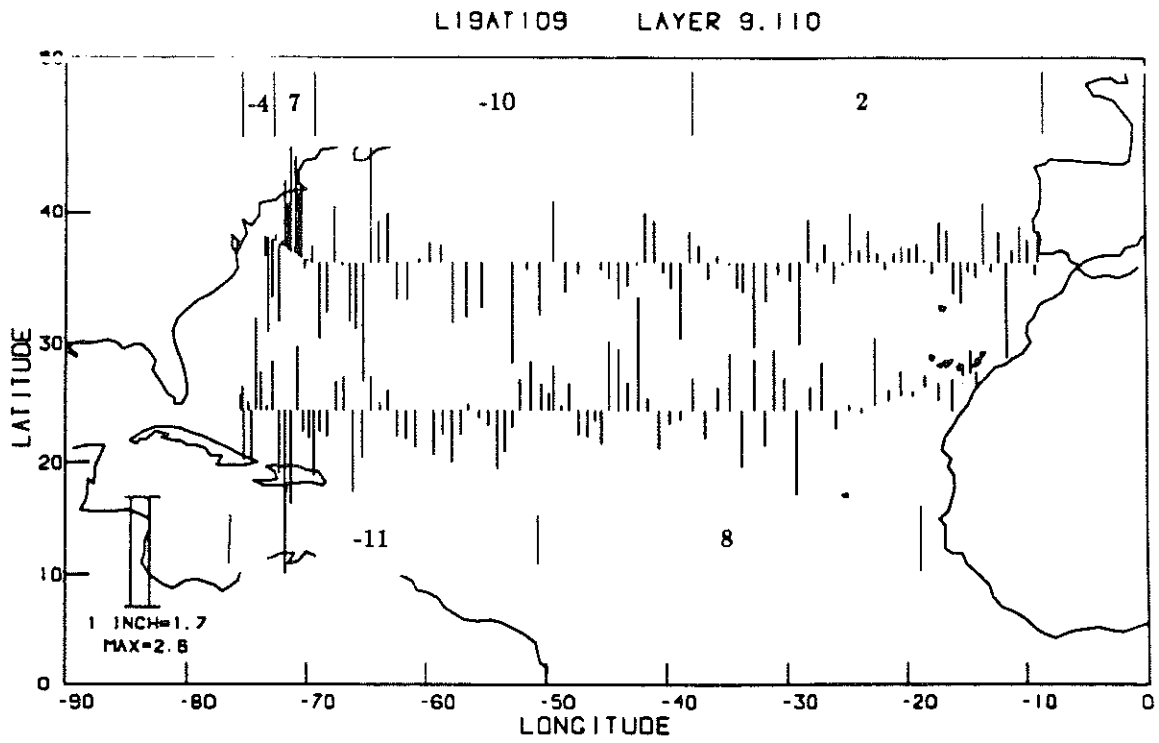


Fig. 5.7 Same as Fig. 5.5 for layers 9-11.

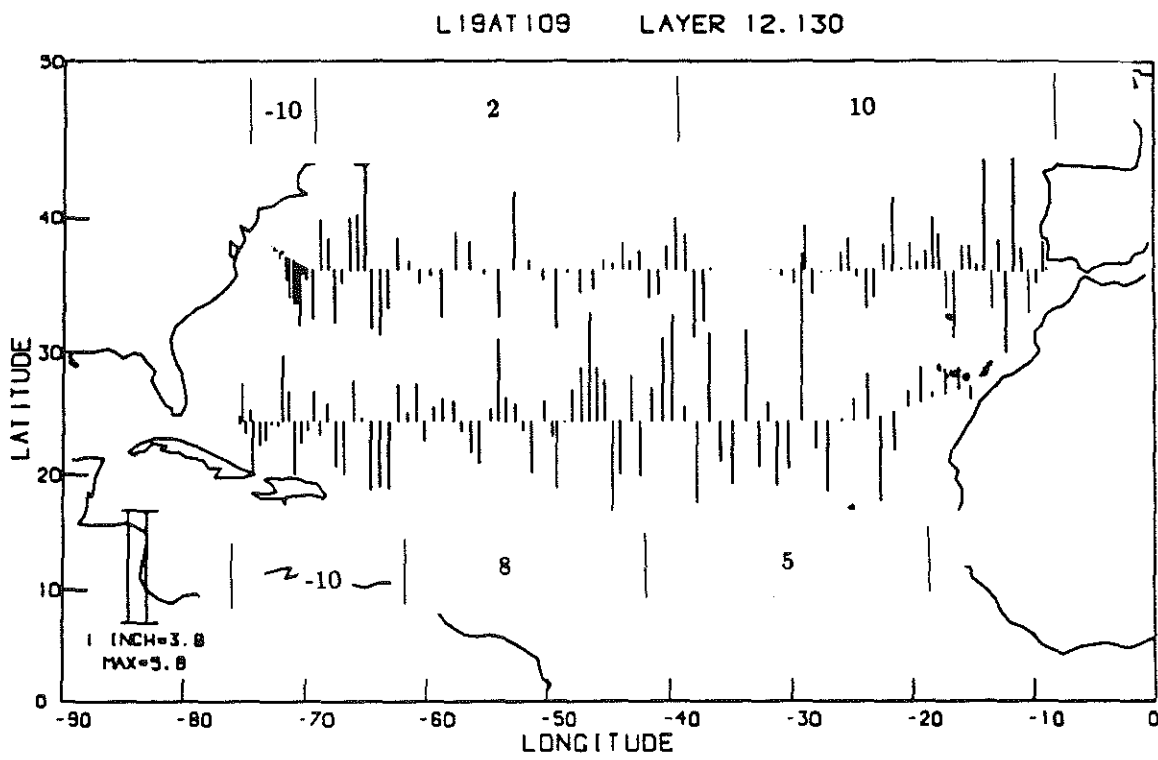
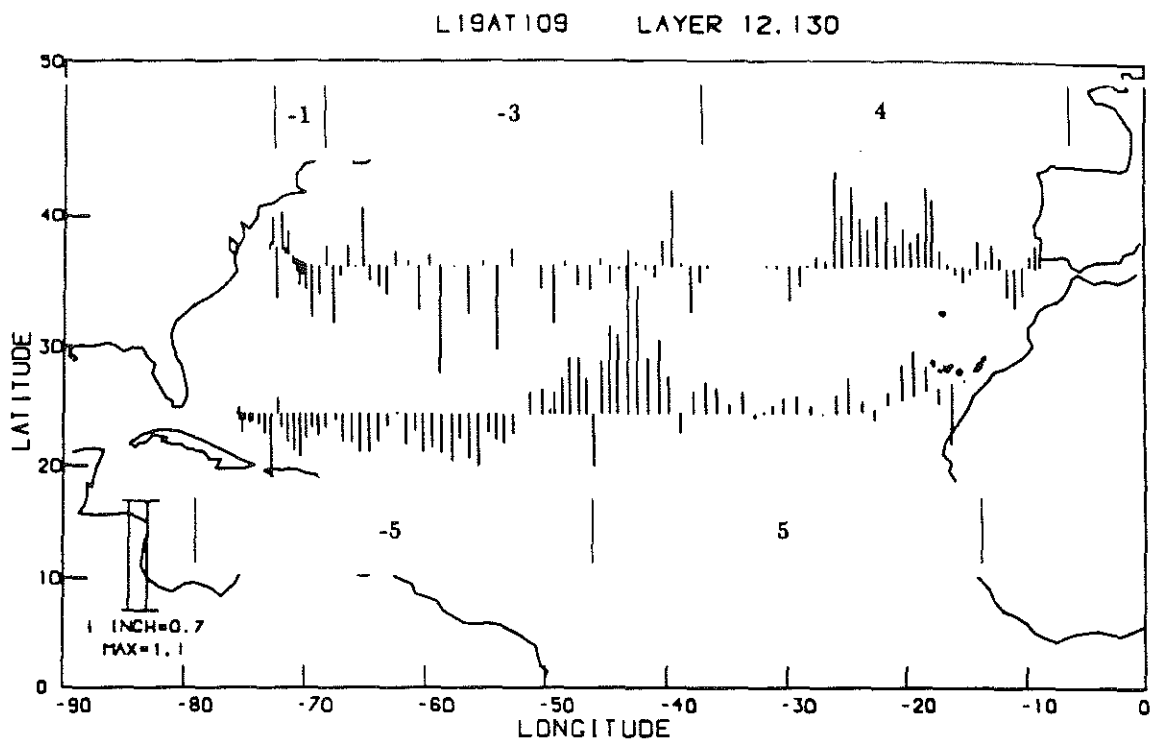


Fig. 5.8 Same as Fig. 5.5 for layers 12-13.

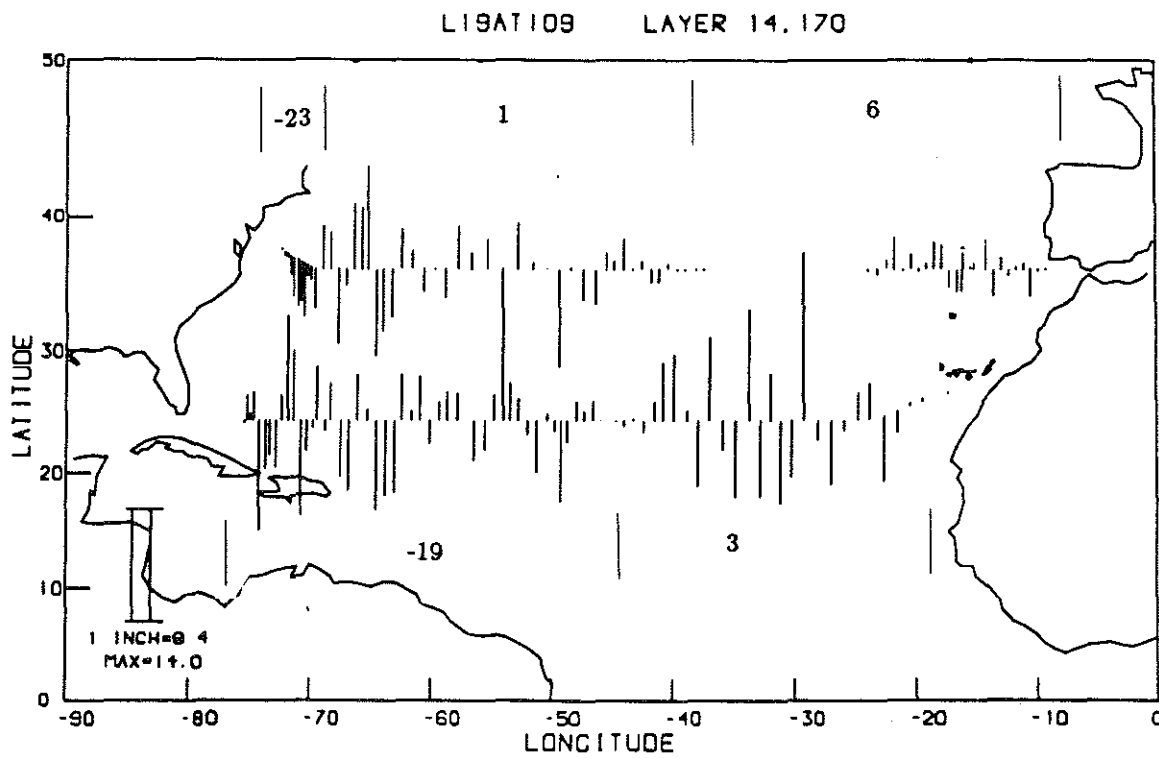
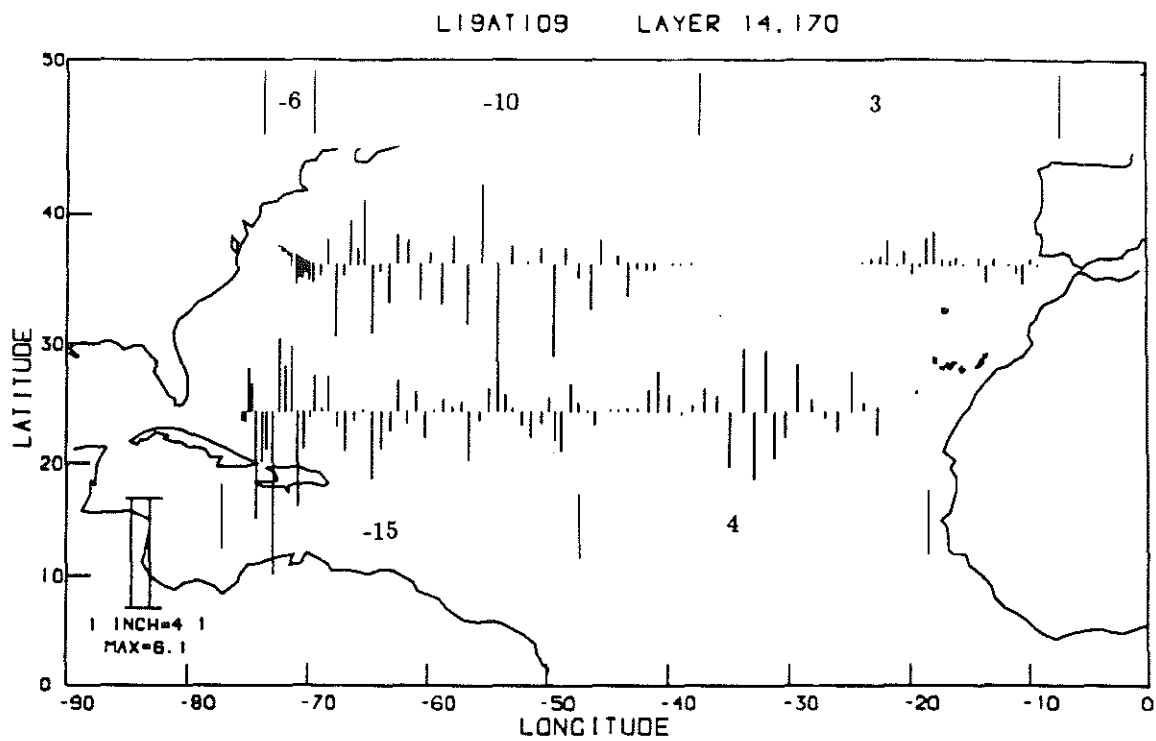


Fig. 5.9 Same as Fig. 5.5 for layers 14-17.

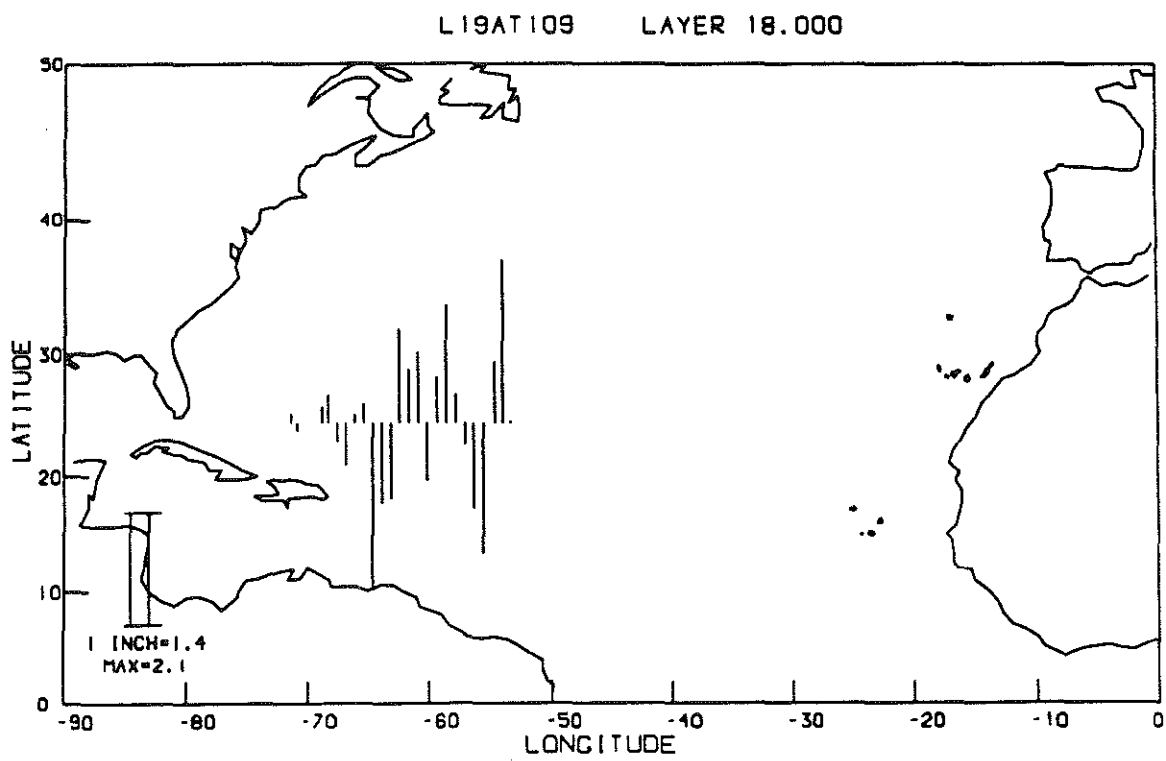
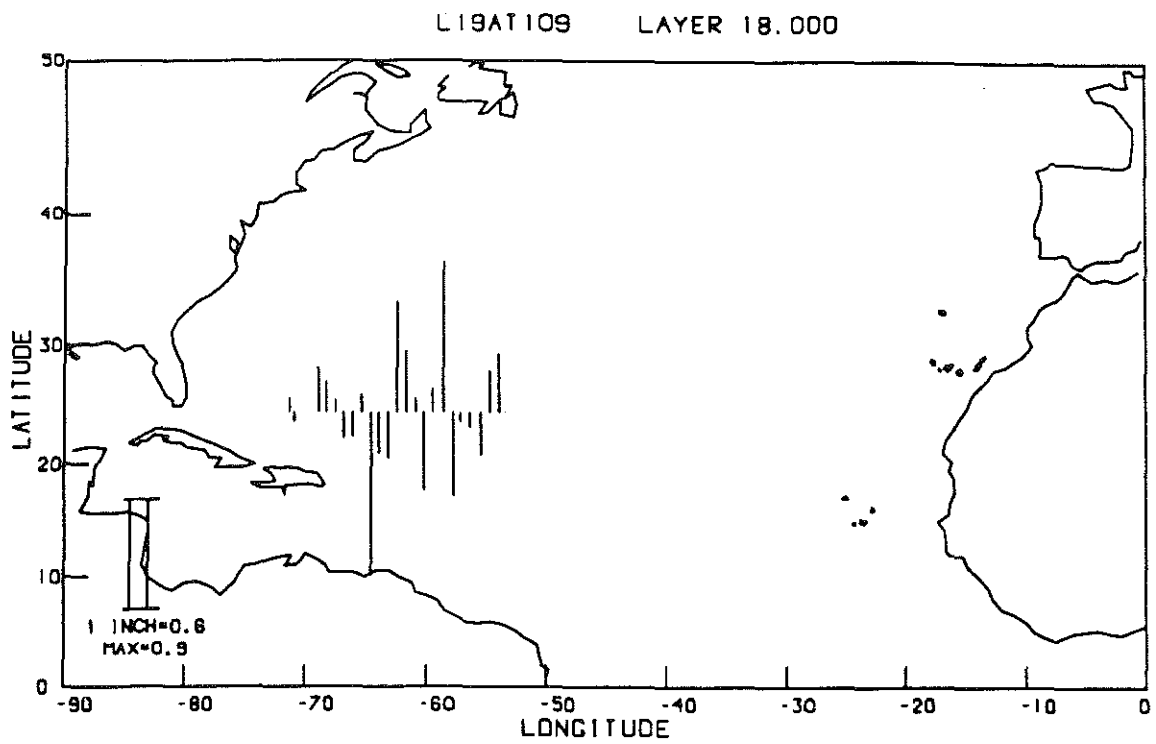


Fig. 5.10 Same as Fig. 5.5 for layer 18.

5.7). The circulation at  $36^{\circ}\text{N}$  consists of southward flow in the WBUC, northward flow in the Gulf Stream, southward flow between  $70^{\circ}\text{W}$  and  $30^{\circ}\text{W}$ , and northward flow between  $30^{\circ}\text{W}$  and the eastern boundary. Note that although the WBUC appears as a strong narrow current, it carries less than half the transport of the broad southward flow in the interior at this section. The net flux is 5 Sv to the south.

For these layers there is a clear southward flow concentrated in the western portion of the  $24^{\circ}\text{N}$  section, although it is difficult to define the limits of the WBUC. Most of this southward flow is compensated by northward flow on the eastern half of the section, and the net flux is about 3 Sv to the south.

In layers 12 and 13 the circulation again changes sign smoothly along both sections and is very weak (Fig. 5.8). At both latitudes there is broad motion to the south in the western basin, offset by general northward flow to the east, and the net flux in each case is less than 1 Sv to the north. At  $24^{\circ}\text{N}$  the northward flow is concentrated along the eastern flank of the Mid-Atlantic Ridge.

The majority of the southward flux of NADW occurs in layers 14-17 (Fig. 5.9). There is now southward flow beneath the Gulf Stream, which carries about half of the net equatorward transport of 12 Sv in these layers. The rest occurs more evenly distributed across the western basin. Reid (1981) also concluded from an analysis of the geostrophic shear and nutrient fields that a significant fraction of the equatorward flow of NADW occurred in the interior rather than in the DWBC. The net flux in the eastern basin is again to the north.

The same pattern is seen at  $24^{\circ}\text{N}$ . These layers lie below the sill depth of the Mid-Atlantic Ridge so that the eastern and western basins are isolated, and mass should be approximately conserved for each basin individually. This is indeed found to be true for this solution.

There is no water as dense as layer 18 at  $36^{\circ}\text{N}$ , or in the eastern basin at  $24^{\circ}\text{N}$  (Fig. 5.10). Despite the presence of eddies, there is a sense of a cyclonic circulation in



the western basin, consistent with the property distributions which show the strongest AABW signature on the flank of the Mid-Atlantic Ridge. The net transport is less than one Sv to the north, consistent with Whitehead and Worthington's (1982) estimate of the inflow of AABW to the North Atlantic.

#### *Transport Results for the 1300 db Model*

The corresponding mass transport maps for the 1300 db reference level model appear as Fig.'s 5.5b-5.10b. There is very little difference between the two model solutions for layers 1-4. At intermediate depths (layers 5-8) the pattern of flow also looks similar, but the shallow reference level leads to a somewhat weaker circulation with fewer eddies, particularly near the western boundary. The Gulf Stream transports only 5 Sv to the north in this case, compared to 23 Sv in the previous model. East of the Gulf Stream, the substantial recirculation of intermediate water seen in the 3000 db model is replaced by weak flow to the north in the western basin. The net transport in the western basin is similar in the two models, although the deep reference level results in a more eddy-rich flow. Note also that the bubble or jet of warm salty water off the coast of Portugal described above is moving to the south in this case.

The pattern of the flow in the upper NADW (layers 9-11) is quite different for the two models, although the net amount of northward and southward moving water at 36°N is similar in each case. In the 3000 db model the southward flow occurs in two parts, a narrow flow along the western boundary isolated from a more diffuse southward drift in the interior by northward flow in the Gulf Stream. In contrast, here the flow beneath the Gulf Stream is strongly to the south and all the southward flow (14 Sv) occurs in a deep western boundary current. The net flux in the western basin interior is small. The northward flow in the interior of the eastern basin, on the other hand, has increased by a factor of five.

The circulation in layers 12 and 13 is also significantly more energetic and eddy-rich with a shallow initial reference level. At  $36^{\circ}\text{N}$  the WBUC transport is larger by a factor of 10, the net flux in the western basin is of opposite sign to that in the previous model, and the northward transport in the eastern basin is more than twice as large, despite changes in sign between nearby station pairs. The zonally-integrated transport across each section has increased from 1 to 3 Sv to the north. The maps show that nearly all this northward flow occurs in the eastern basin.

Although the deep flow to the south along the western boundary at  $24^{\circ}\text{N}$  is significantly greater than in the 3000 db model, it is offset by a northward flow further offshore, so that the net southward flux of deep water in the western basin has decreased. In the eastern part of the section the flow appears much less regular but the net transport is similar in the two models.

A similar pattern is seen in the deeper layers. The 1300 db model results in a much stronger WBUC (23 vs. 6 Sv) in layers 14-17, an interior characterized by flow oscillating in sign and carrying little net transport across the section, and stronger northward flow in the eastern basin. At  $24^{\circ}\text{N}$  the two patterns look very similar, but note that the scale is different for the two plots and the 1300 db model flow is actually much more energetic, particularly in the eastern basin.

#### *Summary and Discussion of the Mass Transport Results*

Despite the similarity in the zonally-integrated fluxes, the details of the circulation do depend strongly on the initial model assumed. In theory, given sufficient information to make the problem fully determined, the solution will be independent of the initial reference level. In practice we often do not have enough information to uniquely determine the solution and are left with a strongly underdetermined problem. Examining the results of different initial models is one way to explore the degree of indeterminacy, or the range of solutions consistent with a particular set of modelling assumptions.

Additional observations not included explicitly as constraints in the model can be used as diagnostics to evaluate which of several model solutions seems most realistic.

The general impression from the transport maps is that the shallow reference level results in a more energetic deep circulation, while the reverse is true for the deep reference level. This is not surprising, since the shear is monotonic with depth at most station pairs, and either choice of reference level leads to an initial flow field that is not very far from satisfying the imposed constraints, even with no reference level velocity correction added. Thus, only a small  $b$  is required to satisfy the constraints that mass and silicate are conserved, and the final solution is not very different from the initial state in either case.

More specifically, the primary differences between the two models can be summarized as follows. The 1300 db reference level results in a shallow Gulf Stream, with strong southward flow below 1500 m, while the deeper level gives northward flow in the boundary current extending below 3000 m. As a result the total top to bottom transport of the Gulf Stream differs dramatically for the two models: 26 Sv and 84 Sv for the 1300 and 3000 db models, respectively. (Again, the limits of the Gulf Stream are taken to be the location at which the top-to-bottom transport per unit width changes sign.)

The debate over whether the Gulf Stream extends to great depth or not is an old one in oceanography, and depends both on location and definition (see Worthington (1976) or Fofonoff (1981) for a review). Direct velocity measurements using neutrally buoyant floats, current meters and transport floats tend to support the existence of flow in the direction of the surface Gulf Stream to at least 2500 m depth, once the Gulf Stream has left the coast at Cape Hatteras (Fuglister, 1963; Warren and Volkmann, 1968; Barrett, 1965; Luyten, 1977). Several more recent studies based on direct velocity observations also support the notion of a deep Gulf Stream, with a large volume transport. Using a year-long record from a current meter mooring with instruments

from 400 to 4000 m, Hall and Bryden (1985) showed that the Gulf Stream extended to  $> 4000$  m and estimated a mean transport of 103 Sv at  $68^{\circ}\text{W}$ . Halkin and Rossby (1985) estimated the mean transport of the Gulf Stream at  $36^{\circ}\text{N}$  to be  $88 \pm 17$  Sv above 2000 db, based on twenty sections across the current using the Pegasus velocity profiler taken over a two year period. Joyce *et al.* (1986) combined acoustic doppler velocity measurements and hydrographic data using an inverse method to estimate the synoptic absolute velocity field for two crossings of the Gulf Stream. They found a total transport of  $107 \pm 11$  Sv near Cape Hatteras, which increased to  $125 \pm 6$  Sv at  $72.5^{\circ}\text{W}$ . The direct velocity measurements therefore tend to support the large Gulf Stream transport values found with the 3000 db reference level model.

Direct velocity measurements have also been made in the WBUC beneath and inshore of the Gulf Stream and can be compared to the model results. The transport maps showed that the shallow reference level led to a more intense WBUC. In terms of transport, the total southward mass flux inshore and beneath the Gulf Stream in layers 5-17 is 54 Sv in the 1300 db case, compared to 18 Sv in the 3000 db case. Richardson (1977) used six current meter records to reference geostrophic velocity sections extending from Cape Hatteras across the Gulf Stream. He estimated the transport of the water moving to the south in the WBUC inshore of the right edge of the Gulf Stream to be 17 Sv. More recently, Hogg (1983) used the available long-term current meter data in the western North Atlantic to construct a circulation scheme for the deep water and concluded that the WBUC carried about 12 Sv to the south below 1000 m at  $70^{\circ}\text{W}$ . Joyce *et al.* (1986) found the transport of the deep western boundary current below 2000 db to be  $9 \pm 3$  Sv, compared to 47 Sv and 11 Sv below this depth for the 1300 db and 3000 db models, respectively. The 3000 db model thus results in a WBUC transport that is more consistent with the direct current measurements.

The two models also differ in the eastern basin, although both solutions show net northward flow below 2000 db. This is consistent with the property distributions,

which suggest that the deep water in the eastern basin is fed by inflow from the western basin at the Romanche Fracture Zone at the equator. The meridional gradients of temperature, salinity and silica indicate general northward flow away from this source (Wüst, 1935; Metcalf, 1969).

For the deepest layers (14-17) the net northward flow is not very different for the two models (6 and 3 Sv for the 1300 and 3000 db models, respectively). These values compare favorably to the estimate of Schlitzer *et al.*(1985), who concluded that a northward transport of 4.8 Sv below 4250 m was necessary to account for the observed  $^{14}\text{C}$  distribution in the eastern basin.

The solutions differ significantly, however, between 2000 and 4000 m (layers 9-13). The shallow level leads to a net northward flux of 19 Sv in the eastern basin, in contrast to 6 Sv with the deep reference level. Dickson *et al.*(1985) concluded on the basis of several long-term deep current meter records that the mean flow is very weak in most of the eastern basin, but that a hint of bottom intensification in the records was consistent with deep flow to the north. Kawase and Sarmiento (1986) showed that the distribution of AOU, silicate and nitrate on isopycnal surfaces in the eastern basin was consistent with northward flow at mid-depth. Broecker *et al.*(1976) also suggested that the nutrient distribution in the eastern Atlantic could be most easily explained by spreading to the north of water receiving a large input of opal and organic debris beneath the upwelling area along the African coast south of  $20^{\circ}\text{N}$ . Although the property distributions thus suggest the flow in the eastern basin is to the north, they do not help in distinguishing between the two models.

Saunders (1982) estimated the circulation in the eastern basin by assuming a reference level chosen to satisfy the Sverdrup relation. He concluded that the net transport between 1200 and 3500 m in the eastern basin was 2 Sv to the south, in contrast to the large northward transport implied by the 1300 db model.

The work of Saunders raises the issue of whether the North Atlantic circulation is in Sverdrup balance, a topic addressed by several investigators in recent years (e.g. Leetma *et al.*, 1977; Wunsch and Roemmich, 1984; Roemmich and Wunsch, 1985). Saunders did not claim to verify Sverdrup balance in the eastern basin; rather, he showed that if a deep reference level was used to calculate the transports, the results were consistent with the observed wind stress. The work of Leetma *et al.* (1977) also implied that the wind-driven transport in the North Atlantic was accounted for by the Sverdrup relation. Wunsch and Roemmich (1984) criticized this demonstration on two grounds: first, that the circulation derived by Leetma *et al.* was inconsistent with estimates of the meridional heat flux; and second, that a proof of the validity of Sverdrup balance required not only a demonstration that the interior equatorward flow balanced the poleward transport in the western boundary current, but also evidence that  $w=0$  at the reference level. Without such evidence, the agreement between the observed transport and that predicted by Sverdrup theory may be fortuitous. Wunsch and Roemmich also presented a simple scaling argument suggesting that vertical velocities forced by flow over a sloping bottom may dominate that due to the wind forcing at the sea surface.

Roemmich and Wunsch (1985) later concluded that not only could one not demonstrate that  $w=0$  at some level, but that even the more limited "consistency check" such as that of Saunders and Leetma *et al.* failed at least in some parts of the North Atlantic subtropical gyre. They showed that while the equatorward transport in the upper layers ( $\sigma_0 < 27.4$ ) across the eastern 4000 km of the  $24^\circ\text{N}$  section was consistent with that expected from the wind stress curl, the flux across  $36^\circ\text{N}$  was less than half that required by Sverdrup balance. (The results of the 1300 and 3000 db models presented here are within 1 or 2 Sv of the RW results in the upper layers of the eastern basin, and support this conclusion.) Saunders rejected the IGY section at  $36^\circ\text{N}$  because the vertical shear did not seem consistent with the pattern observed at the other sections he considered. However, the average vertical shear in the eastern basin in the 1981 section is similar to that observed in the IGY: apparently in neither year was the wind-driven flow at this latitude consistent with Sverdrup balance.

Thus the 3000 db model appears to give results more consistent with the direct velocity measurements and property distributions. For the remainder of the discussion the model that conserves mass and silicate in density layers with an initial reference level at 3000 db will be adopted as my "best estimate" of the circulation. There is no guarantee, of course, that this model solution is an accurate representation of the details of the mean circulation, or the flow in the summer of 1981. Some features of the flow remain undetermined by the available information. For example, Schmitz (1980) has described strong, weakly depth-dependent currents along 55°W, with velocities up to  $9 \text{ cm s}^{-1}$  at 4000 m at 36°N. Such strong barotropic flows will only appear in the inverse solution to the extent that they are required to account for the observed property distributions. The hydrographic and nutrient fields, however, vary on much broader scales than the narrow zonal jets revealed by the direct current meter measurements. These currents can thus have little effect on the net transport of properties, since the gradients are small on this scale, and in turn the distributions contain little information about such flows. One could introduce some of the smaller scale undetermined components of the flow field into the solution by including the current meter observations explicitly as additional constraints. The choice of an initial horizontal reference level is meant to provide an initial model that is reasonably close to the actual state of the ocean. The inverse method then provides a means of adding the least amount of additional structure required to satisfy the constraints. A circulation scheme based on current meter results or float observations could of course be used as an initial model replacing a "level-of-no-motion" by a "level-of-known-motion." However, at this point both the number of direct current observations and our understanding seem too limited to justify the construction of a more elaborate initial model. Moreover, there is a problem with the mismatch of scales in explicitly including such observations. The shear field obtained from a single hydrographic section represents a single "snapshot" of the relative velocity, spatially smoothed on the scale of the station spacing, while a current

meter measurement gives a long-time mean at a single location. The tracer fields represent yet another mixture of space and time scales, as the observed concentration is the product of the advective/diffusive history of a water parcel, not the instantaneous flow field alone.

Although the direct velocity measurements suggest the 3000 db solution is closer to the true circulation, the differences between the 1300 and 3000 db models can be interpreted as one statement of the uncertainty remaining in our estimate of the velocity field. Note that although the mass transports differ significantly in some locations, the net mass and nutrient fluxes described in section 4 are very similar for the two models. In the next section we will demonstrate explicitly that the zonal integrals are well determined, by examining the potential contribution of the null-space vectors to the property fluxes.

While on the subject of reference levels, it is worth commenting on a variation to the inverse procedure introduced by Fiadeiro and Veronis (1982). They suggest performing an empirical search to find the optimal reference level, in which the whole depth range is systematically searched for the horizontal level that gives the smallest residuals in the constraint equations. An inverse correction is then applied if some of the residuals are still larger than the estimated errors. The first step in any inverse procedure is indeed to seek an initial state that is as close as possible to the actual flow, so that by finding the minimal correction to the initial model required to satisfy the observations one obtains a good approximation to the true flow. But consideration of the initial residuals alone can be misleading, especially in models that are not highly constrained. For the models considered here in which only mass was conserved, the 1300 db model had an initial residual norm half that of the 3000 db model, but to drive the residuals to zero (within error) required a larger reference level velocity correction in the 1300 db case. Furthermore, when additional information was included, namely silicate conservation statements, we saw that the 1300 db reference level resulted in



huge residuals in the silicate equations, and a velocity field inconsistent with the direct velocity observations. Predicting the relative success of a candidate reference level from the initial residuals alone is therefore difficult.

Moreover, having performed a systematic search, one may be tempted to conclude that all possibilities have been considered. Yet the method as applied so far is limited to *horizontal* (either constant pressure or constant density) surfaces, and many inverse calculations and current meter measurements have shown that there is no simple horizontal level of no motion in most of the ocean. A safer approach, given that we lack the knowledge to construct a more complicated initial model, would seem to be to calculate solutions for several reference levels, each consistent with water mass distributions, and compare the results. To the extent that different choices lead to flow fields that satisfy the imposed constraints, but differ in detail, one can get a feeling for the range of solutions consistent with the observations.

### 5.3 Heat, oxygen and nutrient transports

In section 5.1 two sources of uncertainty in the solution were discussed: errors due to noise in the data and errors due to a failure to fully resolve the solution. We found that the individual  $b_i$  are generally not very well resolved. The meridional fluxes, however, are much better determined. One way to demonstrate this is simply to compare the results of different models. We have already seen that the range of values for the meridional property transports obtained with different reference levels was dramatically reduced when both silicate and mass were conserved. The sensitivity of the zonal integrals to the modeling assumptions can be examined more thoroughly by considering directly the error in the fluxes arising from noise in the observations and the potential contribution from the unresolved components of the flow. Wunsch *et al.*(1983) showed how one can define the projection of any tracer onto the null-space, and from this calculate the uncertainty in the flux due to the undetermined velocities. The error due to data noise follows directly from eq. (1.3), where instead of the variance of the  $b_i$  we find the variance of the flux of tracer C carried by the  $b_i$ . The details are shown in the Appendix, which follows closely the discussion in Wunsch *et al.*(1983). Estimates of these errors are included with the meridional flux results in Table 4.9. Also given in Table 4.9, and discussed in the Appendix, are errors due to observational errors in the wind stress.

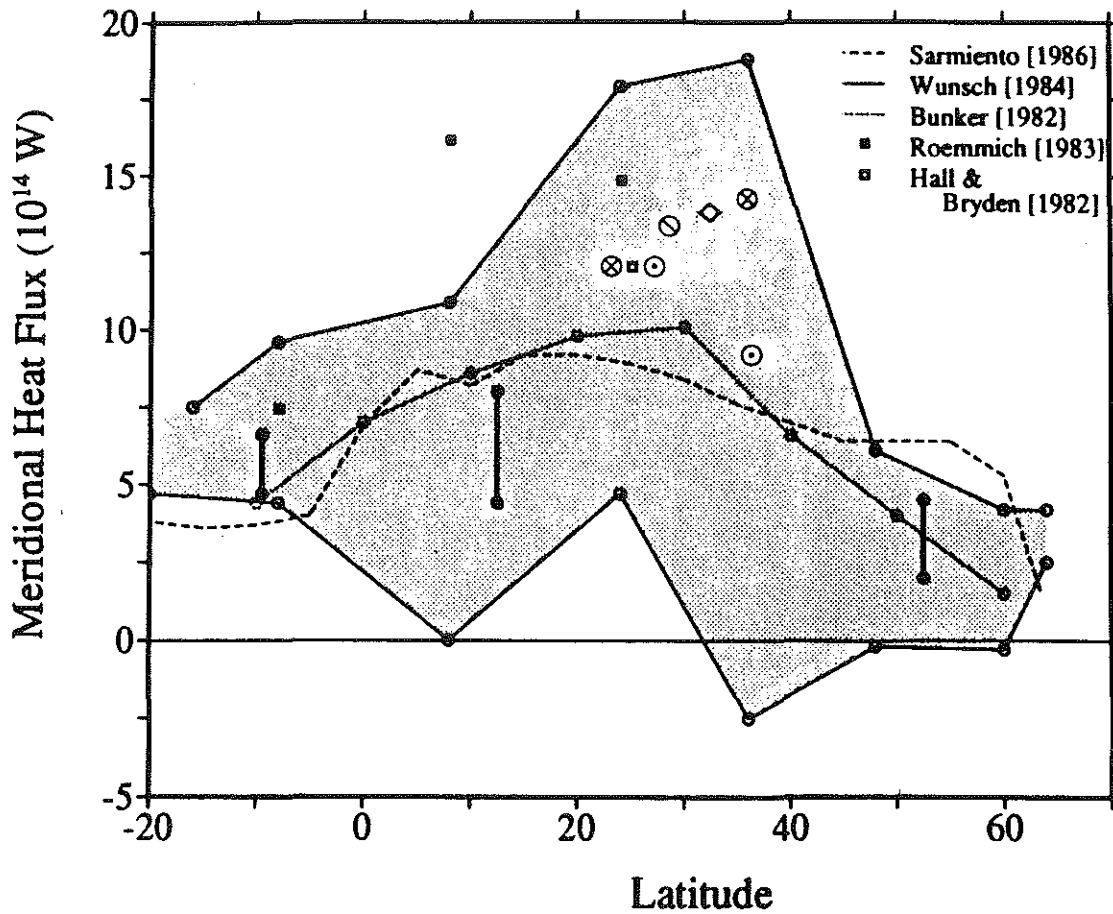
### *Mass and Heat Transport: Comparison to RW Results*

The net temperature flux results for the silica-conserving models are presented in Table 4.9. The meridional heat flux across each latitude, for both models, is  $\approx 1.3 \pm .2$  PW. The dominant source of error in the heat flux estimate is the uncertainty in the Ekman flux. The projection of the total heat content vector on the null-space is very small, and thus the uncertainty due to unresolved components of the flow is also small.

This estimate is in general agreement with other recent estimates of meridional heat flux in the North Atlantic, as seen in Fig. 5.12. However, there is a large discrepancy between these results and those of RW. At 24°N the estimates are similar (1.2 PW) but at 36°N the heat flux is significantly higher than that found by RW: 1.4 PW vs. .8 PW, despite the fact that the same initial reference level and modelling assumptions were used.

As noted in Section 4, the pattern of mass transports found here also differs from that of RW in the near surface layer and in the deep water. It is at first surprising that there is a large difference in the net transport of some layers between these results and those of RW, given that the same data set and similar methods were used. As mentioned earlier, the models differ in two respects: first, RW used a single reference pressure to define the potential density surfaces bounding each layer; second, RW applied an objective mapping procedure before performing the inversion which both smoothed the original data and provided a way to extrapolate below the deepest common sample depth over sloping topography.

To test how using a variable reference pressure to define layer boundaries affects the solution, I ran the mass-conserving model with an initial reference level at 1300 db, using the RW layer definitions and a constant reference pressure for each layer boundary. In Section 3 it was shown that for most layers there was little difference between the areas of layers defined by constant and variable reference pressures, but that at intermediate depths the areas could differ by a factor of two.



- ⊗ this study
- ◇ Rago and Rossby (1987)
- Leeman *et al.* (1987)
- ⊙ Roemmich and Wunsch (1985)

Fig. 5.12 Meridional heat flux in the Atlantic Ocean as a function of latitude, adapted from Fig. 15 of Schlitzer (1987). Shaded area is between the upper and lower bounds determined by Wunsch (1984).

Table 5.1 Comparison of layer transports at 36°N for RW, variable and constant reference pressure cases. Initial reference level = 1300 db in each case. Units=Sv.

| Layer | RW   | variable<br>$P_{ref}$ | constant<br>$P_{ref}$ |
|-------|------|-----------------------|-----------------------|
| 1     | 11.2 | 14.1                  | 14.3                  |
| 2     | -1.7 | -0.1                  | 0.8                   |
| 3     | 1.4  | 1.6                   | 1.8                   |
| 4     | 1.9  | -2.9                  | -3.2                  |
| 5     | 1.6  | 2.4                   | 0.9                   |
| 6     | 2.9  | 3.8                   | 2.2                   |
| 7     | 1.8  | 0.0                   | 0.7                   |
| 8     | -0.6 | -0.6                  | -1.0                  |
| 9     | -0.5 | -0.4                  | -0.1                  |
| 10    | -1.2 | -1.2                  | -1.1                  |
| 11    | -0.4 | 0.2                   | -0.3                  |
| 12    | -0.3 | 0.8                   | 0.8                   |
| 13    | -1.5 | 1.1                   | 0.5                   |
| 14    | -1.5 | -1.5                  | -2.0                  |
| 15    | -8.3 | -8.9                  | -7.3                  |
| 16    | -5.4 | -7.7                  | -6.4                  |
| 17    | 0.3  | -0.6                  | -0.6                  |
| 18    | *    | *                     | *                     |

The zonally-integrated transport in each layer at 36°N for the two cases, and for the RW model, are compared in Table 5.1. Not surprisingly, the transports are similar for most layers. However, the constant  $P_{ref}$  solution has 2.4 Sv less intermediate water (layers 5-7) flowing north and the southward flow of deep water (layers 14-17) is decreased by the same amount. The heat flux is in turn decreased by a small amount ( $\approx .1 \times 10^{15} W$ ).

On the other hand, the different definition of layer boundaries does not account for all of the transport differences between these results and those of RW: the southward flow in layer 4 is slightly increased in the constant  $P_{ref}$  case, and the net flow in layers 12 and 13 is still to the north.

To examine the effect of smoothing the data before applying the inverse method, I first compared the maps of RW to maps of the non-smoothed station data. The two were indistinguishable for most of the section. The two exceptions were in the Gulf Stream and the cold core ring or meander, where the isopleths are nearly vertical in the upper part of the water column. The transport maps discussed above show that most of the northward flow in layer 1 occurs in the Gulf Stream, while the imbalance in north- and southward flow of layer 4 in the cold core ring is alone sufficient to account for the net southward flow in this layer. This suggested that the difference between the two solutions might be explained in part by smoothing, and hence decreased transport, of the very high gradient features in this section.

This hypothesis was tested directly by applying a smoothing filter to the original data and running the inversion again. A simple "box-car" averaging window was used for the test, and experiments were performed with the filter width equal to  $\pm 1$  and  $\pm 2$  station pairs. These two experiments will be referred to as SMOOTH1 and SMOOTH2, respectively. RW used a more involved, two-step procedure (see Roemmich (1983) for details of the mapping technique) but the scale of the averaging is comparable: the smaller-scale features were mapped using an exponential function with an e-folding scale of 2 station pairs, in their case.

The net mass transport in each layer across  $36^{\circ}\text{N}$  for each of the models is shown in Table 5.2. Some differences still remain (the models still differ in the method used to extrapolate below the deepest common sample depth, and the 3000 db and smoothing model runs use variable reference pressures to define the layer boundaries) but smoothing does seem to eliminate the largest discrepancies between the 3000 db results and those of RW. Note that the transports in individual layers are coupled by the conservation and flux constraints (a change in  $b_i$  affects all layers) and thus the transport of all layers is altered by smoothing, including locations distant from the high gradient regions. Thus, significant changes in transport are seen even at depth,

Table 5.2 Layer transports at 36°N for the 3000 db model with mass and silicate conserved in density layers, compared to results of the smoothing experiments and those of RW.

|    | 3000 db | SMOOTH1 | SMOOTH2 | RW   |
|----|---------|---------|---------|------|
| 1  | 15.2    | 12.8    | 10.2    | 11.2 |
| 2  | -1.5    | -1.6    | 2.2     | -1.7 |
| 3  | 2.2     | 1.7     | 1.9     | 1.4  |
| 4  | -4.1    | 0.7     | 2.0     | 1.9  |
| 5  | 2.4     | 2.1     | 3.1     | 1.6  |
| 6  | 3.1     | 2.6     | 2.4     | 2.9  |
| 7  | 1.6     | 0.0     | 0.0     | 1.8  |
| 8  | -2.1    | -1.3    | -1.8    | -0.6 |
| 9  | -3.3    | -1.6    | -1.3    | -0.5 |
| 10 | -1.4    | -1.1    | -1.1    | -1.2 |
| 11 | -0.5    | -1.0    | -1.8    | -0.4 |
| 12 | -0.2    | -1.2    | -2.0    | -0.3 |
| 13 | 1.1     | -1.2    | -2.3    | -1.5 |
| 14 | -0.1    | -0.9    | -1.3    | -1.5 |
| 15 | -5.3    | -4.9    | -4.6    | -8.3 |
| 16 | -6.6    | -4.9    | -5.3    | -5.4 |
| 17 | -.4     | 0.1     | -0.1    | 0.3  |
| 18 | *       | *       | *       | *    |

where the gradients are generally more gentle than in the upper water column: in layers 12-14, for example, the net transport is .8 Sv in the 3000 db model, vs. -5.6 in the SMOOTH2 experiment.

The meridional heat flux is also more in line with the results of RW when the data is smoothed. The net heat flux across 36°N for each of the models is shown in Table 5.3. Both smoothing experiments give a net heat flux of  $\approx 1.1$  PW, midway between the results of the "best estimate" model and that of RW. The gap is further narrowed (by  $\approx 1$  PW) when the effect of using a constant reference pressure to define the isopycnal bounding surfaces is accounted for, as noted above.

The differences in the meridional transport results for each of the models provides some insight into the mechanisms responsible for the poleward heat flux in the North

Table 5.3 Meridional heat flux across 36°N for smoothing experiment comparison (PW).

|                  | 3000 db | SMOOTH1 | SMOOTH2 | RW   |
|------------------|---------|---------|---------|------|
| Total            | 1.4     | 1.1     | 1.1     | .8   |
| overturning cell | 1.1     | 1.1     | 1.1     | 1.0  |
| difference       | .28     | .05     | -0.08   | -.17 |

Atlantic. Also listed in Table 5.3 is the contribution to the net heat flux carried by the zonally-integrated overturning cell, estimated by multiplying the net mass transport in each layer by the layer-average temperature. In each case the overturning cell is responsible for the majority of the net poleward flux of heat. The fact that the meridional overturning circulation dominates the meridional transport of heat, due to the large temperature contrast between the poleward and equatorward flows, has been recognized by many other investigators (e.g. Bryan, 1962; Hall and Bryden, 1982; Wunsch, 1978; Roemmich, 1980; Rago and Rossby, 1987).

It is also interesting to note that the contribution of the overturning cell is nearly the same in each case, even for the 3000 db and RW models, for which the net heat fluxes differ by .6 PW. The large difference in the net heat flux in the 3000 db and RW models is not due to a change in the vigor of the overturning cell, but rather to contributions to the heat flux arising from horizontal correlations of velocity and temperature, whose sum is of opposite sign in the two cases. For example, the larger poleward heat flux in the unsmoothed model is largely due to relatively high temperatures and stronger northward flow in the warm core (upper 100-200 m) of the Gulf Stream.

Smoothing of the data, then, does appear to be responsible for the major differences between these results and those of RW. The important question is which of the two is



more appropriate: should one smooth or not? This issue will be discussed in detail at the end of this section, after considering the oxygen and nutrient fluxes.

### *Oxygen Transport*

The net flux of oxygen is  $-2940 \pm 180 \text{ kmol s}^{-1}$  to the south at  $36^\circ\text{N}$  and  $-2600 \pm 120 \text{ kmol s}^{-1}$  at  $24^\circ\text{N}$  for the 3000 db model. For oxygen the estimated uncertainty due to all three sources of error is small. The transports found here are of the same sign but larger in magnitude than the  $-2080 \text{ kmol s}^{-1}$  estimated by BD. As they point out, two factors contribute to the southward flux. Part of the increase in the southward flow is due to "thermal pumping." The solubility of oxygen increases with decreasing temperature, so that water that equilibrates with the atmosphere at high latitude carries "excess" oxygen when it returns to the south. For reference, the oxygen solubility increases by about 20% for a temperature change from  $18^\circ\text{C}$  to  $10^\circ\text{C}$  at a salinity of  $35\text{‰}$  (Smith and Kalber, 1974).

The overturning cell associated with deep water formation in the North Atlantic is the second important mechanism responsible for the southward flux of oxygen. When the low oxygen sub-surface water carried north by the Gulf Stream is exposed at the sea surface at higher latitude, it equilibrates with the atmosphere as it is cooled and returns to the south at depth with a higher oxygen concentration. The meridional overturning cell is thus the primary mechanism responsible for the equatorward flux of oxygen, as well as the poleward flux of heat. The strong similarity between the zonally-integrated oxygen flux density (Fig. 5.13) and the mass flux density (Fig. 4.13b) for this model further reflects the dominant contribution made by the meridional cell to the transport of oxygen.

The transport estimates result in a small net convergence of oxygen between  $24^\circ$  and  $36^\circ\text{N}$  of  $340 \text{ kmol s}^{-1}$ . This convergence is barely significantly different from zero, but it is consistent in sign with net consumption of oxygen within the box. The

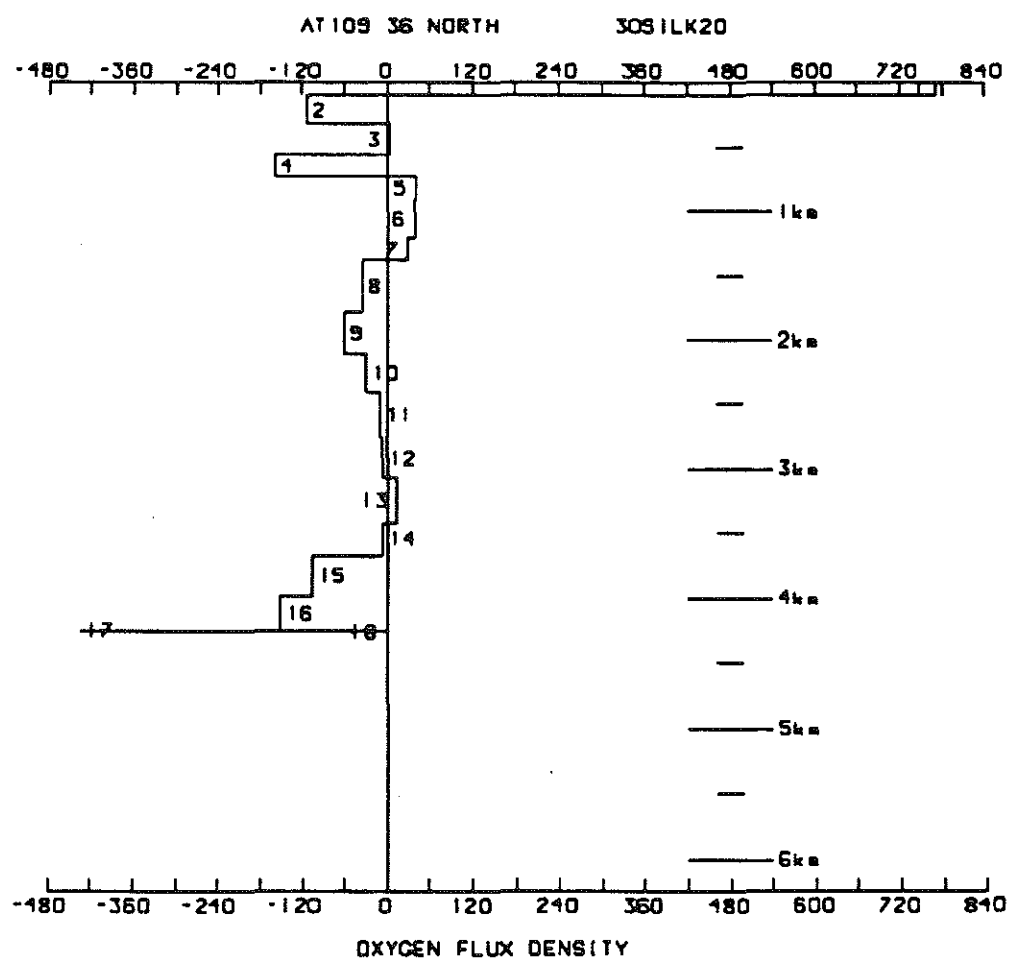


Fig. 5.13 Zonally-integrated oxygen flux density at 36°N for the mass and silicate conserving model with 3000 db reference level ( $kmol s^{-1}/km$ ).

oxygen residuals in each layer (Fig. 4.14) suggest that there is a net input of oxygen to the ocean from the atmosphere in layer 1 and that the net oxygen consumption occurs primarily in layers 2-4. This is in accord with estimates of the oxygen utilization rate (OUR) in the subtropical Atlantic by Riley (1951) and Jenkins (1980) which show that the OUR decreases rapidly with depth. The oxygen residuals are small below layer 4 and there is no evidence for oxygen consumption in the deep water, to within the error in the layer transports.

The North Atlantic Deep Water thus provides a major source of oxygen to the deep water of the world ocean. Indeed the striking high oxygen plume extending along the western boundary of the Atlantic basin led Wüst (1935), and later Mantyla and Reid (1983), to comment on the important role played by the formation and export of NADW in ventilating the deep ocean.

#### *Silicate Transport*

The net transport of silicate, like that of oxygen, is to the south:  $-138 \pm 38 \text{ kmol s}^{-1}$  at  $36^\circ\text{N}$  and  $-152 \pm 56 \text{ kmol s}^{-1}$  at  $24^\circ\text{N}$ . In this case the Ekman flux uncertainty is the dominant source of error. The projection of the total silicate content vector onto the null-space is only 2%, and the resulting errors are 1/3 those due to the Ekman errors quoted above. Errors due to data noise are even smaller.

A plot of the silicate transport per unit depth (Fig. 5.14) suggests that the overturning cell in the North Atlantic also plays an important role in the flux of silicate. Since the poleward flow in the upper layers is lower in silica than the equatorward deep flow, the result is a net equatorward flux of silicate. As noted in Section 2, the concentration of silica increases rapidly with depth, and has significant structure in the deep water. The increase in concentration between 1500 and 3500 m is in fact great enough that although the northward mass flux in layers 12 to 14 is much smaller (.8

Sv) than the southward transport in layers 8-11 (-7.3), the silica transport is actually higher for the deeper layers.

*Importance of the horizontal circulation.* Note also, in comparing Fig. 5.14 to the mass transport per unit depth for this model (Fig. 4.13b), that a net flux of mass to the south in a given layer does not necessarily lead to a net silica flux of the same sign. In fact, although the southward silica flux is largely due to net poleward flow of low silica water in the upper layers balanced by equatorward high silica flow at depth, the horizontal circulation makes a significant contribution to the total transport. The flux due to the zonally-integrated cell at 36°N, obtained by multiplying the mass transport by the average silicate concentration in each layer, is  $-460 \text{ kmol s}^{-1}$ , more than three times greater than the actual flux.

The discrepancy is explained by the observation that silicate, unlike temperature and oxygen, varies significantly along isopycnal surfaces. The variation is particularly large for layers 1-4 and layers 12-15. A useful way to explore the differences in structure of the tracer fields is to compare plots of the depth-averaged concentration against horizontal distance along the sections, as in Fig. 5.15. The variation of the vertically averaged nutrient concentrations is significantly larger than for temperature or oxygen. Hall and Bryden (1982) took advantage of the fact that the depth-averaged temperature at 24°N was nearly constant to make an estimate of the meridional heat flux; they recognized that as long as the average temperature did not vary along the section, one could determine the barotropic component of the heat flux without determining the horizontal structure of the barotropic, or reference level, velocity itself. One clearly cannot make the same assumption when calculating nutrient transports (i.e.  $\int_x \int_z \bar{v}(x) C'(x, z) \neq 0$ , where  $\bar{v}$  is the barotropic velocity and  $C'$  is the deviation from the depth-averaged concentration).

In particular, calculating the silicate transport by the product of the zonally-integrated circulation and the layer average concentration gives an overestimate of the

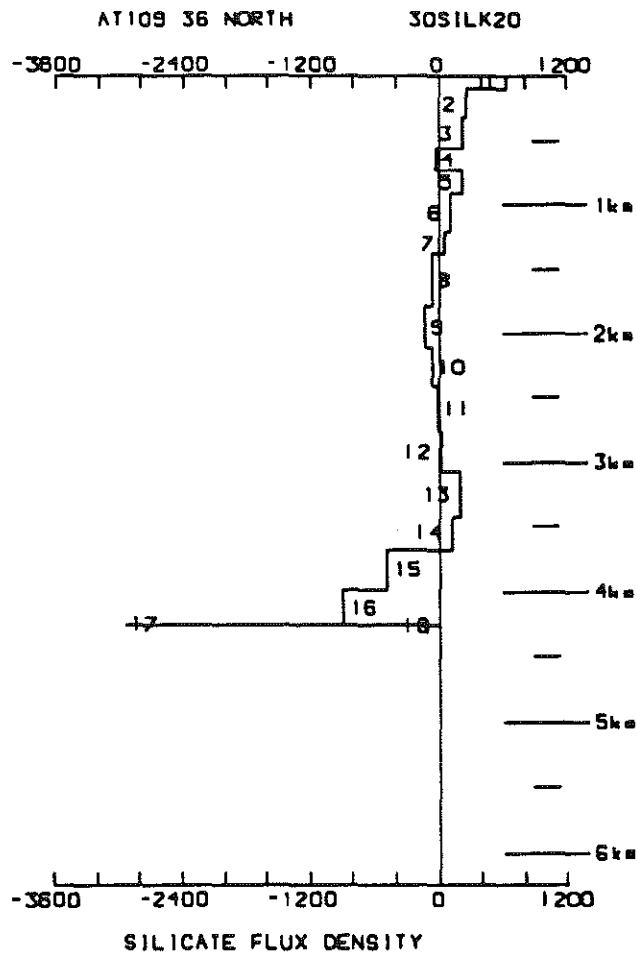


Fig. 5.14 Zonally-integrated silicate flux density at 36°N for the mass and silicate conserving model with 3000 db reference level ( $kmol s^{-1}/km$ ).

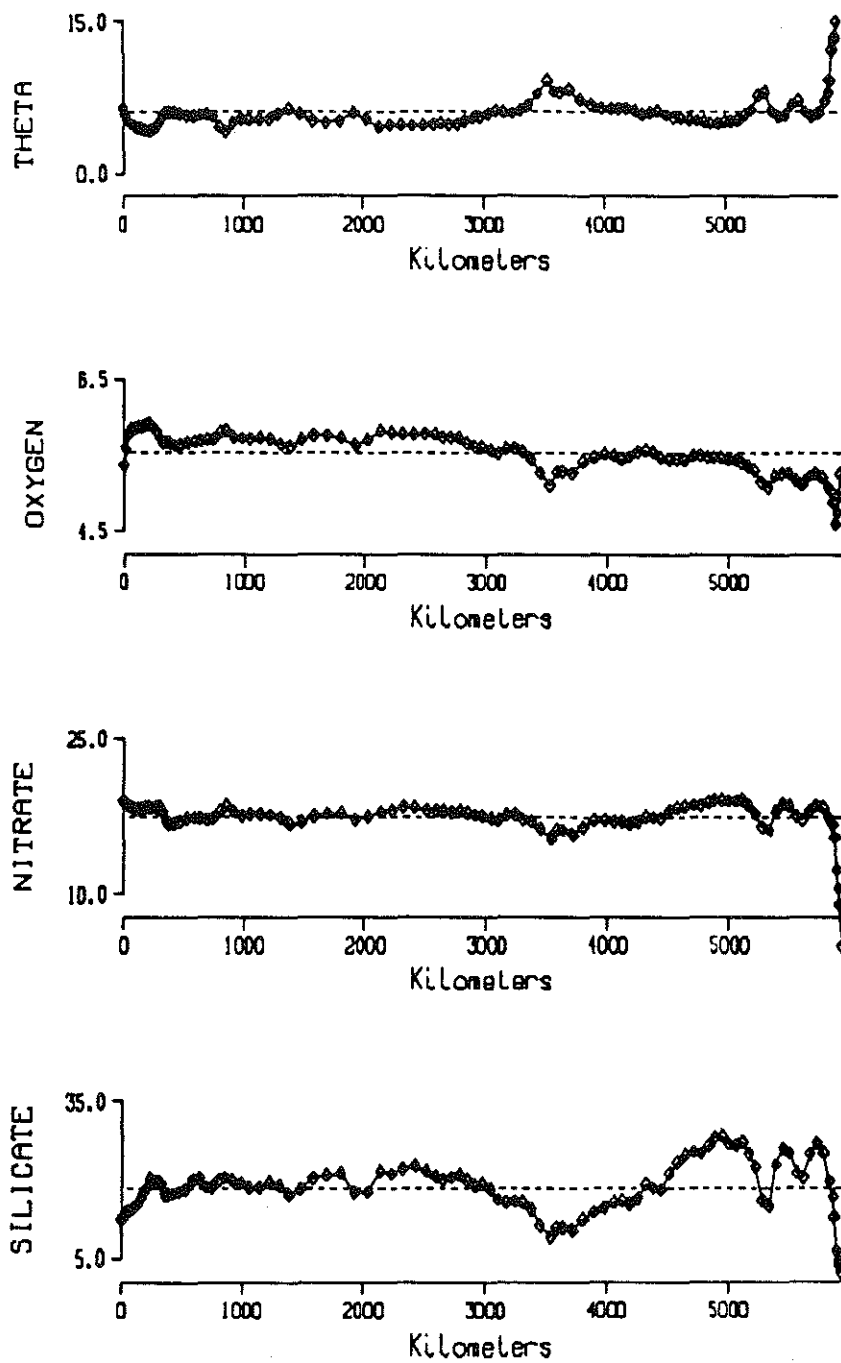


Fig. 5.15a Depth-averaged concentration vs. zonal distance for temperature, oxygen, silicate and nitrate at 36°N. Dashed line is section average.

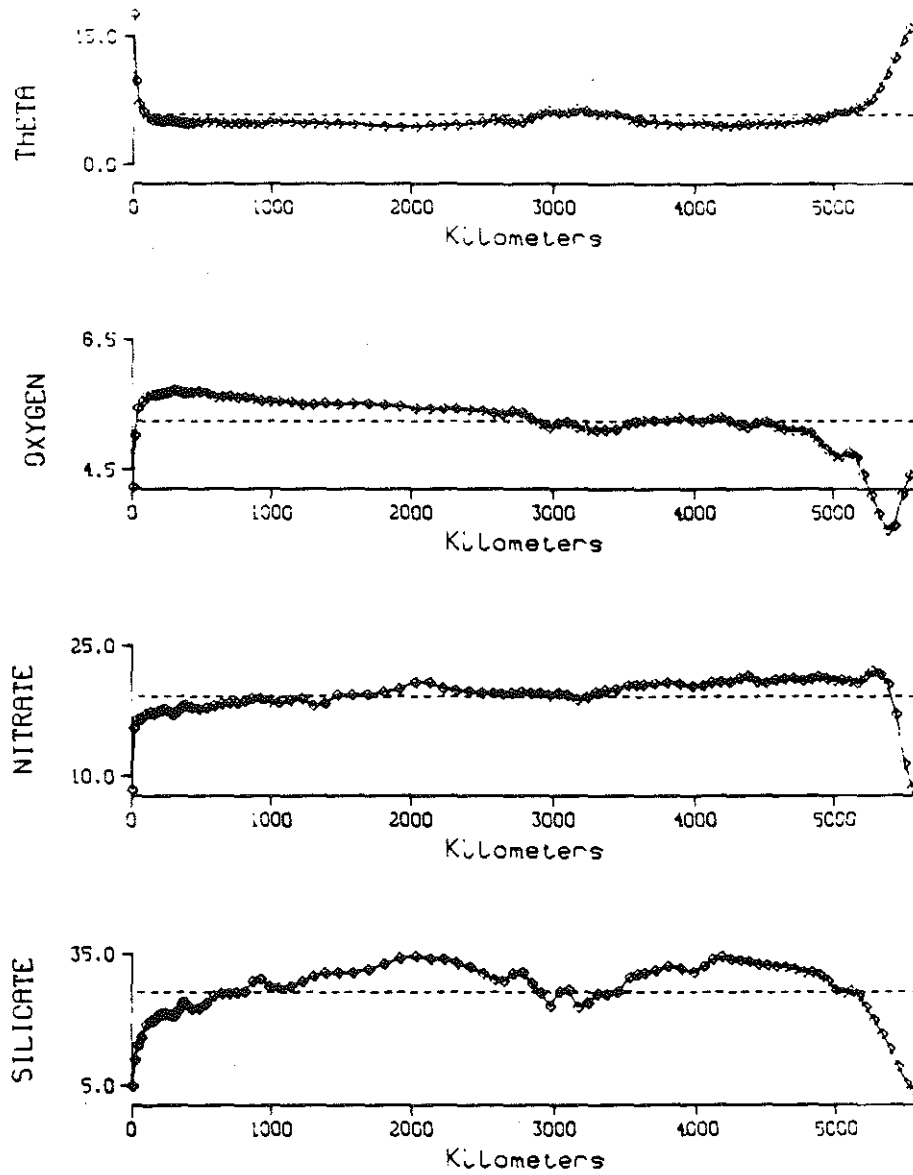


Fig. 5.15b Depth-averaged concentration vs. zonal distance for temperature, oxygen, silicate and nitrate at 24°N. Dashed line is section average.

southward flux because it misses significant transport by the horizontal circulation in two depth intervals. In layers 1-4 the silica concentration in the Gulf Stream is higher than the section average, and the correlation of high concentrations with strong northward flow results in  $160 \text{ kmol s}^{-1}$  more Si carried to the north than that implied by the section average picture. Likewise, in layers 12-15 there is northward flow in the eastern basin, where the concentrations are high, which balances in part the southward flow of newly formed NADW with low silica in the western basin. Consequently there is a significant net equatorward transport of mass in these layers, but only a small net silica transport of  $46 \text{ kmol s}^{-1}$ ,  $120 \text{ kmol s}^{-1}$  less than one would conclude based on the layer average silica concentrations. The importance of the horizontal component of the circulation to the flux of silicate was also suggested by the results of the smoothing experiments: the silicate flux across  $36^\circ\text{N}$  was  $-215$  and  $-320 \text{ kmol s}^{-1}$ , for the SMOOTH1 and SMOOTH2 runs, respectively, compared to  $-138$  in the standard case. The fact that the section average values give misleading estimates of the silicate flux explains in part why BD's estimate was more than twice as large as the value found here.

*Can the silica flux be driven to zero?* The silicate transport of  $-138 \text{ kmol s}^{-1}$  across  $36^\circ\text{N}$  implied by this model, although smaller than the BD estimate, is still twice the rate at which silica is supplied to the North Atlantic found by Anderson *et al.*(1983). Given the probable uncertainties in both numbers, the difference may not be significant (there are no error bars given for the silica source strength). However, the inverse machinery can be used to test directly if a flow consistent with a smaller source of silica can be found.

The 3000 db model was run again with the additional constraint that there be no net flux of silicate across each latitude. To drive the silicate flux to zero requires a 40% increase in the solution norm. The main difference in b is stronger northward flow in the eastern basin (where the average concentration is high) balanced by stronger flow



to the south over the Mid-Atlantic Ridge and along the western boundary (where the concentration is low).

The effect of the changes in  $b$  on the mass transport can be seen by comparing the mass flux density plot in Fig. 5.16 to that of the earlier model (Fig. 4.13b). The transport of the surface and intermediate layers is unchanged, and even at depth the transports differ by only a few Sverdrups. However, as noted above, the large vertical silica gradient between 1500 and 3500 m allows even a weak circulation cell to carry a large flux of silica. In this case, an additional net northward flow of 2 Sv in layers 13 and 14 balanced by southward flow in layers 8-12 is sufficient to bring the net flux across the section to zero. Note that although the net transport across the section in layers 13 and 14 is increased by only 2 Sv, the northward flow of deep water in the eastern basin is increased by more than a factor of two. A doubling of the flow rate implies that the eastern basin is flushed more rapidly than Schlitzer *et al.* (1985) concluded from the  $^{14}\text{C}$  distribution.

The heat and oxygen transports are unchanged by the silica flux constraint, since neither temperature nor oxygen vary significantly over this depth range. Nitrate increases in concentration with depth, although less dramatically than silicate, and the northward flux of nitrate is increased slightly to  $140 \text{ kmol s}^{-1}$  when the silica flux is driven to zero.

Forcing the system to carry no net flux of silicate across  $36^\circ\text{N}$  thus leads to substantial but perhaps not unreasonable changes in the circulation. Relaxing the constraint somewhat to be consistent with the  $-(30-60) \text{ kmol s}^{-1}$  flux expected from the silica input rate estimates of Anderson *et al.* (1983) would clearly require even smaller changes in the flow. Additional information which could set bounds on the maximum northward flux of deep water in the eastern basin would be useful in setting a lower bound on the net silica flux. One possibility would be to include constraints on  $^{14}\text{C}$ , along the lines of Schlitzer *et al.* (1985), although the data available are still sparse. At this

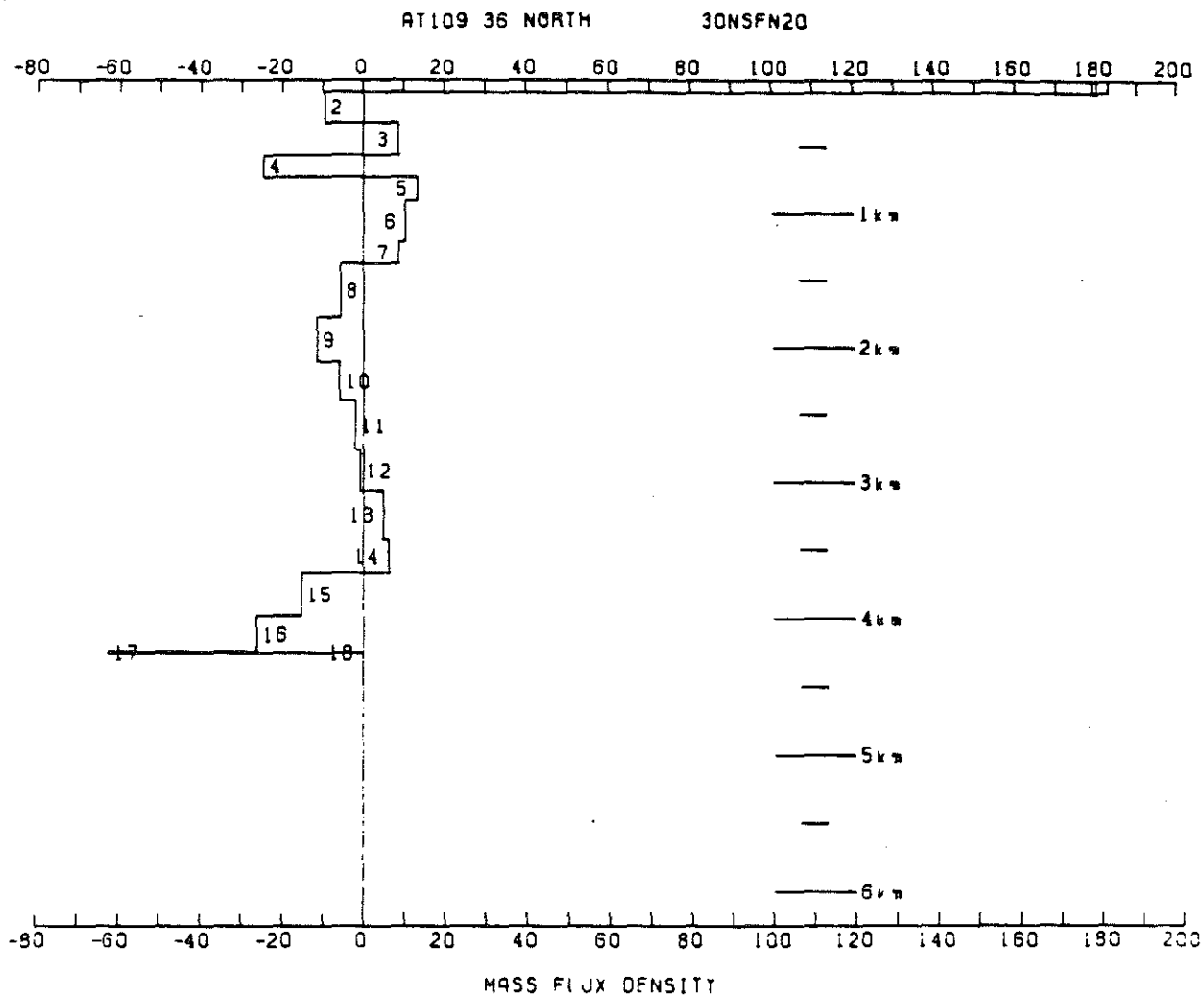


Fig. 5.16 Mass flux density at 36°N for model with silica flux across this latitude set to zero.

point the appropriate conclusion seems to be that current estimates of the silica input to the North Atlantic may be low, but there is no strong contradiction between the flux estimate presented here and estimates of the input rate to the North Atlantic, given the uncertainties in both values. Either estimate implies that the North Atlantic as a whole exports silica to the rest of the world ocean. If one insists that there be no net flux of silica, one must be willing to accept a sizable flow of deep water to the north in the eastern basin, and a large flux of nitrate to the north.

### *Nitrate Transport*

The transport of nitrate, in contrast to silicate, is to the north across  $36^{\circ}\text{N}$  and equal to  $119 \pm 35 \text{ kmol s}^{-1}$ . At  $24^{\circ}\text{N}$  the flux of nitrate through the Florida Straits is nearly equal to that carried to the south in the interior and the net transport,  $-8 \pm 39 \text{ kmol s}^{-1}$ , is indistinguishable from zero. The dominant error is again the Ekman component, as 98% of the length of the nitrate content vector lies in the range of **A** and the error due to data noise is small.

The nitrate flux density at  $36^{\circ}\text{N}$  (Fig. 5.17) shows that the transport of nitrate also appears to be dominated by the overturning meridional cell. In this case, however, the northward flux in the upper layers is larger than the southward flux at depth, so that the net transport across the section is to the north. This is at first counter-intuitive, since nitrate concentrations are generally higher at depth.

The explanation again lies in the fact that the nitrate concentration varies strongly with position in some layers, so that the horizontal circulation can make a significant contribution to the total nitrate flux. In layer 2, for example, although the net mass flux is to the south the flux of nitrate is strongly to the north. Indeed, despite the gross similarity of the pattern of the nitrate flux density to that of mass, the difference between the nitrate flux carried by the zonally-integrated circulation and the actual flux is even larger in this case than was found for silicate. Multiplying the mass transport

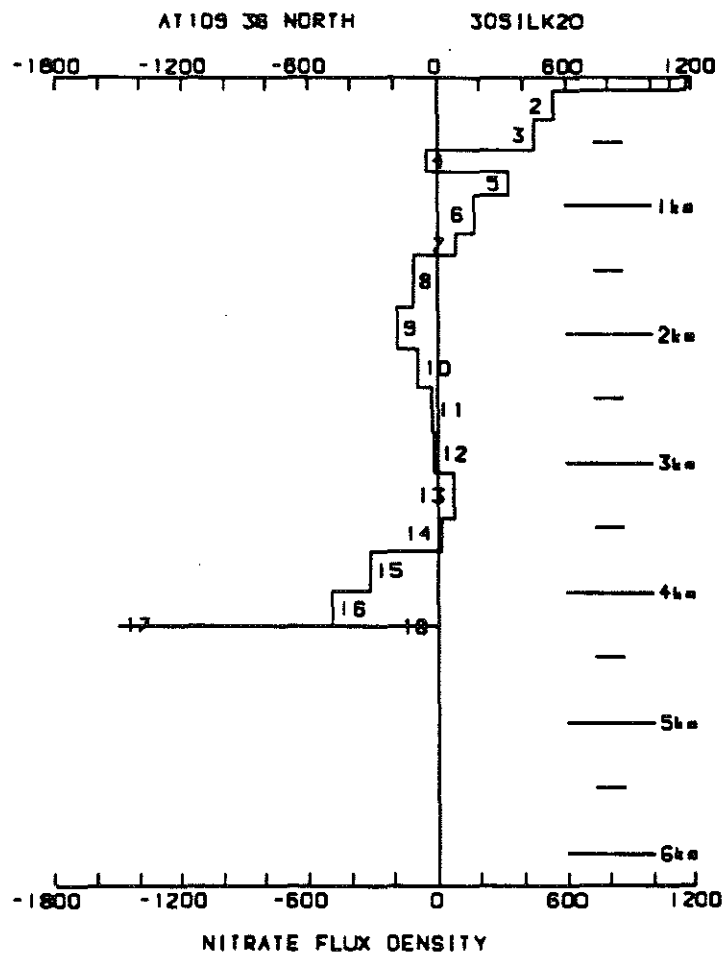


Fig. 5.17 Zonally-integrated nitrate flux density at 36°N for the mass and silicate conserving model with 3000 db reference level ( $\text{kmol s}^{-1}/\text{km}$ ).

and average nitrate concentration for each layer implies a net flux of  $300 \text{ kmol s}^{-1}$  to the south, opposite in sign and much larger in magnitude than the actual flux of  $119 \text{ kmol s}^{-1}$  to the north.

This difference of  $>400 \text{ kmol s}^{-1}$  when the section average values are used is due to a serious underestimate of the actual northward flux in the top 4 layers. Below layer 4 there is little variation in the concentration of nitrate within each layer and the product of the net mass transport and the mean layer concentration provides a good estimate of actual nitrate transport. In the upper layers this is not the case. The upper layers are generally poor in nitrate but between 200 and 600 m nitrate concentrations in the Gulf Stream are several times higher than in the interior. The correlation of high nutrient concentrations and strong northward flow in the Gulf Stream results in a large northward nitrate flux; in fact, this is the dominant mechanism controlling the flux of nitrate across  $36^\circ\text{N}$ . When these correlations are decreased by smoothing the data, the flux decreases rapidly: smoothing over  $\pm 1$  station pair lowers the flux to  $73 \text{ kmol s}^{-1}$ , and to  $18 \text{ kmol s}^{-1}$  when smoothed over  $\pm 2$  station pairs.

Brewer and Dyrssen found a net nitrate flux of  $100 \text{ kmol s}^{-1}$  to the south at  $24^\circ\text{N}$ , in contrast to the near balance between the import of nitrate through the Florida Straits and the export of nitrate in the interior found in this model. The above discussion suggests that BD's calculation, based on zonal average values, overestimated the southward flux in the interior. One of the important results of the present work is the demonstration that property fluxes cannot be reliably estimated from heavily-smoothed or section-average values. This suggests that conclusions concerning property fluxes based on heavily smoothed data sets such as the climatological atlas of Levitus (1982) should be taken with caution. In the case of nitrate, for example, a smoother representation of the field which missed the high values in the high velocity core of the Gulf Stream would result in a net flux of the wrong sign.

Can total nitrate be conserved? Northward nitrate transport across 36°N and a small or southward flux across 24°N leads to a large divergence ( $130 \text{ kmol s}^{-1}$ ), implying that there is a significant source of nitrate within this latitude band. However, BD suggested that a reasonable value for the input of nitrate by rivers to the entire North Atlantic was only  $10 \text{ kmol s}^{-1}$ . To see if the nitrate flux results could be reconciled with the source strength estimates, an experiment was run in which total nitrate was approximately conserved. Initial reference levels at 1300 and 3000 db were considered and gave similar results, so only the deep reference level model will be discussed.

To satisfy the nitrate conservation constraint requires an increase in  $b^t b$  by a factor of two (587 to 1051). The solution contains more smaller-scale structure and there are some reference level velocities  $>5 \text{ cm s}^{-1}$ . The nitrate transport at 36°N is decreased to  $78 \text{ kmol s}^{-1}$  but is still to the north, while at 24°N the flux through the Florida Straits is increased slightly and the southward flux in the interior is reduced, so that the net flux across this latitude is now  $68 \text{ kmol s}^{-1}$  to the north. Thus, the system responds to the requirement that total nitrate be conserved by removing less nitrate to the north at 36°N and changing the sign of the flux at 24°N.

These changes in the circulation lead to an increase in the transport of heat, oxygen and silicate across 36°N to 1.6 PW,  $-3600 \text{ kmol s}^{-1}$  and  $-158 \text{ kmol s}^{-1}$ , respectively. At 24°N the heat flux is decreased and the oxygen and silicate fluxes increased by small amounts. In this model, then, the ocean apparently gains  $\approx .4 \text{ PW}$  of heat between 24 and 36°N, contrary to Bunker's (1982) maps which show this region as one of net heat loss.

In terms of the zonally-integrated mass transport, the primary change at 36°N is an increase in northward flow of 4 Sv in layers 3-6 balanced by an increased southward flow of NADW of the same magnitude in layers 15-17. Moreover, the reference level velocities are distributed in such a way that the average nitrate concentration of the northward flowing intermediate water is decreased by 20%. As a result, the mean

concentration of the intermediate water is now lower than that of the deep water, and this intermediate/deep water cell carries a flux of nitrate to the south. However, since the concentration difference is not large ( $< 2 \mu g - at l^{-1}$ ) this cell is not a very efficient mechanism for transporting nitrate, and the net transport across the section is still to the north. In fact, the strong northward flux in the warm waters of the Gulf Stream is unchanged when total nitrate is conserved.

At  $24^{\circ}N$  the introduction of a horizontal circulation cell, consisting of poleward flow in the eastern basin and equatorward return flow to the west, is responsible for the smaller equatorward flux of nitrate in the interior. Since the vertically-averaged nitrate concentration is higher in the east, the effect is to decrease the southward flux in the interior.

Conserving total nitrate thus leads to dramatic changes in the circulation. The vertical average concentration is fairly constant across the section, and therefore the capacity to transport large amounts of nitrate through some combination of reference level velocities is limited. The solution is forced to vary more energetically on small scales, corresponding to the small changes in average nitrate along the section. Nitrate and temperature are negatively correlated such that changes in the flow which decrease the poleward nitrate flux across  $36^{\circ}N$  (e.g. increasing the strength of the overturning cell), tend to increase the heat flux. The net heat gain of .4 PW between  $24^{\circ}$  and  $36^{\circ}N$  required by this model is difficult to reconcile with estimates of heat loss to the atmosphere in this region (Bunker, 1982; Hsiung, 1986).

These results suggest that the assumption that total nitrate is conserved should be reexamined. Note that the nitrate residuals in layers 5-18 are all zero to within error bars for the model with no nitrate constraints (Fig. 4.14). The net divergence is entirely due to an excess of nitrate leaving the box in the top 4 layers at  $36^{\circ}N$  over that entering the box across  $24^{\circ}N$ . When the system is forced to conserve total nitrate the transports and divergence in the upper layers are unchanged; instead the flow in

the deep layers, in which nitrate was already conserved, is altered so that there is a net convergence at depth to balance the divergence in the upper layers. Given that the deep layers already approximately conserve nitrate, an alternate approach is to consider in more detail the northward flux in layers 1-4. How robust are the transport estimates in the upper layers? Is there a solution consistent with no net flux of nitrate across  $36^{\circ}\text{N}$ ? If not, is there a conceivable source of nitrate to balance the divergence?

*Can the nitrate flux across  $36^{\circ}\text{N}$  be driven to zero?* The model was run again with the total nitrate conservation constraint replaced by a constraint that there be no net flux of nitrate across  $36^{\circ}\text{N}$ . Driving the total nitrate flux to zero leads to dramatic changes in the circulation and property fluxes. The solution norm is now 1080, twice that of the model without nitrate constraints. Comparing the mass transport per unit depth for this model (Fig. 5.18) to the earlier model (Fig. 4.13b), one sees that the flux constraint is met by bringing 5 Sv more low nitrate water to the north in the interior in layers 1 and 2, and an equal transport of high nitrate water to the south in layers 13 and 14. The transport of NADW is increased to 25 Sv.

This increase in the vigor of the meridional cell has a large impact on the other property transports as well. The heat flux is unchanged at  $24^{\circ}\text{N}$  but increased to 1.7 PW at  $36^{\circ}\text{N}$ , resulting in a net heat gain between these latitudes of .5 PW. The net silica transport is increased by a factor of three to  $440 \text{ kmol s}^{-1}$  to the south at both latitudes. The southward flux of nitrate at  $24^{\circ}\text{N}$  is also increased, to  $76 \text{ kmol s}^{-1}$ , so that again there is a large divergence of nitrate within the box.

Requiring that there be no net flux of nitrate across  $36^{\circ}\text{N}$  thus leads to an unreasonable solution. In addition to unrealistically large velocities at 3000 m, the heat and silica fluxes implied are not consistent with the observed sources and sinks of these properties. Moreover, the nitrate transport in layers 1-4 is still unchanged. The near-surface flux occurs primarily in the Gulf Stream and is almost all accounted for by the relative velocity contribution, not by the reference level velocity selected by a particular



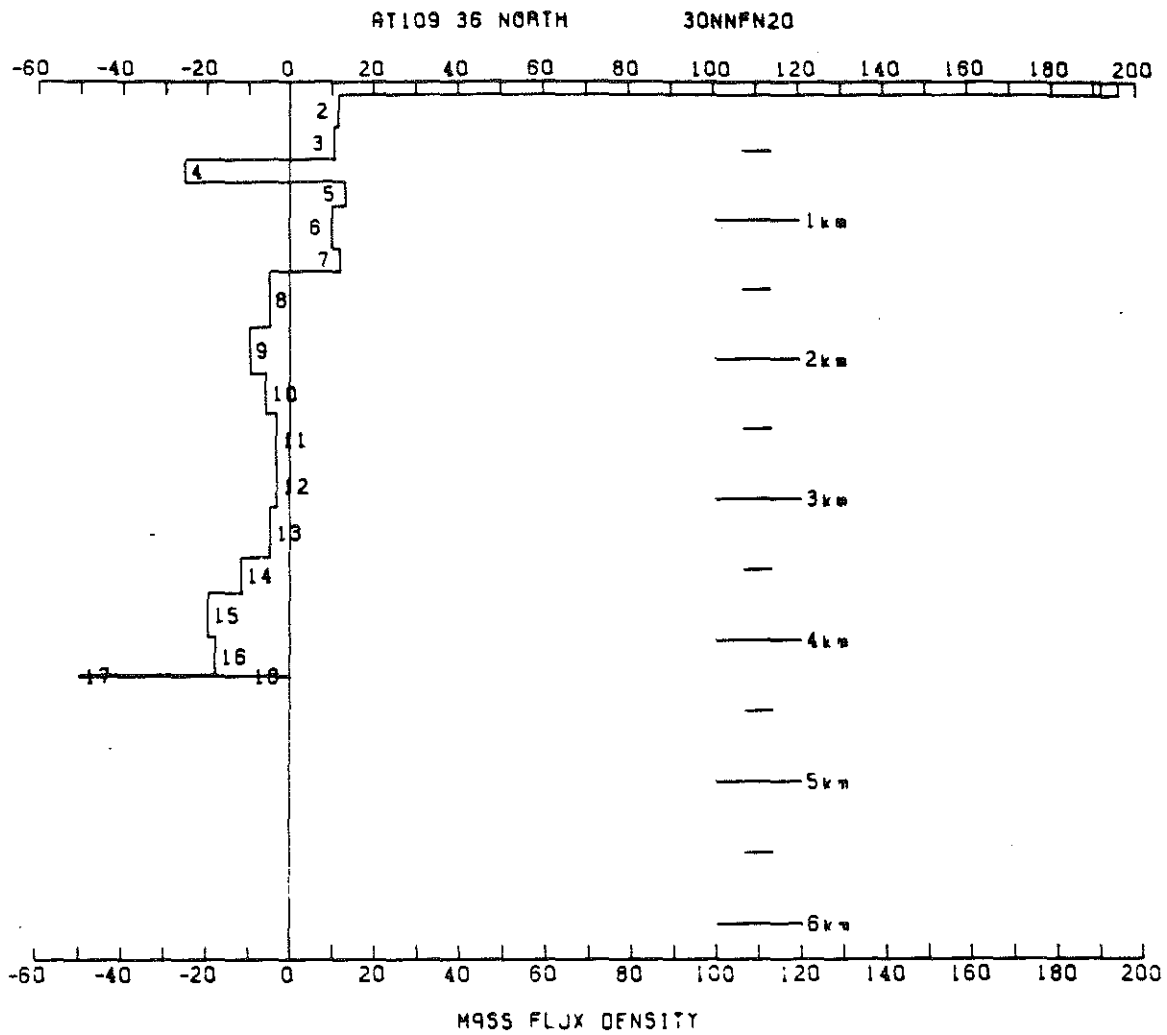


Fig. 5.18 Mass transport density at 36°N for model with zero nitrate flux across 36°N in Sv/km.

model. The only way to change the sign of the nitrate transport is to reverse the flow in the Gulf Stream by selecting a reference level near the sea surface.

*Is there a source of nitrate in the North Atlantic?* The strong poleward flux of nitrate at 36°N is therefore a robust feature that is insensitive to specific model assumptions. We are still left with the problem of finding a source of nitrate to feed this outflow. The flow through the Florida Straits provides an input of  $235 \text{ kmol s}^{-1}$  in the upper 4 layers. Of this,  $60 \text{ kmol s}^{-1}$  returns to the south in the interior, leaving a deficit of  $165 \text{ kmol s}^{-1}$  between what enters in these layers at 24°N and what leaves in the Gulf Stream at 36°N.

Brewer and Dyrssen's estimate of the nitrate transport across 24°N differs from these results, but they also found that the nitrate flux imbalance required an additional source of nitrate north of this latitude. They suggested that either "external sources or deep oxidation of organonitrogen compounds originating in the Gulf Stream flow" could provide the missing nitrate. The discussion above indicates that the requirement is more specific: there must be an input of nitrate to the Gulf Stream between 24 and 36°N.

"External sources" providing nitrate to the Gulf Stream in this latitude band are difficult to find. River run-off from the southeastern U.S. may provide some nitrate but this is unlikely to supply more than a small fraction of what is required. The hypothesis that the oxidation of organic matter carried into the basin through the Florida Straits supplies the necessary nitrate is difficult to test due to the lack of measurements of the concentration of organic matter in the water column. Even those measurements that do exist are difficult to interpret: investigators using different analytical techniques find radically different values for reasons that are not yet understood (Brewer *et al.*, 1986; Suzuki *et al.*, 1985; Sugimura and Suzuki, 1986).

Another active debate that bears on the present discussion concerns recent estimates of "new" production. Jenkins (1982) and Jenkins and Goldman (1985) concluded

from estimates of the oxygen utilization rate (OUR) in the Sargasso Sea that the rate of new production is  $\approx 4-6$  moles C  $m^{-2}$   $yr^{-1}$ , roughly 4 times conventional estimates based on  $^{14}C$  incubations. Shulenberger and Reid (1981) reached a similar conclusion using oxygen data from the Pacific. Platt and Harrison (1985), however, showed that if spatial and temporal variations in the ratio of new to total primary production are accounted for, then the OUR estimates were consistent with the  $^{14}C$  based production estimates. More recently, Martin *et al.* (1987) have shown that sediment trap results from the VERTEX experiment support the traditional values and are inconsistent with the large estimates based on oxygen utilization. Martin *et al.* offered a hypothesis to explain the difference between the two results, based on the evidence from radionuclide work that both large and very small particles must be considered in order to understand the carbon and nutrient cycles in the ocean (Krishnaswami *et al.*, 1976,1981; Bacon and Anderson, 1982; Bacon, 1984; Bacon *et al.*, 1985). The small particles sink slowly in the water column, if at all. Martin *et al.* suggested that oxidation of the slowly-sinking particles as they are carried isentropically around the subtropical gyre could account for the large apparent oxygen utilization rates (AOUR) observed by Jenkins and Goldman. Jenkins and Goldman assumed that the oxygen consumption they observed was solely due to the oxidation of the large particles sinking rapidly out of the overlying photic zone. If a large fraction of the oxygen consumed instead results from the decomposition of small organic particles advected in along isopycnals, then very large production rates are not required to explain the observed AOUR.

Oxidation of the slowly-sinking particulate organic matter would also regenerate nitrate, and could provide the source required to balance the divergence of nitrate found in this study. If the high dissolved organic nitrogen (DON) values obtained by Suzuki *et al.* (1985) are valid, the pool of dissolved organic matter may be an even more important source of regenerated nitrate. Recent experiments performed at Woods Hole

comparing different analytical techniques indeed tend to support the higher (DON) values (Brewer, personal communication).

The net northward flux of nitrate across  $36^{\circ}\text{N}$  thus appears to be a robust result: it is insensitive to the specific model assumptions made, and the flux cannot be driven to zero without unrealistic changes in the circulation. The export of nitrate leads to a net divergence of nitrate between  $24^{\circ}$  and  $36^{\circ}\text{N}$ , and to balance this divergence a substantial input of regenerated nitrate to the Gulf Stream is required, apparently derived from the oxidation of organic material. Given the uncertainty in the measurements of the organic constituents it is difficult to make a definitive statement, but the stability of the flux estimate gives confidence that the divergence is real. Nitrate must be supplied from somewhere, and the regeneration of organic matter seems the most likely source.

The poleward flux of nitrate leads to a net *convergence* north of  $36^{\circ}\text{N}$ . The flux of organic matter may be important in this case as well. There is no obvious sink of nitrate north of  $36^{\circ}\text{N}$ . Inflow from the Pacific through the Arctic Ocean and river run-off are in fact a net *source* of nitrate to the North Atlantic, adding to the net convergence (Kinney *et al.*, 1977). The evidence from sediment cores suggests that organic matter is not being buried in the sediments in the northern North Atlantic in large amounts at the present time (Broecker and Peng, 1982). Since total nitrogen is conserved, if there is no sink of nitrate the nitrogen entering the North Atlantic in inorganic form must return across  $36^{\circ}\text{N}$  as particulate or dissolved organic nitrogen (PON or DON).

Lacking good observations of the distribution of DON or PON any conclusions concerning the role of the organic constituents in the nitrogen cycle must remain speculative. However, if one believes that the evidence from sediment cores is sufficient to rule out extensive removal of organic material to the sediments, then there seems to be little alternative.

A general picture of the nitrogen cycle in the North Atlantic can be constructed along the lines of Martin *et al.*'s argument that is consistent with these observations.

This scenario is shown schematically in Fig. 5.19. It is hypothesized that the recirculation gyre plays a role in increasing the nitrate transport of the Gulf Stream analogous to the role it plays in boosting the mass transport between the Florida Straits and Cape Hatteras. North of  $36^{\circ}\text{N}$  the nitrate carried in the sub-surface ( $\approx 150\text{-}600\text{ m}$ ;  $26.4 < \sigma_0 < 27.3$ ) layers of the Gulf Stream is exposed to the atmosphere as the warm waters of the Stream are cooled. The vertical mixing driven by this strong cooling introduces a large flux of nutrients into the sunlit surface layers and supports the very high productivity observed along the axis of the North Atlantic Current by satellite measurements of ocean color (Esaias *et al.*, 1986). A significant fraction of this production is then assumed to be carried back to the south along isopycnals in the Gulf Stream return flow, so that the transport of organic nitrogen (either DON or PON) to the south balances the northward flux of inorganic nitrogen (nitrate) in the Gulf Stream across  $36^{\circ}\text{N}$ . This pool of organic nitrogen is consumed during its transit of the subtropical gyre, accounting for the large (AOUR) observed by Jenkins and Goldman (1985) near Bermuda, and nitrate is regenerated, providing the required source to the Gulf Stream when the recirculated water is incorporated into the Gulf Stream south of Cape Hatteras.

The recirculation cell described above accounts for roughly one third of the nitrate flux carried by the Gulf Stream at  $36^{\circ}\text{N}$ . The remainder enters the region through the Florida Straits and continues north of  $36^{\circ}\text{N}$  in the portion of the Gulf Stream flow that ultimately reaches the deep water formation regions in the northern part of the basin. The nitrate carried to the north in this branch of the circulation is returned to the south in the NADW. As a result, the import of nitrate through the Florida Straits is balanced by an export of nitrate in the NADW and there is no net flux across  $24^{\circ}\text{N}$ .

Thus it is suggested that two distinct mechanisms are responsible for the transport of nitrate in the North Atlantic: a shallow cell coincident with the Gulf Stream recirculation gyre and involving substantial conversion between organic and inorganic

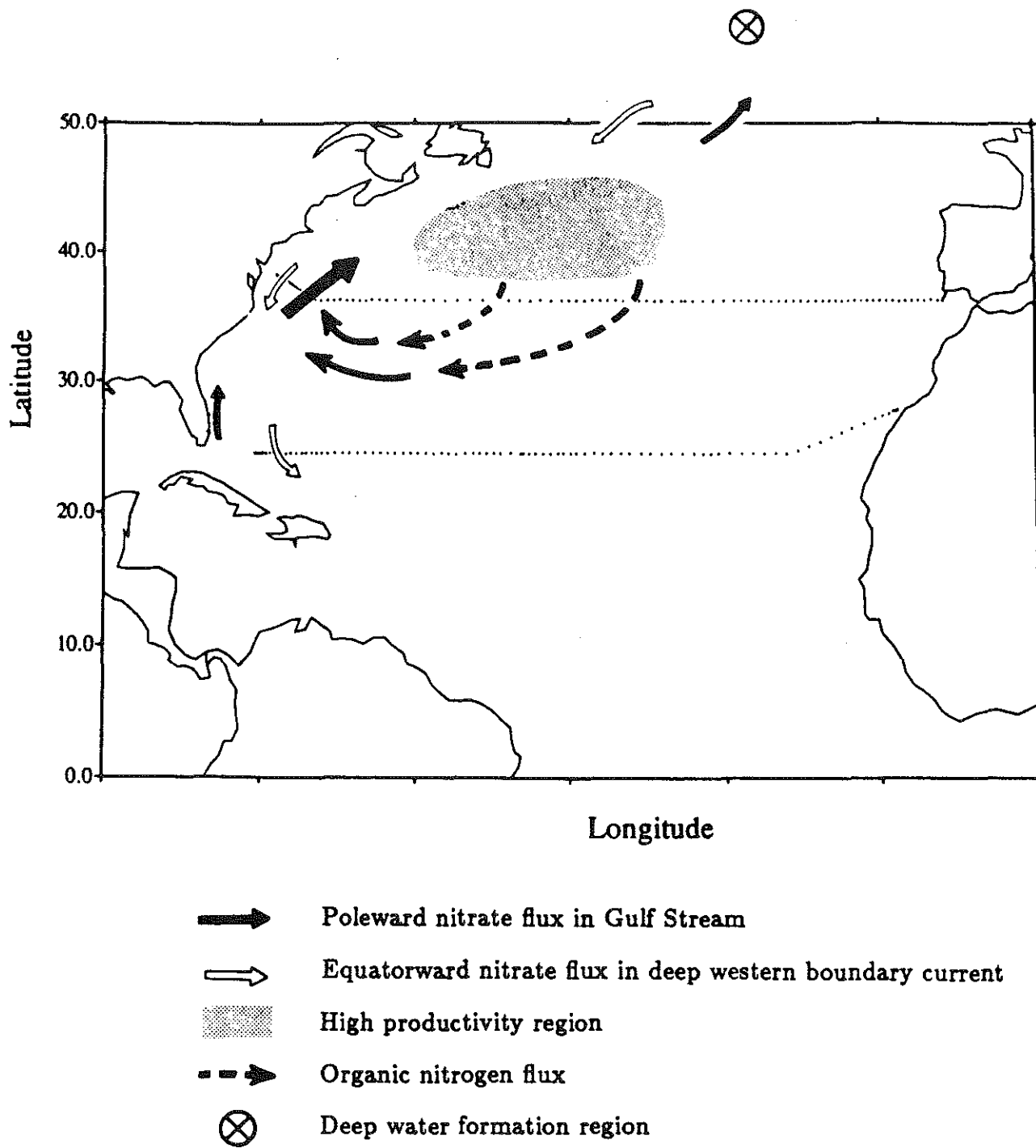


Fig. 5.19 Schematic picture of the nitrogen cycle in the subtropical North Atlantic.

forms of nitrogen, and an overturning meridional cell associated with the formation of NADW. Such a scenario reconciles the sediment trap and AOU productivity estimates, along the lines of Martin *et al.* The existence of a recirculating cell that is limited in latitudinal extent carrying a large flux of nitrogen is also consistent with there being no net flux at 24°N, and with the results of a model by Schlitzer (1987) showing no net flux across 52.5°N. (This model is discussed in more detail below.) How the large seasonal oxygen production observed by Jenkins and Goldman (1985) in the Sargasso Sea fits into such a scheme is not clear.

Many more measurements are required to verify the existence of the hypothesized "nitrate recirculation." However, provided that the nitrate cycle sketched above is reasonably correct, the stability of the nitrate flux results can be exploited to estimate the net new production north of 36°N. That is, since there is no source of organic matter at depth, the organic nitrogen carried to the south must have sunk out of the euphotic zone. Using the "Redfield" ratio estimated by Takahashi *et al.* (1985), a flux of 119  $kmol\ s^{-1}$  of nitrogen implies a carbon flux of  $119 \times (103/16) = 766\ kmol\ s^{-1}$  C. This value is a lower bound on the total new production to the extent that some "new" carbon is oxidized before it is carried to the south across 36°N. Dividing by the area of the North Atlantic between 36 and 60°N ( $\approx 1.2 \times 10^{13}\ m^2$ ) gives a new production rate of  $2.1\ moles\ C\ m^{-2}\ yr^{-1}$ , similar to the estimates based on sediment trap data ( $1.5\ moles\ C\ m^{-2}\ yr^{-1}$ , Martin *et al.*, 1987) and somewhat lower than the estimates of Jenkins and Goldman (1985) based on AOU ( $4\ moles\ C\ m^{-2}\ yr^{-1}$ ).

Such a calculation demonstrates the potential for deriving estimates of basin scale production from consideration of the large scale nutrient budgets. The fact that the net nutrient transports can be well determined in this type of calculation imposes strong constraints on models of the biological and chemical cycles. New production is a notoriously difficult quantity to measure that is of great importance to an understanding of the carbon cycle and the ocean's role in climate, since the sinking of particles is a

primary mechanism by which carbon is transferred from the sea surface to the deep ocean. These results suggest that simple flux calculations such as these provide perhaps the most direct and straightforward way to make estimates of average basin-scale production.

*Final comments on spatial averaging.* The nutrient fluxes found here can be compared to the results of a model of the nutrient and carbon cycles in the North Atlantic recently presented by Schlitzer (1987). He divided the North Atlantic into 3 boxes defined by zonal sections constructed from the climatological data of Levitus (1982) at  $52.5^{\circ}\text{N}$ ,  $12.5^{\circ}\text{N}$  and  $9.5^{\circ}\text{S}$ . The nutrient and carbon data were objectively interpolated onto these sections using smoothing scales of 1000 km and 500 km in the zonal and meridional directions, respectively. In the vertical the water column was divided into 5 layers corresponding to the major water masses. Linear programming methods were used to find the reference level velocities, which were also heavily smoothed (length scale = 800 km), and to set bounds on physical quantities of interest such as the meridional heat flux and the magnitude of the mixing coefficients.

Schlitzer found that the nutrients in each of his boxes balanced and there was no net flux of nutrients across the 3 latitudes he considered, in contrast to the model results discussed above. He also found no evidence that the organic constituents played an important role in the nutrient cycle. In fact, he concluded that no feasible solution could be found consistent with the high values reported by Sugimura and his colleagues. There is no real contradiction between these results: I have only found the nutrient fluxes at  $24^{\circ}\text{N}$  and  $36^{\circ}\text{N}$ , and can say nothing about what happens north or south of these latitudes. If the recirculation cell does not extend to  $50^{\circ}\text{N}$  then the scenario described above is consistent with no net flux across  $50^{\circ}\text{N}$ . Furthermore, as noted by Schlitzer, estimates based on climatological data may not agree with those based on quasi-synoptic data sets. However, the two models do paint different pictures of the nutrient cycles in the North Atlantic and it is worth examining possible reasons for



the difference in results in more detail. In particular, if we can demonstrate that the difference in results does reflect a real difference between the synoptic and climatic mean transports, then this is a significant statement concerning the variability of the nutrient fluxes in the ocean.

Schlitzer suggested that the discrepancy could be explained by several weaknesses in the model presented here; namely, that iso- and diapycnal mixing and vertical particle fluxes due to biological productivity are not included. To consider these criticisms in reverse order, particle fluxes are included implicitly in the model to the extent they are required to account for the observed distributions and fluxes. That is, if there is substantial vertical transport of nutrients into some layers due to sinking and dissolution of particles then the sum of the advective terms will leave a large residual in these layers. As we have seen, the residuals for all properties are small below the upper few hundred meters.

Diapycnal mixing is also allowed for in the model, to some degree. The cross-isopycnal transfer term included in the model equations permits the exchange of properties across density surfaces. The assumption we have made is not that diapycnal mixing does not occur, but that with the data available we can determine only the net cross-isopycnal flux due to a variety of diffusive and advective processes active in the ocean.

Isopycnal mixing is not included in the model. We have found that a model that is purely advective in the horizontal is sufficient to explain the observations. Moreover, it is not clear in this model what mechanism would be responsible for this mixing. It is a standard, if ad hoc, practice in oceanography to parameterize the mixing due to eddies by the product of an "Austausch" mixing coefficient times the mean concentration gradients. However, in this case the eddies are relatively well-resolved by the station spacing, as shown by RW from an analysis of the temperature spectra, and the eddy contribution due to mesoscale features is to a large extent included explicitly. The

assumption made here is that the fluxes due to velocity and concentration correlations on horizontal scales less than 50 km are small relative to the contribution due to advection by the synoptic flow field. This assumption was supported by the error analysis demonstrating that the flux due to unresolved components of the flow in the null-space is small.

Therefore the fact that these processes were not explicitly included in the model seems unlikely to account for the difference in results. Rather, the discussion presented above of the mechanisms responsible for the transport of silicate and nitrate in this model suggests that the heavily-smoothed, low resolution model of Schlitzer may have missed significant components of the total nutrient flux. For example, the net northward flux of nitrate was primarily due to relatively high concentrations in the narrow, high velocity core of the Gulf Stream. If these fields were smoothed over 1000 km scales, as in Schlitzer's model, most of this flux would be missed. Even when smoothed over much smaller scales, as in the smoothing experiments (100 km vs. 1000 km in Schlitzer's case), a large fraction of the net transport was omitted.

Other features of Schlitzer's model conflict with present estimates and cast further doubt on the reliability of results obtained from smoothed climatological fields. Schlitzer finds very large particle fluxes at 1000 m near 50°N: 300  $kmol\ s^{-1}$  of silicate and 830  $kmol\ s^{-1}$  of organic carbon. The new production rate implied by this organic carbon flux over the outcrop area of his layer 3 is 5.2 moles C  $m^{-2}\ yr^{-1}$ , slightly higher than the estimates quoted above. However, most of the organic carbon sinking out of the euphotic zone is consumed in the upper few hundred meters. To support a particle flux of 830  $kmol\ s^{-1}$  of organic C at 1000 m requires a new production rate roughly 7 times that above, or >50 moles C  $m^{-2}\ yr^{-1}$ , if the results of Martin *et al.*(1987) for the northeast Pacific are characteristic of the north Atlantic as well.

The large particle fluxes may be an artifact of the very low spatial resolution of Schlitzer's model. Below 400 m and north of 12.5°N the model represents the North

Atlantic as a two layer system, so that the nutrient transport in the upper layer must equal that in the lower layer. The nutrient concentrations in the lower layer, corresponding to southward flowing NADW, increase dramatically between the boundaries of box II at  $52.5^{\circ}\text{N}$  and  $12.5^{\circ}\text{N}$ . To offset the divergence caused by equatorward flow through the box in this layer the model pumps in a large particulate flux of nutrients. As we have seen, the new production rate implied by the required particle flux is 15-40 times larger than present estimates.

Using very few layers in the vertical and heavily-smoothed fields in the horizontal may misrepresent the true flux in two ways. The property fields suggest that the very high silica near the bottom north of  $12.5^{\circ}\text{N}$  which Schlitzer includes in his NADW layer is actually northward flowing AABW. The results of the model presented here also show that zonal variations in the nutrient concentrations are important in determining the net flux of these properties. For example, the strongest equatorward flows of NADW occur in the DWBC, where the silica concentration is low, while the high-silica deep water in the eastern basin is moving to the north. As Schlitzer noted, data smoothed on the scale of the Levitus atlas does a poor job of reproducing the boundary currents and it is not clear that one or two reference level velocities in the eastern basin is adequate to reproduce the circulation. Both these effects would tend to relax the requirement for the vary large particle fluxes found by Schlitzer.

The model presented here has provided some valuable insight into the specific mechanisms responsible for the transport of nutrients in the North Atlantic. In particular, the nutrient fluxes are strongly dependent on relatively small scale features of the flow, such as the boundary currents. The flux due to the correlation of strong velocities and deviations in concentration from the section average in these small scale features is largely lost when the fields are smoothed. Spatial smoothing of high gradient, permanent features such as the Gulf Stream will not give the same results as time-averaging of many transport estimates based on synoptic data. The proper conclusion to draw,

then, is not that the situation in the summer of 1981 differed dramatically from the climatic mean, but that nutrient transport estimates based on heavily smoothed averages of synoptic data will not represent the "true" climatic or long-term mean flux. Schlitzer, at the end of his paper, reaches a similar conclusion concerning the possible inadequacies of the climatological fields.

## 6. Summary and Conclusions

In part II of the thesis I have applied an inverse method to hydrographic and nutrient data along two sections in the subtropical North Atlantic to estimate the absolute velocity field and the property transports. A series of models were considered in the search for a "best estimate" of the circulation, defined to be the simplest model consistent with the observations. By starting with the most basic model and gradually adding constraints, we were able to explicitly explore the impact of different types of information on the solution obtained. The main results are summarized in this section.

Mass conservation statements alone lead to models whose results are very sensitive to the initial model assumed. Different initial reference levels result in flows that conserve mass in isopycnal layers but differ from each other substantially, particularly in the deep water. The differences in the deep circulation, in turn, lead to drastically different estimates of the nutrient transports. The low-order models in which only mass is conserved thus leave both the velocity field and the transports largely undetermined.

The silicate flux is particularly sensitive to the choice of initial reference level, since the silica distribution has a great deal of structure in the deep water. Silicate conservation constraints were next added to the model to test whether the independent information contained in the silica field could be exploited to reduce the degree of indeterminacy.

Conserving mass and silica dramatically decreases the range of meridional transport estimates obtained starting with different initial reference levels. However, despite the similarity of the zonally-integrated mass flux results, the horizontal and vertical structure of the velocity field still shows some dependence on the initial model assumed. A shallow reference level leads to a shallow Gulf Stream and an energetic deep circulation, while the reverse is true for a deep initial level. Analysis of the residuals

suggested that there was little additional information to extract from the oxygen or nutrient distributions to further resolve the flow field.

Comparison of these results with direct current measurements in the Gulf Stream and Western Boundary Undercurrent indicated that the deep reference level led to a circulation more consistent with the observed transports of these currents. This model was selected as the best estimate of the absolute velocity field in the summer of 1981.

The flow in this semi-synoptic snapshot is visually dominated by eddies, particularly near the Gulf Stream at  $36^{\circ}\text{N}$ . Northward flow in the Gulf Stream reaches to 3000 m, with a total top-to-bottom transport of 84 Sv. The return flow of the Gulf Stream occurs mostly in the western basin, but any sign of a coherent, tight recirculation gyre is masked by the eddy field. Inshore and beneath the Gulf Stream there is a well-defined WBUC with a transport to the south of 18 Sv, of which 7 Sv is intermediate water. However, there is a general southward drift in the western basin offshore of the WBUC which makes a significant contribution to the net NADW transport of 19 Sv. In the eastern basin the flow is generally to the north below the thermocline.

The discussion of resolution in Section 5.1 makes it clear that we have resolved the reference level component of the velocity field only on broad scales. The fact that we have not completely resolved the velocity field with the available information is also reflected in the differences between the flow field for initial reference levels at 1300 and 3000 db. It was suggested that strong barotropic flows with small horizontal scales, such as those described by Schmitz (1977,1980), are unlikely to be included in an inverse solution unless direct current observations are included as constraints because the tracer fields contain little or no information on these scales.

In contrast to the velocity field itself, the zonal integral of the property fluxes is well determined. This was shown directly by comparing the results of different models and more formally by considering the potential contribution to the flux by the unresolved components of the flow lying in the null-space. For the sections considered here, the

projection of the tracer fields onto the null-space vectors is small and hence so is the transport carried by the undetermined part of the velocity field.

The meridional flux of heat is  $1.3 \pm 0.2$  PW poleward and is equal at both latitudes to within estimated error. The poleward heat flux is primarily due to the overturning thermohaline cell: warm water in the surface and thermocline layers flows to the north, is made more dense by cooling and evaporation at high latitude, and sinks to return to the south as NADW, with a much lower temperature.

The overturning cell is also responsible for a net equatorward transport of oxygen ( $\approx -3000 \text{ kmol s}^{-1}$ ) across both sections. When the low oxygen sub-surface waters carried to the north in the Gulf Stream and North Atlantic Current are exposed to the atmosphere in the deep water formation regions, they both lose heat and gain oxygen. The large export of oxygen from the North Atlantic plays a major role in ventilating the deep waters of the world ocean.

The net flux of silicate is also to the south:  $-138 \pm 38 \text{ kmol s}^{-1}$  at  $36^\circ\text{N}$  and  $-152 \pm 56 \text{ kmol s}^{-1}$  at  $24^\circ\text{N}$ . These estimates are somewhat higher than the estimated source of silicate to the North Atlantic but given the uncertainties in both estimates the conflict is not strong. In contrast to heat and oxygen, the meridional overturning cell is not the only important mechanism responsible for transporting silicate in the North Atlantic. The concentration of silicate varies significantly along density surfaces; consequently a "horizontal" circulation can carry a significant flux of silicate. In particular, northward flow at depth in the eastern basin, where concentrations are high, balanced by southward flow of relatively low-silica deep water in the western basin results in a significant flux of silica to the north. Estimates based on the net meridional mass transport and average concentration in each layer will largely miss this component of the silica flux and overestimate the net southward transport.

Nitrate is the only property considered that shows a significant divergence in the box. The net flux across  $36^\circ\text{N}$  is  $119 \pm 35 \text{ kmol s}^{-1}$  to the north, while at  $24^\circ\text{N}$  the

transport is indistinguishable from zero ( $-8 \pm 39 \text{ kmol s}^{-1}$ ). Forcing the system to conserve nitrate or to drive the net flux across  $36^\circ\text{N}$  to zero results in an unreasonable circulation. As for silicate, the product of the section average concentrations and net mass fluxes in each layer lead to poor estimates of the nitrate transport. In fact, the dominant contribution to the nitrate flux at  $36^\circ\text{N}$  comes from the correlation of strong flows and relatively high nitrate concentrations in the sub-surface waters of the Gulf Stream.

The poleward transport of nitrate across  $36^\circ\text{N}$  leads to a divergence between  $24^\circ$  and  $36^\circ\text{N}$ , and a net convergence north of this latitude. In Section 5.5 I suggested that the nitrate cycle in the North Atlantic could be thought of as a two component system. Roughly  $2/3$  of the northward nitrate flux carried by the Gulf Stream at  $36^\circ\text{N}$  is compensated at depth by the southward flow of relatively nitrate-rich NADW. The overturning cell, which dominates the transport of heat and oxygen, results in little net transport of nitrate because the average concentration of the poleward branch is roughly equal to that of the deep equatorward branch.

The net flux of nitrate is due to the second component, a horizontal recirculation that coincides with the Gulf Stream gyre. Nitrate carried to the north in the sub-surface layers of the Gulf Stream supports the high primary production north of this latitude. Organic nitrogen produced in these regions returns to the south in the Gulf Stream return flow, balancing the flux of inorganic nitrogen, and is consumed during its transit of the subtropical gyre, accounting for the large oxygen consumption rates observed and supplying regenerated nitrate to the Gulf Stream when it rejoins the boundary current.

Thus the transport of each property is dominated by a different combination of physical processes: heat and oxygen by the meridional overturning cell; silicate by both the overturning cell and a recirculation of deep waters; and nitrate by a shallow cell involving the conversion between organic and inorganic forms of nitrogen. Each



property considered contains independent and complementary information that is of use in resolving different aspects of the circulation.

Several of the results presented here could be tested with additional observations. Measurements with which to constrain the northward flow of deep water in the eastern basin would be useful in confirming the silicate flux estimates. Such measurements might include direct velocity observations using either current meters or floats, or tracer work along the lines of Schlitzer *et al.*(1985). The proposed role of organic matter in the nitrate cycle also needs to be tested against measurements of DON and PON concentrations in different parts of the basin.

The models I have discussed suggest that the synthesis of physical and chemical data is a fruitful one. The nutrients provide information that is useful in determining the velocity field and mass transport, and accurate estimates of the chemical fluxes in turn depend on relatively detailed knowledge of the circulation. The extent to which this will be true in other basins, or to which additional tracers not considered here will provide further information, is not known. However, the approach seems very promising. Recent data sets which provide better spatial coverage and a more complete suite of tracer measurements, such as the TTO data in the North Atlantic, several recent long lines in the North Pacific, and the sections to be done as part of the SAVE in the South Atlantic, provide good opportunities to extend these ideas.

### Concluding Remarks

In the preceding chapters, an inverse method has been used to investigate a variety of ocean circulation problems. The method allows one to find an estimate of the circulation which conserves mass and other properties, and satisfies a variety of additional constraints. Furthermore, we have seen that the inverse machinery provides a powerful tool with which to test specific hypotheses for consistency with the data.

The first problem addressed concerned the interbasin exchange of mass and heat in the South Atlantic. The "best estimate" of the circulation suggested that the Atlantic as a whole acts to convert intermediate water entering the basin through Drake Passage into deep and bottom water which leaves the basin to the east in the Circumpolar Current. This, in turn, suggested that the global thermohaline cell associated with the formation and export of North Atlantic Deep Water is closed primarily by a "cold water path," in which the deep water leaving the basin ultimately returns as intermediate water entering through Drake Passage. By including additional constraints we were able to use the inverse machinery to demonstrate explicitly that the data used here were inconsistent with the alternative, "warm water path," in which the deep water is replaced by thermocline water entering the basin from the Indian Ocean.

The method also proved to be useful for studying the meridional flux of heat across  $32^{\circ}\text{S}$ . The optimal solution resulted in a smaller heat flux ( $.25 \times 10^{15} \text{ W}$ ) than several recent estimates; altering the model constraints to force the system to accommodate a larger heat flux led to an unreasonable circulation.

The circulation of the subtropical North Atlantic was considered in Chapter 3, focusing on the transport of oxygen and the nutrients as well as mass and heat. We found that combining nutrient and hydrographic observations was useful for addressing questions of concern to both physicists and chemists. The nutrients, particularly silica,

were found to contribute information independent of temperature and salinity and provided useful constraints on the circulation. In turn, accurate estimates of the chemical fluxes were shown to depend on detailed knowledge of the circulation: smoothing of small-scale features of the property fields led to large changes in the transport. In the case of the nitrate flux across  $36^{\circ}\text{N}$ , for example, spatial-averaging can reverse the sign of the net transport.

The oxygen and nutrient flux estimates presented here are the first based on a physically-realistic model of the North Atlantic circulation. Through the export of newly-formed North Atlantic Deep Water, the North Atlantic is found to provide a major input of oxygen to the deep waters of the world ocean. The North Atlantic was also found to be a net source of silicate. The magnitude of the flux suggested that current estimates of the input of silica to the Atlantic may be low, although given the uncertainty in both numbers the discrepancy is barely significant.

The nitrate cycle was found to be somewhat more complicated. To account for the observed poleward flux of nitrate across  $36^{\circ}\text{N}$ , and the resulting divergence to the south and convergence to the north of this latitude, apparently requires a shallow recirculating cell in which the production, transport and eventual regeneration of dissolved or particulate organic nitrogen plays an active role. The sketch of the nitrogen cycle proposed here is in keeping with several recent ideas emerging in the biological and chemical communities concerning estimates of primary production, oxygen utilization and the role of dissolved organic matter in the carbon and nutrient cycles.

The flexibility of the inverse method made it especially well-suited to the problems addressed in this work. The ability to run the model repeatedly while varying the imposed constraints allowed us to not only estimate the property fluxes, and to check the stability of the results, but also to learn a great deal about the physical mechanisms responsible for the transport of each property.

Finally, the sensitivity of the nutrient flux results to the details of the flow field has important, and somewhat sobering, implications for attempts to model "climatological mean" transports in the ocean. Due to the lack of data, one usually makes the assumption that temporal- and spatial-averaging of measurements obtained at different times and in different places is equivalent to a time-average over many synoptic realizations. Hence, heavily-smoothed compilations of historical data, such as that of Levitus (1982), are generally referred to as "climatological" atlases of the world ocean. However, a property flux is a fundamentally nonlinear operation, in the sense of being the product of a velocity and a concentration, and the results will thus be sensitive to the smoothing applied to each of the fields. To the extent that small-scale correlations of velocity and concentration make a significant contribution to the net flux, as found here to be the case for nitrate, climatological atlases will give misleading estimates of the transports. The same will be true of data with insufficient spatial resolution, and it is not clear that we have yet "done it right." Valid estimates of the "mean" transports of physical and chemical properties may then require many more observations, or perhaps a more creative solution to the problem of how best to combine historical data sets in a way that preserves the essential character of the fields.

## Acknowledgements

I would first like to thank my thesis adviser, Carl Wunsch, for generously sharing his time and ideas whenever I asked, while also giving me the freedom to work through problems independently. Carl's specific suggestions have improved this work a great deal, but his most lasting contribution may be in teaching by example how to think critically and communicate effectively; that is, how to do good science.

The members of the physical oceanography departments at WHOI and MIT have almost all made some contribution along the line. In particular, my thesis committee - Nelson Hogg, Terry Joyce and John Toole - provided encouragement and many helpful suggestions, and the manuscript was much improved by their careful reading of several early drafts. Harry Bryden also provided useful comments which helped to make the final presentation clearer and more complete.

I am indebted to Barbara Grant for computing assistance beyond the call of duty, as well as her friendship and frequent reminders of my senator's phone number. Joe Reid and Worth Nowlin kindly provided access to the AJAX data before publication.

Those responsible for the nonscientific support during my Joint Program career are too numerous to mention - you know who you are. Without you I might have made it through graduate school, but it certainly wouldn't have been worth it.

Finally, my greatest thanks go to my mother, my grandfather and my grandmother, who have supported my education, academic and otherwise, in every way possible, and have always shared my enthusiasm for whatever I chose to do.

This research was supported by NASA under contract NAG5-534 and NSF under contract OCE-8521685.

## Appendix

### Sensitivity of property flux estimates

In this section the details of the error analysis for the property fluxes are presented. The discussion summarizes the presentation in the Appendix of Wunsch *et al.* (1983) and is included here for completeness; those interested in a more complete treatment are referred to their paper.

The "true" velocity at a hydrographic section can be written

$$\mathbf{v} = \mathbf{v}_R + \mathbf{v}_E + \mathbf{b} + \sum_{l=k+1}^N \alpha_l \mathbf{Q}_l$$

or

$$\mathbf{v} = A_1 + A_2 + A_3 + A_4$$

where  $\mathbf{Q}$  are the "null-space" vectors (Wunsch and Grant, 1982),  $\mathbf{v}_R$  is the relative velocity,  $\mathbf{v}_E$  is the Ekman velocity, and  $\mathbf{b}$  is the reference level velocity. The flux of a tracer  $C$  across a section becomes

$$F_C = B_1 + B_2 + B_3 + B_4$$

where  $B_{1,2,3,4}$  are the fluxes obtained by integrating the velocities  $A_{1,2,3,4}$  times the concentrations along the section.  $B_3$  and  $B_4$  can be written

$$B_3 = \mathbf{C}^t \mathbf{b} = \sum_{l=1}^k \alpha_l \mathbf{C}^t \mathbf{V}_l$$

$$B_4 = \sum_{l=k+1}^N \alpha_l \mathbf{C}^t \mathbf{Q}_l.$$

Errors in  $F_C$  result from errors in each of the individual components of the flux.  $B_1$ , the flux contribution from the thermal wind, has errors due to noise in the observations, navigation errors and interpolation errors, as discussed in Chapter 1. Errors in  $B_2$  arise

from errors in the wind stress. The contribution from the reference level velocity,  $B_3$ , also contains errors resulting from noise in the observations; as discussed in Chapter 1, the inverse method provides a formal estimate of the error in the  $b_i$  due to data noise. This can be converted into an estimate of the error in the flux due to this source, as seen below.  $B_4$  represents the flux due to the unresolved components of the flow lying in the null-space of the coefficient matrix  $\mathbf{A}$ . Since the set of eigenvectors of  $\mathbf{A}$  ( $\mathbf{V}, \mathbf{Q}$ ) form a complete set,  $B_4$  represents the difference between all models based on the same data and constraints.

In Chapter 1 an expression for the variance in the solution element  $b_i$  from Wiggins (1972) was given (equation 1.3):

$$\langle b_i b_j \rangle = \sigma^2 \sum_l \frac{V_{li} V_{lj}}{\lambda_l^2}.$$

The formal error in the flux carried by this component,  $C_i b_i$ , follows in a straightforward way:

$$\langle (\sum_i C_i b_i) (\sum_j C_j b_j) \rangle = \sigma^2 \sum_i \sum_j C_i C_j \frac{(V_{li} V_{lj})}{\lambda_l^2}.$$

The errors due to data noise calculated using this formula are tabulated in Table 4.7 under the column heading "noise."

To estimate the error in  $B_4$  we first use the fact that the  $\mathbf{V}$  and  $\mathbf{Q}$  vectors form a complete set to rewrite the vector of (vertically-integrated) tracer concentrations  $\mathbf{C}$

$$\mathbf{C} = \sum_{l=1}^k (\mathbf{C}^t \mathbf{V}_l) \mathbf{V}_l + \sum_{l=k+1}^N (\mathbf{C}^t \mathbf{Q}_l) \mathbf{Q}_l.$$

Wunsch *et al.* (1983) show that the squared magnitude of  $B_4$  is then given by

$$\begin{aligned} |B_4|^2 &\leq \left( \sum_i \alpha_i^2 \right) \mathbf{C}^t \mathbf{C} \frac{\mathbf{C}^t \mathbf{Q} \mathbf{Q}^t \mathbf{C}}{\mathbf{C}^t \mathbf{C}} \\ &= \left( \sum_i \alpha_i^2 \right) \mathbf{C}^t \mathbf{C} \Delta \end{aligned}$$

$$\Delta \equiv \frac{C^t Q Q^t C}{C^t C} = 1 - \frac{C^t V V^t C}{C^t C}$$

where  $C^t V V^t C$  is the squared projection of  $C$  onto the range of  $A$ . If the problem is fully determined and there is no null-space, then  $\Delta=0$ , and this uncertainty is zero. For the problems considered here, the projection of  $C$  onto the null-space tends to be small. The error estimates listed in Table 4.7 give the change in the transport of each property that would result from an increase in the rms null-space velocity (i.e.  $\alpha^2$ ) of  $1 \text{ cm s}^{-1}$ .

The third error estimate given in Table 4.7 is that due to variations in the observed wind. The magnitude of the errors in the fluxes expected from errors in the Ekman transport are difficult to estimate, since the depth at which the compensating geostrophic flow occurs is not known. Here I have assumed that changes in the Ekman flux are balanced by a flow with the section-average concentration of each property. To the extent that variations in the Ekman flux are balanced by changes in the near-surface geostrophic flow, these values will be overestimates.



## References

- Aagard, K., J.H. Swift, and E.C. Carmack, 1985. Thermohaline circulation in the Arctic Mediterranean Seas. *J. Geophys. Res.* 90:4833-4846.
- Anderson, L. and D.W. Dyrssen, 1981. Chemical constituents of the Arctic Ocean in the Svalbard area. *Oceanol. Acta* 4:305-311.
- Anderson, L., D.W. Dyrssen, E.P. Jones and M. G. Lowings, 1983. Inputs and outputs of salt, freshwater, alkalinity and silica in the Arctic Ocean. *Deep-Sea Res.* 30:87-94.
- Bacon, M.P., 1984. Radionuclide fluxes in the ocean interior. In: *Global Ocean Flux Study, Proceedings of a Workshop*, Sept. 10-14, 1984, Woods Hole, MA. National Academy Press, Washington, D.C., pp. 180-220.
- Bacon, M.P. and R.F. Anderson, 1982. Distribution of thorium isotopes between dissolved and particulate forms in the deep sea. *J. Geophys. Res.* 87:2045-2056.
- Bacon, M.P., C.A. Huh, A.P. Fleer and W.G. Deuser, 1985. Seasonality in the flux of natural radionuclides and plutonium in the deep Sargasso Sea. *Deep-Sea Res.* 32:273-286.
- Bang, N.D., 1970. Dynamic interpretations of a detailed surface temperature chart of the Agulhas Current retroflexion and fragmentation area. *S. Afr. geogr.* 52:67-76.
- Barrett, J.R., 1965. Subsurface currents off Cape Hatteras. *Deep-Sea Res.* 12:173-184.
- Baumgartner, A. and E. Reichel, 1975. *The World Water Balance*, Elsevier, 179 pp.
- Bennett, A.F., 1978. Poleward heat fluxes in southern hemisphere oceans. *J. Phys. Oceanogr.* 8:785-798.
- Brewer, P.G. and D.W. Dyrssen, 1987. Ocean chemical fluxes across 25°N in the Atlantic Ocean. Discussion paper prepared for the International GOFS meeting, Paris, February 17-20, 1987, 25 pp.
- Brewer, P.G., W.S. Broecker, W.J. Jenkins, P.B. Rhines, C.G. Rooth, J.H. Swift, and T. Takahashi, 1983. A climatic freshening of the deep North Atlantic (north of 50°N) over the past 20 years. *Science* 222:1237-1239.
- Broecker, W.S., 1974. "NO", a conservative water mass tracer. *Earth Planet Sci. Lett.* 23:100-107.
- Broecker, W.S. and T.-H. Peng, 1982. *Tracers in the Sea*, Lamont-Doherty Geological Observatory, Columbia University, Palisades, N.Y., 690 pp.
- Broecker, W.S., T. Takahashi and Y.-H. Li, 1976. Hydrography of the Central Atlantic - I. The two-degree discontinuity. *Deep-Sea Res.* 23:1083-1104.
- Broecker, W.S. and H.G. Östlund, 1979. Property distributions along the  $\sigma_\theta = 26.8$  isopycnal in the Atlantic Ocean. *J. Geophys. Res.* 84:1145-1154.

- Broecker, W.S., T. Takahashi and M. Stuiver, 1980. Hydrography of the central Atlantic - II. Waters beneath the Two-Degree Discontinuity. *Deep-Sea Res.* 27A:397-419.
- Broecker, W.S. and T. Takahashi, 1980. Hydrography of the central Atlantic - III. The North Atlantic deep water complex. *Deep-Sea Res.* 27A:591-613.
- Broecker, W.S. and T. Takahashi, 1981. Hydrography of the central Atlantic - IV. Intermediate waters of Antarctic origin. *Deep-Sea Res.* 28A:177-193.
- Bryan, K., 1962. Measurements of meridional heat transport by ocean currents. *J. Geophys. Res.* 67:3403-3414.
- Bryan, K., 1982. Poleward heat transport by the ocean: observation and models. *Ann. Rev. Earth Planet. Sci.*, 10:15-38.
- Bryden, H., 1979. Poleward heat flux and conversion of available potential energy in Drake Passage. *J. Mar. Res.* 37:1-22.
- Bryden, H.L. and R.D. Pillsbury, 1977. Variability of deep flow in the Drake Passage from year-long current measurements. *J. Phys. Oceanogr.* 7:803-810.
- Bryden, H.L. and M.M. Hall, 1980. Heat transport by currents across 25°N latitude in the Atlantic Ocean. *Science* 207:884-886.
- Bunker, A.F., 1980. Trends and variables and energy fluxes over the Atlantic Ocean from 1948 to 1972. *Monthly Weath. Rev.* 108:720-732.
- Bunker, A.F., 1982. Surface energy fluxes of the South Atlantic Ocean. *Monthly Weather Review* (submitted).
- Buscaglia, J.L., 1971. On the circulation of the Intermediate Water in the southwestern Atlantic Ocean. *J. Mar. Res.* 29:245-255.
- Carmack, E.C. and T.D. Foster, 1975. On the flow of water out of the Weddell Sea. *Deep-Sea Res.* 22: 711-724.
- Chapman, P., C.M. Duncombe Rae and B.R. Allanson, 1987. Nutrients, chlorophyll and oxygen relationships in the surface layers at the Agulhas Retroflexion. *Deep-Sea Res.* 34:1399-1416.
- Chelton, D.B., 1982. Statistical reliability and the seasonal cycle: Comments on "Bottom pressure measurements across the Antarctic Circumpolar Current and their relation to the wind." *Deep-Sea Res.* 29A:1381-1388.
- Clarke, A.J., 1982. The dynamics of large-scale, wind-driven variations in the Antarctic Circumpolar Current. *J. Phys. Oceanogr.* 12:1092-1105.
- Codispoti, L.A. and T.G. Owens, 1975. Nutrient transports through Lancaster Sound in relation to the Arctic Ocean's reactive silica budget and the outflow of Bering Strait waters. *Limnology and Oceanography*, 20:115-119.

- Cooper, L.H.N., 1952. Factors affecting the distribution of silicate in the North Atlantic Ocean and the formation of North Atlantic Deep Water. *Journal of the Marine Biological Association of the United Kingdom* 30:511-526.
- Deacon, G.E.R., 1937. The hydrology of the Southern Ocean. *Discovery Reports* 15:1-124.
- Deacon, G.E.R., 1979. The Weddell gyre. *Deep-Sea Res.* 26A:981-995.
- de Ruijter, W.P.M., 1982. Asymptotic analysis of the Agulhas Current. *Rev. of Pure and Appl. Geophysics* 12:361-373.
- de Ruijter, W.P.M. and D.B. Boudra, 1985. The wind-driven circulation in the South Atlantic-Indian Ocean - I. Numerical experiments in a one-layer model. *Deep-Sea Res.* 32:557-574.
- de Szoeko, R.A. and M.D. Levine, 1981. The advective flux of heat by mean geostrophic motions in the Southern Ocean. *Deep-Sea Res.* 28A:1057-1085.
- Defant, A., 1961. *Physical Oceanography, Vol. I & II*. Pergamon Press, New York, 1327 pp.
- Dickson, R.R., W.J. Gould, T.J. Müller and C. Maillard, 1985. Estimates of the mean circulation in the deep (>2000 m) layer of the eastern North Atlantic. *Prog. in Oceanog.* 14:103-127.
- Edmond, J.M. and G.C. Anderson, 1971. On the structure of the North Atlantic Deep Water. *Deep-Sea Res.* 18:127-131.
- Esaias, W.E., G.C. Feldman, C.R. McClain and J.A. Elrod, 1986. Monthly satellite-derived phytoplankton pigment distribution for the North Atlantic basin. *EOS, Trans. Am. Geophys. Union* 67:835-837.
- Evans, D.L. and S.S. Signorini, 1985. Vertical structure of the Brazil Current. *Nature* 315:48-50.
- Fiadeiro, M.E. and G. Veronis, 1982. On the determination of absolute velocities in the ocean. *J. Mar. Res.* 40(Suppl.):159-182.
- Fofonoff, N.P., 1981. The Gulf Stream system. In: *Evolution of Physical Oceanography*, B.A. Warren and C. Wunsch, ed.'s, The MIT Press, Cambridge, pp. 112-138.
- Foster, L.A., 1972. Current measurements in the Drake Passage. M.S. Thesis, Dalhousie Univ., Halifax, N.S., Canada, 61 pp.
- Foster, T.D. and E.C. Carmack, 1976. Frontal zone mixing and Antarctic Bottom Water formation in the southern Weddell Sea. *Deep-Sea Res.* 23:301-318.
- Fu, L.-L., 1981. The general circulation and meridional heat transport of the subtropical South Atlantic determined by inverse methods. *J. Phys. Oceanogr.* 11:1171-1193.

- Fu, L.-L. and D.B. Chelton, 1984. Temporal variability of the Antarctic Circumpolar Current observed from satellite altimetry. *Science* 226:343-346.
- Fuglister, F.C., 1960. Atlantic Ocean atlas of temperature and salinity profiles and data from the International Geophysical Year of 1957-1958. *Woods Hole Oceanographic Institution Atlas Series* 1:209 pp.
- Fuglister, F.C., 1963. Gulf Stream '60. *Progress in Oceanography* 1:265-373.
- Georgi, D.T., 1981. Circulation of bottom waters in the southwestern South Atlantic. *Deep-Sea Res.* 28A:959-979.
- Georgi, D.T. and J.M. Toole, 1982. The Antarctic Circumpolar Current and the oceanic heat and freshwater budgets. *J. Mar. Res.* 40(suppl.):183-197.
- Gill, A.E., 1973. Circulation and bottom water production in the Weddell Sea. *Deep-Sea Res.* 20:111-140.
- Gordon, A.L., 1967. Structure of Antarctic waters between 20°W and 170°W. *Antarct. Map Folio Ser.* folio 6, V. Bushnell, ed., Am. Geograph. Soc., New York, 10 pp., 14 pl.
- Gordon, A.L., 1971. Oceanography of Antarctic waters. In: *Antarctic Oceanology I*, J.L. Reid, ed., *Antarctic Research Series* 15:169-203.
- Gordon, A.L., 1975. General ocean circulation. In: *Numerical Models of the Ocean Circulation*, pp. 39-53, National Academy of Sciences, Washington, D.C.
- Gordon, A.L., 1978. Deep Antarctic convection west of Maud Rise. *J. Phys. Oceanogr.* 8:600-612.
- Gordon, A.L., 1981. South Atlantic thermocline ventilation. *Deep-Sea Res.* 28:1239-1264.
- Gordon, A.L., 1981. Seasonality of Southern Ocean sea ice. *J. Geophys. Res.* 86:4193-4197.
- Gordon, A.L., 1985. Indian-Atlantic transfer of thermocline water at the Agulhas retroflection. *Science* 227:1030-1033.
- Gordon, A.L., 1986. Interocean exchange of thermocline water. *J. Geophys. Res.* 91:5037-5046.
- Gordon, A.L. and H.W. Taylor, 1975. Heat and salt balance within the cold water of the world ocean. In: *Numerical Models of the Ocean Circulation*, pp. 54-56, National Academy of Sciences, Washington, D.C.
- Gordon, A.L., D.T. Georgi and H.W. Taylor, 1977. Antarctic Polar Front Zone in the western Scotian Sea - summer, 1975. *J. Phys. Oceanogr.* 7:309-328.
- Gordon, A.L., D.G. Martinson, and H.W. Taylor, 1981. The wind-driven circulation in the Weddell-Enderby Basin. *Deep-Sea Res.* 28A:151-163.

- Gordon, A.L. and E.J. Molinelli, 1982. *Southern Ocean Atlas*, Columbia University Press, New York, 11 pp., 213 pl.
- Gordon, A.L. and C.L. Greengrove, 1986. Geostrophic circulation of the Brazil-Falkland confluence. *Deep-Sea Res.* 33:573-585.
- Halkin, D. and T. Rossby, 1985. The structure and transport of the Gulf Stream at 73°W. *J. Phys. Oceanogr.* 15:1439-1452.
- Hall, M.M. and H.L. Bryden, 1982. Direct estimates and mechanisms of ocean heat transport. *Deep-Sea Res.* 29:339-360.
- Hall, M.M. and H.L. Bryden, 1985. Profiling the Gulf Stream with a current meter mooring. *Geophys. Res. Lett.* 12:203-206.
- Han, Y.-J. and S.W. Lee, 1981. A new analysis of monthly mean wind stress over the global ocean. *Rep.* 26, 148 pp., Clim. Res. Inst., Oreg. State Univ., Corvallis.
- Harris, T.F.W., R. Legeckis and D. Van Foreest, 1978. Satellite infra-red images in the Agulhas Current System. *Deep-Sea Res.* 25:543-548.
- Harris, T.F.W. and L.V. Shannon, 1979. Satellite-tracked drifters in the Benguela Current system. *South African Journal of Science* 75:316-317.
- Hart, T.J. and R.I. Currie, 1960. The Benguela Current. *Discovery Rep.* 31:123-298.
- Hastenrath, S., 1980. Heat budget of tropical ocean and atmosphere. *J. Phys. Oceanogr.* 10:159-170.
- Hastenrath, S., 1982. On meridional heat transports in the world ocean. *J. Phys. Oceanogr.* 12:922-927.
- Hellerman, S. and M. Rosenstein, 1983. Normal monthly wind stress over the world ocean with error estimates. *J. Phys. Oceanogr.* 13:1093-1104.
- Hogg, N.G., P. Biscaye, W. Gardner, and W.J. Schmitz, Jr., 1982. On the transport and modification of Antarctic Bottom Water in the Vema Channel. *J. Mar. Res.* 40(Suppl.):231-263.
- Hogg, N.G., 1983. A note on the deep circulation of the western North Atlantic: its nature and causes. *Deep-Sea Res.* 30:945-961.
- Hsiung, J., 1985. Estimates of global oceanic meridional heat transport. *J. Phys. Oceanogr.* 15:1405-1413.
- Hsiung, J., 1986. Mean surface energy fluxes over the global ocean. *J. Geophys. Res.* 91:10,585-10,606.
- Iselin, C.O'D., 1936. A study of the circulation of the western North Atlantic. *Papers in Physical Oceanography and Meteorology* 4:4, 101pp.
- Jacobs, S.S. and D.T. Georgi, 1977. Observations on the southwest Indian/Antarctic Ocean. In: *A Voyage of Discovery: George Deacon 70th Anniversary Volume*, M. Angel ed., Supplement to *Deep-Sea Res.*, Pergamon Press, Oxford, pp. 43-84.

- Jenkins, W.J., 1980. Tritium and  $^3\text{He}$  in the Sargasso Sea. *J. Mar. Res.* 38:533-569.
- Jenkins, W.J. and J.C. Goldman, 1985. Seasonal cycling and primary production in the Sargasso Sea. *J. Mar. Res.* 43:465-491.
- Johnson, D.A., S.E. McDowell, L.G. Sullivan and P.E. Biscaye, 1976. Abyssal hydrography, nephelometry, currents and benthic boundary layer structure in the Vema Channel. *JGR* 81:5771-5786.
- Joyce, T.M., C. Wunsch and S.D. Pierce, 1986. Synoptic Gulf Stream velocity profiles through simultaneous inversion of hydrographic and acoustic doppler data. *J. Geophys. Res.* 91:7573-7585.
- Jung, G.H., 1952. Note on the meridional transport of energy by the oceans. *J. Mar. Res.* 11:2.
- Jung, G.H., 1955. Heat transport in the Atlantic Ocean. *Ref. 53-34T*, Dept. of Oceanography, Texas A. and M., College Station.
- Kawase, M. and J.L. Sarmiento, 1985. Nutrients in the Atlantic thermocline. *J. Geophys. Res.* 90:8961-8979.
- Kawase, M. and J.L. Sarmiento, 1986. Circulation and nutrients in middepth Atlantic waters. *J. Geophys. Res.* 91:9749-9770.
- Killworth, P.D., 1977. Mixing on the Weddell Sea continental slope. *Deep-Sea Res.* 24:427-448.
- Kirwan, A.D., 1963. Circulation of Antarctic Intermediate Water deduced through isentropic analysis. *Ref. No. 63-34 F*, Texas A & M University, College Station, Texas, 34 pp.
- Krishnaswami, S., D. Lal, B.L.K. Somayajulu, R.F. Weiss and H. Craig, 1976. Large volume *in situ* filtration of deep Pacific waters: mineralogical and radioisotope studies. *Earth and Planetary Science Letters* 32:420-429.
- Krishnaswami, S., M.M. Sarin, and B.L.K. Somayajulu, 1981. Chemical and radiochemical investigations of surface and deep particles of the Indian Ocean. *Earth and Planetary Science Letters* 54:81-96.
- Knauss, J.A., 1969. A note on the transport of the Gulf Stream. *Frederick C. Fuglister Sixtieth Anniversary Volume, Deep Sea Research* 16(Suppl.):117-123.
- Lanczos, C., 1961. *Linear Differential Operators*, Van Nostrand, Reinhold, N.Y., 564 pp.
- Lawson, C.L. and R.J. Hanson, 1974. *Solving Least Squares Problems*, Prentice-Hall, Englewood Cliffs, N.J., 340 pp.
- Leeman, K.D., R.L. Molinari and P.S. Vertes, 1987. Structure and variability of the Florida Current at 27°N: April 1982 - July 1984. *J. Phys. Oceanogr.* 17:565-583.

- Levitus, S., 1982. Climatological atlas of the world ocean, *NOAA Prof. Pap. 19*, U.S. Government Printing Office, Washington, D.C.
- Lutjeharms, J.R.E., 1981. Features of the southern Agulhas Current circulation from satellite remote sensing. *S. Afr. J. Sci.* 77:231-236.
- Lutjeharms, J.R.E. and D.J. Baker, 1980. A statistical analysis of the meso-scale dynamics of the Southern Ocean. *Deep-Sea Res.* 27:145-159.
- Lutjeharms, J.R.E. and P.L. Stockton, 1987. Kinematics of the upwelling front off southern Africa. *The Benguela and Comparable Ecosystems*, A.I.L. Payne, J.A. Gulland and K.H. Brink, ed.'s, *S. Afr. J. Mar. Sci.* 5:35-49.
- Lutjeharms, J.R.E. and R.C. van Ballegooyen, 1987. The Agulhas Current retroflection. *J. Phys. Oceanogr.* (submitted).
- Luyten, J.R., 1977. Scales of motion in the deep Gulf Stream and across the Continental Rise. *J. Mar. Res.* 35:49-74.
- Luyten, J.R., J. Pedlosky and H. Stommel, 1983. The ventilated thermocline. *J. Phys. Oceanogr.* 13:292-309.
- Mann, C.R., A.R. Coote and D.M. Garner, 1973. The meridional distribution of silicate in the western Atlantic Ocean. *Deep-Sea Res.* 20:791-801.
- Mantyla, A.W. and J.L. Reid, 1983. Abyssal characteristics of the World Ocean waters. *Deep-Sea Res.* 30:805-833.
- Martin, J.H., G.A. Knauer, D.M. Karl and W.W. Broenkow, 1987. VERTEX: carbon cycling in the northeast Pacific. *Deep-Sea Res.* 34:267-285.
- Martineau, D.P., 1953. The influence of the current systems and lateral mixing upon Antarctic Intermediate Water in the South Atlantic. *W.H.O.I. Technical Report 53-72*, Woods Hole Oceanographic Institution, Woods Hole, MA, 12 pp.
- McCartney, M.S., 1977. Subantarctic Mode Water. In: *A Voyage of Discovery: George Deacon 70th Anniversary Volume*, M.V. Angel, ed., Supplement to *Deep-Sea Res.*, Pergamon Press, Oxford, pp. 103-119.
- McCartney, M.S., 1982. The subtropical recirculation of Mode Waters. *J. Mar. Res.* 40(Suppl.):427-464.
- McDougall, T.J., 1984. The relative roles of diapycnal and isopycnal mixing on sub-surface water-mass conversion. *J. Phys. Oceanogr.* 14:1577-1589.
- McDougall, T.J., 1987. Thermobaricity, cabbeling, and water-mass conversion. *J. Geophys. Res.* 92:5448-5464.
- Menzel, D.W. and J.H. Ryther, 1968. Organic carbon and the oxygen minimum in the South Atlantic Ocean. *Deep-Sea Res.* 15:327-337.
- Metcalfe, W.G., 1969. Dissolved silicate in the deep North Atlantic. *Frederick C. Fuglister Sixtieth Anniversary Volume, Deep-Sea Res.* 16(Suppl.):139-145.

- Model, F., 1950. Warmwasserheizung Europas, *Ber. deut. Wetterdienstes* 12:51-60.
- Montgomery, R.B., 1938. Circulation in upper layers of southern North Atlantic deduced with use of isentropic analysis. *Papers in Physical Oceanography and Meteorology* 6:2, 55 pp.
- Montgomery, R.B. and M.J. Pollack, 1942. Sigma-T surfaces in the Atlantic Ocean. *J. Mar. Res.* 5:20-27.
- Niiler, P.P. and W.S. Richardson, 1973. Seasonal variability of the Florida Current. *J. Mar. Res.* 31:144-167.
- Nowlin, W.D., T. Whitworth and R.D. Pillsbury, 1977. Structure and transport of the Antarctic Circumpolar Current at Drake Passage from short-term measurements. *J. Phys. Oceanogr.* 7:788-802.
- Nowlin, W.D. and J.M. Klinck, 1986. The physics of the Antarctic circumpolar current. *Rev. Geophys.* 24:469-491.
- Olson, D.B. and R.H. Evans, 1986. Rings of the Agulhas Current. *Deep-Sea Res.* 33:27-42.
- Parker, R.L., 1970. The inverse problem of electrical conductivity in the mantle. *Geophys. J. Roy. Astronom. Soc.* 22:121-138.
- Parker, R.L., 1977. Understanding inverse theory. *Annu. Rev. Earth Planet. Sci.* 5:35-64.
- Piola, A. and D.T. Georgi, 1982. Circumpolar properties of Antarctic Intermediate Water and Subantarctic Mode Water. *Deep-Sea Res.* 29:687-711.
- Rago, T.A. and H.T. Rossby, 1987. Heat transport into the North Atlantic Ocean north of 32°N latitude. *J. Phys. Oceanogr.* 17:854-871.
- Redfield, A.C., 1942. The processes determining the concentration of oxygen, phosphate and other organic derivatives within the depths of the Atlantic Ocean. *Pap. Phys. Oceanogr. Meteorol.* 9:1-22.
- Redfield, A.C., B.H. Ketchum and F.A. Richard, 1963. The influence of organisms on the composition of sea water. *The Sea*, Vol. 2, M.N. Hill, ed., Interscience, New York, pp. 26-77.
- Reid, J.L., Jr., 1965. Intermediate waters of the Pacific Ocean. *The Johns Hopkins Oceanographic Studies* 5:96 pp.
- Reid, J.L., Jr., 1979. On the contribution of the Mediterranean Sea outflow to the Norwegian-Greenland Sea. *Deep-Sea Res.* 26:1199-1223.
- Reid, J.L., Jr., 1981. On the mid-depth circulation of the World Ocean. In: *Evolution of Physical Oceanography*, The MIT Press, Cambridge, 623 pp.



- Reid, J.L., Jr. and R.J. Lynn, 1971. On the influence of the Norwegian-Greenland and Weddell seas upon the bottom waters of the Indian and Pacific oceans. *Deep-Sea Res.* 18:51-64.
- Reid, J.L. and W.D. Nowlin, 1971. Transport of water through the Drake Passage. *Deep-Sea Res.* 18:51-64.
- Reid, J.L., Jr., W.D. Nowlin and W.C. Patzert, 1977. On the characteristics and circulation of the southwestern Atlantic Ocean. *J. Phys. Oceanogr.* 7:62-91.
- Rhines, P.B. and W.R. Young, 1982. A theory of the wind-driven circulation, I: Mid-ocean gyres. *J. Mar. Res.* 40(Suppl.):559-596.
- Richards, F.A., 1958. Dissolved silicate and related properties of some western North Atlantic and Caribbean waters. *J. Mar. Res.* 17:449-465.
- Richardson, P.L., 1977. On the crossover between the Gulf Stream and the Western Boundary Undercurrent. *Deep-Sea Res.* 24:139-159.
- Riley, G.A., 1951. Oxygen, phosphate and nitrate in the Atlantic Ocean. *Bull. Bingham Oceanogr. Collect.* 12:3, 169 pp.
- Roemmich, D., 1980. The application of inverse methods to problems in ocean circulation. Ph.D. thesis, MIT/WHOI, 193 pp.
- Roemmich, D., 1983. The balance of geostrophic and Ekman transports in the tropical Atlantic Ocean. *J. Phys. Oceanogr.* 13:1534-1539.
- Roemmich, D., 1983. Optimal estimation of hydrographic station data and derived fields. *J. Phys. Oceanogr.* 13:1544-1549.
- Roemmich, D. and C. Wunsch, 1985. Two transatlantic sections: meridional circulation and heat flux in the subtropical North Atlantic Ocean. *Deep-Sea Res.* 32:619-664.
- Roemmich, D. and C. Wunsch, 1984. Apparent changes in the climatic state of the deep North Atlantic Ocean. *Nature* 307:447-450.
- Sarmiento, J.L., 1986. On the north and tropical Atlantic heat balance. *J. Geophys. Res.* 91:11,677-11,689.
- Saunders, P.M., Circulation in the eastern North Atlantic. *J. Mar. Res.* 40(Suppl.): 641-657.
- Schink, D.R., 1967. Budget for dissolved silica in the Mediterranean Sea. *Geochim. Cosmochim. Acta* 31:897-899.
- Schlitzer, R., 1987. Modeling the nutrient and carbon cycles of the North Atlantic. Part I: circulation, mixing coefficients, and heat fluxes. *in preparation*.
- Schlitzer, R., W. Roether, U. Weidmann, P. Kalt and H.H. Loosli, 1985. A meridional  $^{14}\text{C}$  and  $^{39}\text{Ar}$  section in northeast Atlantic deep water. *J. Geophys. Res.* 90:6945-6952.

- Schmitt, R.W. and D.B. Olson, 1985. Wintertime convection in Warm-Core Rings: Thermocline ventilation and the formation of mesoscale lenses. *J. Geophys. Res.* 90:8823-8837.
- Schmitz, W.J., Jr., 1977. On the deep general circulation in the Western North Atlantic. *J. Mar. Res.* 35:21-28.
- Schmitz, W.J., Jr., 1980. Weakly depth-dependent segments of the North Atlantic circulation. *J. Mar. Res.* 38:11-135.
- Shannon, L.V., 1985. The Benguela Ecosystem I: Evolution of the Benguela, physical features and processes. *Oceanog. Mar. Biol. Annu. Rev.* 23:105-182.
- Shulenberger, E. and J.L. Reid, 1981. The Pacific shallow oxygen minimum, deep chlorophyl maximum and primary productivity, reconsidered. *Deep-Sea Res.* 28: 901-919.
- Sievers, H.A. and W.D. Nowlin, 1984. The stratification and water masses in Drake Passage. *J. Geophys. Res.* 83:10,489-10,514.
- Smith, F.G.W. and F.A. Kalber, 1974. *Handbook of Marine Science*, Vol. II, CRC Press Inc., Cleveland, 390 pp.
- Stefànsson, U., 1968. Dissolved nutrients, oxygen and water masses in the Northern Irminger Sea. *Deep-Sea Res.* 15:541-575.
- Stefànsson, U. and L.P. Atkinson, 1971. Relationship of potential temperature and silicate in the deep waters between Cape Lookout, North Carolina, and Bermuda. *J. Mar. Res.* 29:306-318.
- Stommel, H., 1957. A survey of ocean current theory. *Deep-Sea Res.* 4:149-184.
- Stommel, H., 1980a. Asymmetry of interoceanic freshwater and heat fluxes. *Proc. National Academy of Sciences* 77:2377-2381.
- Stommel, H., 1980b. How the ratio of meridional flux of freshwater to flux of heat fixes the latitude where low salinity intermediate water sinks. *Tellus* 32:562-566.
- Stommel, H. and A.B. Arons, 1960. On the abyssal circulation of the world ocean - I. Stationary planetary flow patterns on a sphere. *Deep-Sea Res.* 6:140-154.
- Stommel, H. and G.T. Csanady, 1980. A relation between the T-S curve and global heat and atmospheric water transports. *J. Geophys. Res.* 85:495-501.
- Sugimura, Y. and Y. Suzuki, 1986. A high temperature catalytic oxidation method of non-volatile dissolved organic carbon in sea water by direct injection of a liquid sample. *Mar. Chem.*, in press.
- Sundquist, E.T., 1985. Geological perspectives on carbon dioxide and the carbon cycle. In: *The carbon cycle and atmospheric CO<sub>2</sub>: natural variations Archean to present*. E.T. Sundquist and W.S. Broecker, ed.'s, American Geophysical Union, Washington, D.C., pp. 5-59.

- Suzuki, Y., Y. Sugimura and T. Itoh, 1985. A catalytic oxidation method for the determination of total nitrogen in seawater. *Mar. Chem.* 16:83.
- Sverdrup, H.U., 1933. On vertical circulation in the ocean due to the action of the wind with application to conditions within the Antarctic Circumpolar Current. *Discovery Rep., Vol. VII* pp. 139-170.
- Sverdrup, H.U., 1938. On the exploration of the oxygen minima and maxima in the ocean. *J. Coun. Intern. 13*, Kopenhagen, 163 pp.
- Sverdrup, H.U., M.W. Johnson and R.H. Fleming, 1942. *The Oceans: Their Physics, Chemistry and General Biology*. Prentice Hall, Englewood Cliffs, New Jersey, 1087 pp.
- Taft, B.A., 1963. Distribution of salinity and dissolved oxygen on surfaces of uniform potential specific volume in the South Atlantic, South Pacific and Indian Oceans. *J. Mar. Res.* 21:129-146.
- Taylor, H.W., A.L. Gordon and E. Molinelli, 1978. Climatic characteristics of the Antarctic Polar Front Zone. *J. Geophys. Res.* 83:4572-4578.
- Thompson, R.O.R.Y. and G. Veronis, 1980. Transport calculations in the Tasman and Coral Seas. *Deep-Sea Res.* 27A:303-323.
- Tsuchiya, M., 1985. Evidence of a double cell subtropical gyre in the South Atlantic Ocean. *J. Mar. Res.* 43:57-65.
- Warren, B. A., 1981. The deep circulation of the world ocean. In: *Evolution of Physical Oceanography*, The MIT Press, Cambridge, pp. 6-41.
- Warren, B.A. and G.H. Volkmann, 1968. Measurement of the volume transport of the Gulf Stream south of New England. *J. Mar. Res.* 26:110-126.
- Wearn, R.B., Jr., and D.J. Baker, 1980. Bottom pressure measurements across the Antarctic Circumpolar Current and their relation to wind. *Deep-Sea Res.* 27:857-888.
- Whitehead, J.A. and L.V. Worthington, 1982. The flux and mixing rates of Antarctic bottom water within the North Atlantic. *J. Geophys. Res.* 87:7903-7924.
- Whitworth, T., III, 1980. Zonation and geostrophic flow of the Antarctic Circumpolar Current at Drake Passage. *Deep-Sea Res.* 27:497-507.
- Whitworth, T., III, 1983. Monitoring the transport of the Antarctic Circumpolar Current at Drake Passage. *J. Phys. Oceanogr.* 13:2045-2057.
- Whitworth, T., III, and W.D. Nowlin, 1987. Water masses and currents of the Southern Ocean at the Greenwich Meridian. *J. Geophys. Res.* 92:6462-6476.
- Wiggins, R.A., The general linear inverse problem: Implication of surface waves and free oscillations for earth structure. *Rev. Geophys. Space Phys.* 10:251-285.

- Wooster, W.S. and J.L. Reid, 1963. Eastern boundary currents. In: *The Sea, Vol. 2*, M.N. Hill, ed., pp. 253-276.
- Worthington, L.V., 1959. The 18° water in the Sargasso Sea. *Deep-Sea Res.* 5:297-305.
- Worthington, L.V., 1976. On the North Atlantic Circulation. *The Johns Hopkins Oceanographic Studies* 6:110 pp.
- Wright, W.R., 1969. Northward transport of Antarctic Bottom Water in the western Atlantic Ocean. *Deep-Sea Res.* 17:367-371.
- Wright, W.R. and L.V. Worthington, 1970. The Water Masses of the North Atlantic Ocean; a Volumetric Atlas of Temperature and Salinity. *Serial Atlas of the Marine Environment*, Folio 19, American Geographical Society, New York, 8 pp. and 7 plates.
- Wunsch, C., 1978. The general circulation of the North Atlantic west of 50°W determined from inverse methods. *Reviews of Geophysics and Space Physics* 16:583-620.
- Wunsch, C., 1980. Meridional heat flux of the North Atlantic Ocean. *Proceedings of the National Academy of Sciences* 77:5043-5047.
- Wunsch, C., 1984. An eclectic Atlantic Ocean circulation model. Part I: the meridional flux of heat. *J. Phys. Oceanogr.* 14:1712-1733.
- Wunsch, C. and B. Grant, 1982. Towards the general circulation of the North Atlantic Ocean. *Prog. in Oceanography* 11:1-59.
- Wunsch, C., D. Hu and B. Grant, 1983. Mass, heat and nutrient fluxes in the South Pacific Ocean. *J. Phys. Oceanogr.* 13:725-753.
- Wüst, G., 1935. *The Stratosphere of the Atlantic Ocean*, W.J. Emery, ed., 1978, Amerind, New Delhi, 112 pp.
- Wunsch, C. and D. Roemmich, 1985. Is the North Atlantic in Sverdrup balance? *J. Phys. Oceanogr.* 15:1876-1880.
- Wüst, G., 1935. Schichtung und Zirkulation des Atlantischen Ozeans. Die Stratosphäre. In *Wissenschaftliche Ergebnisse der Deutschen Atlantischen Expedition auf dem Forschungs- und Vermessungsschiff "Meteor" 1925-1927*, 6: 1st Part, 2, 180 pp. (*The Stratosphere of the Atlantic Ocean*, W.J. Emery, ed., 1978, Amerind, New Delhi, 112 pp.
- Wüst, G., 1964. *Stratification and circulation in the Antillean-Caribbean Basins*, Columbia University Press, New York, 201 pp.
- Wüst, G. and A. Defant, 1936. Atlas zur Schichtung und Zirkulation des Atlantischen Ozeans. Schnitten und Karten von Temperatur, Salzgehalt und Dichte. In *Wissenschaftliche Ergebnisse der Deutschen Atlantischen Expedition auf dem Forschungs- und Vermessungsschiff "Meteor" 1925-1927*, 6: Atlas, 103 plates.
- Wyrtki, K., 1962. The oxygen minimum in relation to ocean circulation. *Deep-Sea Res.* 9:11-23.